CONTROL SYSTEM DESIGN FOR ROBUST PERFORMANCE DESPITE MODEL PARAMETER UNCERTAINTIES: APPLICATION TO CROSS-DIRECTIONAL RESPONSE CONTROL IN PAPER MANUFACTURING

Thesis by

Daniel Lee Laughlin

In Partial Fulfillment of the Requirements

for the Degree of

Doctor of Philosophy

California Institute of Technology

Pasadena, CA 91125

1988

(Submitted April 25, 1988)

My love

I give and

this work I dedicate

to my parents Vicki and Dave,

to my grandparents Doris, Elgin, and Matilda,

to my late great-grandmother Lynne.

The rare joy of their love

remains with me always,

brightens my spirit,

ends despair.

ACKNOWLEDGEMENTS

I am grateful to my advisor Manfred Morari for his support and guidance. I appreciate the many hours he devoted to me in discussing this work and directing my education in process control. I thank him for providing Internal Model Control and CONSYD research tools utilized in this work.

I am thankful to the AMOCO Foundation and the National Science Foundation for providing financial support for my graduate education.

I am thankful to John Doyle for providing structured-singular-value analysis, μ-synthesis, and HONEYX research tools utilized in this work.

I respect and admire the intelligence, dedication, and persistence of my fellow research group members: Pete Campo, Richard Colberg, Mike Creed, Frank Doyle, Costas Economou, Philippe Engel, Pierre Grosdidier, Eric Hanzyc, Roland Heersink, Ken Jordan, Jorge Mandler, Lionel Laroche, Jay Lee, Dan Lewin, Dan Rivera, Tony Skjellum, Sigurd Skogestad, Chris Webb, and Evangelos Zafiriou. I thank all of them for their encouragement and friendship.

ABSTRACT

The problem of robust performance analysis is solved for SISO control systems with uncorrelated model parameter uncertainties. The robust performance problem is formulated in a manner consistent with structured singular value μ-analysis – for SISO systems this means restricting the magnitude of a weighted closed-loop sensitivity function. The solution to the problem is graphical in nature and well suited to a computer-aided controller-design procedure. It utilizes region boundaries on the complex plane that contain specified sets of process models at each frequency. An algorithm is presented for locating the region boundaries corresponding to model transfer-functions with uncertain real coefficients and time-delay. Convergence and containment properties of the algorithm are proven.

The region-based analysis is combined with the Internal Model Control design procedure to form a controller synthesis method for robust performance. Tradeoffs between performance and robustness are transparent to the designer in the proposed synthesis method. Useful tables of controller parameters are presented in tabular form for a wide range of parameter uncertainty levels in a first-order-with-time-delay model. The controller resulting from the IMC design procedure is compared with the μ-optimal controller. Although the new synthesis procedure is generally applicable to SISO systems, it can be used to design decentralized controllers for MIMO systems with uncertain scalar dynamics and symmetric interactions. The particular application of cross-machine-direction basis-weight control in paper manufacturing is discussed in detail. Robust performance and robust failure tolerance of desirable decentralized controllers for this system are proven.

TABLE OF CONTENTS

LIST OF FIGURES

LIST OF TABLES

CHAPTER I: INTRODUCTION

INTRODUCTION

Modelling errors are inseparable, undesirable companions of modelling – like *Ignorance* and *Want* clinging to the feet of Dickens' *Ghost of Christmas Present.* The objective of the control engineer is to design controllers that satisfy system requirements despite these modelling errors. Control system designs that meet the objective are said to exhibit robust performance. It is perhaps true that control systems have always been designed for robust performance even if the early designers didn't recognize it – physical systems have not just recently become difficult to model. Early control-system designers lacked rigorous mathematical tools to measure robust performance. Development of structured-singular-value analysis and synthesis [Doyle, 1982] provided the needed tools.

This work utilizes the tools of structured-singular-value analysis and synthesis for control-system design. Evaluating control-system designs with these tools allows development of attractive necessary and sufficient conditions for robust performance despite modelling errors. It is not always possible, however, to formulate control-system design problems so that they are compatible with existing tools for robust performance analysis and synthesis. For example, uncertain time-delays, real model parameter variations, and synthesis of desirable decentralized controllers – important issues in chemical engineering control problems – are all inadequately addressed by existing analysis and synthesis techniques. An objective of this work is to eliminate these deficiencies of existing techniques with intuitively appealing and practical new controller-design techniques. The focus and advantages of new results

in this work are best appreciated after reviewing the present status of structured-singular-value analysis and synthesis.

1. The Structured Singular Value μ and Robust Performance

In structured-singular-value analysis, a control structure is proposed as illustrated in Figure 1 with nominal model $\tilde{P}(s)$, controller $K(s)$, expected disturbances $d(s)$, output $y(s)$, and modelling error $W_1(s)\Delta_1(s)$. Matrices Δ_i in such structures are usually bounded in the sense that $\sigma_{max}(\Delta_i) \leq 1\ \forall\omega$ to represent model uncertainty in all directions from the nominal model. The weight $W_1(s)$ is used to shape the modelling error as a function of frequency ω. The requirements of the control system in Figure 1 are that the system be stable and that the system perform attenuation of disturbances $d(s)$ in the output $y(s)$. The control system is robustly stable if it is stable for all models $P(s) = \tilde{P}(s)\left[I+W_1(s)\Delta_1(s)\right]$. The Small Gain Theorem states that this will be the case if and only if the nominal system with $\tilde{P}(s)$ is stable and the gain in the loop containing Δ_1 is less than one; that is, the control system in Figure 1 is robustly stable for all $\sigma_{max}(\Delta_1) \leq 1$ if and only if the nominal system is stable and $\sigma_{max}\left(W_1(s)\tilde{P}(s)K(s)\left[I+\tilde{P}(s)K(s)\right]^{-1}\right) < 1\ \forall s = i\omega$. Acceptable attenuation of disturbances in the output, or performance, is described in terms of a bound on the closed-loop sensitivity function by $\sigma_{max}\left(W_2(s)\left[I+\tilde{P}(s)K(s)\right]^{-1}\right) < 1$. The system exhibits robust performance if it exhibits performance for all models $P(s)$.

A key insight of Doyle was recognition that robust performance of the system in Figure 1 is equivalent to robust stability of the system in Figure 2. In Figure 2 a second uncertainty block Δ_2 and weight $W_2(s)$ connect output $y(s)$ to disturbances $d(s)$. Once again, the Small Gain Theorem states that the system in Figure 2 is robustly stable if and only if it is nominally stable and the gain in the loop containing

Δ_2 is less than one; that is, the control system in Figure 2 is robustly stable for all $\sigma_{max}(\Delta_2) \leq 1$ if and only if it is nominally stable and

$$\mu = \sup_{w,P(s)} \sigma_{max}\left(W_2(s)\left[I + P(s)K(s)\right]^{-1}\right) < 1. \tag{1}$$

Since the sensitivity function $\left[I + P(s)K(s)\right]^{-1}$ relates output $y(s)$ to disturbances $d(s)$, the performance weight $W_2(s)$ can be used to shape the disturbance attenuation as a function of frequency. Since $P(s) = \tilde{P}(s)\left[I + W_1(s)\Delta_1(s)\right]$ appears in the condition $\mu \leq 1$ for the system in Figure 2, the level of performance specified by $W_2(s)$ is guaranteed for the whole set of models $P(s)$. Therefore, the structured singular value μ is a rigorous measure of the robust performance of a control system.

The control structure in Figure 2 is equivalent to the two structures illustrated in Figure 3. Matrix transfer-functions Δ, $G(s)$, and $M(s)$ are given by:

$$\Delta = \begin{pmatrix} \Delta_1 & 0 \\ 0 & \Delta_2 \end{pmatrix} \tag{2}$$

$$G(s) = \begin{pmatrix} 0 & 0 & W_1\tilde{P} \\ W_2 & W_2 & W_2\tilde{P} \\ -I & -I & -\tilde{P} \end{pmatrix} \tag{3}$$

$$M(s) = \begin{pmatrix} -W_1\tilde{P}K\left[I + \tilde{P}K\right]^{-1} & -W_1\tilde{P}K\left[I + \tilde{P}K\right]^{-1} \\ -W_2\left[I + PK\right]^{-1} & -W_2\left[I + PK\right]^{-1} \end{pmatrix}. \tag{4}$$

Figure 3 (top) is typically associated with μ-synthesis; Figure 3 (bottom), with μ-analysis. When $\sigma_{max}(\Delta) \leq 1\ \forall\omega$, the robust performance condition given by 1 can also be defined as nominal stability and $\mu\left[M(s)\right] < 1\ \forall s = i\omega$, where μ is calculated according to the structure associated with Δ. The μ-optimal controller is defined as the stabilizing controller $K(s)$ in Figure 3 (bottom) that minimizes μ of the associated matrix transfer-function $M(s)$ [Doyle, 1987]. The beauty of the structured-singular-value framework is that all control structures can be written

as in Figure 3, with matrices Δ, $G(s)$, and $M(s)$ taking appropriate forms to accommodate specified model uncertainties and performance requirements. Although robust performance of all control structures can be defined in terms of the structured singular value, methods for computing μ and for synthesizing the μ-optimal controller exist for a limited number of structures Δ.

Currently the method of Fan and Tits [1986] is employed to calculate a tight lower bound on $\mu[M(s)]$ when Δ is composed of nonrepeated complex blocks Δ_i. The method of Doyle [1982] is used to calculate an upper bound on $\mu[M(s)]$, when Δ is composed of complex blocks Δ_i. Both methods are guaranteed to converge to the actual value of μ when Δ has no more than three blocks. Methods are being developed to enable calculation of μ when Δ contains real scalar blocks [Sideris and de Gaston, 1987]. Extensions of μ-analysis are being applied when Δ is a structured cone-bounded nonlinearity [Doyle and Packard, 1987]. No existing method enables efficient calculation of μ when Δ contains repeated real parameter variations or enables synthesis of the μ-optimal controller, when Δ contains repeated and/or real parameter uncertainties. An active area of research is the development of additional methods to calculate μ when Δ is more highly structured. Enabling more information about model uncertainty to be incorporated into Δ results in less conservative robust-performance analysis.

2. Model Parameter Uncertainties and Region-Based Analysis

In this work a new algorithm is presented for calculating μ as defined by Equation 1 for SISO systems with real parameter uncertainties in the process model. The set π of Laplace transfer-function models that can be accommodated by the algorithm is given by 5. Terms $x(s)$, $y(s)$, $n_j(s)$, and $d_l(s)$ are assumed to be exact transfer-functions, while real numerator coefficients a_j, denominator coefficients b_l, gain k, and time-delay θ are inexactly known.

$$\pi = \left\{ p(s) | p(s) = x(s) + y(s)\ k \left[\frac{a_j n_j(s) + ... + a_1 n_1(s) + a_0 n_0(s)}{b_l d_l(s) + ... + b_1 d_1(s) + b_0 d_0(s)} \right] e^{-\theta s} \right\} \quad (5)$$

$$a_j \in [a_{j_{min}}, a_{j_{max}}],\ b_l \in [b_{l_{min}}, b_{l_{max}}]$$

$$k \in [k_{min}, k_{max}],\ \theta \in [\theta_{min}, \theta_{max}]$$

Through the bounded real parameters, the set π can capture uncertainty in models derived from basis principles and uncertainty in models extracted from experimental data. In order to calculate the structured singular value μ for systems with the set of process models π, the new algorithm locates regions on the complex plane containing $\pi(i\omega)$ at each frequency ω.

For SISO systems in Figure 1 with controller $c(s)$, the robust performance test 1 with W_2 equal to scalar w_2 is equivalent to the requirement that the distance of regions $\pi(i\omega)c(i\omega)$ from $(-1, 0)$ exceeds $|w_2(i\omega)|$ for all frequencies ω. It is clearly important that regions $\pi(i\omega)c(i\omega)$ contain all models in 5 without containing any extra models to avoid conservativeness. Previous algorithms for locating boundaries for regions $\pi(i\omega)$ by Chen [1984], Saeki [1986], East [1982], and Longdon and East [1979] are either excessively conservative or cannot guarantee that all models are contained. The new algorithm presented here was developed to solve these deficiencies of previous algorithms. Programming solutions from the field of computational geometry (see Lee and Preparata [1984]) applied to steps in the new algorithm enable efficient and accurate location of regions $\pi(i\omega)$.

The SISO robust performance test based on uncertainty regions $\pi(i\omega)c(i\omega)$ motivates graphical techniques for control-system analysis. Several researchers have offered controller-design techniques that utilize regions on the complex plane or Nichols chart to represent process uncertainty [Chen, 1984] [East, 1982] [Horowitz, 1982]. Horowitz [1982] associates with such graphical design techniques a property he calls "transparency", where the relationship between model characteristics and control-system requirements are clearly visible to the control-system designer. With

graphical analysis techniques, for example, it is possible to recognize immediately that time-delay uncertainty is limiting the achievable performance of a control-system design – this in contrast to strict μ-analysis, where such a condition would be much more difficult to recognize. To illustrate the property of transparency, regions $\pi(i\omega)$ corresponding to combinations of 20 percent uncertainty in parameters k, τ, and θ in the familiar first-order with time-delay model 6 are illustrated in Figures 4–10 for 60 frequencies in the range $0.01 \leq \omega \leq 10.0$.

$$\pi = \left\{ p(s) \middle| p(s) = \frac{ke^{-\theta s}}{\tau s + 1} \right\} \tag{6}$$

$$k \in [k_{min}, k_{max}],\ \tau_a \in [\tau_{min}, \tau_{max}],\ \theta \in [\theta_{min}, \theta_{max}]$$

Note in the figures that characteristics of gain, time-constant, and delay uncertainty are easily recognizable – they are transparent to the control-system designer. Any controller-design method can be used in conjunction with graphical robust performance analysis based on regions $\pi(i\omega)$.

3. Internal Model Control and Smith Predictors

The Internal Model Control (IMC) design method extensively developed by Morari et al. [1988] is particularly compatible with graphical robust performance analysis based on uncertainty regions $\pi(i\omega)$. The IMC structure is illustrated in Figure 11 with process $p(s)$, model $\tilde{p}(s)$, controller $q(s)$, disturbances $d(s)$ and outputs $y(s)$. Principal advantages of the IMC structure include:

1) The IMC control structure is a stable parameterization of the feedback controller $c(s)$ in Figure 11. The control system is guaranteed to be nominally stable, if both $\tilde{p}(s)$ and $q(s)$ are stable.

2) The restrictions placed on $q(s)$ by robustness requirements are clear, since any nominal transfer function relating inputs to outputs is affine in $q(s)$. For example, the nominal sensitivity function $1/\big(1+\tilde{p}(s)c(s)\big)$ is equal to $1-\tilde{p}(s)q(s)$.
3) Usually, only a single IMC tuning parameter is required – with a transparent relationship to robustness and performance. Controller tuning to satisfy system requirements is straightforward.

The IMC design procedure involves two steps: 1) a controller $\tilde{q}(s)$ is designed to be H_2–optimal for the nominal model and the expected input to the system, and 2) the controller is "detuned" by the addition of a low-pass filter $f(s)$ to meet robustness requirements. The resulting IMC controller is given by $q(s)=\tilde{q}(s)f(s)$.

When the process model is open-loop stable with time-delay, the IMC structure is a parameterization of the Smith predictor control structure introduced by O. J. M. Smith [1957]. In the absence of modelling error, the Smith predictor has been shown to lead to optimal response to step disturbances. Since the chemical process industries are replete with transport delays and composition analysis delays, the IMC parameterization is particularly useful in designing controllers for chemical processes. The proposed IMC controller-design procedure employing graphical robust-performance analysis is a powerful tool for control-system design in the face of model parameter uncertainties.

4. CD Response Control in Paper Manufacturing

The problem of cross-machine-direction (CD) response control in paper manufacturing is ideally suited for the proposed IMC robust-controller-design procedure. Models relating CD paper sheet properties to actuator adjustments are typically given by $P_{CD}^{n,m}(s)=p(s)P_{CD}^{n,m}$, where $p(s)$ are uncertain actuator dynamics with time-delay (as in Equation 5), and $P_{CD}^{n,m}$ is an interaction matrix given by Equation 7.

$$P_{CD}^{n,m} = \underbrace{\begin{pmatrix} p_1 & p_2 & \cdots & p_m & 0 & \cdots & \cdots & 0 \\ p_2 & p_1 & p_2 & \cdots & p_m & \ddots & \ddots & \vdots \\ \vdots & p_2 & p_1 & p_2 & \cdots & \ddots & \ddots & \vdots \\ p_m & \vdots & p_2 & \ddots & \ddots & \vdots & p_m & 0 \\ 0 & p_m & \vdots & \ddots & \ddots & p_2 & \vdots & p_m \\ \vdots & \ddots & \ddots & \cdots & p_2 & p_1 & p_2 & \vdots \\ \vdots & \ddots & \ddots & p_m & \cdots & p_2 & p_1 & p_2 \\ 0 & \cdots & \cdots & 0 & p_m & \cdots & p_2 & p_1 \end{pmatrix}}_{n \times n} \tag{7}$$

Uncertain interaction parameters in $P_{CD}^{n,m}$ are bounded real numbers given by

$$p_i \in \left[P_{i_{min}}, p_{i_{max}}\right]. \tag{8}$$

Since models $P_{CD}^{n,m}$ are typically of very large dimension n, μ-synthesis and model-inverse-based techniques for controller design lead to hugely complicated control algorithms. Moreover, models $P_{CD}^{n,m}$ are characterized by high condition numbers, so robust performance can be difficult to achieve with model-inverse-based controllers. Tight bounds on the singular values of positive-definite models $P_{CD}^{n,m}$ despite interaction parameter uncertainties enable application of the IMC robust-controller-design procedure. The design procedure leads to desirable diagonal and banded controllers with valuable robust-stability, robust-performance, and failure-tolerance properties.

If the robust-performance-analysis problem involving $P_{CD}^{n,m}$ with uncertain interaction parameters were written in terms of M and Δ as in Figure 3, matrix Δ would contain m repeated real blocks of dimension $n \times n$ in addition to real blocks corresponding to uncertain scalar dynamic parameters – a problem entirely beyond the capabilities of existing software for calculating $\mu\left[M\right]$. Application of μ-synthesis to design either a diagonal or banded controller for this problem is equally hopeless without the results in this work.

Significant raw-material savings often accompany successful control of cross-machine-direction sheet properties in paper manufacturing. World paper and paperboard production now amounts to some 140 million metric tons – a single percent reduction in fiber use translates into the preservation of some 300 square miles of forest.† Such raw material savings often accompany successful control of cross-machine-direction (CD) sheet properties. For example, Eastman Kodak reported a 2.4 percent reduction in fiber usage as a result of CD control [Carey et al., 1975]. Operators can produce thinner paper closer to specifications when variations in CD sheet properties are eliminated. Successful application of the proposed controller-design procedure to CD paper-response control is therefore an opportunity for significant, beneficial impact on a major industry.

---

†This 140 million metric tons is a 1982 production Figure from *Statistical Yearbook 1983/84*. In 1985 the United States consumed 84.1 million cords of pulpwood in production of 76.5 million short tons of paper and paperboard [*Statistical Abstract of the United States*, 1987]. George S. Witham, Sr., author of a classic 1942 text *Modern Pulp and Paper Making* estimates "average Adirondack Spruce runs 15 to 20 markets to the acre" [Witham, 1942]. Therefore, a one-percent reduction in fiber usage saves approximately

$$
\begin{aligned}
1,400,000\ \textit{metric tons paper} \times \left(\frac{84.1\ \textit{cords pulpwood}}{76.5\ \textit{short tons paper}}\right) \times \left(\frac{0.907\ \textit{short ton}}{1\ \textit{metric ton}}\right) \\
&= 1,396,000\ \textit{cords pulpwood} \times \left(\frac{3\ \textit{markets wood}}{1\ \textit{cord wood}}\right) \\
&= 4,188,000\ \textit{markets pulpwood} \\
&= 209,000\ \textit{acres average Adirondack Spruce} \\
&= 327\ \textit{square miles forest.}
\end{aligned}
$$

5. Thesis Overview

In Chapter II the new algorithm for locating model uncertainty regions $\pi(i\omega)$ corresponding to 5 is presented. The containment and convergence properties of the algorithm are proven. Advantages of the new algorithm over factorial and region-mapping methods are discussed. Figures in Chapter II illustrate each step in the algorithm. Chapter III presents the IMC controller-design procedure for robust performance based on the regions $\pi(i\omega)$. The performance/robustness tradeoff associated with selection of the IMC filter tuning parameter is illustrated. Performance of the Smith predictor resulting from the design procedure is compared with that of a PID controller for different levels of uncertainty. In Chapter IV the design and tuning of Smith predictors are addressed in detail. Translation of parameter uncertainty into norm-bounded uncertainty is discussed – a particularly useful formula for multiplicative error in the first-order with time-delay model 6 is derived. A method for selecting the form of performance weight $w_2(s)$ is suggested. Useful tables of controller tuning parameters are presented in tabular form for a wide range of uncertainty levels in the first-order with time-delay model. The Smith predictor controller resulting from the IMC design procedure is compared with the μ-optimal controller in Chapter IV. In Chapter V the IMC robust-controller-design procedure is applied to the problem of CD response control in paper manufacturing. Characteristics of the physical process that relate to model structure are discussed. Properties of special matrix forms that model CD response interactions are established. In particular, bounds on the singular values of uncertain CD response models are developed. The bounds enable design of desirable decentralized and banded controllers for large-dimension CD response control problems. Robust stability, robust performance, and robust failure tolerance of the controllers despite interaction parameter uncertainties are proven. The importance of a dimensionless

slice actuator design parameter on the CD response control problem is also illustrated in Chapter V. Chapter VI presents a study on μ-synthesis of decentralized controllers. Repeated sequential application of the μ-synthesis algorithm is found to be most effective for optimizing decentralized controllers. Properties of uncertainty structures designed to penalize the magnitude of off-diagonal controller blocks are summarized. Advantages, applications, and limitations of new results in this work are summarized in Chapter VII, along with recommendations for future research.

References

Carey, E. W., with C. R. Bietry and H. W. Stoll, "Performance Factors Associated with Profile Control of Basis Weight on a Paper Machine," *Tappi*, 58, June 1975, pp. 75–78.

Chen, S., *Control System Design for Multivariable Uncertain Processes*, Ph.D. Thesis (Supervised by C. B. Brosilow), Case Western Reserve University, August 1984.

Doyle, J. C., "Analysis of Feedback Systems with Structured Uncertainties," *Proc. Inst. Elect. Engrs.*, Pt. D, 129, 1982, pp. 242–250.

Doyle, J. C., "A Review of μ for Case Studies in Robust Control," *IFAC World Congress*, Munich, July 1987.

Doyle, J. C., and A. Packard, "Uncertain Multivariable Systems from a State Space Perspective," *Proceedings of the American Control Conference*, Minneapolis, June 10-12, 1987, pp. 2147–2152.

East, D. J., "On the Determination of Plant Variation Bounds for Optimum Loop Synthesis," *International Journal of Control*, 35, 1982, pp. 891–908.

Fan, M. K., and A. L. Tits, "Characterization and Efficient Computation of the Structured Singular Value," *IEEE Transactions on Automatic Control*, AC-31, August 1986, pp. 734–743.

Horowitz, I., "Quantitative Feedback Theory," *IEE Proc.*, D-129, November 1982, pp. 215–226.

Lee, D. T., and F. P. Preparata, "Computational Geometry," *IEE Transactions on Computers*, C-33, December 1984, pp. 1072–1102.

Longdon, L., and D. J. East, "A Simple Geometrical Technique for Determining Loop Frequency Response Bounds which Achieve Prescribed Sensitivity Specifications," *Int. J. Control*, 30, 1979, pp. 153–158.

Morari, M., with E. Zafirou and C. Economou, *Robust Process Control*, Springer Verlag, to be published 1988.

Saeki, M., "A Method of Robust Stability Analysis with Highly Structured Uncertainties," *IEEE Transactions on Automatic Control*, AC-31, October 1986, pp. 935–940.

Sideris, A., and R. R. E. de Gaston, "Multivariable Stability Margin Calculation with Uncertain Correlated Parameters," *IEEE Transactions on Automatic Control*, to be submitted 1987.

Smith, O. J. M., "Closer Control of Loops with Dead Time," *Chemical Engineering Progress*, 53, 1957, pp. 217–219.

Statistical Abstract of the United States, U. S. Department of Commerce, 107th ed., 1987, pp. 660–661.

Statistical Yearbook 1983/1984, Department of International Economics and Social Affairs, (United Nations: New York), 34th ed., pp. 686–687.

Wallace, B. W., "Economic Benefits Offered by Computerized Profile Control of Weight, Moisture, and Caliper," *Tappi*, 64, 1981, pp. 79-83.

Witham, G. S., *Modern Pulp and Paper Making: A Practical Treatise*, (Reinhold Publishing Co.: New York), 2nd Ed., 1942.

FIGURES FOR CHAPTER I

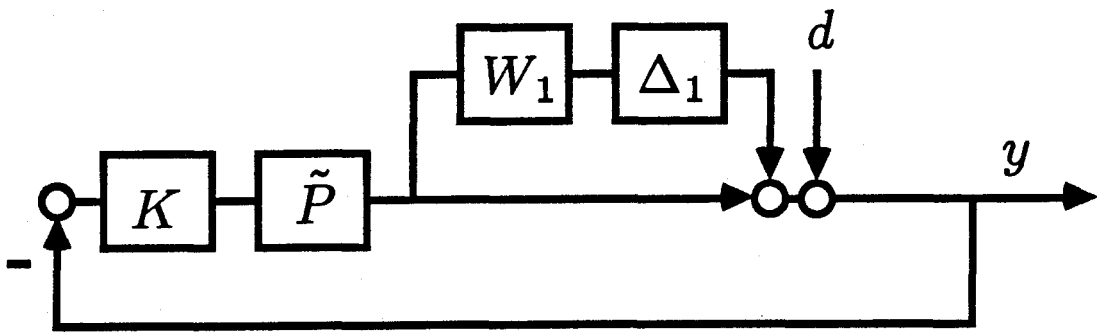

Figure 1: Standard feedback control structure with nominal process $\tilde{P}(s)$, multiplicative uncertainty $W_1(s)\Delta_1$, controller $K(s)$, disturbances $d(s)$ and outputs $y(s)$.

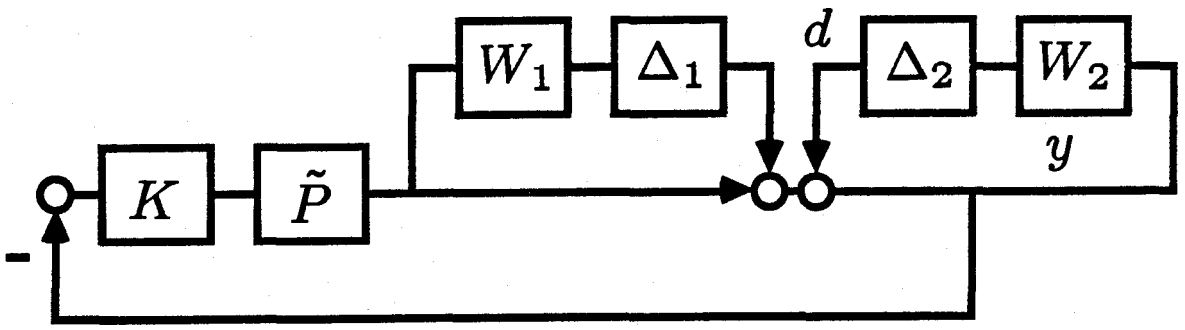

Figure 2: Standard feedback control structure in Figure 1 with performance requirement $W_2(s)\Delta_2$ in the loop between $y(s)$ and $d(s)$.

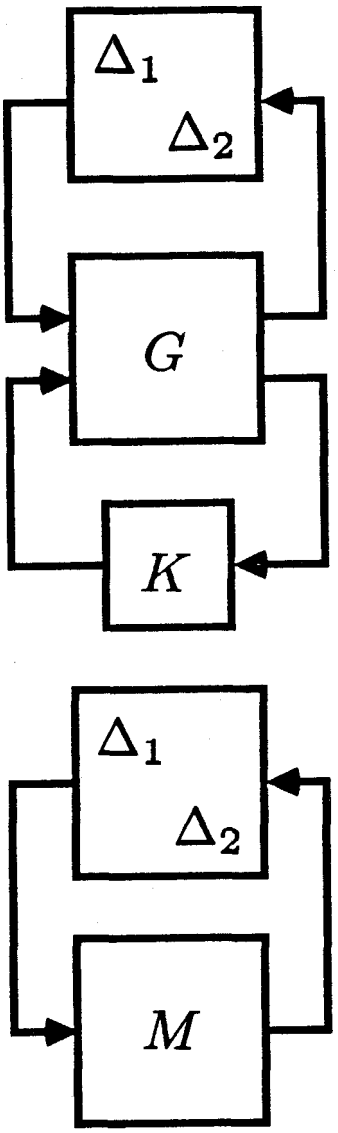

Figure 3: The block structures for μ-synthesis (top) and μ-analysis (bottom) are equivalent to that in Figure 2.

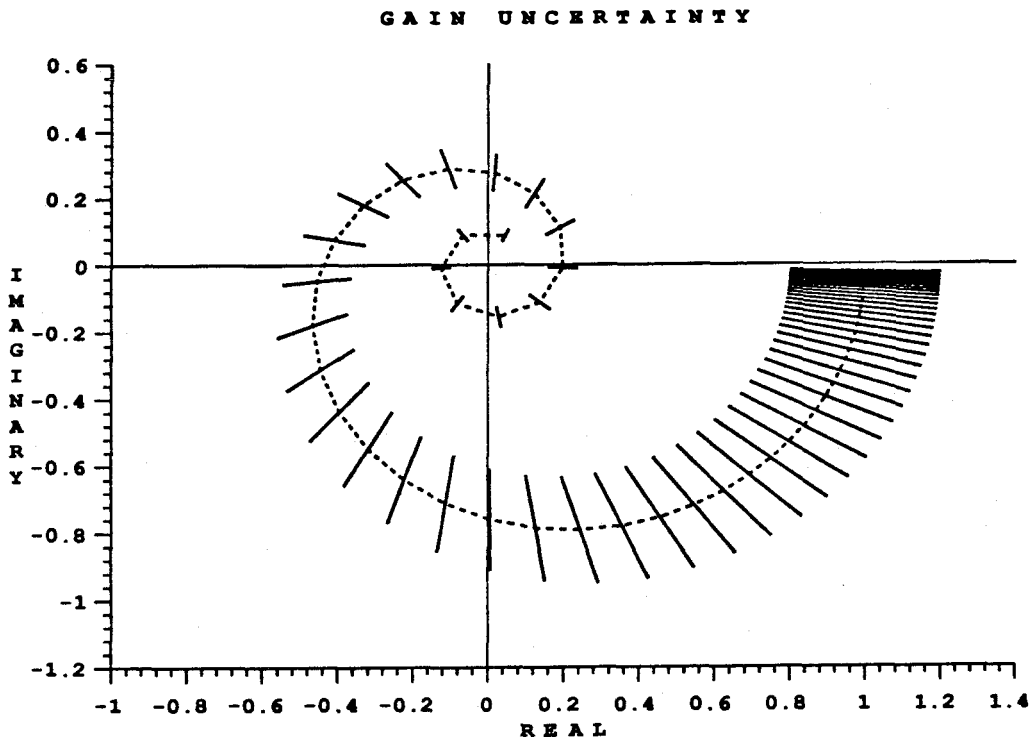

Figure 4: Twenty percent gain uncertainty in $e^{-s}/(s+1)$ for sixty frequencies in the range 0.01 to 10.

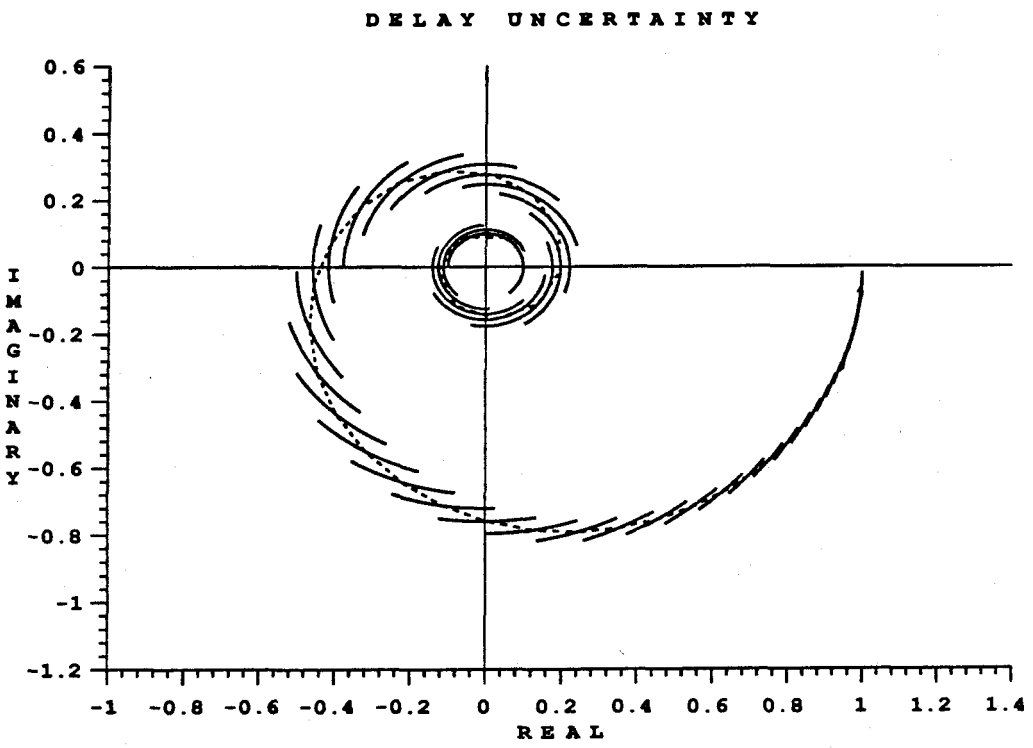

Figure 5: Twenty percent time-delay uncertainty in $e^{-s}/(s+1)$ for sixty frequencies in the range 0.01 to 10.

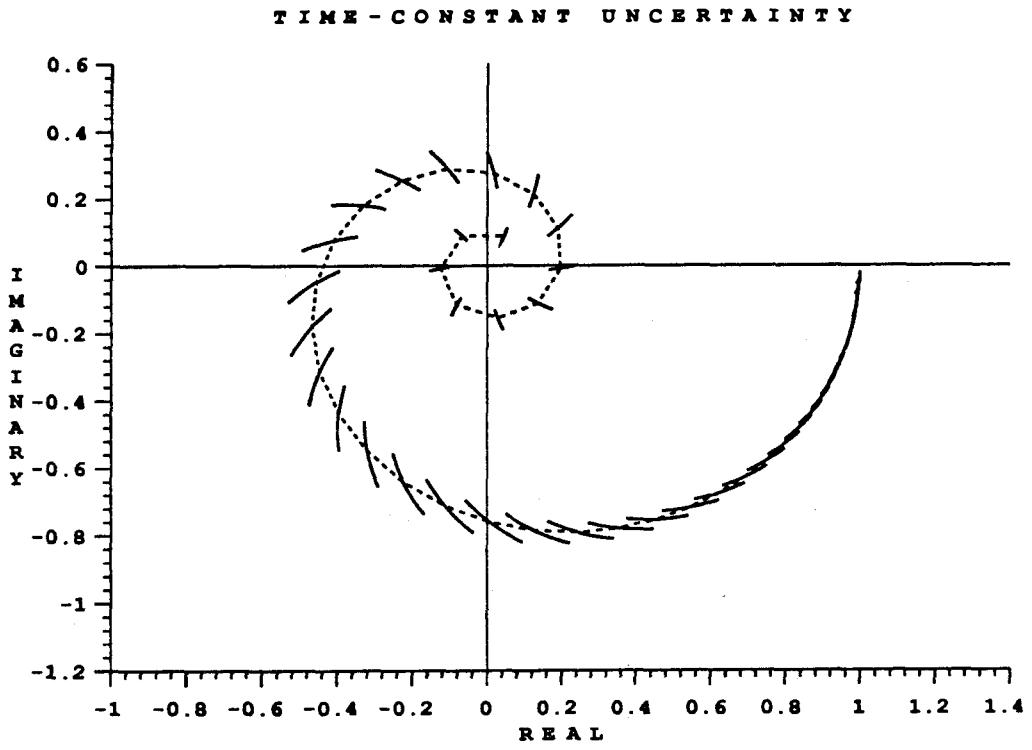

Figure 6: Twenty percent time-constant uncertainty in $e^{-s}/(s+1)$ for sixty frequencies in the range 0.01 to 10.

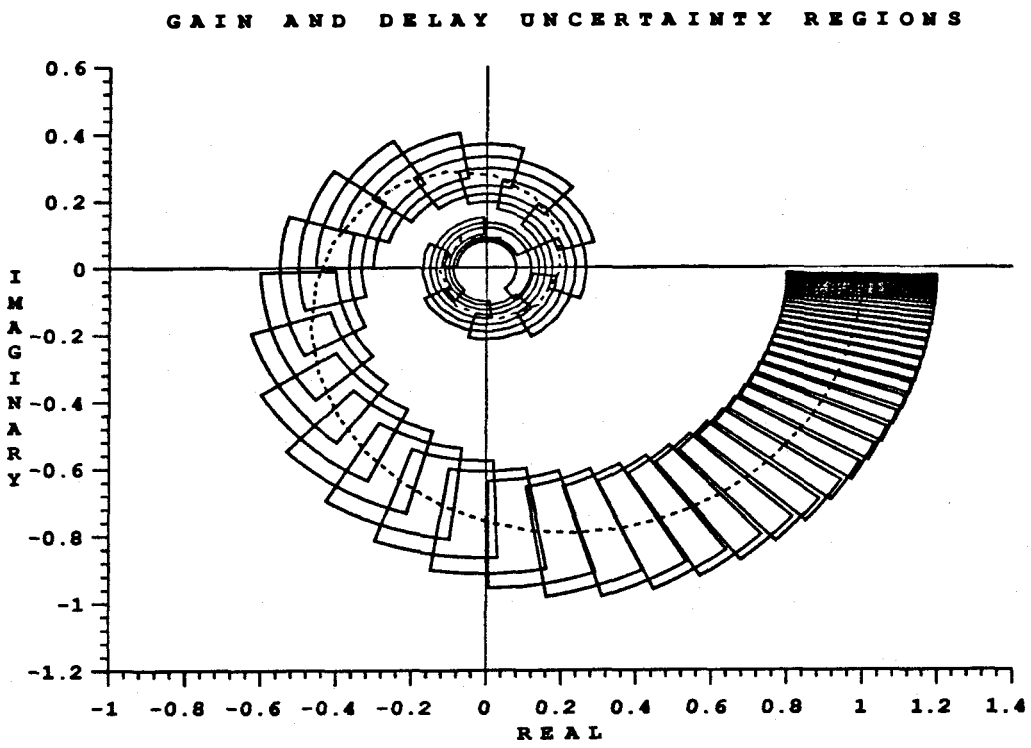

Figure 7: Twenty percent gain and time-delay uncertainty in $e^{-s}/(s+1)$ for sixty frequencies in the range 0.01 to 10.

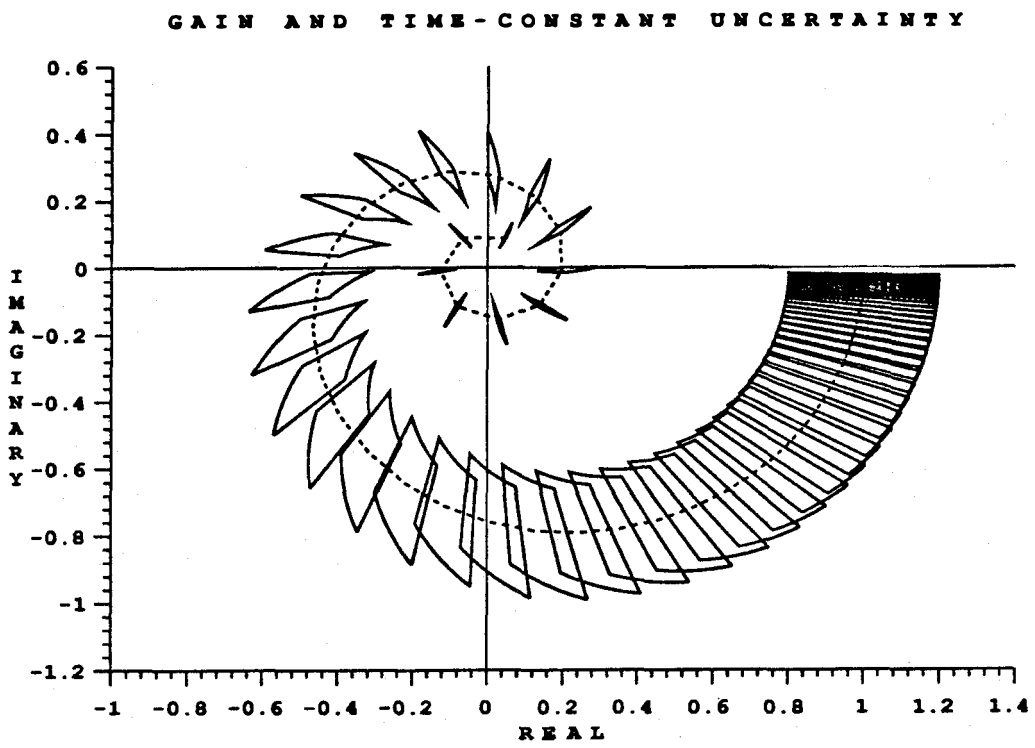

Figure 8: Twenty percent gain and time-constant uncertainty in $e^{-s}/(s+1)$ for sixty frequencies in the range 0.01 to 10.

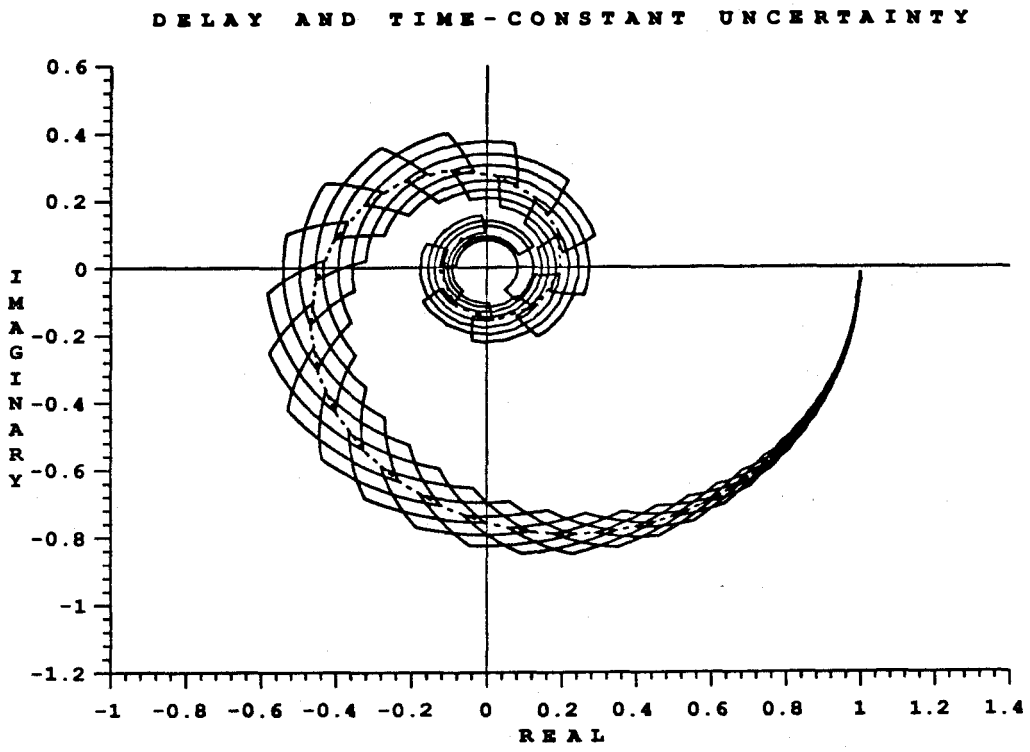

Figure 9: Twenty percent time-delay and time-constant uncertainty in $e^{-s}/(s+1)$ for sixty frequencies in the range 0.01 to 10.

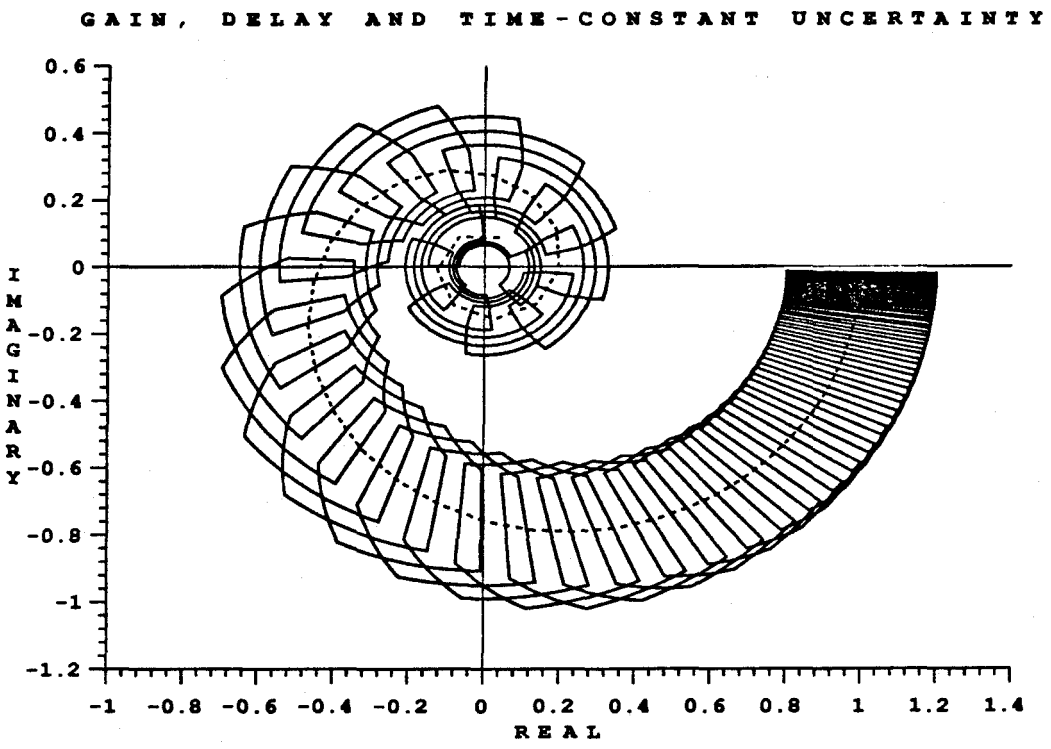

Figure 10: Twenty percent gain, time-delay, and time-constant uncertainty in $e^{-s}/(s+1)$ for sixty frequencies in the range 0.01 to 10.

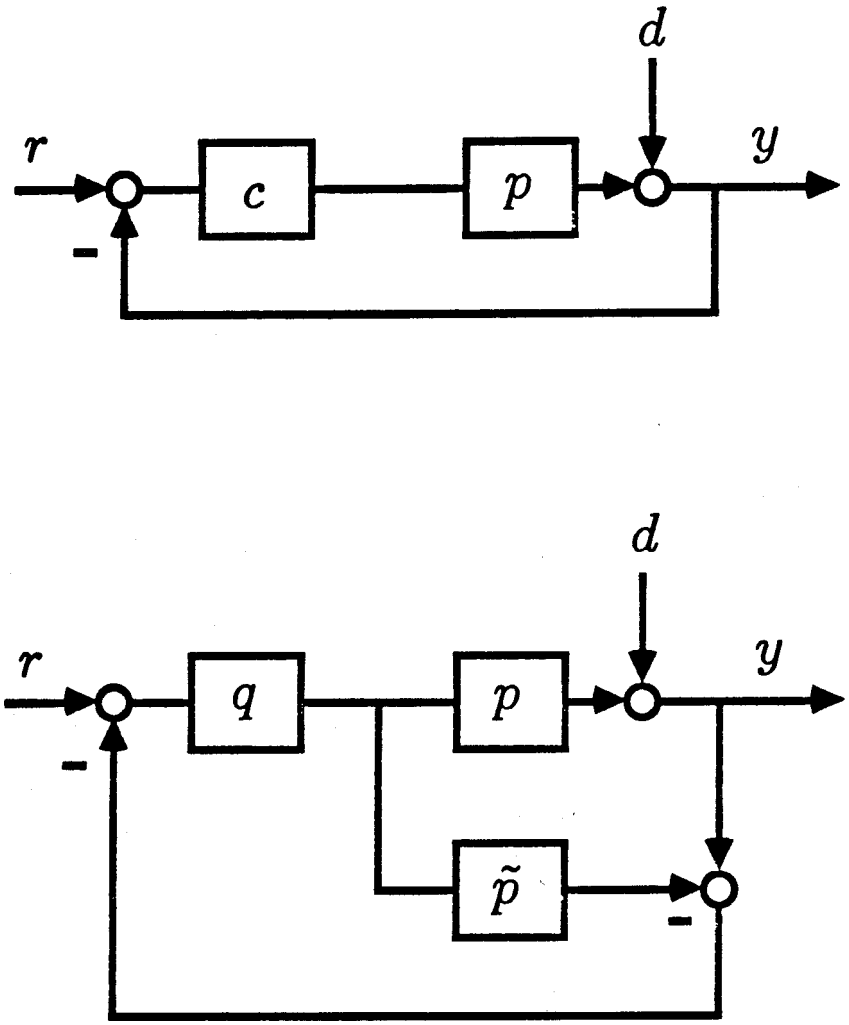

Figure 11: Internal Model Control (IMC) parameterization of standard feedback control system with process $p(s)$, nominal model $\tilde{p}(s)$, controller $q(s)$, set-point $r(s)$, disturbances $d(s)$ and output $y(s)$.

CHAPTER II: GRAPHICAL STABILITY ANALYSIS FOR CONTROL SYSTEMS WITH MODEL PARAMETER UNCERTAINTIES

GRAPHICAL STABILITY ANALYSIS FOR CONTROL SYSTEMS WITH MODEL PARAMETER UNCERTAINTIES

Daniel L. Laughlin and Manfred Morari

Abstract

Regions on the complex plane are employed in a version of the Nyquist stability test for control systems when the system model contains parameter uncertainties. Generally, the uncertain parameters are real and bounded and appear as numerator and denominator coefficients in a rational function of frequency. Through the function, the parameters decribe a set of model points at each frequency. The problem of locating such sets is defined for a model useful in describing the frequency response of physical processes. A new algorithm for locating region boundaries enclosing the set of models is presented. Boundary points connected by straight line segments are determined by the algorithm. The algorithm offers two principal advantages over previously available methods: 1) The region boundaries are guaranteed to enclose the set of models, and 2) the algorithm preserves concave sides on the region enclosing the set.

1. Introduction

An objective of control-system design is to guarantee system stability and performance despite error in modelling the physical system. Error, or uncertainty in

modelling, is anticipated in control-system design by specifying a set of models encompassing the error. If a controller can be designed to deliver stability and performance for the set, it is termed robust with respect to the modelling error. The frequency response of a physical system is conveniently modelled by a rational function of frequency with bounded real numerator and denominator coefficients. As such, the function describes a set of possible frequency response models for the system. The problem of locating regions enclosing this set of models is an integral part of a robust-stability analysis test for single-input, single-output (SISO) control systems.

1.1. Problem Definition

The continuous frequency response of a physical process is conveniently modelled by the set defined in 1. In 1, the terms $x(s)$, $y(s)$, $n_j(s)$, and $d_l(s)$ are assumed to be exact functions, while real numerator coefficients a_j, denominator coefficients b_l, gain k, and time-delay θ are bounded by some minimum and maximum values. Since the real parameters in 1 are inexactly known, π represents a set of process models. Through the uncertain parameters, the set π can capture uncertainty, or error, in models.

$$\pi = \left\{ p(s) \middle| p(s) = x(s) + y(s)\ k\left[\frac{a_j n_j(s) + \ldots + a_1 n_1(s) + a_0 n_0(s)}{b_l d_l(s) + \ldots + b_1 d_1(s) + b_0 d_0(s)}\right] e^{-\theta s} \right\} \qquad (1)$$

$$a_j \in [a_{j_{min}}, a_{j_{max}}],\ b_l \in [b_{l_{min}}, b_{l_{max}}]$$

$$k \in [k_{min}, k_{max}],\ \theta \in [\theta_{min}, \theta_{max}]$$

Uncertain real parameters in 1 are assumed to be uncorrelated; that is, each may take on all values within its specified range irrespective of values taken on by other parameters.

1.1.1 Nomenclature

To avoid confusion, the following nomenclature will be used in this paper:

π – the set of frequency-response models of a physical system as given by 1.

$\tilde{p}(s)$ – one model in the set π with all bounded real parameters fixed at one point in their allowed range.

$\pi(i\omega)$ – the exact region containing the set of frequency response models π evaluated at one frequency $s = i\omega$, including no extra points for all possible combinations of bounded real parameters in 1.

$N(\omega, a_j)$ – the convex hull (the smallest convex polygon containing a set of points) defined by the numerator in 1 with bounded real coefficients a_j.

$N(\omega, a_j, k)$ – the convex hull containing $N(\omega, a_j)$ after multiplication by an uncertain gain k.

$D(\omega, b_l)$ – the convex hull defined by the denominator in 1 with bounded real coefficients b_l.

$D(\omega, b_l, \theta)$ – the boundary containing $D(\omega, b_l)$ after multiplication by the inverse of an uncertain delay $e^{\theta i\omega}$.

$D^{-1}(\omega, b_l, \theta)$ – the inverse of boundary $D(\omega, b_l, \theta)$.

$d_i^{-1}(\omega, b_l, \theta)$ – line segments and triangles defined to enclose the entire boundary $D^{-1}(\omega, b_l, \theta)$.

$\pi_i(\omega, a_j, b_l, \theta, k)$ – convex hulls resulting from the multiplication of $N(\omega, a_j, k)$ by each $d_i^{-1}(\omega, b_l, \theta)$.

1.1.2 Analysis Test for SISO Robust Stability

Graphical performance-analysis techniques in control require that the model $p(s)$ be evaluated at frequencies $s = i\omega$, where $0 \leq \omega \leq \infty$. When all real parameters in 1 are exactly known, $\pi(i\omega)$ is exactly one point on the complex plane at each frequency ω. However, when the real parameters are bounded by minimum and maximum values, $\pi(i\omega)$ is a connected region on the complex plane at each frequency. Use of the regions $\pi(i\omega)$ in SISO control-system robust-stability analysis is described by Analysis Test 1 based on the familiar Nyquist stability test.

Nyquist Stability Test – SISO Nominal Stability: The SISO system in Figure 1 with controller $c(s)$ and nominal model $\tilde{p}(s)$ is stable if and only if the number of clockwise (positive) encirclements of $(-1,0)$, by $\tilde{p}(s)c(s)$ as s encircles (clockwise) the Nyquist contour (the right-half plane excluding singularities on the imaginary axis), is equal to the negative of the number of open-loop unstable poles.

Analysis Test 1 – SISO Robust Stability: The SISO system in Figure 1 with controller $c(s)$ and model $p(s) \in \pi$ is robustly stable if and only if the system is nominally stable for one $\tilde{p}(s) \in \pi$ and regions $\pi(i\omega)c(i\omega)$ exclude $(-1,0)$ for all frequencies ω.

(See Laughlin et al. [1986] for more information about this type of control-system robust-stability analysis). If boundaries resulting from an algorithm are used in Analysis Test 1, it is important that they enclose the set of models $\pi(i\omega)$ in 1 so that the test is not indeterminate. Additionally, they must not contain any extra models in order to avoid unwanted conservativeness in the robust-stability analysis test.

The new algorithm presented in this paper locates a boundary consisting of points connected by straight line segments. In Section 3, proof is given that both

the points and the line segments are on, or outside, the set $\pi(i\omega)$. The boundary located by the algorithm converges on concave boundaries of $\pi(i\omega)$ if they exist in order to avoid conservativeness. Advantages of the new algorithm can be best appreciated by examining methods reported by other authors for locating regions approximating $\pi(i\omega)$.

1.2. Other Methods for Bounding Uncertain Transfer-Functions

1.2.1. Factorial Methods

The use of factorial methods for locating region boundaries is reported by several authors (e.g. Chen [1984], East [1981, 1982], Saeki [1986]). Each of n real parameters defining a set of models through a function as in 1 is chosen to take on d values within its bounds. The function is then evaluated at each of d^n possible combinations of the parameters. The result of these evaluations is a "shotgun" pattern of points on the complex plane. A boundary is then usually defined as the set of line segments connecting points on the outer edge of the "shotgun" pattern. In general, such factorial methods cannot guarantee that $\pi(i\omega)$ will be interior to the located boundary. For example, if $\pi(i\omega)$ is a disk, some of the points in the shotgun pattern may be on the edge of the disk, but segments connecting these points will always be on the interior of $\pi(i\omega)$. The factorial method can take into account correlation between parameters in the function. For example, if $a_j = b_l$ in 1, $p(i\omega)$ can be evaluated at each of the d^n points while maintaining this equality. The factorial method converges on $\pi(i\omega)$ as d is increased, but the number of required computations grows exponentially with n.

1.2.2. Region Arithmetic Methods

The result of a mathematical operation between two regions can be formally defined to contain all possible results of the same operation between points in each region. For example, Bolton [1981] and Henrici [1974] define operations between disks on the complex plane. A set of such operations between regions is a "region

arithmetic." In previous work, authors have used region-arithmetic methods to bound sets of models $\pi(i\omega)$. East [1981] locates convex hulls containing factors in $\pi(i\omega)$ and defines their product as the convex hull about all possible products of vertices on the factor hulls. Although these region-arithmetic methods in general locate a boundary that is guaranteed to contain $\pi(i\omega)$, they are usually excessively conservative; that is, the formally defined boundary resulting from a mathematical operation between two regions may contain many points that are not in $\pi(i\omega)$. Concave edges on $\pi(i\omega)$ are universally approximated by straight lines. Since these region-arithmetic methods are in general one-step operations, no sequence of improving approximations to $\pi(i\omega)$ is possible. Therefore, the region-arithmetic methods as defined do not converge to the actual set $\pi(i\omega)$.

2. Algorithm for Locating Uncertainty Region Boundary

The new algorithm for locating the boundary of $\pi(i\omega)$ utilizes the attractive convergence and containment properties of the factorial and region-arithmetic methods without their deficiencies. The algorithm is closely related to the structure of the function $p(s)$ in 1. When the real parameters are assumed to be uncorrelated, Lemma 1 in Section 3 shows that both the numerator sum involving uncertain a_j and the denominator sum involving uncertain b_l are contained exactly by convex hulls at each frequency $s = i\omega$. The problem of bounding $\pi(i\omega)$ becomes one of bounding $p(i\omega)$ given by

$$p(i\omega) = x(i\omega) + y(i\omega)\ k\left[\frac{N(\omega, a_j)}{D(\omega, b_l)}\right] e^{-\theta i\omega} \qquad (2)$$

$$k \in [k_{min}, k_{max}],\ \theta \in [\theta_{min}, \theta_{max}],$$

where $N(\omega, a_j)$ and $D(\omega, b_l)$ are convex hulls containing the numerator and denominator sums, respectively.

The new algorithm involves eight steps:

1) Locate $N(\omega, a_j)$ and $D(\omega, b_l)$.
2) Multiply $N(\omega, a_j)$ by $k \in [k_{min}, k_{max}]$.
3) Multiply $D(\omega, b_l)$ by $e^{\theta i \omega}$ with $\theta \in [\theta_{min}, \theta_{max}]$.
4) Invert $D(\omega, b_l, \theta)$ analytically.
5) Bound $D^{-1}(\omega, b_l, \theta)$ with segments and triangles $d_i^{-1}(\omega, b_l, \theta)$.
6) Multiply $N(\omega, a_j, k)$ by each $d_i^{-1}(\omega, b_l, \theta)$.
7) Locate the union of products $\pi_i(\omega, a_j, b_l, \theta, k)$.
8) Multiply by $y(i\omega)$ and add $x(i\omega)$.

The eight steps in the algorithm are explained in detail below. Figures 2–9 illustrate the steps in the algorithm used to locate the boundary of the set $\pi(i\omega)$ containing models $p(s)$ given by

$$p(s) = \frac{1}{2} + \frac{1}{4s} k \left[\frac{a_1 s + a_0}{b_2 s^2 e^{-\frac{\pi}{4} s} + b_1 s + b_0} \right] e^{-\theta s} \tag{3}$$

$$a_1 \in [1, 2], \; a_0 \in [-2, -1]$$

$$b_2 \in [\sqrt{2}, 2\sqrt{2}], \; b_1 = -1, \; b_0 \in [-1.5, -0.5]$$

$$k \in [1, 2], \; \theta \in [0, \frac{\pi}{2}], \; s = i,$$

evaluated at $s = i$ (frequency ω equal to one radian per second). Efficient routines for performing the required geometrical computations are cited.

2.1. Locate $N(\omega, a_j)$ and $D(\omega, b_l)$

The first step in the algorithm is to locate convex polygons $N(\omega, a_j)$ and $D(\omega, b_l)$ that exactly contain numerator and denominator sums in 1. The numerator sum involving uncertain coefficients a_j is given in Equation 4. Since the a_j in Equation 4 are bounded real numbers and the $n_j(i\omega)$ are fixed complex numbers, each term in the sum represents variation along a segment of a ray extending

from the origin on the complex plane. The assumption that the real coefficients are uncorrelated allows each term in the sum to take on all its values independent of the other terms. Lemma 1 in Section 3 states that the sum of j nonparallel line segments is exactly contained by a convex $2j$-gon with two sides parrallel to each line segment – no additional points are contained. Vertices of the polygon $N(\omega, a_j)$ containing the sum result from adding terms with extreme values of the a_j. The value of the sum varies along sides of $N(\omega, a_j)$ parallel to a line segment, as the uncertain a_j corresponding to that segment varies between its extreme values.

$$N(\omega, a_j) = a_j n_j(i\omega) + ... + a_1 n_1(i\omega) + a_0 n_0(i\omega) \tag{4}$$

$$a_j \in [a_{j_{min}}, a_{j_{max}}]$$

The convex polygons $N(\omega, a_j)$ and $D(\omega, b_l)$ are efficiently located by using a factorial method. The numerator and denominator sums are evaluated for all possible combinations of extreme coefficient values; 2^j sums are calculated for the numerator and 2^l sums are calculated for the denominator. Note that this is many fewer calculations than the number required to approximate the whole function $p(i\omega)$ by a factorial method. The computational geometry literature is replete with algorithms for locating the smallest polygon, or convex hull, about a set of points. The fastest of these algorithms calculates the convex hull in order $n \times log(n)$ time where n is the number of points in the set [Kurozumi and Davis, 1982], [Preparata and Hong, 1977]. Such an algorithm is used to find the convex hulls $N(\omega, a_j)$ and $D(\omega, b_l)$ about the 2^j numerator sums and 2^l denominator sums, respectively. Regions $N(\omega, a_j)$ and $D(\omega, b_l)$ are located in Figure 2 for $p(i\omega)$ in Equation 3.

2.2. *Multiply $N(\omega, a_j)$ by $k \in [k_{min}, k_{max}]$*

The effect of multiplying a convex region $N(\omega, a_j)$ by an uncertain real gain k is to stretch it along rays extending from the origin on the complex plane. This effect is shown in Figure 3, where $N(\omega, a_j)$ corresponding to Equation 3 is multiplied by

$k \in [1,2]$. Possible product regions $N(\omega, a_j, k)$ resulting from such a multiplication are easy to describe. If $N(\omega, a_j)$ contains the origin, the region containing the product is just $k_{max}N(\omega, a_j)$. If $N(\omega, a_j)$ does not contain the origin, the boundary containing the product is composed of segments on $k_{min}N(\omega, a_j)$ closest to the origin, segments on $k_{max}N(\omega, a_j)$ farthest from the origin, and segments on rays extending from the origin connecting corresponding points on $k_{min}N(\omega, a_j)$ and $k_{max}N(\omega, a_j)$ having minimum and maximum phase. The boundary $N(\omega, a_j, k)$ containing the product is convex since $N(\omega, a_j)$ is convex.

A convenient way to compute the region $N(\omega, a_j, k)$ containing the product of $N(\omega, a_j)$ and an uncertain gain k is to multiply vertices of the $N(\omega, a_j)$ by both k_{min} and k_{max} and then locate the convex hull about the resulting set of points. In general, beginning this procedure with a convex $2j$-gon $N(\omega, a_j)$ excluding the origin results in a convex $(2j+2)$-gon containing the numerator multiplied by the uncertain gain. A $(2j+1)$-gon or a $2j$-gon results when the numerator hull has one or two sides on rays extending from the origin, respectively.

2.3. *Multiply $D(\omega, b_l)$ by $e^{\theta i\omega}$ with $\theta \in [\theta_{min}, \theta_{max}]$*

Multiplying the ratio $N(\omega, a_j)/D(\omega, b_l)$ in Equation 2 by $e^{-\theta i\omega}$ is clearly equivalent to multiplying $D(\omega, b_l)$ by $e^{\theta i\omega}$. In this algorithm, $D(\omega, b_l)$ is multiplied by $e^{\theta i\omega}$ to preserve the convexity of the numerator region $N(\omega, a_j, k)$ – this convexity is exploited in step 6. The effect of multiplying $D(\omega, b_l)$ by an uncertain $e^{\theta i\omega}$ is to stretch it along concentric circles centered at the origin. This effect is shown in Figure 4, where $D(\omega, b_l)$ corresponding to Equation 3 is multiplied by $e^{\theta i\omega}$ with $\theta \in [0, \pi/2]$. Possible product regions $D(\omega, b_l, \theta)$ are easily described. If $|\theta_{max} - \theta_{min}| \geq 2\pi/\omega$, the region $D(\omega, b_l, \theta)$ will be an annulus or circle centered at the origin, depending on whether or not the origin is contained in $D(\omega, b_l)$. If $|\theta_{max} - \theta_{min}| < 2\pi/\omega$, the product region $D(\omega, b_l, \theta)$ will be be composed of sections of $D(\omega, b_l)e^{\theta_{min}i\omega}$, sections of $D(\omega, b_l)e^{\theta_{max}i\omega}$, and arcs of circles centered at the origin. The arcs of

circles centered at the origin connect points on $D(\omega, b_l)e^{\theta_{min}i\omega}$ and $D(\omega, b_l)e^{\theta_{max}i\omega}$ at relative minimum and relative maximum distances from the origin as shown in Figure 4.

2.4. *Invert $D(\omega, b_l, \theta)$ Analytically*

At this point the denominator region boundary $D(\omega, b_l, \theta)$ consists of line segments and arcs of circles centered at the origin. Line segments and arcs are conveniently parameterized in terms of the real number t through the linear fractional transformation 5 with complex coefficients α, β, and γ.

$$f(t) = \frac{\alpha t + \beta}{\gamma t + 1} \tag{5}$$
$$t \in [t_{min}, t_{max}],\ \alpha - \beta\gamma \neq 0$$

When $\gamma = 0$ in Equation 5, $f(t)$ is a line segment – otherwise $f(t)$ is an arc of a circle. Since $1/f(t)$ is also a linear fractional transformation, the inverses of line segments and arcs on the complex plane are also line segments and arcs. Specifically, segments on lines containing the origin and arcs of circles containing the origin ($f(t) = 0$ for some t: $-\infty \leq t \leq \infty$) invert to segments on lines containing the origin. All other line segments and arcs invert to arcs. Therefore, the inverse of the denominator region boundary $D^{-1}(\omega, b_l, \theta)$ will consist of line segments and arcs. Note that this means that $D^{-1}(\omega, b_l, \theta)$ will in general be nonconvex. For example, see Figure 5 showing the inverse of $D(\omega, b_j, \theta)$ in Figure 4. Since recording of circle centers, endpoints and orientation of individual arcs and line segments is easily done by computer, $D(\omega, b_l, \theta)$ can be inverted analytically. If the origin is outside $D(\omega, b_l, \theta)$, the interior of $D(\omega, b_l, \theta)$ maps to the interior of $D^{-1}(\omega, b_l, \theta)$. If the origin is inside $D(\omega, b_l, \theta)$, the interior of $D(\omega, b_l, \theta)$ maps to the exterior of $D^{-1}(\omega, b_l, \theta)$ – this case, however, has limited application in control-system analysis, since it means that $p(i\omega)$ is unbounded at this frequency.

2.5. Bound $D^{-1}(\omega, b_l, \theta)$ with Segments and Triangles $d_i^{-1}(\omega, b_l, \theta)$

Until now, no approximation has been made to located either $N(\omega, a_j, k)$ or $D^{-1}(\omega, b_l, \theta)$. The uncertain numerator sum multiplied by the uncertain gain is exactly bounded by convex $N(\omega, a_j, k)$ (see Lemma 1 in Section 3). The region containing the inverse of $D(\omega, b_j, \theta)$ is exactly bounded by line segments and arcs on $D^{-1}(\omega, b_j, \theta)$. The problem that remains is to locate the boundary of the product of $N(\omega, a_j, k)$ multiplied by $D^{-1}(\omega, b_l, \theta)$. The product region will be contained by a boundary that results from multiplying points on the two factor-region boundaries (see Lemma 2 in Section 3). Use of a factorial method based on points to locate the product boundary – multiplying a large number of points on $N(\omega, a_j, k)$ by a large number of points on $D^{-1}(\omega, b_l, \theta)$ – would not guarantee containment of the actual product region. Bounding $D^{-1}(\omega, b_l, \theta)$ by a single convex hull and locating the product boundary by region arithmetic introduce unwanted conservativeness and fail to locate concave product boundaries where they exist. The region-arithmetic method will, however, locate a boundary that is guaranteed to contain all possible products of $N(\omega, a_j, k)$ multiplied by $D^{-1}(\omega, b_l, \theta)$.

The solution to the problem of locating the product region is to use a combination of factorial and region-arithmetic methods. Curved boundaries of inverted denominator region $D^{-1}(\omega, b_l, \theta)$ are approximated by many convex line segments and triangles $d_i^{-1}(\omega, b_l, \theta)$. The $d_i^{-1}(\omega, b_l, \theta)$ approximating $D^{-1}(\omega, b_l, \theta)$ in Figure 5 are shown in Figure 6. Each line segment on $D^{-1}(\omega, b_l, \theta)$ is divided into 2^{r+1} smaller line segments, where r is an integer resolution parameter. Arcs of more than π radians are bisected into two smaller arcs. Each arc is then approximated by 2^r equal-sized, smallest triangles containing the arc. One side of each triangle is inside the arc. The other two sides of each triangle are outside the arc and tangent to the arc at the two vertices on the arc. Defined in this way, the triangles are the 2^r convex polygons of least area containing the arc. As resolution parameter r increases, the approximation of $D^{-1}(\omega, b_l, \theta)$ becomes less conservative – fewer points

not in $D^{-1}(\omega, b_l, \theta)$ are contained. The product of each $d_i^{-1}(\omega, b_l, \theta)$ multiplied by $N(\omega, a_j, k)$ is located by multiplying convex hulls in step 6. The union of these product regions will contain the product of $D^{-1}(\omega, b_l, \theta)$ multiplied by $N(\omega, a_j, k)$ by Lemmas 2 and 3 in Section 3.

2.6. Multiply $N(\omega, a_j, k)$ by Each $d_i^{-1}(\omega, b_l, \theta)$

Every line segment and triangle $d_i^{-1}(\omega, b_l, \theta)$ used to approximate $D^{-1}(\omega, b_l, \theta)$ must now be multiplied by $N(\omega, a_j, k)$. A set of product points is generated by multiplying all vertices of $N(\omega, a_j, k)$ by all vertices or endpoints of one $d_i^{-1}(\omega, b_l, \theta)$. The convex hull $\pi_i(\omega, a_j, b_l, \theta, k)$ about this set of points is then located. The convex $\pi_i(\omega, a_j, b_l, \theta, k)$ is guaranteed to contain all possible products resulting from multiplying individual points on the two factor convex hulls (see Lemma 3 in Section 3). It may, however, contain additional points that are not in the actual product region. This step in the algorithm can therefore introduce conservativeness into the result by locating a boundary outside $\pi(i\omega)$. This conservativeness is related to the resolution parameter r. As parameter r, increases the size of line segments and triangles $d_i^{-1}(\omega, b_l, \theta)$ used to approximate $D^{-1}(\omega, b_l, \theta)$ decreases. The actual product region that results by multiplying such a small convex hull by $N(\omega, a_j, k)$ converges to $N(\omega, a_j, k)$ multiplied by a single complex number – a convex region. Approximating the products $\pi_i(\omega, a_j, b_l, \theta, k)$ of $N(\omega, a_j, k)$ multiplied by very small $d_i^{-1}(\omega, b_l, \theta)$ by convex hulls introduces relatively little conservativeness. The product hulls $\pi_i(\omega, a_j, b_l, \theta, k)$ of $N(\omega, a_j, k)$ in Figure 3 multiplied by each of the $d_i^{-1}(\omega, b_l, \theta)$ in Figure 6 are illustrated in Figure 7 for resolution parameter $r = 1$.

2.7. Locate the Union of Products $\pi_i(\omega, a_j, b_l, \theta, k)$

Each $\pi_i(\omega, a_j, b_l, \theta, k)$ located in step 6 contains all points that result when a piece of $D^{-1}(\omega, b_l, \theta)$ is multiplied by $N(\omega, a_j, k)$. The union of all $\pi_i(\omega, a_j, b_l, \theta, k)$ will therefore contain (by Lemma 3) <u>all</u> points that result from multiplying the

whole boundary $D^{-1}(\omega, b_l, \theta)$ by $N(\omega, a_j, k)$. What remains is to locate the outer boundary of the union of all $\pi_i(\omega, a_j, b_l, \theta, k)$. When $D(\omega, b_l, \theta)$ does not contain the origin, this boundary will lie wholely on or outside the region corresponding to the uncertain part of $p(i\omega)$ in 1 (by Theorem 1 in Section 3.1). When $D(\omega, b_l, \theta)$ does contain the origin, this boundary will lie wholely on or outside the region of the complex plane not given by the region corresponding to the uncertain part of the function in 1. Unions of regions $\pi_i(\omega, a_j, b_l, \theta, k)$ for the example function 3 are shown in Figure 8 for resolution parameters r equal to 1, 2, and 3. Note in Figure 8 that the algorithm converges on $\pi(i\omega)$ from the outside in, as parameter r increases.

Efficient algorithms for finding intersections between geometric figures can be found in the literature (see for example Chin and Wang [1983], Edelsbrunner et al. [1982], Nievergelt and Preparata [1982], or Sedgewick [1983]). Typically, figures are decomposed into segments whose intersections are searched. The union of many overlapping geometric figures can be found as follows: 1) locate an extreme point of the union (for example the point farthest from the origin); 2) decompose the figures into vectors employing uniform clockwise or counter-clockwise direction; 3) trace the outer boundary one vector at a time while searching for intersecting vectors, and 4) select the correct outer boundary vector based on the vector cross product when intersections are encountered.

2.8. Multiply by $y(i\omega)$ and Add $x(i\omega)$

The terms $y(s)$ and $x(s)$ in 1 are known exactly, so they are each equal to a single complex number at frequency $s = i\omega$. Multiplication of the uncertainty region by $y(i\omega)$ results in a simple polygon similar to the original one but translated and/or rotated on the complex plane. Addition of $x(i\omega)$ to the uncertainty region simply translates it on the complex plane. Therefore, multiplying each boundary point of the union of $\pi_i(\omega, a_j, b_l, \theta, k)$ by $y(i\omega)$ and adding $x(i\omega)$ are sufficient to locate the final region boundary containing $\pi(i\omega)$. Figure 9 shows the final region boundary

for the example in Equation 3. Note that the new algorithm preserves concave sides on $\pi(i\omega)$.

3. Containment, Convergence and Conservativeness

Proof of important containment and convergence properties of the algorithm for locating the region boundary containing $\pi(i\omega)$ is given in this section. Theorem 1 (containment) and Theorem 2 (convergence) are based on the following three lemmas:

Lemma 1: The sum of n line segments on the complex plane is contained exactly within the convex hull about the set of 2^n points that result from adding all combinations of endpoints of the segments.

Proof: The equation of a line segment on the complex plane can be written as $a_i = a_{i\ min} + t_i(a_{i\ max} - a_{i\ min})$ where $0 \leq t_i \leq 1$ and endpoints $a_{i\ min}$ and $a_{i\ max}$ are nearest to and farthest from the origin, respectively. The sum of n such line segments is therefore

$$S = \sum_{i=1}^{n} a_i = \sum_{i=1}^{n} a_{i\ min} + \sum_{i=1}^{n} t_i(a_{i\ max} - a_{i\ min}) \qquad (6)$$
$$0 \leq t_i \leq 1\ \forall i = 1, n.$$

That S is convex will now be proven. Consider arbitrary points Q and R in S:

$$Q = \sum_{i=1}^{n} a_{i\ min} + \sum_{i=1}^{n} t_i^Q(a_{i\ max} - a_{i\ min})$$
$$R = \sum_{i=1}^{n} a_{i\ min} + \sum_{i=1}^{n} t_i^R(a_{i\ max} - a_{i\ min})$$
$$0 \leq t_i^Q \leq 1\ ;\ 0 \leq t_i^R \leq 1\ \forall i = 1, n.$$

The line segment L connecting Q and R can be parameterized by T as follows:

$$L(T) = Q + T(R - Q) = \sum_{i-1}^{n} a_{i\ min} + \sum_{i=1}^{n} (t_i^Q + T(t_i^R - t_i^Q))(a_{i\ max} - a_{i\ min})$$

$$0 \leq T \leq 1.$$

Since $0 \leq (t_i^Q + T(t_i^R - t_i^Q)) \leq 1$ for all i, line segment $L(T)$ is entirely in S. Therefore, S is convex. In fact, Equation 6 is that of a parallelogram on the complex plane with at most $2n$ edges. Two sides on the parallelogram are parallel to each segment a_i. The vertices of S are among the set of points corresponding to values of t_i equal to one or zero. These points result from adding endpoints of the n line segments.

QED.

Lemma 2: The boundary of the product of two regions on the complex plane is composed of products of boundary points on each region.

Proof: (After that of property 4 in Chen [1984]) Define P as the set of all products of n multiplied by d, where n is a complex number in region N and d is a complex number in region D. Denote the boundary P by $\hat{P}$. Assume that $n_i \times d \in \hat{P}$, where n_i is an interior point in N. Then there exists a disk around n_i of radius ϵ in N. But this means that there is a disk of radius $|d|\epsilon$ around $n_i \times d$ in P, so $n_i \times d$ cannot be a boundary point of P. The same contradiction is obtained by assuming that $n \times d_i \in \hat{P}$, where d_i is an interior point in D. Therefore, the boundary of the product region results from multiplication between boundary points of the two factor regions.

QED.

Lemma 3: The smallest convex polygon containing the product of two convex regions on the complex plane is the convex hull about all products of vertices of the two factor regions.

Proof: (After that of Theorem VI.6 in Jordan [1985]) First, it is necessary to prove that the product of two line segments is contained by the convex hull about the four products of segment endpoints. The convex hull P about four points a_1b_1, a_1b_2,

a_2b_1, and a_2b_2 contains all line segments connecting these points by definition of convexity. Now consider two line segments parameterized as follows:

$$a = a_1 + t_a(a_2 - a_1) \; ; \; 0 \leq t_a \leq 1$$

$$b = b_1 + t_b(b_2 - b_1) \; ; \; 0 \leq t_b \leq 1.$$

The line segment that results by multiplying a by any point $b(t_b)$ on b is given by:

$$ab(t_b) = a_1b(t_b) + t_a\big(a_2b(t_b) - a_1b(t_b)\big)$$

$$0 \leq t_a \leq 1.$$

But $a_1b(t_b)$ is just a line segment connecting a_1b_1 and a_1b_2 in P, and $a_2b(t_b)$ is just a line segment connecting a_2b_1 and a_2b_2 in P. The line segment $ab(t_b)$ connects two points in P and is itself contained in P because P is convex. Therefore, the product of two line segments is contained within the convex hull about the four products of segment endpoints.

Since boundaries of two factor convex hulls are composed of line segments, the product of the two convex boundaries is contained within the union of convex hulls containing all combinations of segment products. The product region of the two convex hulls is bounded by this union of convex hulls by Lemma 2. Since all vertices of hulls containing the segment products are themselves products of vertices of the two factor hulls, the convex hull about all products of vertices of the two convex factor regions is the smallest convex polygon containing the product region.

QED.

3.1. Theorem 1 – The Algorithm Boundary Contains $\pi(i\omega)$

Now Lemmas 1–3 can be applied to prove that the boundary resulting from the algorithm contains $\pi(i\omega)$.

Theorem 1: All points on the boundary located by the algorithm lie on or outside the actual set $\pi(i\omega)$ in 1.

Proof:

a) The exact boundary $N(\omega, a_j)$ of the uncertain numerator sum in 1 is found – in step 1 by Lemma 1.

b) The exact boundary $D(\omega, b_l)$ of the uncertain denominator sum in 1 is found – in step 1 by Lemma 1.

c) The exact boundary $N(\omega, a_j, k)$ of $N(\omega, a_j)$ multiplied by the uncertain gain k is found – in step 2.

d) The exact boundary $D(\omega, b_l, \theta)$ containing $D(\omega, b_l)$ multiplied by the uncertain $e^{\theta i\omega}$ is found – in step 3.

e) The region $D(\omega, b_l, \theta)$ is inverted analytically – in step 4.

f) One line segment or triangle $d_i^{-1}(\omega, b_l, \theta)$ contains one portion of $D^{-1}(\omega, b_l, \theta)$. The union of the $d_i^{-1}(\omega, b_l, \theta)$ contains the entire boundary $D^{-1}(\omega, b_l, \theta)$ – by definition in step 5.

g) The convex hull $\pi_i(\omega, a_j, b_l, \theta, k)$ about the product of vertices of one $d_i^{-1}(\omega, b_l, \theta)$, multiplied by the vertices of $N(\omega, a_j, k)$, contains all products of the enclosed portion of $D^{-1}(\omega, b_l, \theta)$ multiplied by $N(\omega, a_j, k)$ – by f) and Lemma 3.

h) The union of convex hulls $\pi_i(\omega, a_j, b_l, \theta, k)$ contains the entire product region of $N(\omega, a_j, k)$ multiplied by $D^{-1}(\omega, b_l, \theta)$ – by f), g), and Lemma 2.

Since multiplication of the union containing $N(\omega, a_j, k)$ multiplied by $D^{-1}(\omega, b_l, \theta)$ by $y(i\omega)$ and addition with $x(i\omega)$ simply translates and rotates it on the complex plane, the entire set $\pi(i\omega)$ in 1 is contained within the boundary located by the algorithm.

QED.

3.2. Theorem 2 – The Algorithm Boundary Converges to $\pi(i\omega)$

It is important to establish that the algorithm converges to the actual set $\pi(i\omega)$ in 1 as the resolution parameter r increases to enable nonconservative application of the SISO robust-performance test. Theorem 2 and Lemma 2 establish that this is true.

Theorem 2: All points on the boundary located by the algorithm with r_1 lie on or outside the boundary located with r_2 if $r_1 < r_2$.

Proof: Consider one line segment or triangle $d_q^{-1}(\omega, b_l, \theta, r_1)$ containing a portion of $D^{-1}(\omega, b_l, \theta)$ for an arbitrary r_1. The product of $d_q^{-1}(\omega, b_l, \theta, r_1)$ multiplied by $N(\omega, a_j, k)$ is guaranteed to be contained in a convex polygon $\pi_q(\omega, a_j, b_l, \theta, k, r_1)$ by Lemma 3. Now consider a resolution parameter $r_2 = r_1 + 1$. Following step 5 of the algorithm leads to two smaller line segments or triangles $d_s^{-1}(\omega, b_l, \theta, r_2)$ and $d_t^{-1}(\omega, b_l, \theta, r_2)$ in $d_q^{-1}(\omega, b_l, \theta, r_1)$, containing the same portion of $D^{-1}(\omega, b_l, \theta)$. Multiplication of the two smaller line segments or triangles by $N(\omega, a_j, k)$ results in products $\pi_s(\omega, a_j, b_l, \theta, k, r_2)$ and $\pi_t(\omega, a_j, b_l, \theta, k, r_2)$ in $\pi_q(\omega, a_j, b_l, \theta, k, r_1)$ by Lemma 3. Therefore, the union of all such products with $r_2 = r_1 + 1$ will be contained by the union of all such products with r_1. The same result holds for arbitrary $r_2 > r_1$ by induction.

QED.

In the limit of $r_2 = \infty$, the $d_i^{-1}(\omega, a_j, b_l, \theta, k)$ defined in step 5 of the algorithm are points along the boundary $D^{-1}(\omega, b_l, \theta)$. If each point on $D^{-1}(\omega, b_l, \theta)$ could be multiplied by $N(\omega, a_j, k)$ and the union of infinitely many product points located, Lemma 2 assures us that the boundary of this union would exactly contain the product region. In practice, the algorithm is executed for a few values of the resolution parameter r and the resulting region boundaries are compared. Experience has indicated that boundaries resulting from small values of r (e.g., 3 and 4) are practically indistinguishable from one another and closely approximate curved boundaries on $\pi(i\omega)$.

Conservativeness introduced by the algorithm can be attributed to two factors: 1) additional points included in the products $\pi_i(\omega, a_j, b_l, \theta, k)$, when large line segments or triangles $d_i^{-1}(\omega, b_l, \theta)$ are multiplied by $N(\omega, a_j, k)$, and 2) additional points included in triangles $d_i^{-1}(\omega, b_l, \theta)$ containing portions of arcs on $D^{-1}(\omega, b_l, \theta)$. Specifying a larger resolution parameter r decreases the conservativeness introduced by both of these factors at the expense of additional computation.

4. *Discussion and Conclusions*

It has been demonstrated that the proposed algorithm locates region boundaries containing the set $\pi(i\omega)$ in 1. The set of models in 1, though quite general, does not encompass all frequency response models useful for describing physical processes. For example, the second-order system given by Equation 7 does not fit the form of 1, if uncorrelated variations of parameters β and γ are allowed.

$$g(s) = k\left[\frac{s+\alpha}{(s+\beta)(s+\gamma)}\right]e^{-\theta s} \tag{7}$$

$$\alpha \in [\alpha_{min}, \alpha_{max}],\ \beta \in [\beta_{min}, \beta_{max}],\ \gamma \in [\gamma_{min}, \gamma_{max}]$$

$$k \in [k_{min}, k_{max}],\ \theta \in [\theta_{min}, \theta_{max}]$$

Multiplying the denominator terms in Equation 6 results in $s^2 + (\beta + \gamma)s + \beta\gamma$. Interpreted in the form of 1, coefficients $b_0 = \beta\gamma$ and $b_1 = \beta + \gamma$ would be correlated.

The proposed algorithm can be extended, at the expense of additional computation, to locate region boundaries containing functions of the form given in Equation 7. If Equation 7 is considered to be the product of two functions of the form given in 1, the product region boundary can be located as follows: 1) Locate each factor region boundary using the proposed algorithm; 2) locate convex hulls containing products of all combinations of line segments on the two factor-region boundaries, and 3) locate the boundary of the union of the resulting array of convex

hulls. Since all segments of the factor boundaries are on or outside the actual region containing factor functions, the product boundary located in this way is on or outside the actual region containing the product. Clearly, the number of required computations becomes large as the number of segments on each factor boundary increases. It is worth mentioning, however, that the computational effort required is no greater than that required by the factorial methods discussed above.

Robust stability of discrete systems can also be evaluated through application of the proposed algorithm. For discrete systems, a set of pulse-transfer function models $h(z)$ would replace the set of Laplace transfer-functions $p(s)$ in 1; exact functions $x(z)$, $y(z)$, $n_j(z)$, and $d_l(z)$ would appear in 1. In the discrete version of the the Nyquist Stability Test, encirclements of $(-1,0)$ by $\tilde{h}(z)c(z)$, as z encircles the discrete Nyquist contour (the unit disk excluding positive real axis and singularities on the unit circle), are determined. The nominal closed-loop system is stable if and only if the number of encirclements is equal to the negative of the number of open-loop unstable poles. Since functions $x(z)$, $y(z)$, $n_j(z)$, and $d_l(z)$ evaluated at $z = e^{i\omega}$ are complex numbers, the proposed algorithm can be applied to locate region boundaries for the sets $h(z)c(z)$ at points z on the discrete Nyquist contour. If these regions exclude $(-1,0)$ and the system is nominally stable, then the system is robustly stable despite parameter uncertainties in $h(z)$.

The proposed algorithm enables calculation of boundaries that are guaranteed to enclose the set $\pi(i\omega)$ in 1. The algorithm boundaries converge on the actual sets $\pi(i\omega)$ from the outside in, as additional computational effort is expended. The boundaries resulting from the algorithm preserve concave sides of the actual set, thereby minimizing the enclosed area. These properties make the algorithm a valuable tool for meeting sufficient conditions of the SISO control-system robust-performance test without introducing excessive conservativeness.

5. *Appendix – Implementation of Algorithm in Program REGIONS*

The new algorithm for bounding sets π of models from uncertain model parameters has been incorporated into program REGIONS, a computer graphics tool for control-system design. Versions of program REGIONS have been written for both VAX and IBM-PC. The particular implementation of the algorithm in REGIONS is explained in this appendix when not fully described above. Methods from computational geometry used to solve graphical problems are cited. Implemented in program REGIONS, the algorithm is a useful tool for control-system-robustness analysis.

Step 1

The method of Kurozumi and Davis [1982] is used in program REGIONS to locate convex hulls $N(\omega, a_j)$ and $D(\omega, b_l)$.

Step 3

In program REGIONS, the points on $D(\omega, b_l)$ at relative minimum and maximum distances from the origin are identified. The two convex hulls $D(\omega, b_l, \theta_{max}) = D(\omega, b_l)e^{\theta_{max}i\omega}$ and $D(\omega, b_l, \theta_{min}) = D(\omega, b_l)e^{\theta_{min}i\omega}$ are located. Arcs of circles centered at $(0,0)$ connecting counter-clockwise, from relative extrema on $D(\omega, b_l, \theta_{max})$ to the corresponding extrema on $D(\omega, b_l, \theta_{min})$, are located. The boundary of this set of structures is $D(\omega, b_l, \theta)$. The arc connecting the global minimum on $D(\omega, b_l, \theta_{max})$ and $D(\omega, b_l, \theta_{min})$ is always part of the boundary $D(\omega, b_l, \theta)$. Portions of the arcs and hulls interior to the denominator boundary can be discarded by starting at the global minimum of $D(\omega, b_l, \theta_{max})$ and searching the outer boundary counter-clockwise for intersection points. At each intersection point a decision is made to follow the outer boundary based on the cross product of alternative routes until the starting point is reached.

Let ρ equal the total phase uncertainty of $D(\omega, b_l)$. If $|\theta_{max} - \theta_{min}| > (2\pi/\omega) - \rho$, the region $D(\omega, b_l, \theta)$ can overlap itself around the origin. Whether or not this is the case can be determined by searching the boundary $D(\omega, b_l, \theta)$ for intersections with itself. Program REGIONS does not concern itself with such overlap in $D(\omega, b_l, \theta)$ because step 7 eliminates overlap when the union of $\pi_i(\omega, a_j, b_l, \theta, k)$ is found.

Step 7

In program REGIONS, the method used to locate the union of $\pi_i(\omega, a_j, b_l, \theta, k)$ product convex hulls involves the "plane-sweep" line intersection routine presented by Sedgwick [1983]. In REGIONS, a routine locates the simple polygon that contains the union of a simple polygon and an intersecting convex polygon. The routine is called repeatedly until the union of all convex $\pi_i(\omega, a_j, b_l, \theta, k)$ is found.

Robustness Analysis

In practice, it is necessary to plot out enough of the boundaries for $\pi(i\omega)c(i\omega)$ over a relevant frequency range to allow determination of the envelope, or Nyquist band, of the uncertain loop-transfer function on the complex plane. In REGIONS, visual inspection of the $\pi(i\omega)c(i\omega)$ plot is utilized for stability determination. The minimum distance between the critical point $(-1, 0)$ and the region boundary, related to control-system performance, is determined by selecting the smallest distance between each boundary segment and $(-1, 0)$. Efficient algorithms can be found in the literature for this search when boundaries have special characteristics (e.g., Chin and Wang [1983], and Schwartz [1981]). An alternative (and conservative) analysis method utilizes disk-shaped approximations to regions $\pi(i\omega)$. The determination of containment of the critical point and distance from the critical point is simplified when $\pi(i\omega)$ is a disk. In REGIONS, this option is offered through an algorithm for fitting disks around simple polygons based on Bass and Schubert [1967] and Graham and Yao [1983].

References

Bass, L. J., and S. R. Schubert, "On Finding the Disc of Minimum Radius Containing a Given Set of Points," *Mathematical Computation*, 21, 1967, pp. 712–714.

Bolton, A. G., "Inverse Nyquist Design Using Region Algebra," *International Journal of Control*, 33, 1981, pp. 575–584.

Chen, S., *Control System Design for Multivariable Uncertain Processes*, Ph.D. Thesis, Case Western Reserve University, 1984.

Chin, F. and C. Wang, "Optimal Algorithms for the Intersection and the Minimum Distance Problem Between Planar Polygons," *IEEE Transactions on Computers*, C-32, 1983, pp. 1203–1207.

East, D. J., "A New Approach to Optimum Loop Synthesis," *International Journal of Control*, 34, 1981, pp. 731–748.

East, D. J., "On the Determination of Plant Variation Bounds for Optimum Loop Synthesis," *International Journal of Control*, 35, 1982, pp. 891–908.

Edelsbrunner, H., with H. A. Maurer and D. G. Kirkpatrick, "Polygonal Intersection Searching," *Information Processing Letters*, 14, April 20, 1982, pp. 74–79.

Graham, R. L., and F. F. Yao, "Finding the Convex Hull of a Simple Polygon," *Journal of Algorithms*, 4, 1983, pp. 324–331.

Henrici, P., "Circular Arithmetic and the Determination of Polynomial Zeros," *Applied and Computational Complex Analysis*, 1, 1974, pp. 86–92.

Jordan, K., *A Novel Analysis Technique for Processes With Uncertain Parameters*, M.S. Research Report, California Institute of Technology, 1985.

Kurozumi, Y. and W. Davis,"Polygon Approximation by the Mini-max Method," *Computer Graphics and Image Processing*, 19, 1982, pp. 248–264.

Laughlin, D., with K. Jordan and M. Morari, "Internal Model Control and Process Uncertainty: Mapping Uncertainty Regions for SISO Controller Design," *International Journal of Control*, 44, 1986, pp. 1675–1698.

Nievergelt, J., and F. P. Preparata, "Plane-Sweeping Algorithms for Intersecting Geometric Figures," *Communications of the ACM*, 25, October 1982, pp. 739–747.

Preparata F. P., and S. J. Hong, "Convex Hulls of Finite Sets of Points in Two and Three Dimensions," *Communications of the ACM*, 20, February 1977, pp. 87–93.

Saeki, M., "A Method of Robust Stability Analysis with Highly Structured Uncertainties," *IEEE Transactions on Automatic Control*, AC-31, 1986, pp. 935–940.

Schwartz, J. T., "Finding the Minimum Distance Between Two Convex Polygons," *Information Processing Letters*, 13, 1981, pp. 168–170.

Sedgwick, R., *Algorithms*, (Addison Wesley: London), 1983.

FIGURES FOR CHAPTER II

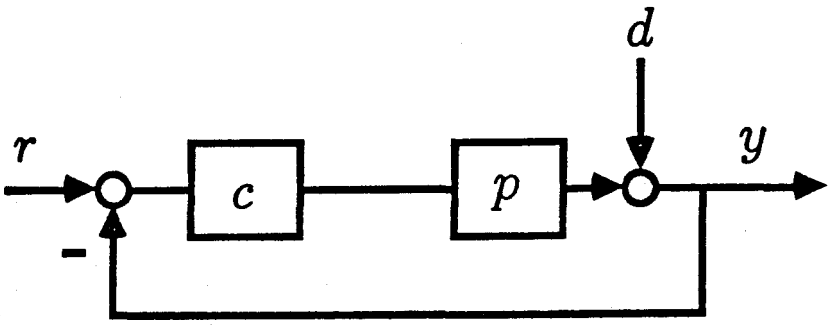

Figure 1: Standard feedback control structure with process $p(s)$, controller $c(s)$, set-point $r(s)$, disturbances $d(s)$ and output $y(s)$.

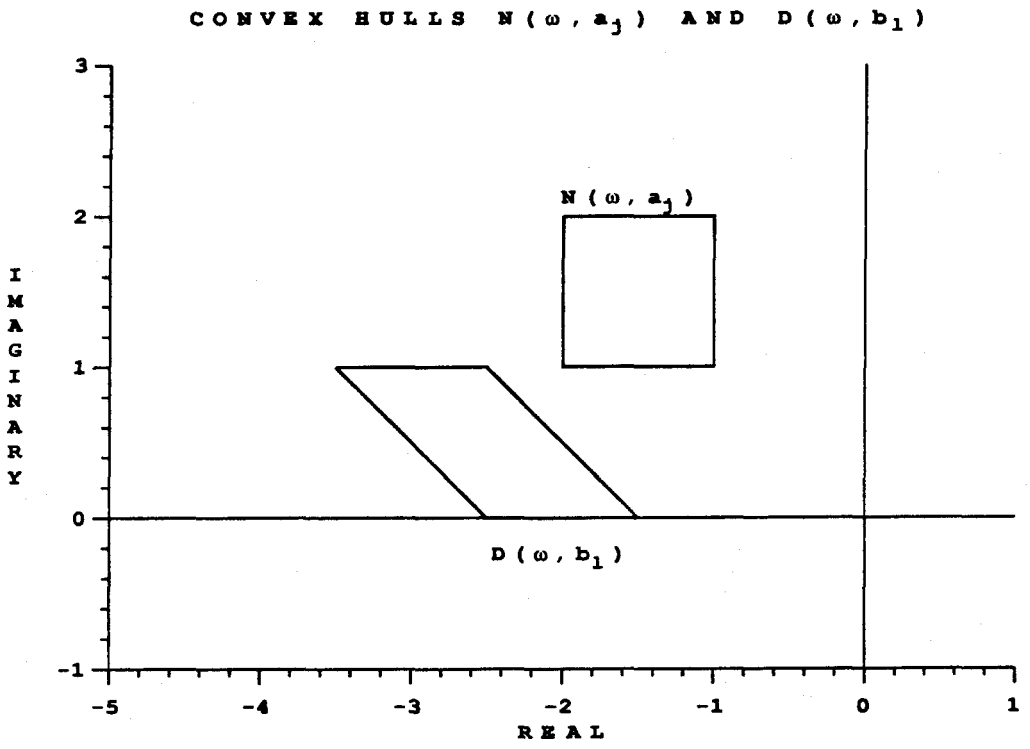

Figure 2: Convex hulls $N(\omega, a_j)$ containing the uncertain numerator sum and $D(\omega, b_l)$ containing the uncertain denominator sum in Equation 3 are located here following step 1 of the algorithm.

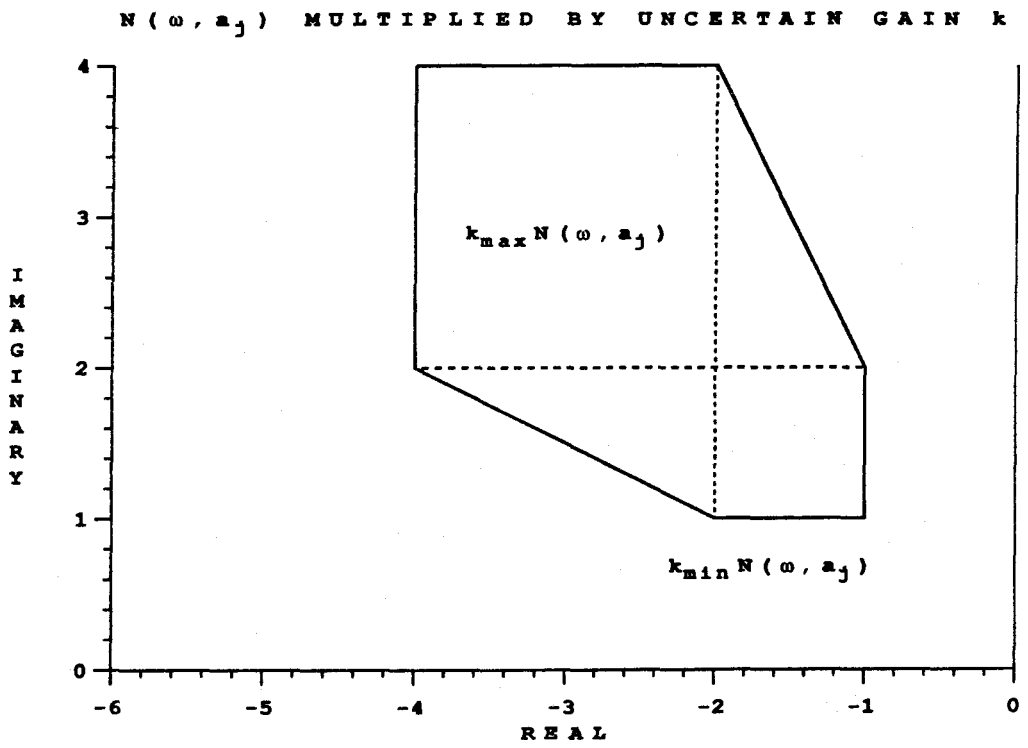

Figure 3: Multiplication of $N(\omega, a_j)$ in Figure 2 by an uncertain gain ($1 \leq k \leq 2$) stretches the region along rays extending from the origin. Note that the region containing the product is still convex.

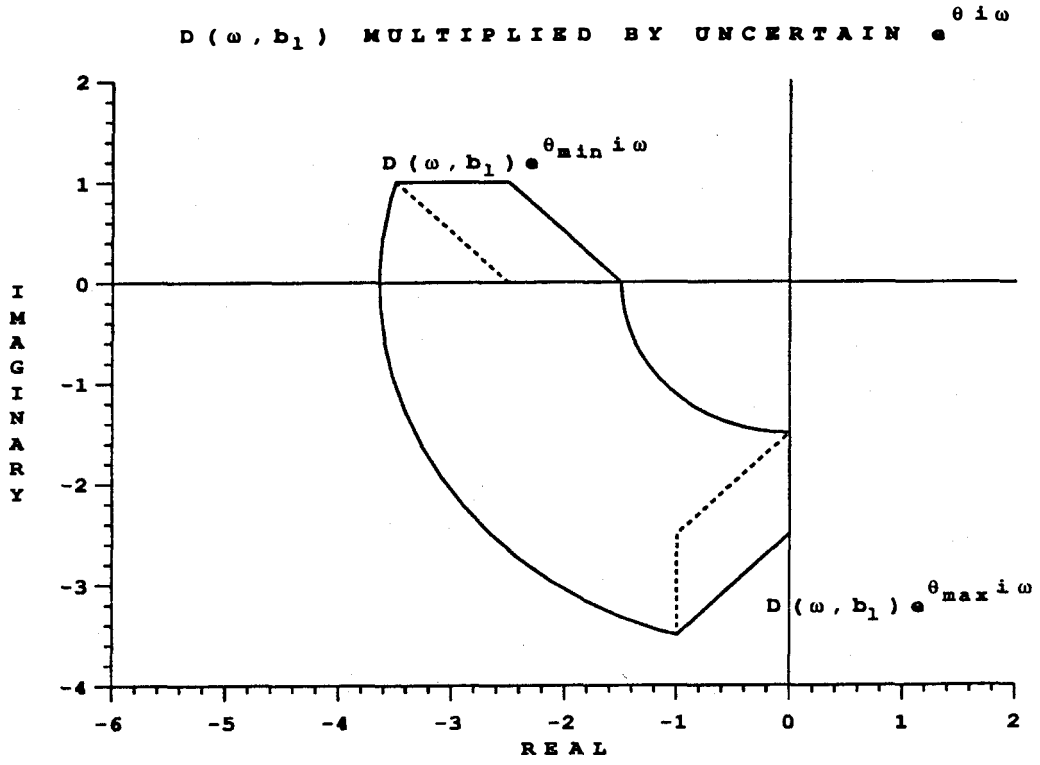

Figure 4: Multiplication of $D(\omega, b_l)$ in Figure 2 by $e^{i\theta}$ with $0 \leq \theta \leq \pi/2$ rotates it about the origin. Points on $D(\omega, b_l)e^{i\omega\theta min}$ and $D(\omega, b_l)e^{i\omega\theta max}$ at relative minimum and maximum distances from the origin are connected by arcs of circles centered at the origin.

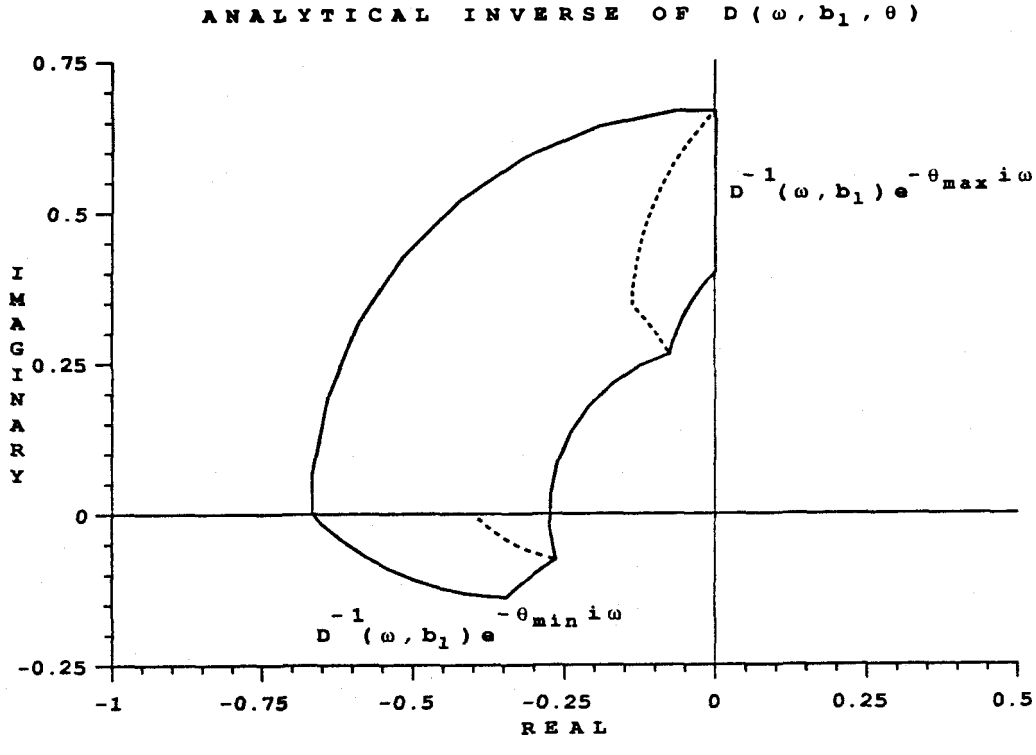

Figure 5: The inverse of the denominator region $D(\omega, b_l, \theta)$ in Figure 4 can be located analytically, since circles centered at the origin invert to circles centered at the origin and line segments invert to arcs or segments.

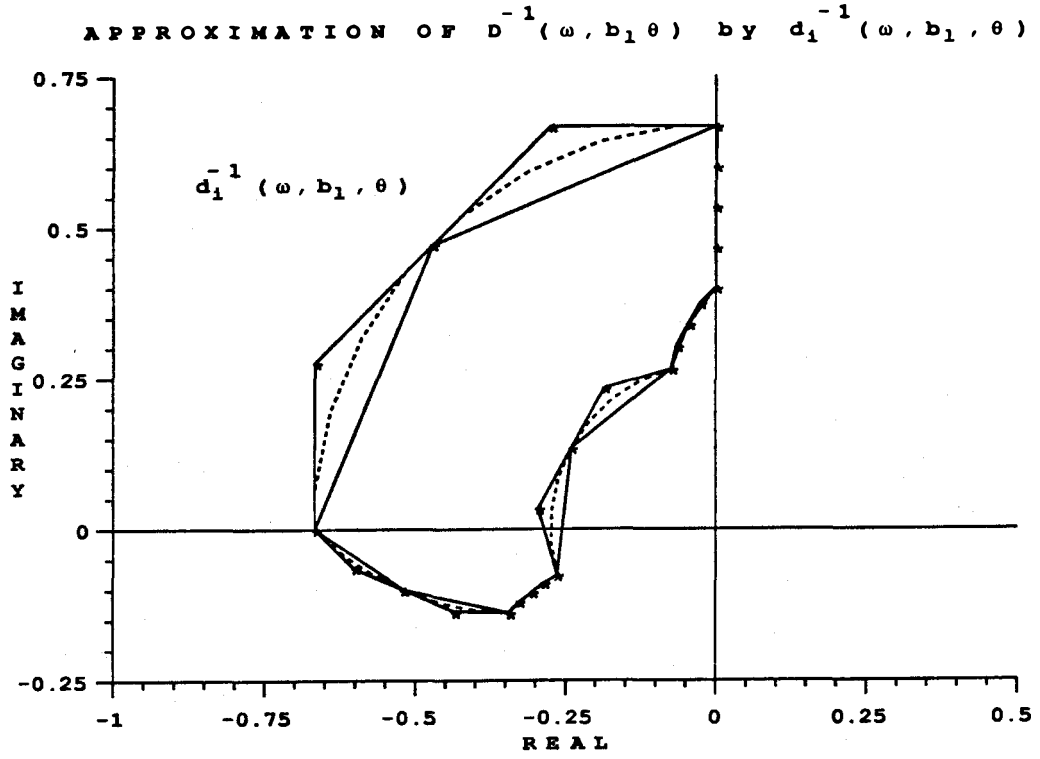

Figure 6: The entire boundary of $D^{-1}(\omega, b_l, \theta)$ in Figure 5 is contained within the union of line segments and triangles $d_i^{-1}(\omega, b_l, \theta)$. Here the number of triangles and segments used to approximate the boundary corresponds to a resolution parameter $r = 1$.

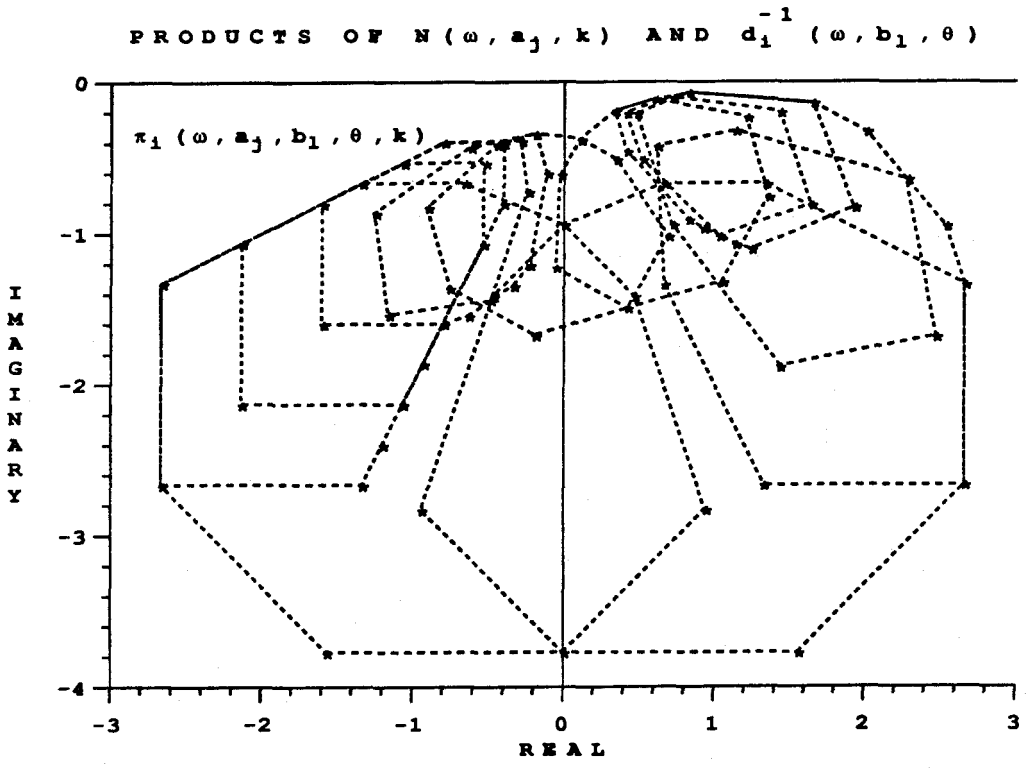

Figure 7: Convex hulls $\pi_i(\omega, a_j, b_l, \theta, k)$ result when each of the $d_i^{-1}(\omega, b_l, \theta)$ in Figure 6 is multiplied by the numerator hull $N(\omega, a_j, k)$ in Figure 3. The resolution parameter here is $r = 1$.

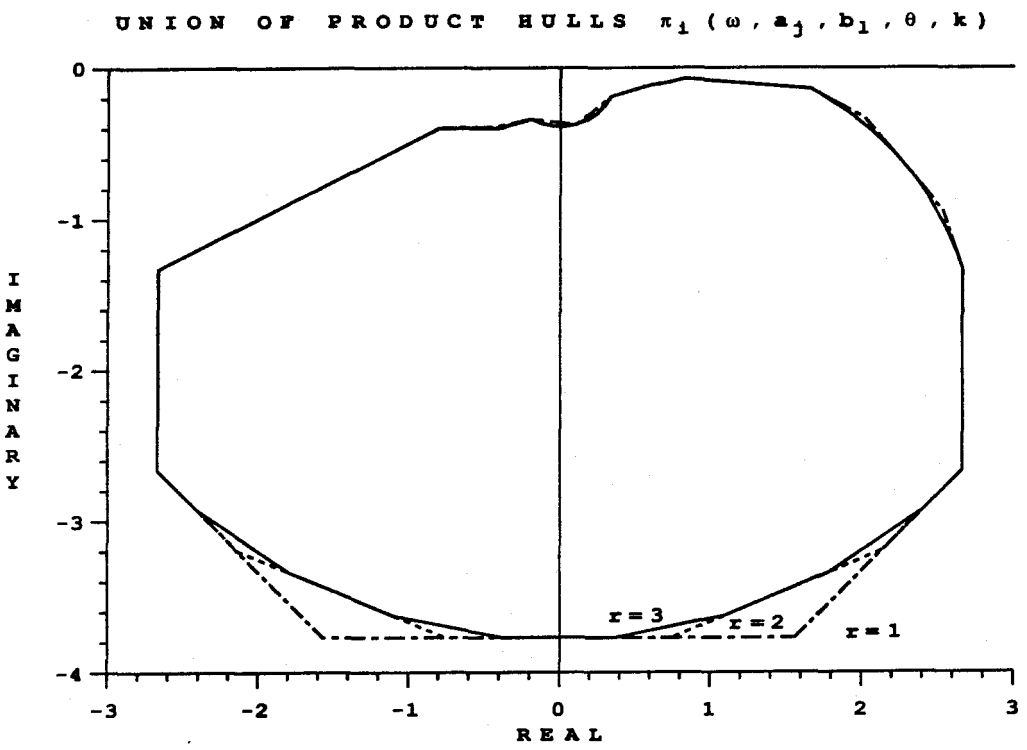

Figure 8: The outer edge of the convex hulls $\pi_i(\omega, a_j, b_l, \theta, k)$ in Figure 7 ($r = 1$) illustrated by long dashes contains the boundary of the product of $N(\omega, a_j, k)$ and $D^{-1}(\omega, b_l, \theta)$. Convergence of the algorithm can be seen here with intermediate ($r = 2$) and least conservative boundary ($r = 3$) illustrated with short dashes and solid lines, respectively.

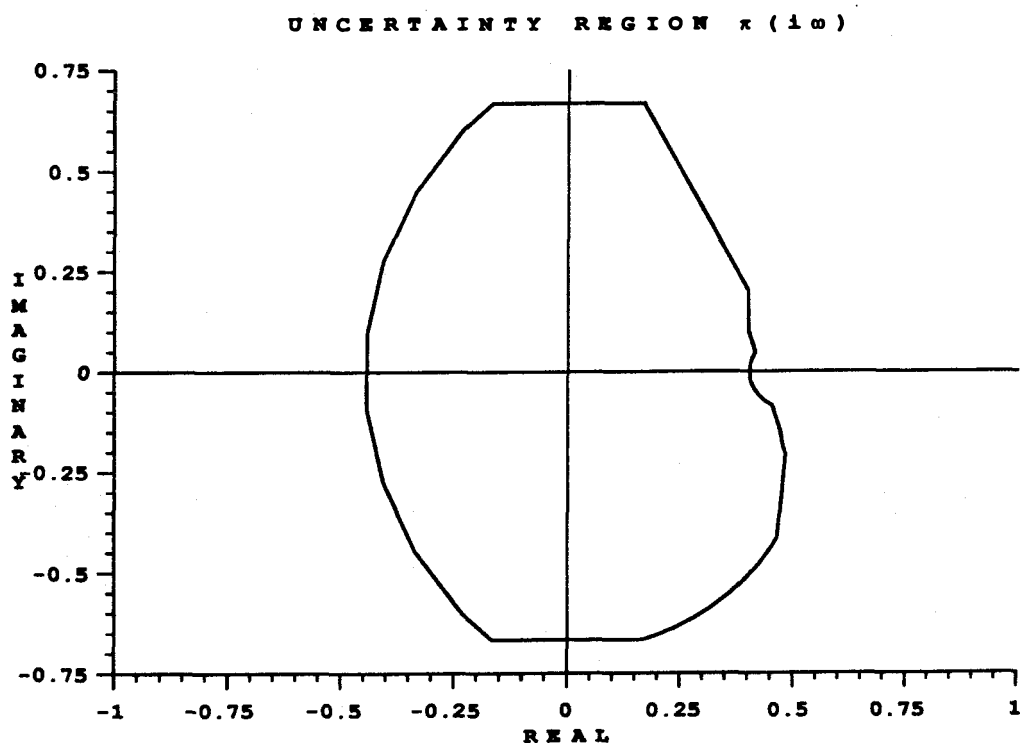

Figure 9: The region boundary with resolution $r = 3$ in Figure 8 has been multiplied by $1/4i$ and added to $1/2$. The uncertain function of ω in Equation 3 is contained within the boundary shown here at $\omega = 1.0$ *rad/sec.*

CHAPTER III: INTERNAL MODEL CONTROL AND PROCESS UNCERTAINTY: MAPPING UNCERTAINTY REGIONS FOR SISO CONTROLLER DESIGN

INT. J. CONTROL, 1986, VOL. 44, NO. 6, 1675–1698

Internal model control and process uncertainty: mapping uncertainty regions for SISO controller design

DANIEL L. LAUGHLIN†, KENNETH G. JORDAN† and MANFRED MORARI†

A complete SISO controller design technique is presented that allows robust controller design in the face of process uncertainty. Process-uncertainty descriptions with meaningful physical interpretations are compatible with the technique. A test for robust performance can be applied when the process is described by a transfer function with real parameter variations. First a method is presented for locating all possible complex variations of a transfer function resulting from real parameter uncertainties. The possible variations are pictured as model uncertainty regions on the complex plane. Next a controller design technique based on the internal model control structure is outlined. The controller is used to map the process uncertainty regions to the Nyquist plane for stability and performance analysis. The region-mapping technique offers a unique opportunity to compare robust performance of PID and Smith Predictor controllers. Finally, applications of the proposed technique to structured singular-value analysis are discussed.

1. Introduction

1.1. *The robust control problem*

The challenge for the control engineer is to design a robust controller for a process that cannot be modelled exactly. It is not enough to design a controller that provides stability and adequate performance for a nominal model. A robust controller guarantees stability and adequate performance for a whole family of linear models used to represent the actual process. The SISO *robust control problem* formulated here involves three steps: (i) representing the diversity of plants to be controlled by a mathematical uncertainty description; (ii) translating desired response characteristics into mathematical performance requirements; and (iii) designing a controller and testing to ensure that all performance requirements can be met by all plants within the uncertainty description. A valuable robust performance guarantee is obtained by following the recommended procedure for each step.

1.1.1. *Selecting the process uncertainty description*

A set of linear models must be selected to represent the actual process. This set of models is best selected after considering the origins of process uncertainty. One source of process uncertainty is variation of real parameters affecting plant operation. For example, ambient temperature and pressure can stray from nominal conditions. A second source of process uncertainty is the inherent non-linearity of most processes. Linearizing the process model around different steady states results in different

Received 17 February 1986.

† Chemical Engineering, 206–41, California Institute of Technology, Pasadena, California 91125, U.S.A.

transfer-function descriptions. A third source of uncertainty is experimental identification of the process. A 'fuzzy' plant description on the complex plane results when input/output data is Fourier-transformed to extract a frequency-domain model. Uncertainty originating from all three sources can be considered by defining model uncertainty regions on the complex plane. Let $\pi(\omega)$ be a simply or multiply connected domain on the complex plane at each frequency ω. The set Π of all possible process models is defined as follows:

$$\Pi = \{p(s) \mid p(i\omega) \in \pi(\omega), \forall\omega\} \tag{1}$$

Note that in general the set Π is infinite, since a never-ending variety of transfer functions $p(s)$ can lie inside the regions $\pi(\omega)$ when evaluated at frequency ω. The set Π is meaningful in the context of the robust control problem when the boundaries of each $\pi(\omega)$ reflect uncertainties identified above. A method for locating these region boundaries will be presented.

1.1.2. *Establishing performance requirements*

The control structure in Fig. 1 must be closed-loop-stable for all plants in the set Π. Additional SISO performance objectives are typically 'good' command-following and disturbance-rejection. These performance objectives are achieved if the error signal $e(s) = r(s) - y(s)$ is kept 'small'. Exactly what is meant by 'good' and 'small' is established by considering the nature of inputs to the control system. The inputs $r(t) - d(t)$ are assumed to belong to a set of norm-bounded functions such that

$$\left\| \frac{r(t) - d(t)}{w_d(t)} \right\|_2^2 = \frac{1}{2\pi} \int_{-\infty}^{+\infty} \left| \frac{r(i\omega) - d(i\omega)}{w_d(i\omega)} \right|^2 d\omega \leqslant 1 \tag{2}$$

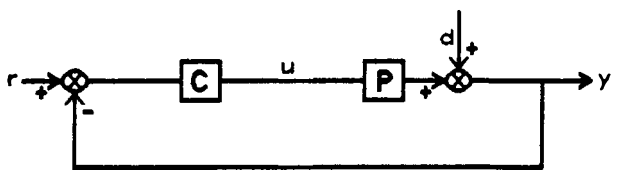

Figure 1. Standard feedback structure with commands $r(s)$, disturbances $d(s)$ and outputs $y(s)$.

The class of permissible inputs is determined by the choice of $w_d(i\omega)$. The magnitude of a typical input weight $w_d(i\omega)$ is shown in Fig. 2 (*a*). When such a weight is selected, high-frequency inputs are expected to have small amplitudes. If the disturbance spectrum is a narrow band concentrated near ω (i.e. the disturbance looks almost like $\sin \omega t$) the disturbance power (amplitude) is limited to $|w_d(i\omega)|$. For all inputs described by (2) the error $e(s)$ is required to belong to a similar set of norm-bounded functions:

$$\| e(t)w_e(t) \|_2^2 = \frac{1}{2\pi} \int_{-\infty}^{+\infty} |e(i\omega)w_e(i\omega)|^2 \, d\omega \leqslant 1 \tag{3}$$

Error weight $w_e(i\omega)$ can be interpreted as follows: if the spectrum of $e(i\omega)$ is concentrated near ω (i.e. the error looks almost like $\sin \omega t$) then the error power is limited to $|1/w_e(i\omega)|$. Usually $|w_e(i\omega)|$ resembles the curve in Fig. 2 (b), indicating that only small small low-frequency errors will be tolerated.

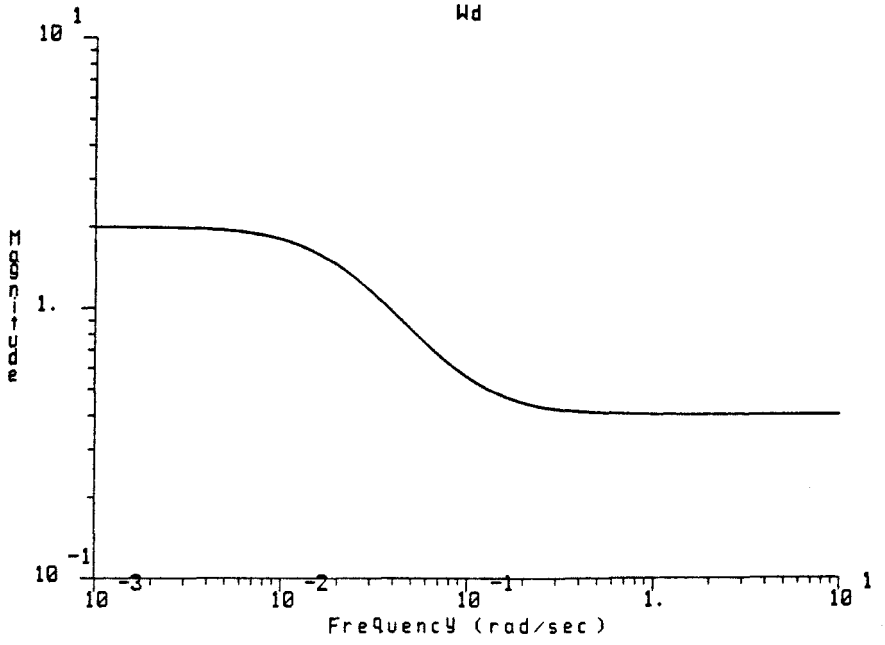

Figure 2(*a*)

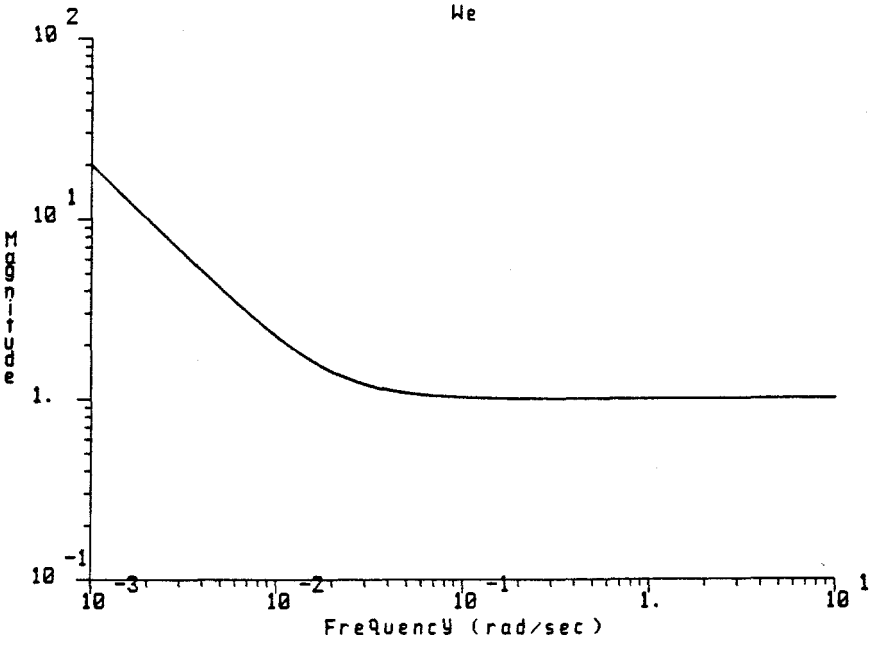

Figure 2(*b*)

Figure 2. (*a*) Weight $w_d(s) = (s + 0{\cdot}1)/2{\cdot}5(s + 0{\cdot}02)$. (*b*) Weight $w_e(s) = (s + 0{\cdot}02)/s$. (*c*) Performance weight $w_2(s) = (s + 0{\cdot}1)/2{\cdot}5s$. (*d*). The magnitude of the sensitivity function must be less than $|w_2(i\omega)|$ for all frequencies in order to achieve robust performance.

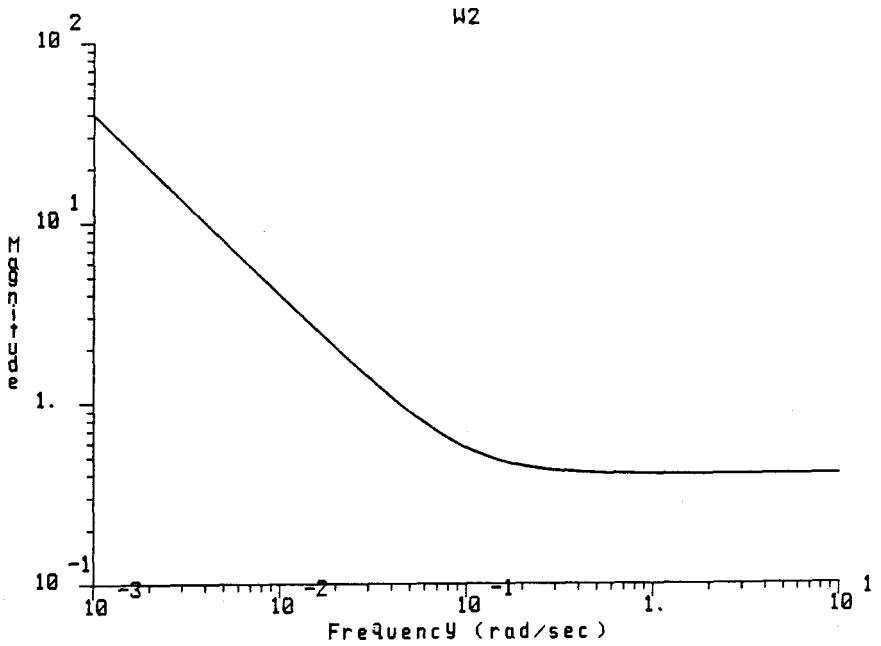
W2
Magnitude
Frequency (rad/sec)

(*c*)

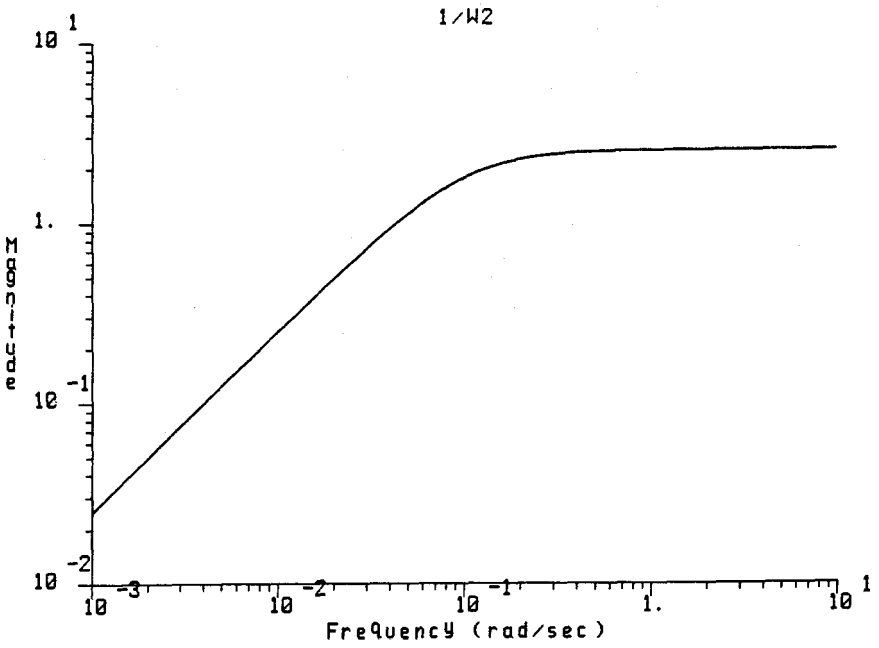
1/W2
Magnitude
Frequency (rad/sec)

(*d*)

1.1.3. *Testing for robustness*

Robust stability and robust performance must be guaranteed for all plants in Π. Robust stability is evaluated by applying the Nyquist stability criterion to regions $\pi(\omega)c(i\omega)$. The system is closed-loop-stable if the net number of counterclockwise encirclements of $(-1, 0)$ by $pc(s)$ as s traverses the Nyquist contour is equal to the number of unstable open-loop poles. When $pc(s)$ is represented by regions $\pi(\omega)c(i\omega)$ at each frequency $s = i\omega$ the additional constraint that no region $\pi(\omega)c(i\omega)$ contain $(-1, 0)$ must be met to ensure stability. If any region $\pi(\omega)c(i\omega)$ contains $(-1, 0)$ the number of encirclements is indeterminate and closed-loop stability cannot be guaranteed.

Robust performance is evaluated by examining the magnitude of the sensitivity function $s(i\omega)$. Equation (3) is satisfied for all inputs described by (2) for all plants in Π if and only if $s(i\omega)$ satisfies

$$|s(i\omega)| = \left|\frac{1}{1 + p(i\omega)c(i\omega)}\right| \leqslant \left|\frac{1}{w_2(i\omega)}\right| \quad \forall\omega, \forall p(s) \in \Pi \tag{4}$$

The weight $w_2(i\omega)$ in (4) is related to the weights $w_d(i\omega)$ and $w_e(i\omega)$ by

$$w_2(i\omega) = w_e(i\omega)w_d(i\omega) \tag{5}$$

The weight $w_2(i\omega)$ corresponding to previously selected $w_d(i\omega)$ and $w_e(i\omega)$ is illustrated in Fig. 2 (*c*). For convenience, (4) can be written as

$$|1 + p(i\omega)c(i\omega)| \geqslant |\omega_2(i\omega)| \quad \forall\omega, \forall p(s) \in \Pi \tag{6}$$

Since all plants $p(s) \in \Pi$ are restricted to lie within region $\pi(\omega)$ at frequency ω, the requirement (6) can be met by ensuring that the distance of regions $\pi(\omega)c(i\omega)$ from $(-1, 0)$ is greater than $|w_2(i\omega)|$.

1.2. *The issue of conservativeness*

Unless a robust controller can be synthesized directly from the uncertainty description and performance requirements an iterative design procedure must be used: (i) describe process uncertainty and specify performance requirements; (ii) perform analysis tests to determine whether or not robust stability and performance have been achieved; and (iii) if the stability and performance requirements are not met then select another controller and repeat the analysis tests. Conservativeness enters the design procedure if the tests cannot be applied to exactly the same set of plants used to describe the process uncertainty. A useful solution to the robust control problem has eluded researchers because of the incompatibility of uncertainty descriptions that accurately represent process behaviour with convenient tests for robust performance.

The proposed solution to the robust control problem eliminates the incompatibility of meaningful uncertainty descriptions with convenient analysis tests. Controller design can begin with the uncertainty description given by

$$\Pi = \left\{p(s) \mid p(s) = \left[\frac{a_n s^n + a_{n-1}s^{n-1} + \ldots + a_1 s + a_0}{b_m s^m + b_{m-1}s^{m-1} + \ldots + b_1 s + b_0}\right] \exp(-\theta s)\right\} \tag{7}$$

$$a_i \in [a_{i\min}, a_{i\max}], \quad b_i \in [b_{i\min}, b_{i\max}], \quad \theta \in [\theta_{\min}, \theta_{\max}]$$

The set Π can accurately represent physical parameter variations in the process or linearization of the process about different steady states. This uncertainty description also enables controller design to begin where many experimental identification methods end—with transfer-function coefficients described by a standard deviation about their mean. When the proposed design method is employed, uncertainty regions $\pi(\omega)$ corresponding to Π will be found. Initially a nominal model with all parameters at their mean values will be used to design a controller $c(s)$. Regions $\pi(\omega)c(i\omega)$ will be located on the Nyquist plane to evaluate robust stability and performance. The controller $c(s)$ will be adjusted until robust stability and performance can be guaranteed for all models in Π. Advantages of the design procedure proposed in this paper are best appreciated after examining some currently available design techniques.

1.2.1. *Other region-mapping methods*

Several researchers have offered controller-design techniques using arbitrarily shaped regions $\pi(i\omega)$ to represent process uncertainty (East 1982, Chen 1984, Horowitz 1982). In particular, Chen outlines a region-arithmetic-based design technique where process uncertainty regions are mapped to regions that describe the closed-loop transfer function. He offers an algorithm for locating the boundary of each new region. Unfortunately, his algorithm does not guarantee that all possible closed-loop transfer functions are contained within the region boundary. An unstable system might be considered to be stable if Chen's algorithm is used. Perhaps the best aspect of Chen's work is that he uses the internal model control (IMC) design procedure to determine the controller after selecting a nominal plant. Advantages associated with the IMC design procedure have been noted by several authors (Garcia and Morari 1982; Holt and Morari 1985 a, b; Rivera *et al.* 1986; Morari and Skogestad 1985). Chen and the others are not the first to have considered use of a region arithmetic to find bounds on closed-loop transfer-function elements. Bolton (1981) employed a circular region arithmetic in a procedure he called 'inverse Nyquist design'. Bolton's arithmetic was similar to that defined by Henrici (1974) to locate regions containing polynomial zeros. Horowitz (1982) described a 'quantitative feedback theory' where plant uncertainties are described as arbitrarily shaped regions on the complex plane at each frequency. Horowitz applied a controller to these regions and mapped them to a Nichols chart. From this mapping Horowitz was able to adjust controller parameters that lead to robust stability and performance. The parameter adjustments were based largely on experience. A SISO example using Horowitz's design method was given by Krishnan and Cruickshanks (1977).

1.2.2. *Loop-shaping*

Multiplicative perturbations on a nominal plant can be accounted for in the control system design process through loop-shaping (Doyle and Stein 1981). Consider a set of plants $p(i\omega)$ represented by

$$p(s) = \tilde{p}(s)[1 + l_m(s)], \quad |l_m(i\omega)| < |w_1(i\omega)| \tag{8}$$

Using the norm-bounded multiplicative error $l_m(s)$ is equivalent to representing process uncertainty by a disc-shaped uncertainty region $\pi(\omega)$ with radius $|\tilde{p}(i\omega)w_1(i\omega)|$ on the complex plane. A feedback system with controller $c(i\omega)$ is stable for all $l_m(i\omega)$ such that $|l_m(i\omega)| \leqslant |w_1(i\omega)|$ if and only if

$$\left|\frac{\tilde{p}(i\omega)c(i\omega)}{1+\tilde{p}(i\omega)c(i\omega)}\right| < \frac{1}{|w_1(i\omega)|} \quad \forall\omega \tag{9}$$

When $\tilde{p}(i\omega)c(i\omega) \ll 1$ at high frequencies, (9) is approximated by

$$|\tilde{p}(i\omega)c(i\omega)| < \frac{1}{|w_1(i\omega)|} \tag{10}$$

The sensitivity function $s(i\omega) = (1 + p(i\omega)c(i\omega))^{-1}$ is required to be small to yield good performance:

$$\left|\frac{1}{1+p(i\omega)c(i\omega)}\right| = \left|\frac{1}{1+(1+l_m(i\omega))\tilde{p}(i\omega)c(i\omega)}\right| < \frac{1}{|w_2(i\omega)|} \quad \forall\omega \tag{11}$$

In (11) $w_2(i\omega)$ is selected as a performance criterion. The restriction that (11) places on $\tilde{p}(i\omega)c(i\omega)$ is expressed clearly by

$$\begin{aligned} |1+(1+l_m(i\omega))\tilde{p}(i\omega)c(i\omega)| &\geqslant |w_2(i\omega)| \\ &\Leftarrow -1+|(1+l_m(i\omega))\tilde{p}(i\omega)c(i\omega)| \geqslant |w_2(i\omega)| \\ &\Leftarrow |\tilde{p}(i\omega)c(i\omega)| \geqslant \frac{|w_2(i\omega)|+1}{1-|w_1(i\omega)|} \end{aligned} \tag{12}$$

The transfer function $\tilde{p}(i\omega)c(i\omega)$ is shaped to satisfy the performance specification (12) at low frequencies and the stability requirement (10), which usually limits performance at high frequencies. The loop-shaping method causes conservativeness to enter the design procedure when actual process uncertainty cannot be represented by discs on the complex plane. Additionally, loop-shaping cannot guarantee that the closed-loop system will be stable. Perhaps the greatest weakness of loop-shaping is that it gives the controller designer no information about the crossover region—only low- and high-frequency ranges are considered.

1.2.3. *Structured singular-value analysis*

The most promising new developments in robust controller design are based on structured singular-value analysis. Doyle (1982) has developed a single necessary and sufficient test for robust stability and performance when norm-bounded perturbations $\Delta(s)$ can be used to describe process uncertainty. Doyle constructs the SISO robust control problem as shown in Fig. 3. Both Δ_1 and Δ_2 are bounded such that $|\Delta_i(i\omega)| \leqslant 1$. Blocks w_1 and Δ_1 represent the same multiplicative error $l_m(s)$ as in (8). Blocks w_d, w_e and Δ_2 combine into the same performance requirement expressed through (2)–(5). Figure 3 is equivalent to the simple two-block structure shown in

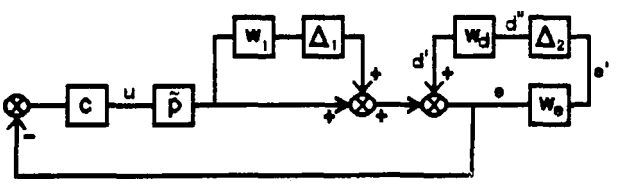

Figure 3. A SISO robust control problem is written in terms of this block structure for structured singular-value analysis. The actual input d' and error e are modified by weights w_d and w_e so signals d'' and e' are 2-norm-bounded by 1.

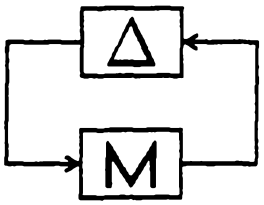

Figure 4. Structured singular-value analysis requires reconstruction of the control problem in terms of a two-block structure. Matrix M contains information about the nominal model, the controller, the uncertainty weights and the performance specifications. Elements in the matrix Δ are norm-bounded uncertainties.

Fig. 4. Matrices M and Δ are given by

$$\Delta = \begin{bmatrix} \Delta_1 & 0 \\ 0 & \Delta_2 \end{bmatrix} \tag{13}$$

$$M = \begin{bmatrix} \dfrac{-w_1(i\omega)c(i\omega)\tilde{p}(i\omega)}{1 + c(i\omega)\tilde{p}(i\omega)} & \dfrac{-w_1(i\omega)c(i\omega)\tilde{p}(i\omega)w_d(i\omega)}{1 + c(i\omega)\tilde{p}(i\omega)} \\ \dfrac{w_e(i\omega)}{1 + c(i\omega)\tilde{p}(i\omega)} & \dfrac{w_e(i\omega)w_d(i\omega)}{1 + c(i\omega)\tilde{p}(i\omega)} \end{bmatrix} \tag{14}$$

Both robust stability and robust performance of the control system are guaranteed if and only if the structure singular value $\mu(M)$ is less than unity:

$$\mu(M) = |(1 - \tilde{s}(i\omega))w_1(i\omega)| + |\tilde{s}(i\omega)w_2(i\omega)| < 1 \tag{15}$$

Here $\tilde{s}(i\omega) = (1 + c(i\omega)\tilde{p}(i\omega))^{-1}$ is the nominal sensitivity function. The weight $w_2(i\omega)$ in (15) is given by (5). The ability to guarantee robust stability and robust performance if and only if $\mu(M) < 1, \forall\ \omega$, establishes the strength of structured singular-value analysis.

Unfortunately, structured singular-value analysis cannot be applied unless the process uncertainty is represented by a disc-shaped region on the complex plane at each frequency. The proposed design method begins with uncertainty descriptions like that given in (7) that do not appear as disc-shaped regions. A design method based on the uncertainty description (7) will be a powerful tool for the control-system designer.

2. SISO robust controller design procedure

2.1. *Translating parameter variations into uncertainty regions*

When a transfer function with coefficients restricted to intervals on the real axis describes the process, it is necessary to locate the corresponding uncertainty regions $\pi(\omega)$ for robustness analysis. Translating coefficient uncertainties into uncertainty regions always introduces conservativeness. Conservativeness enters because regions $\pi(\omega)$ represent a structure-free process description; that is, a specific transfer function form is not selected.

A method has been developed for locating the regions $\pi(\omega)$ corresponding to the transfer function in (7) with any required degree of accuracy. The essential requirement throughout development of the method was that the regions located be *guaranteed* to contain all plants represented by (7). First the control engineer must specify a frequency range of interest. Enough regions $\pi(\omega)$ must be located to allow

construction of the envelope around all uncertainty regions within this frequency range. At a given frequency the region $\pi(\omega)$ can be located by performing steps given in §§ 2.1.1–2.1.4.

2.1.1. *Locating polynomial rectangles*

All coefficients a_i, b_i and θ in (7) are assumed to be uncorrelated. When upper and lower bounds are given for the parameters a_i a hyper-rectangle in a_i parameter space is defined. This hyper-rectangle representing possible values for the a_i is mapped into a rectangle on the complex plane by the numerator polynomial. The denominator polynomial maps a hyper-rectangle in b_i parameter space to another rectangle on the complex plane. This fact is easily established by considering the numerator polynomial $N(s, a_i)$:

$$N(s, a_i) = a_n s^n + a_{n-1} s^{n-1} + \ldots + a_1 s + a_0 \tag{16}$$

When the polynomial is evaluated at $s = i\omega$, the following equation is obtained:

$$N(i\omega, a_i) = (a_0 - a_2\omega^2 + a_4\omega^4 - \ldots) + i(a_1\omega - a_3\omega^3 + a_5\omega^5 - \ldots) \tag{17}$$

The real and imaginary parts of $N(i\omega)$ are given by

$$\text{Re}\,[N(i\omega, a_i)] = a_0 - a_2\omega^2 + a_4\omega^4 - \ldots \tag{18}$$

$$\text{Im}\,[N(i\omega, a_i)] = a_1\omega - a_3\omega^3 + a_5\omega^5 - \ldots \tag{19}$$

The sides of the rectangle are parallel to the real and imaginary axes. Real and imaginary coordinates of points inside the rectangle are bounded by the following values:

$$\max\,[\text{Re}\,(N)] = a_{0\,\max} - a_{2\,\min}\omega^2 + a_{4\,\max}\omega^4 - \ldots \tag{20}$$

$$\min\,[\text{Re}\,(N)] = a_{0\,\min} - a_{2\,\max}\omega^2 + a_{4\,\min}\omega^4 - \ldots \tag{21}$$

$$\max\,[\text{Im}\,(N)] = a_{1\,\max}\omega - a_{3\,\min}\omega^3 + a_{5\,\max}\omega^5 - \ldots \tag{22}$$

$$\min\,[\text{Im}\,(N)] = a_{1\,\min}\omega - a_{3\,\max}\omega^3 + a_{5\,\min}\omega^5 - \ldots \tag{23}$$

Knowledge of the upper and lower bounds for each coefficient a_i and b_i is sufficient to map the numerator and denominator polynomials to rectangles on the complex plane. Numerator and denominator rectangles for the set of linear models described by (24) are located in Fig. 5 for frequency $\omega = 1{\cdot}0$ rad/s.

2.1.2. *Inverting the denominator rectangle*

Once the numerator and denominator rectangles $N(i\omega, a_i)$ and $D(i\omega, b_i)$ have been located, the denominator rectangle must be inverted. This operation is restricted to denominator rectangles that do not contain the origin. If $D(i\omega, b_i)$ contains the origin then the inverse region will extend to infinity on the complex plane. Such a denominator rectangle indicates the possibility of a process pole on the imaginary axis. Since the mapping $f(z) = 1/z$ is a special case of a linear fractional transformation, it maps line segments either to circular arcs or to line segments. Inverting the boundary of the rectangle $D(i\omega, b_i)$ results in a closed curve of connected line segments and circular arcs (see Fig. 5). If $D(i\omega, b_i)$ does not contain the origin then the interior of $D(i\omega, b_i)$ maps to the interior of this closed curve.

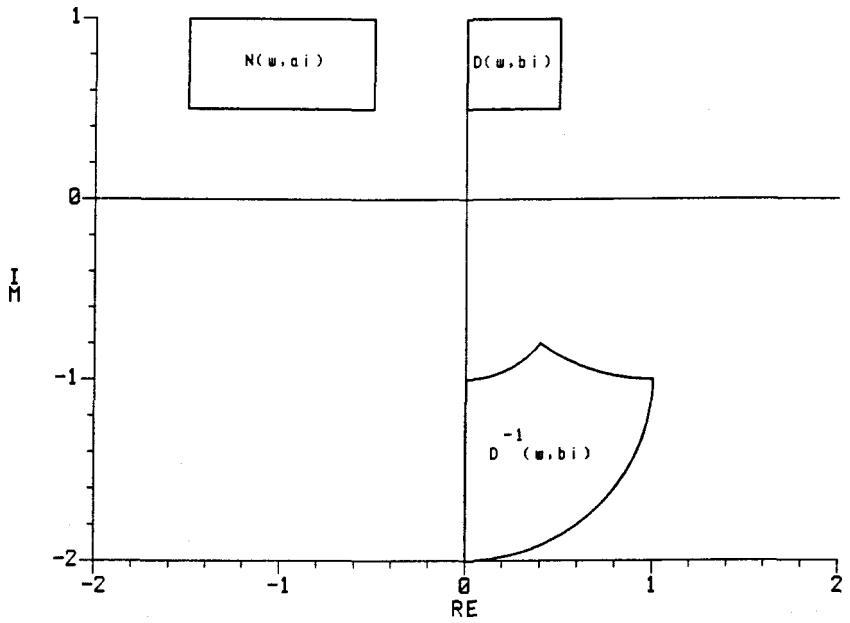

Figure 5. Rectangles representing uncertainty in the numerator and denominator polynomials $N(\omega, a_i)$ and $D(\omega, b_i)$. The inverse of the denominator rectangle $D^{-1}(\omega, b_i)$ is also shown.

2.1.3. *Locating the rational uncertainty region*

Once the denominator inverse region $D^{-1}(i\omega, b_i)$ has been located, it must be multiplied by the numerator rectangle $N(i\omega, a_i)$. The product of this multiplication will be the uncertainty region corresponding to the rational part of the transfer function. A method utilizing multiplication of convex hulls has been developed for locating the rational uncertainty region.

(i) Each circular arc on the boundary of $D^{-1}(i\omega, b_i)$ is covered by 2^n triangles as shown in Fig. 6 for $n = 1$. The line containing collinear sides of adjacent triangles is tangent to the arc.

(ii) Each line segment on the boundary of $D^{-1}(i\omega, b_i)$ is divided into 2^n smaller line segments. Denote the triangles and line segments by d_i^{-1}. The d_i^{-1} number $2^{(n+2)}$.

(iii) Multiplication operations are carried out between the numerator rectangle and each d_i^{-1}. The product region in each operation is defined as the convex hull about the set of points formed by multiplying each vertex on a d_i^{-1} by all four vertices of the numerator rectangle. An algorithm for locating the convex hull about a set of points was given by Kurozumi and Davis (1982).

(iv) The final rational uncertainty region is the union of $2^{(n+1)}$ convex hulls resulting from multiplications between $N(i\omega, a_i)$ and the d_i^{-1}. This region is guaranteed to contain all points that can result from multiplication of an arbitrary point on $N(i\omega, a_i)$ by an arbitrary point on $D^{-1}(i\omega, b_i)$.

Defining the product of each d_i^{-1} times $N(i\omega, a_i)$ as a convex hull introduces some conservativeness; that is, the convex hull contains extra points that do not result from

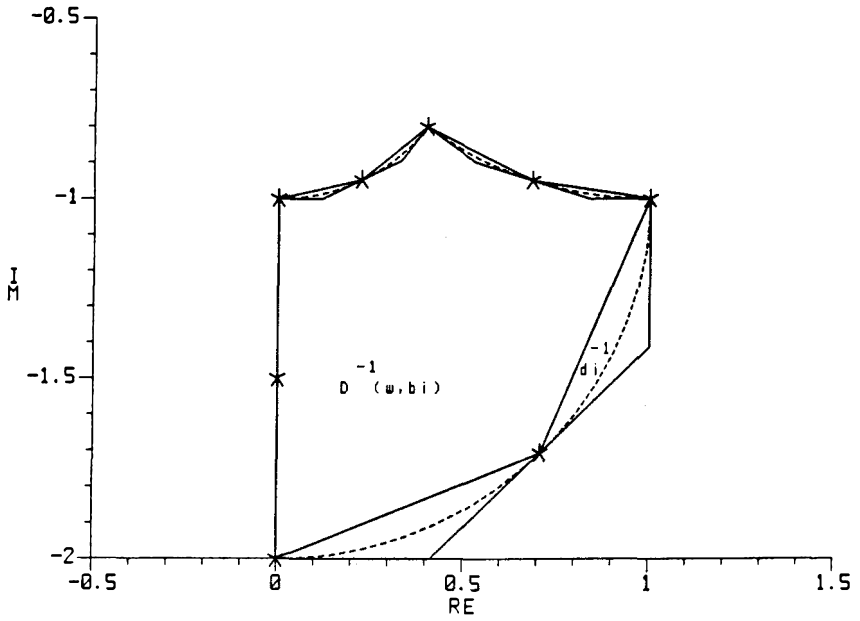

Figure 6. The boundary of the inverted denominator rectangle is covered by line segments and triangles d_i^{-1}.

the multiplication. The conservativeness is reduced as the parameter n is increased. Naturally, computational effort increases as n increases. Experience indicates that $n = 3$ or 4 strikes an acceptable balance between computational intensity and accuracy in locating uncertainty regions.

2.1.4. *Multiplying by the time-delay uncertainty*

The final step in locating the region $\pi(\omega)$ corresponding to (7) is multiplication of the rational uncertainty region by the time-delay uncertainty. First the boundary of the rational uncertainty region is multiplied by $\exp(-i\theta_{\min}\omega)$. Next the boundary of the rational uncertainty region is multiplied by $\exp(-i\theta_{\max}\omega)$. New regions resulting from these two multiplications are located on the complex plane. Corresponding points on the regions located at relative minimum and maximum distances from the origin are connected by circular arcs as shown in Fig. 7. The interior of this construction is the final uncertainty region guaranteed to contain all plants described by (7) at frequency ω.

2.1.5. *Example*

This example will illustrate the procedure used to locate regions $\pi(i\omega)$ corresponding to transfer functions with uncertain coefficients; a region corresponding to the model in (24) will be located at $\omega = 1{\cdot}0$ rad/s:

$$p(s) = \frac{a_1 s + a_0}{b_2 s^2 + b_1 s + b_0} \exp(-\theta s) \tag{24}$$

$$a_0 \in [-1{\cdot}5, -0{\cdot}5], \quad a_1 \in [0{\cdot}5, 1{\cdot}0], \quad \theta \in [0, 2{\cdot}0]$$

$$b_0 \in [0{\cdot}8, 1{\cdot}2], \quad b_1 \in [0{\cdot}5, 1{\cdot}0], \quad b_2 \in [0{\cdot}7, 0{\cdot}8]$$

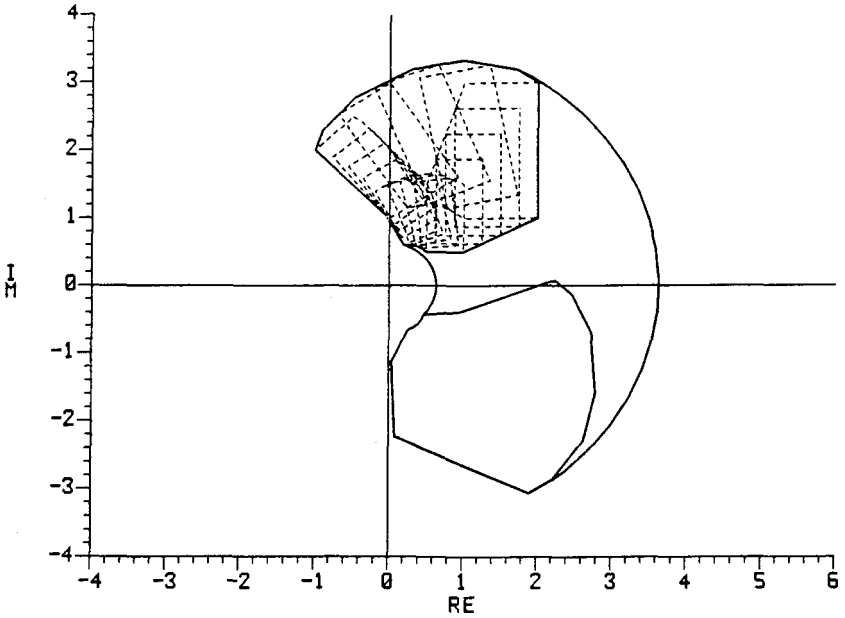

Figure 7. Convex hulls representing the product of each d_i^{-1} times $N(\omega, a_i)$ are illustrated with dashed lines. The union of these convex hulls is the uncertainty regions corresponding to the rational part of the transfer function. Time-delay uncertainty sweeps the uncertainty region about the origin.

Numerator and denominator polynomials in (24) map to the rectangles $N(i\omega, a_i)$ and $D(i\omega, b_i)$ in Fig. 5 at $\omega = 1{\cdot}0$ rad/s. The inverse of the denominator rectangle $D^{-1}(i\omega, b_i)$ is shown in Fig. 5 as well. Line segments and triangles d_i^{-1} used to cover the boundary of $D^{-1}(i\omega, b_i)$ are shown in Fig. 6. Parameter n is equal to 1 in Fig. 6—note that there are a total of $2^{(n+2)} = 8$ triangles and line segments. When each of the d_i^{-1} is multiplied by $N(i\omega, a_i)$ the convex hulls indicated by dashed lines in Fig. 7 are formed. Parameter n is equal to 2 in Fig. 7, so there are a total of $2^{(n+2)} = 16$ convex hulls. The union of these convex hulls is the uncertainty region corresponding to the rational part of the transfer function. Rational uncertainty regions multiplied by low- and high-time-delay terms are located in Fig. 7. (Since $\theta_{\min} = 0$ in (24) the union of convex hulls is one of these regions.) The final uncertainty region $\pi(i\omega)$ is enclosed when the two regions are connected by circular arcs as shown.

2.2. *Using the internal model control design procedure*

Once the process uncertainty regions $\pi(\omega)$ have been located following the procedure outlined above, controller design can begin. A robust controller design procedure for open-loop stable systems based on Internal Model Control (IMC) has been developed. The IMC structure is illustrated in Fig. 8. The IMC design procedure is used because it requires an engineer to vary only a small number of filter parameters when tuning the controller for robustness. First a controller $\tilde{q}(s)$ is designed to yield H_2 optimal performance for the nominal plant (model). Then a filter is employed to 'detune' the controller ($q(s) = \tilde{q}(s)f(s)$) and achieve robustness. In many instances (see the example) only a single filter parameter need be adjusted. The IMC structure guarantees stability of the nominal closed-loop system for *any* stable filter. This and

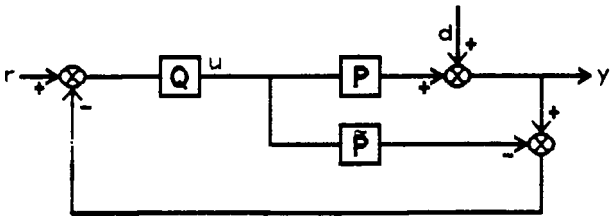

Figure 8. The internal model control structure with plant $\tilde{p}$ and controller q.

the transparent relationship between filter parameters and control system performance is largely responsible for the effectiveness of IMC as a design tool.

IMC is used for controller synthesis in the example. However, region mapping techniques presented here can be used for control system analysis in conjunction with any controller design method. The procedure involves the steps in §§ 2.2.1–2.2.7.

2.2.1. *Specifying performance criteria*

The maximum magnitude of the sensitivity function for all plants within the uncertainty description is specified as a function of frequency according to (4).

2.2.2. *Designing a controller for the nominal plant*

The nominal model $\tilde{p}(s)$ is chosen as that given by (7) with all parameters a_i, b_i and θ at their mean values. An H_2 optimal controller $\tilde{q}(s)$ is designed for this nominal model. The optimal $\tilde{q}(s)$ depends on the type of inputs expected. For step inputs the optimal $\tilde{q}(s)$ can be designed as follows: (i) factor the nominal plant into $\tilde{p}(s) = p_+(s)p_-(s)$, where $p_-^{-1}(s)$ is stable and causal and $|p_+(s)| = 1$; and (ii) set the controller $\tilde{q}(s)$ equal to $p_-^{-1}(s)$. Methods for performing this factorization and designing the H_2 optimal controller can be found in Holt and Morari (1985 a, b).

2.2.3. *Selecting the IMC filter*

The IMC controller $q(s)$ given by (25) below is equal to the H_2 optimal controller multiplied by a filter $f(s)$; a convenient form for the filter is $f(s) = (\varepsilon s + 1)^{-n}$, where the power n is selected large enough for q to be proper or to have a zero-pole excess of one if derivative action is desired; for a model given by (26) the filter $f(s) = (\varepsilon s + 1)^{-1}$:

$$q(s) = \tilde{q}(s)f(s) \tag{25}$$

$$\tilde{p}(s) = \frac{k \exp(-\theta s)}{\tau s + 1} \tag{26}$$

The filter parameter ε is adjusted to meet stability and performance requirements. A small value for ε yields faster system response, whereas a large ε detunes the system and results in greater stability margins.

2.2.4. *Determining the controller $c(i\omega)$*

The standard feedback controller $c(s)$ is related to the IMC controller $q(s)$ by

$$c(s) = \frac{q(s)}{1 - \tilde{p}(s)q(s)} \tag{27}$$

2.2.5. *Mapping the regions* $\pi(\omega)c(i\omega)$

Regions $\pi(\omega)c(i\omega)$ that describe uncertainty in the loop transfer function must be located for stability and performance analysis. The boundary of $\pi(\omega)$ is multiplied by the controller transfer function evaluated at the same frequency to locate the new regions. Multiplication of region $\pi(\omega)$ by a complex number simply scales and translates the region on the complex plane. When the process uncertainty regions are multiplied by the controller in this manner it will be referred to as mapping the regions to the Nyquist or *pc* plane.

2.2.6. *Testing stability robustness*

Regions $\pi(\omega)c(i\omega)$ are examined to evaluate robust stability. Nominal stability is not an issue because the nominal closed-loop system is stable for any stable filter. If none of the regions $\pi(\omega)c(i\omega)$ contain $(-1, 0)$ then robust stability has been achieved. If the closed-loop system is found to be unstable when process uncertainty regions are mapped to the Nyquist plane the filter bandwidth is decreased (by increasing the parameter ε) requiring the designer to return to step 2.2.5.

2.2.7. *Testing performance robustness*

Performance robustness is evaluated by finding the minimum distance from each region $\pi(\omega)c(i\omega)$ to the critical point $(-1, 0)$. If this minimum distance satisfies (6) then performance robustness has been guaranteed. Increasing the filter parameter ε will increase the distance from the critical point for open-loop stable systems.

2.2.8. *Example*

In this example a controller is designed following the recommended procedure for the model given by (28); graphical outputs that could be included in a computer-aided controller design program illustrate the example:

$$p(s) = \frac{k \exp(-\theta s)}{\tau s + 1} \tag{28}$$

$$k \in [11, 14], \quad \theta \in [9, 11], \quad \tau \in [7, 13]$$

$$\tilde{p}(s) = p_n(s) = \frac{12{\cdot}5 \exp(-10s)}{10s + 1}$$

$$p_1(s) = \frac{11 \exp(-9s)}{7s + 1}, \quad p_2(s) = \frac{14 \exp(-9s)}{7s + 1}$$

$$p_3(s) = \frac{14 \exp(-11s)}{7s + 1}, \quad p_4(s) = \frac{14 \exp(-11s)}{13s + 1}$$

$$p_5(s) = \frac{11 \exp(-11s)}{13s + 1}, \quad p_6(s) = \frac{11 \exp(-9s)}{13s + 1}$$

One process uncertainty region corresponding to the model in (28) evaluated at $\omega = 0{\cdot}15$ rad/s is displayed with a solid boundary in Fig. 9. Regions $\pi(\omega)$ for several frequencies within the range of interest are shown in Fig. 10. Discs centred at $\tilde{p}(i\omega)$ have been included in Fig. 10 to enable comparison between designs based on the actual and approximate uncertainty regions.

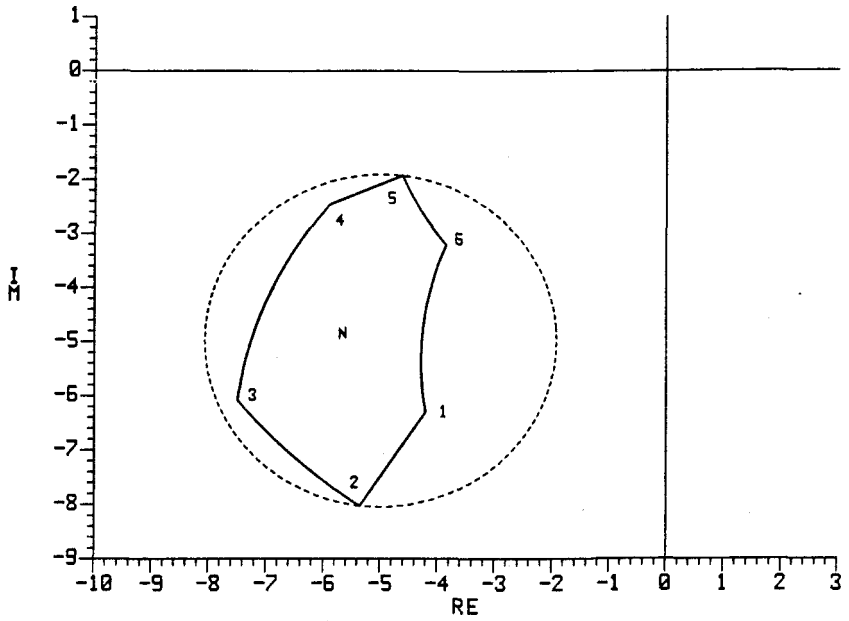

Figure 9. The uncertainty region $\pi(\omega)$ corresponding to the model in (28) evaluated at $\omega = 0{\cdot}15$ rad/s. The smallest circle containing $\pi(\omega)$ could be used as a norm-bounded approximation to the actual uncertainty.

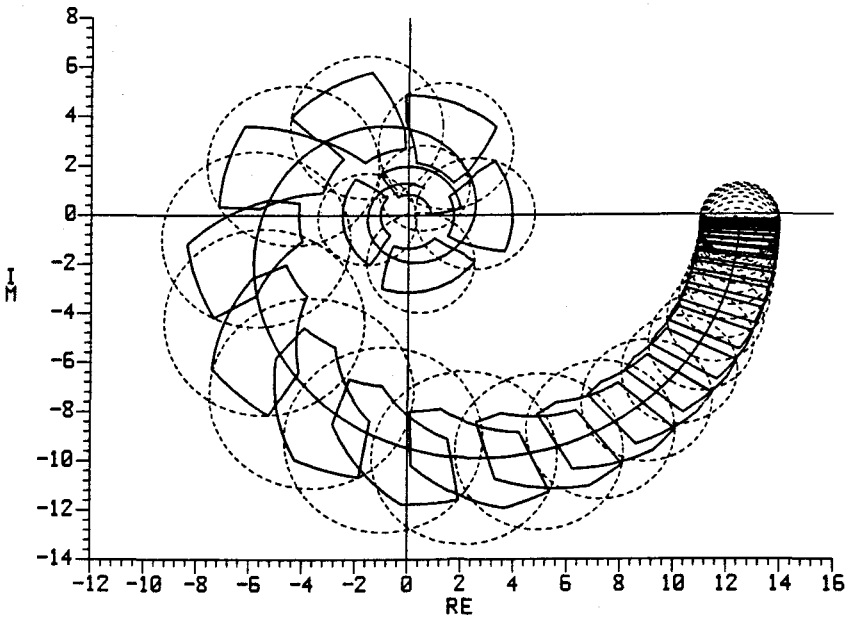

Figure 10. Uncertainty regions $\pi(\omega)$ corresponding to the model in (28) for 30 frequencies in the range $0{\cdot}001 \leqslant \omega \leqslant 1$. The nominal model passes through the center of each region. Discs centred at the nominal model containing the actual uncertainty regions are shown.

The weighting functions illustrated in Fig. 2 are used in this example. Transfer functions for the weights $w_d(s)$, $w_e(s)$ and $w_2(s)$ are given by

$$w_d(s) = \frac{s + 0{\cdot}1}{2{\cdot}5(s + 0{\cdot}02)} \tag{29}$$

$$w_e(s) = \frac{s + 0{\cdot}02}{s} \tag{30}$$

$$w_2(s) = \frac{s + 0{\cdot}1}{2{\cdot}5s} \tag{31}$$

With these weights the bound $|1/w_2(i\omega)| = |2{\cdot}5i\omega/(i\omega + 0{\cdot}1)|$ is placed on the magnitude of the sensitivity function. This bound is illustrated in Fig. 2 (*d*).

The nominal model is factored into $\tilde{p}(s) = p_+(s)p_-(s)$, where $p_+(s) = \exp(-10\ s)$ and $p_-(s) = 12{\cdot}5/(10s + 1)$. The IMC filter is selected to be $f(s) = (\varepsilon s + 1)^{-1}$. This results in an IMC controller given by $q(s) = (10s + 1)/(12{\cdot}5(\varepsilon s + 1))$. The filter parameter ε is varied as directed in §§ 2.2.6 and 2.2.7 until robust performance is achieved with $\varepsilon = 7$. Uncertainty regions $\pi(\omega)c(i\omega)$ are located as shown in Fig. 11.

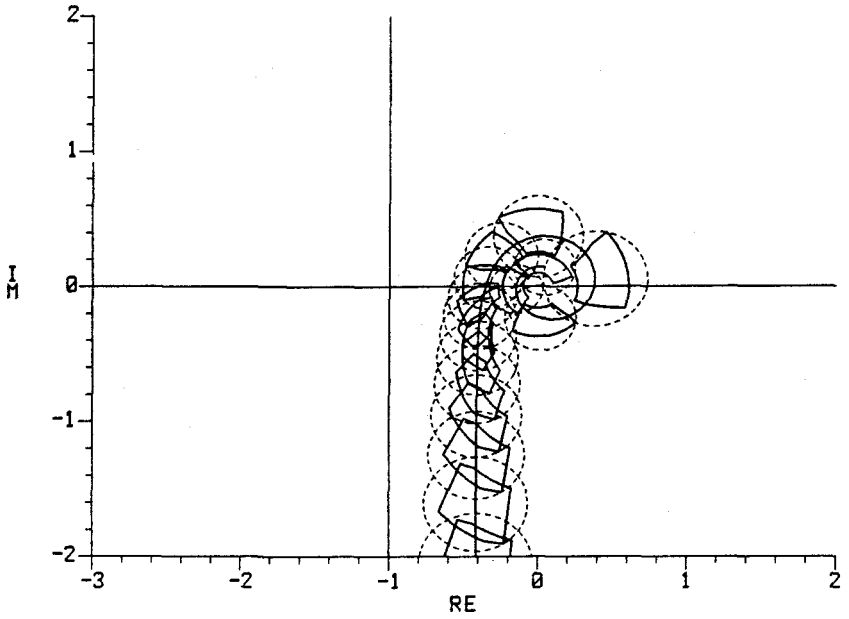

Figure 11. Uncertainty regions $\pi(\omega)c(i\omega)$ on the Nyquist plane. Robust stability requires that none of the regions contain the critical point $(-1, 0)$.

Since none of the regions *pc* intersect $(-1, 0)$ when $\varepsilon = 7$, the Nyquist stability criterion is satisfied. The maximum peak in the sensitivity function generated by the actual process uncertainty regions is determined to be approximately 2·15. Figure 12 illustrates that (4) is satisfied to achieve performance robustness. If the disc-shaped uncertainty regions are used to approximate the actual uncertainty regions, Fig. 12

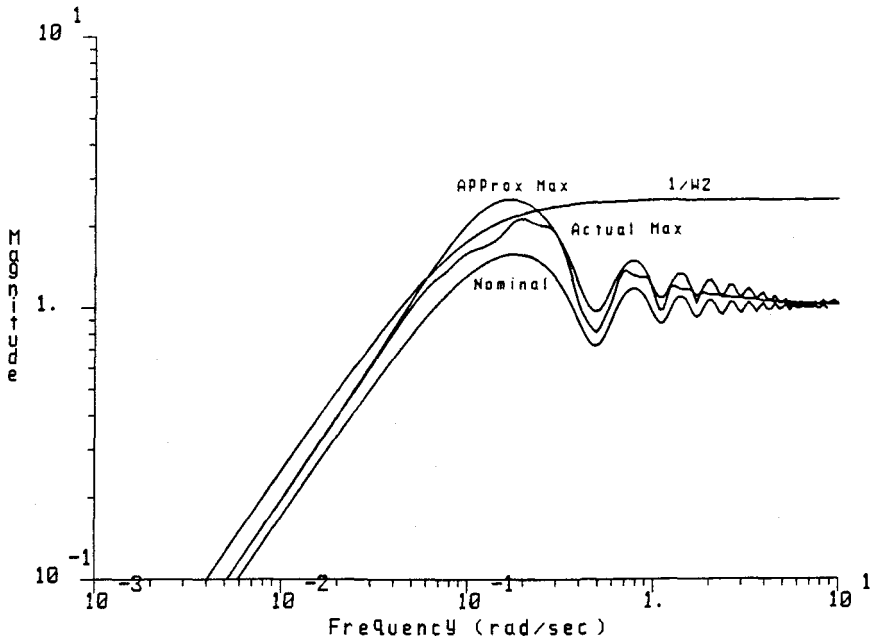

Figure 12. Maximum peaks in the sensitivity function with $\varepsilon = 7$ for the nominal model in (28), the actual uncertainty regions $\pi(\omega)$, and the disc-shaped approximations. Performance requirement $|1/w_2(i\omega)|$ is also shown.

indicates that (4) will not be satisfied. The maximum peak in the sensitivity function generated by the disc-shaped regions is greater than that caused by the actual uncertainty regions. Use of the approximate uncertainty regions results in a more conservative design since the controller must be further detuned to meet performance specifications.

When the disc-shaped uncertainty regions are used, the structured singular value $\mu(M)$ for the system with $\varepsilon = 7$ can be calculated via (15). Figure 13 indicates that $\mu(M) > 1$ for a range of frequencies around 0·1 rad/s, so robust performance cannot be guaranteed for all plants within the disc-shaped uncertainty specification. The frequency range where $\mu(M) > 1$ corresponds to that where the maximum magnitude of the sensitivity function exceeds $|1/w_2(i\omega)|$ in Fig. 12. Once again, this illustrates that approximating parameter uncertainty descriptions by norm-bounded uncertainty descriptions will introduce conservativeness into the controller design procedure.

The effect of different filter parameters ε on the maximum magnitude of the sensitivity function is illustrated in Fig. 14. Note the transparent relationship between the IMC filter parameter and performance. Increasing ε lowers both the maximum peak in the sensitivity function and the bandwidth.

Once the maximum magnitude of the sensitivity function satisfies performance requirements the analysis is complete. The IMC controller is then guaranteed to provide robust stability and performance for all plants within the uncertainty specification. Closed-loop step responses achieved with the IMC controller having $\varepsilon = 7$ are illustrated in Fig. 15. Responses for both the nominal plant and the 'extreme' plants given by (28) are included.

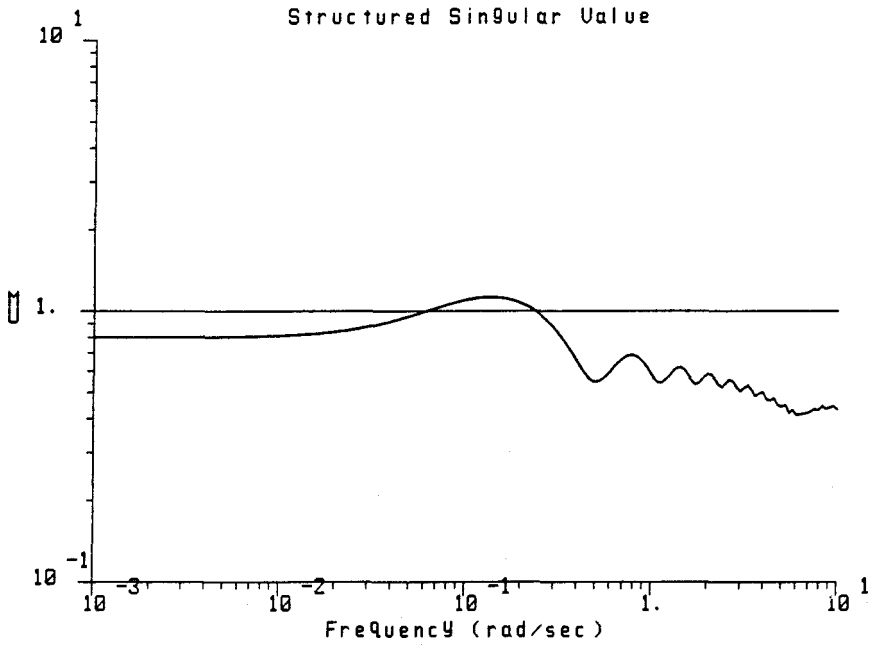

Figure 13. Structured singular-value $\mu(M)$ for the system with $\varepsilon = 7$. Disc-shaped uncertainty regions in Fig. 10 were used to calculate weight $w_1(i\omega)$ in (15).

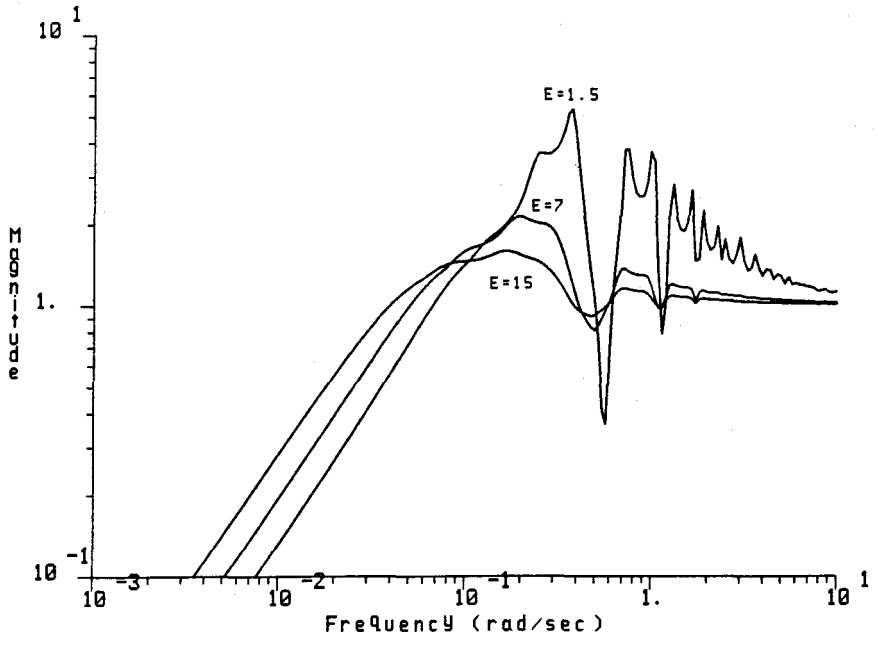

Figure 14. Maximum peaks in the sensitivity function for different values of the filter parameter ε.

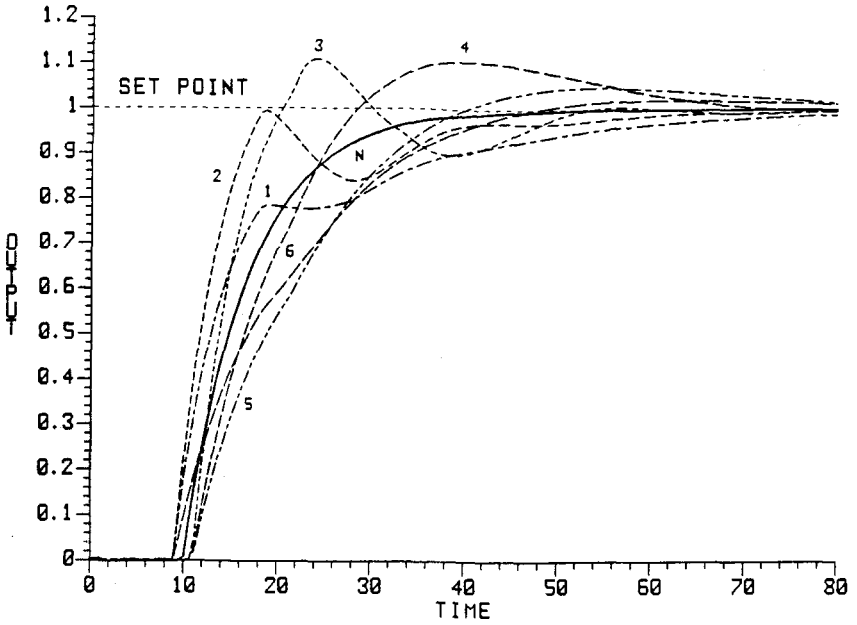

Figure 15. Closed-loop step responses of the nominal model and several 'extreme' plants for the system with IMC filter parameter $\varepsilon = 7$.

2.3. *Comparing Smith predictor with PID control*

The region mapping technique affords a unique opportunity to examine the relative robustness of Smith predictor and PID-with-first-order-filter controllers. The IMC design procedure leads to a PID controller with first-order lag when a first order Padé is used to approximate the time-delay in (26) (Rivera 1984). General expressions for Smith predictor and PID controllers resulting from the model in (28) are given by

$$c_{\text{Smith}}(s) = \frac{\tau s + 1}{k(1 + \varepsilon s - \exp(-\theta s))} \tag{32}$$

$$c_{\text{PID}}(s) = \frac{(\tau s + 1)(\frac{1}{2}\theta s + 1)}{ks(\varepsilon + \theta + \frac{1}{2}\theta\varepsilon s)} \tag{33}$$

Both controllers were applied with $\varepsilon = 7$ to the family of plants described by (28). Maximum peaks in the sensitivity function for both controllers are compared in Fig. 16, which indicates that there is relatively little difference in the maximum magnitude of the sensitivity functions when either a PID or Smith predictor controller is used to control the process in (28). The closed-loop step responses of the nominal and 'extreme' plants with a PID controller are indistinguishable from those in Fig. 15 with a Smith predictor controller.

It should be realized that the process represented by (28) has quite a large variation in each of the parameters. When smaller variations in the parameters occur, as in (34), the maximum magnitudes of the sensitivity functions are less alike. Figure 17 illustrates maximum magnitudes of the sensitivity function for both PID and Smith

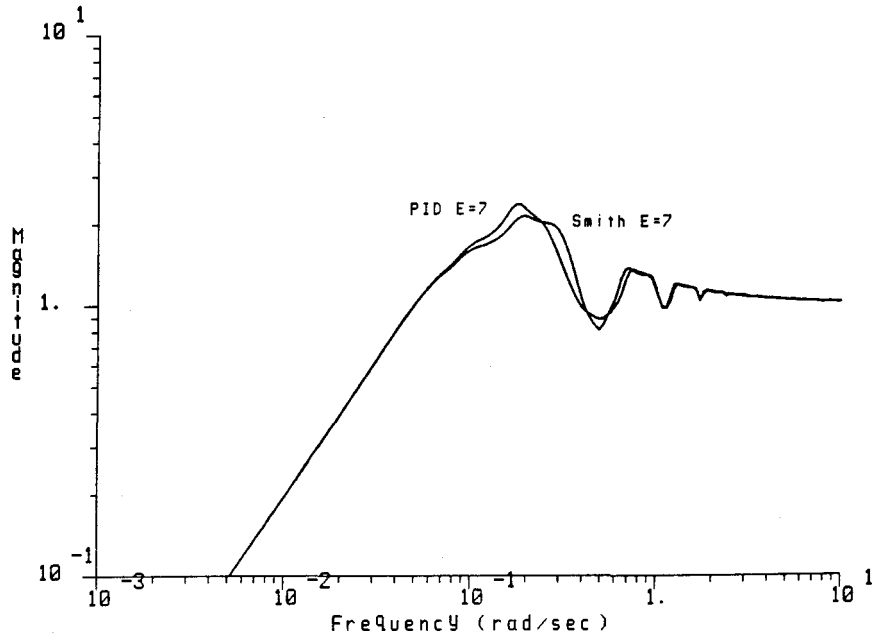

Figure 16. Maximum peaks in the sensitivity function for $c_{\text{Smith}}(s)$ and $c_{\text{PID}}(s)$ applied to the set of models (28).

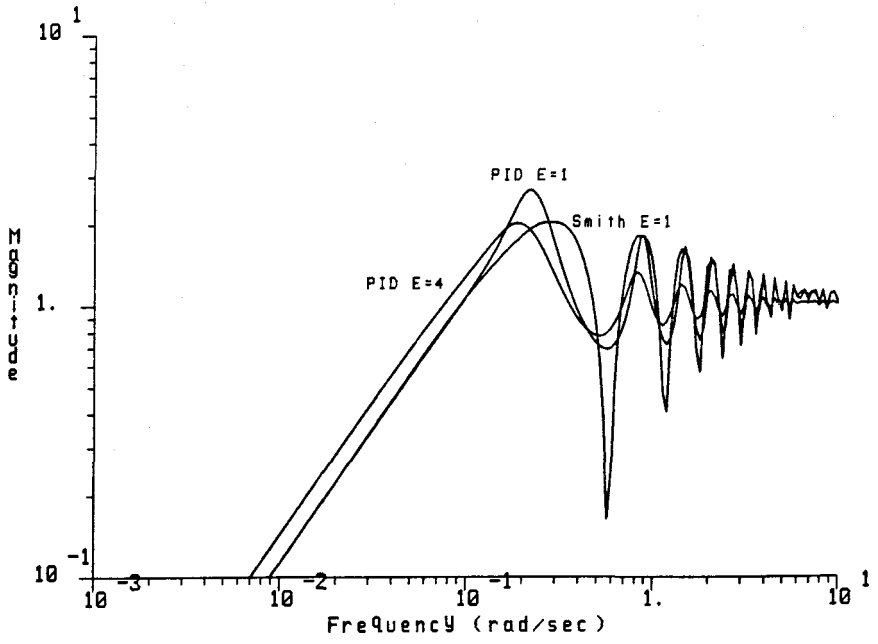

Figure 17. Maximum peaks in the sensitivity function for $c_{\text{Smith}}(s)$ and $c_{\text{PID}}(s)$ applied to the set of models (34).

predictor controllers applied to the process described by

$$p(s) = \frac{k \exp(-\theta s)}{\tau s + 1} \tag{34}$$

$$k \in [12{\cdot}25, 12{\cdot}75], \quad \theta \in [9{\cdot}9, 10{\cdot}1], \quad \tau \in [9{\cdot}8, 10{\cdot}2]$$

For the smaller uncertainty regions described by (34), the maximum peak with the PID controller is higher than that with the Smith Predictor having the same filter parameter. When a filter parameter $\varepsilon = 1$ is used in the Smith predictor, a filter parameter of $\varepsilon = 4$ must be used in the PID controller to yield the same maximum peak. The resulting PID controller has narrower bandwidth and worse performance than the Smith predictor. Closed-loop step responses of nominal and 'extreme' plants with the two controllers are illustrated in Figs. 18 and 19. It is clear from these figures that the Smith predictor step response is superior to the PID step response for the given process. This example suggests that, although relatively little difference in PID versus Smith Predictor performance is observed when there is large process uncertainty, greater difference in performance will result when the process is more accurately known.

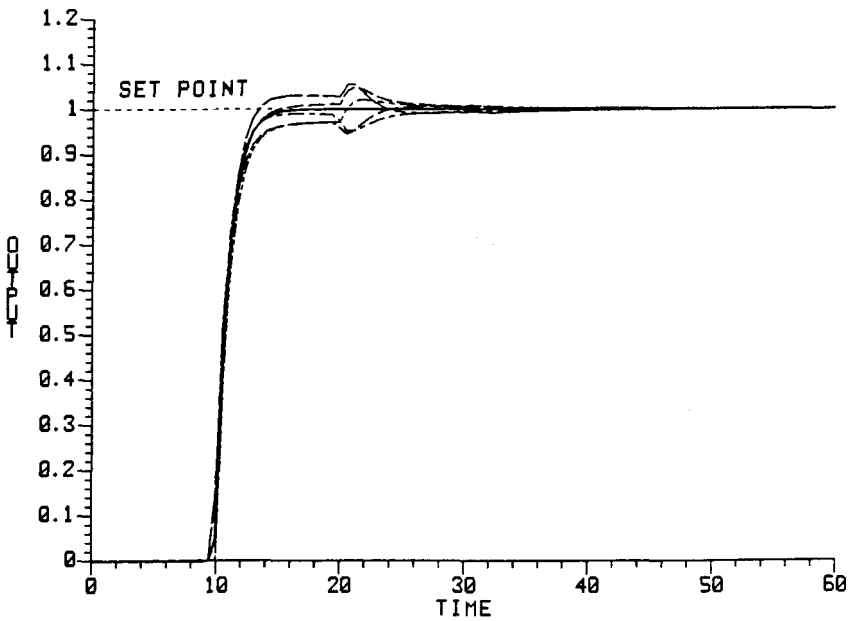

Figure 18. Closed-loop step responses of the nominal model and several 'extreme' models in (34) with Smith predictor controller. The IMC filter parameter is $\varepsilon = 1$.

2.4. *MIMO applications*

Exact uncertainty regions for the SISO transfer function *pc* are easily located once process uncertainty regions are specified. In contrast, exact uncertainty regions for elements in the MIMO transfer matrix *PC* cannot be located when individual element uncertainty regions are specified. If region-mapping is used to locate an uncertainty

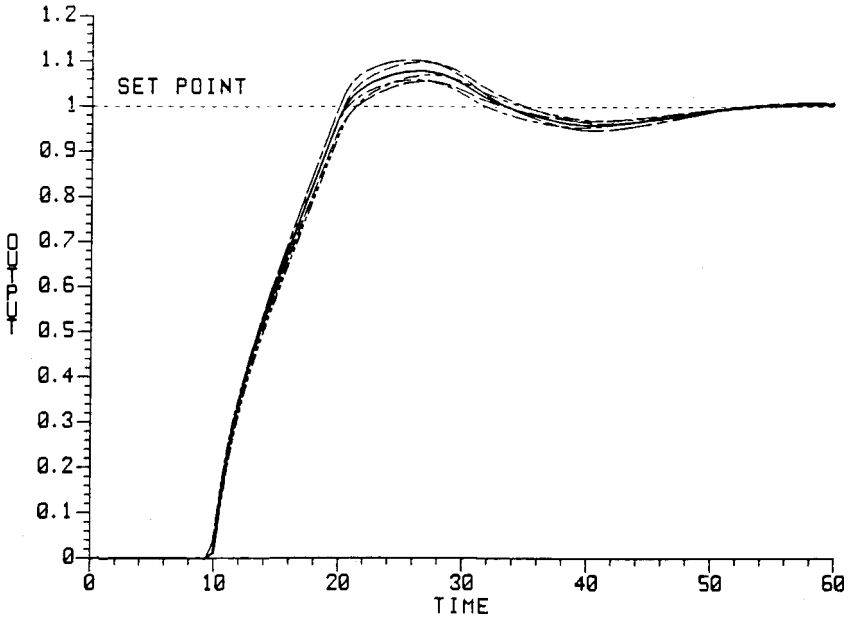

Figure 19. Closed-loop step responses of the nominal model and several 'extreme' models in (34) with PID and first-order lag controller. The IMC filter parameter is $\varepsilon = 4$.

region corresponding to an element in PC the result will always be conservative. The origin of this conservativeness is easily understood by considering the 2×2 transfer matrix PC below:

$$C = \begin{bmatrix} c_{11} & c_{12} \\ c_{21} & c_{22} \end{bmatrix}$$

$$P = \begin{bmatrix} p_{11} & p_{12} \\ p_{21} & p_{22} \end{bmatrix}$$

$$PC = \begin{bmatrix} p_{11}c_{11} + p_{12}c_{21} & p_{11}c_{12} + p_{12}c_{22} \\ p_{21}c_{11} + p_{22}c_{21} & p_{21}c_{12} + p_{22}c_{22} \end{bmatrix} \tag{35}$$

More than one element in the MIMO loop-transfer matrix contain the same plant transfer function element. For example, both $[PC]_{11}$ and $[PC]_{12}$ contain the plant element p_{11}. If regions on the complex plane are used to represent $[PC]_{11}$ and $[PC]_{12}$ the correlation between these elements caused by p_{11} is lost; that is, all occurrences of p_{ij} in the matrix PC are assumed to be independent uncertainties. Since the loss of correlation between elements in the MIMO loop-transfer matrix introduces arbitrary conservativeness, region-mapping is impractical in the MIMO case.

Structured singular-value analysis preserves correlation between elements in the MIMO loop-transfer matrix. However, application of structured singular-value analysis requires that disc-shaped uncertainty regions be used to represent elements in the MIMO plant matrix P. The proposed method for locating uncertainty regions can be used to locate these discs when elements in P are described by Laplace transfer

functions with uncertain coefficients. If the smallest disc containing the actual process uncertainty region at each frequency has radius $W_{ij}(\omega)$ an approximate additive uncertainty $E_{ij}(s)$ can be specified such that $P_{ij}(s) = \tilde{P}_{ij}(s) + E_{ij}(s)$ and $|E_{ij}(i\omega)| \leqslant W_{ij}(\omega)$. A multiplicative uncertainty $L_{ij}(s)$ can then be defined such that $P_{ij}(s) = [1 + L_{ij}(s)]\tilde{P}_{ij}(s)$ where $|L_{ij}(i\omega)\tilde{P}_{ij}(i\omega)| \leqslant W_{ij}(\omega)$. Once a multiplicative uncertainty has been specified, the controller design problem can be rewritten in a form allowing application of structured singular value analysis. Figure 9 illustrates how an additive uncertainty can be used to approximate parameter uncertainties in (28). The accuracy of the approximation depends on the shape of the actual region representing the parameter uncertainties. If the actual region is very nearly disc-shaped the approximation will be quite accurate. The regions representing parameter uncertainties in (28) are closer to disc shapes than those in

$$p(s) = \frac{k \exp(-\theta s)}{\tau_i s + 1} \tag{36}$$

$$k \in [12{\cdot}25, 12{\cdot}75], \quad \theta \in [8, 12], \quad \tau \in [9{\cdot}8, 10{\cdot}2]$$

Comparatively large time-delay uncertainty in (36) stretches the corresponding uncertainty regions into shapes that are not accurately approximated by discs. Conservativeness that results from approximating the parameter uncertainties in (36) by discs can be seen by comparing the maximum magnitudes of the sensitivity functions in Fig. 20. Peaks due to the disc-shaped approximations are considerably higher than the actual peaks.

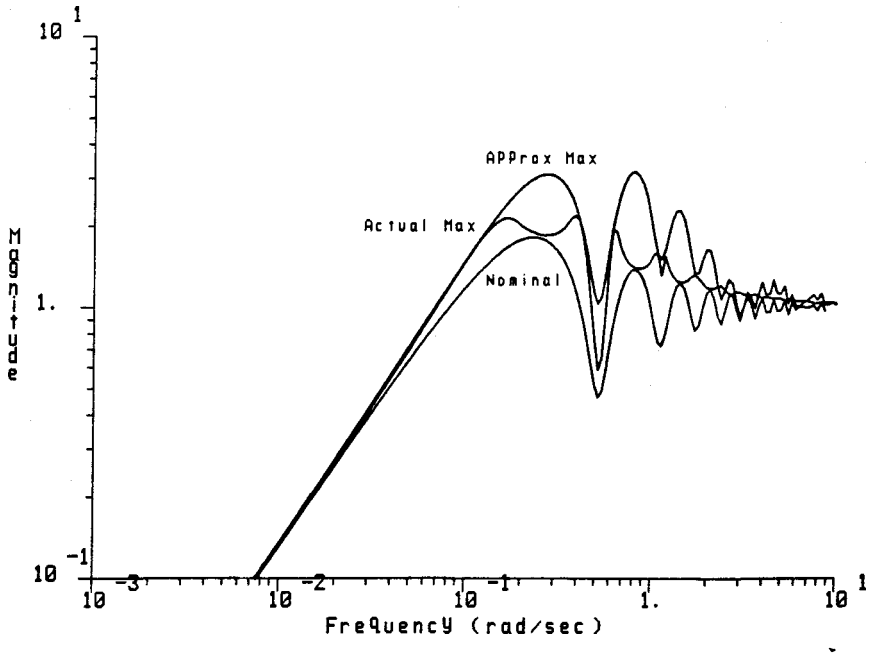

Figure 20. Maximum peaks in the sensitivity function corresponding to the nominal model in (36), the actual uncertainty regions $\pi(\omega)$, and the disc-shaped approximations.

3. Discussion and conclusions

The proposed techniques for locating process uncertainty regions on the complex plane and for mapping them to the Nyquist plane are useful control system design tools. They are particularly applicable when process identification results in models with parameter uncertainties. Required calculations are quickly performed by personal computers found in most engineering environments. Moreover, process uncertainty regions can be displayed on modern graphics terminals. With these computer resources in hand, the proposed technique can be conveniently applied to control system design problems. By viewing process uncertainty regions and noting how they map to the Nyquist plane, the designer can see transparent relationships between adjustable IMC filter parameters and performance.

Computer-aided design can make the proposed region-mapping techniques accessible to the control engineer. The software will allow the user to enter either parameter uncertainties or uncertainty region boundaries. The user will also enter weights $w_d(i\omega)$ and $w_e(i\omega)$ to specify performance requirements. The computer can then locate and store uncertainty region boundaries for a desired number of frequencies. The computer can be programmed to calculate the IMC controller automatically and map the regions $\pi(\omega)c(i\omega)$ to the Nyquist plane. The Nyquist plot can be furnished to the user for a visual stability evaluation. Maximum peaks in the sensitivity function can be output to the user and compared with performance requirements. If performance requirements are not met the user will specify changes in the IMC filter until a robust controller has been designed.

The proposed technique offers several advantages over existing control system analysis methods. First, the proposed technique allows incorporation of arbitrarily shaped uncertainty regions into the analysis procedure, whereas loop-shaping and structured singular-value analysis require the use of norm-bounded uncertainties. Secondly, the proposed method allows the designer to see the exact characteristics of the loop transfer function and the sensitivity function in the critical crossover region. Thirdly, the proposed method for locating process uncertainty regions results in a region guaranteed to contain the actual process uncertainty region. Fourthly, the use of IMC control structure allows the designer to tune the system by adjusting relatively few filter parameters. Finally, by following the recommended procedure the control system designer can accurately determine norm-bounded uncertainties to approximate uncertainty descriptions that result directly from process identification.

References

BOLTON, A. G., 1981, *Int. J. Control*, **33**, 575.

Chen, S., 1984. Control system design for multivariable uncertain processes. Ph.D. thesis, Case Western Reserve University.

DOYLE, J. C., 1982, *Proc. Instn elect. Engrs*, Pt.D, **129**, 242.

DOYLE, J. C., and STEIN, G., 1981, *I.E.E.E. Trans. autom. Control*, **26**, 4.

EAST, D. J., 1982, *Int. J. Control*, **35**, 891.

GARCIA, C. E., and MORARI, M., 1982, *I & EC Process Des. & Dev.*, **21**, 308.

HENRICI, P., 1974, *Applied and Computational Complex Analysis*, Vol. 1 (New York: Wiley).

HOLT, B. R., and MORARI, M., 1985 a, *Chem. Engng Sci.*, **40**, 59; 1985 b, *Ibid.*, **40**, 1229.

HOROWITZ, I. M., 1982, *Proc. Instn. elect. Engrs*, Pt.D, **129**, 215.

KUROZUMI, Y., and DAVIS, W., 1982, *Comput. Graph. Image Process*, **19**, 248.

KRISHNAN, K. R., and CRUICKSHANKS, A., 1977, *Int. J. Control*, **25**, 610.

MORARI, M., and SKOGESTAD, S., 1985, Effect of model uncertainty on dynamic resilience. *Proc. PSE 85*, Cambridge, April 1985; *IChE Symp. Ser.*, No. 92.

RIVERA, D. E., MORARI, M., and SKOGESTAD, S., 1986, *I & EC Process Des. Dev.*, **25**, 252.

CHAPTER IV: SMITH PREDICTOR DESIGN FOR ROBUST PERFORMANCE

INT. J. CONTROL, 1987, VOL. 46, NO. 2, 477–504

Smith predictor design for robust performance

DANIEL L. LAUGHLIN†, DANIEL E. RIVERA† and MANFRED MORARI†

A method is outlined for designing Smith predictor controllers that provide robust performance despite real parameter uncertainties in the process model. Insight into the design process is gained by viewing the Smith predictor from the perspective of internal model control. Performance requirements are written in terms of a frequency-domain weight restricting the magnitude of the closed-loop sensitivity function. A general method for approximating multiple parameter uncertainties by a single multiplicative uncertainty is developed—an exact bound is derived for the magnitude of multiplicative uncertainty used to approximate simultaneous uncertainties in process gain, time-constant, and time-delay. Three different tuning methods are demonstrated; each is applied to a wide range of parameter uncertainties in a first-order with time-delay model. The first tuning method locates loop transfer-function uncertainty regions to test for robust performance—real parameter uncertainties are considered exactly. The second tuning method approximates real parameter uncertainties by multiplicative uncertainty and uses structured singular value analysis to guarantee robust performance. The third is a 'quick design' method that considers the unit magnitude crossing of the multiplicative uncertainty. Finally, the Smith predictor controller is compared with the structured-singular-value-optimal controller.

1. Introduction

Callender *et al.* (1936) recognized the importance of time-lag in a control system more than fifty years ago. In the last five decades their 'controlling gear' and 'control apparatus' has given way to high speed digital computers, but the basic problem remains the same: robust controllers must be designed for systems with time-delay. In particular, the chemical process industries require controllers that can cope with material transport delays, composition analysis delays and other delays that cannot be avoided.

1.1. *Smith predictors*

Early researchers addressed the problem of controller design for systems with time-delay by correlating PID controller settings with model gain, time-constants and time-delay (e.g. Cohen and Coon 1953). Low loop gains were required to avoid instability when time-constants were small compared to the time-delay, leading to poor system performance. Smith enabled larger loop gains to be used by incorporating a minor feedback loop around a conventional controller (see Fig. 1) to stabilize the system (Smith 1957). The effect of the minor feedback loop has been described as similar to that of a lead network with considerable lead (Åström 1977). The Smith predictor controller has been particularly successful in tracking step commands when applied to systems with the ability to respond quickly (systems with small time-constants) despite large time-delays between the controller and the plant input

Received 9 September 1986. Revised 31 October 1986.

† Chemical Engineering 206-41, CALTECH, Pasadena, CA 91125, U.S.A.

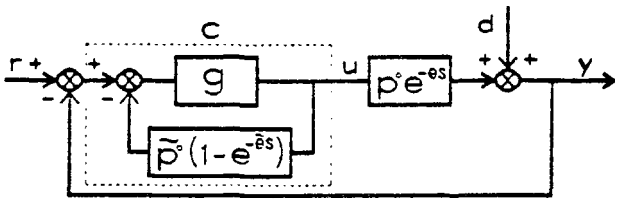

Figure 1. The Smith predictor control structure. A conventional controller g and a minor feedback loop are used to control systems with time-delay.

(Horowitz 1983). In the absence of modelling error the Smith predictor has been shown to lead to optimal response to step disturbances. Although first suggested for use in single-input–single-output (SISO) systems, the Smith predictor concept for controlling systems with time-delay has been extended to multivariable systems (e.g. Holt 1984, Palmor 1985, Bhaya and Desoer 1985, Jerome and Ray 1986).

1.2. *Robust performance for systems with time-delay*

Only recently have researchers attempted to quantify the Smith predictor controller's robustness to modelling errors. In several studies stability boundaries were plotted as functions of error in a single plant parameter (Ioannides *et al.* 1979, Palmor 1980, Palmor and Shinnar 1981). Brosilow (1979) proposed a method for tuning the Smith predictor when one model parameter was uncertain: either gain, time-constant, or time-delay. Owens and Raya (1982) consider the effect of additive plant/model mismatch on the robust stability of Smith predictor controllers and derive an expression for a bound on the magnitude of multiplicative uncertainty used to approximate time-delay uncertainty. All these studies failed to consider the effect of *simultaneous* uncertainties in gain, time-constant, and time-delay on the robustness of Smith predictors. Finally, Chen (1984) addressed this failure by locating regions on the complex plane corresponding to first-order models with uncertain gain, time-constant, and time-delay. Chen correctly evaluated *robust stability* of Smith predictor controllers using these regions. The question of *robust performance* of Smith predictor controllers despite simultaneous parameter uncertainties remained unanswered.

The research results presented here address the question of robust performance of Smith predictor controllers. A systematic design procedure is presented that will guarantee robust Smith predictors despite uncertainties in model parameters. Specific results include:

(1) a concise method for designing robust Smith predictor controllers with a single tuning parameter;

(2) a method for tuning the controllers for robustness with respect to simultaneous uncertainties in gain, time-constant, and time delay or with respect to uncertainty in an even greater number of model parameters; and

(3) a rigorous test for robust performance with respect to parameter uncertainties.

2. Modelling uncertainty in processes with time-delay

It is often convenient to model processes with transfer-functions containing real-parameter uncertainties as in

$$\Pi' = \left\{ p(s) \mid p(s) = p'(s)\left[\frac{a_n s^n + a_{n-1}s^{n-1} + \ldots + a_1 s + a_0}{b_m s^m + b_{m-1}s^{m-1} + \ldots + b_1 s + b_0}\right]\exp(-\theta s)\right\} \qquad (1)$$

$$a_i \in [a_{i_{\min}}, a_{i_{\max}}], \quad b_i \in [b_{i_{\min}}, b_{i_{\max}}], \quad \theta \in [\theta_{\min}, \theta_{\max}]$$

or

$$\Pi' = \left\{ p(s) \mid p(s) = p'(s)\left[\frac{k\Pi_i((1/z_i)s+1)}{\Pi_i((1/p_i)s+1)}\right]\exp(-\theta s)\right\} \tag{2}$$

$$z_i \in [z_{i_{\min}}, z_{i_{\max}}], \quad p_i \in [p_{i_{\min}}, p_{i_{\max}}], \quad k \in [k_{\min}, k_{\max}], \quad \theta \in [\theta_{\min}, \theta_{\max}]$$

For example, the parameter bounds may represent uncertain process flow rates, uncertainty introduced by linearizing a model at different steady states or variations in environmental operating conditions (temperature, pressure, relative humidity, etc.). The factor $p'(s)$ in (1) and (2) is known exactly and does not contain parameter uncertainties. A special case of (1) and (2) is the popular first-order with time-delay model (3).

$$\Pi' = \left\{ p(s) \mid p(s) = p'(s)\frac{k\exp(-\theta s)}{\tau s+1}\right\} \tag{3}$$

$$k \in [k_{\min}, k_{\max}], \quad \tau \in [\tau_{\min}, \tau_{\max}], \quad \theta \in [\theta_{\min}, \theta_{\max}]$$

The model (3) has been used extensively to describe chemical processes. Time-delay is often used in the simple model to incorporate additional phase-lag caused by ignored higher-order dynamics or to approximate the dynamics of a distributed parameter system. For example, Ogunnaike (1986) uses (3) to represent almost every element in a multivariable model for a distillation column.

The method proposed in this paper for designing robust Smith predictor controllers applies to all models (1) and (2) that are open-loop stable. The particular case (3) with simultaneous uncertainties in gain, time-constant, and time-delay will be studied in detail. Controller parameters leading to robust performance for various levels of uncertainty in these three parameters will be presented.

2.1. *Locating model uncertainty regions from parameter uncertainties*

The set of possible process models indicated by (1)–(3) can be represented at each frequency by a simply connected region $\pi(\omega)$ on the complex plane. A method has been developed for locating the regions $\pi(\omega)$ corresponding to the transfer functions in equation (1) with any required degree of accuracy (Laughlin *et al.* 1986). East (1981, 1982) outlined a conservative method for locating convex polygons containing regions corresponding to (2) when the time-delay is known exactly. A set Π of all possible process models can be defined as follows:

$$\Pi = \{ p(s) \mid p(i\omega) \in \pi(\omega), \quad \forall\omega \} \tag{4}$$

The set Π given by (4) is almost always larger than the corresponding set Π' given by (1)–(3) since some elements of Π might not be expressed by a transfer-function with the specified structure. To prove robustness requirements are met for all models in (1)–(3) it is sufficient to show that they are met for all models in the corresponding set Π.

2.2. *Translating parameter uncertainty into multiplicative error*

When modelling error is represented by uncertainty in several real parameters it is often mathematically convenient to approximate the uncertainty with a single multiplicative perturbation. Multiplicative perturbations on a nominal plant are represented by (5).

$$p(s) = \tilde{p}(s)[1 + l_m(s)], \quad |l_m(i\omega)| < l(\omega) \tag{5}$$

Using the norm-bounded multiplicative error $l_m(s)$ is equivalent to representing process uncertainty by a disc-shaped uncertainty region $\pi(\omega)$ with radius $|\tilde{p}(i\omega)|l(\omega)$ on the complex plane. The multiplicative uncertainty description can be incorporated into controller optimization techniques where parameter uncertainty descriptions are less tractable.

It is straightforward to determine the bound $l(\omega)$ on the magnitude of the multiplicative error for the general cases of parameter uncertainty (1) and (2). First the boundaries of a sufficient number of uncertainty regions $\pi(\omega)$ must be located over the frequency range of interest. Next a nominal model $\tilde{p}(i\omega)$ must be specified—in the proposed design procedure parameters will be fixed at their mean values in the nominal model. Finally the maximum distance $d(\omega)$ from $\tilde{p}(i\omega)$ to any point on the boundary of $\pi(\omega)$ is determined at each frequency. This distance $d(\omega)$ is related to the bound on the magnitude of the multiplicative error through $d(\omega) = |\tilde{p}(i\omega)|l(\omega)$.

For the special case of simultaneous uncertainties in gain, time-constant and time-delay in the first-order model (3), an exact analytical expression for the bound $l(\omega)$ can be derived. Owens and Raya (1982) derived the simple expression $l(\omega) = |\exp(\Delta\theta i\omega) - 1|$ for the bound when only uncertainties in time-delay are considered. Bound 1 specifies the smallest possible magnitude $|l_m(i\omega)| = l(\omega)$ such that all plants given by (3) with *simultaneous* errors in gain, time-constant and time-delay can be represented by $p(s) = \tilde{p}(s)[1 + l_m(s)]$.

Bound 1: *Gain, time-delay and pole uncertainty*

Consider the following set of process models:

$$p(s) = p'(s)\frac{(\bar{k} + \delta k)\exp[-(\bar{\theta} + \delta\theta)s]}{(\bar{\tau} + \delta\tau)s + 1} \tag{6}$$

where $p'(s)$ does not contain parameter uncertainties and $\bar{k}$, $\bar{\tau}$, $\bar{\theta}$, δk, $\delta\tau$ and $\delta\theta$ are defined by:

$$\bar{k} = \frac{k_{\min} + k_{\max}}{2}, \quad \bar{\tau} = \frac{\tau_{\min} + \tau_{\max}}{2}, \quad \bar{\theta} = \frac{\theta_{\min} + \theta_{\max}}{2}$$

$$|\delta k| \leqslant \Delta k = |k_{\max} - \bar{k}| < |\bar{k}|, \quad |\delta\tau| \leqslant \Delta\tau = |\tau_{\max} - \bar{\tau}| < |\bar{\tau}|, \quad |\delta\theta| \leqslant \Delta\theta = |\theta_{\max} - \bar{\theta}| < |\bar{\theta}|$$

Define a nominal model $\tilde{p}(s)$ with gain, time-constant and time-delay at their mean values:

$$\tilde{p}(s) = p'(s)\frac{\bar{k}\exp(-\bar{\theta}s)}{\bar{\tau}s + 1} \tag{7}$$

The smallest possible bound $l(\omega)$ on the multiplicative error $l_m(s)$ such that all models in (6) are contained in the set $p(s) = \tilde{p}(s)[1 + l_m(s)]$, $|l_m(i\omega)| < l(\omega)$, is given by:

$$l(\omega) = \left|\left(\frac{|\bar{k}| + \Delta k}{|\bar{k}|}\right)\left(\frac{\bar{\tau}i\omega + 1}{(\bar{\tau} \mp \Delta\tau)i\omega + 1}\right)\exp(\pm\Delta\theta i\omega) - 1\right|, \quad \forall\,\omega < \omega^* \tag{8}$$

$$l(\omega) = \left|\left(\frac{|\bar{k}| + \Delta k}{|\bar{k}|}\right)\left(\frac{\bar{\tau}i\omega + 1}{(\bar{\tau} \mp \Delta\tau)i\omega + 1}\right)\right| + 1, \quad \forall\,\omega \geqslant \omega^* \tag{9}$$

where ω^* is defined implicitly by:

$$\pm\Delta\theta\omega^* + \arctan\left[\frac{\pm\Delta\tau\omega^*}{1 + \bar{\tau}(\bar{\tau} \mp \Delta\tau)\omega^{*2}}\right] = \pm\pi, \quad \frac{\pi}{2} \leqslant \Delta\theta\omega^* \leqslant \pi \tag{10}$$

Bound 1 applies to both stable and unstable models (6). Top signs are selected in (8)–(10) if $\bar{\tau}$ is positive indicating a left-half-plane pole. Bottom signs are selected in (8)–(10) if $\bar{\tau}$ is negative indicating a right-half-plane pole. Note that Bound 1 simplifies to the expression derived by Owens and Raya (1982) when $\Delta k = \Delta\tau = 0$. Proof of Bound 1 is given in the appendix along with a similar bound on multiplicative error for the case of simultaneous variations in gain, time-delay and one process zero location. The bounds $l(\omega)$ for $\Delta k/\bar{k} = \Delta\tau/\bar{\tau} = \Delta\theta/\bar{\theta} = 0{\cdot}1$ and for $\Delta k/\bar{k} = \Delta\tau/\bar{\tau} = \Delta\theta/\bar{\theta} = 0{\cdot}5$ are shown in Fig. 2.

3. Selecting performance requirements

3.1. *Robust stability*

The standard feedback control structure is shown in Fig. 3 with commands $r(s)$, disturbances $d(s)$, outputs $y(s)$, control actions $u(s)$ and errors $e(s)$. The control structure must be stable for all process models in the set Π. Once a controller $c(s)$ is selected, robust stability can be evaluated with respect to the actual parameter uncertainties or with respect to the multiplicative uncertainty approximation. When considering the actual parameter uncertainties the closed-loop system is stable for all plants in Π if and only if a nominal system with $p(s) = \tilde{p}(s) \in \Pi$ is stable and the regions $\pi(\omega)c(i\omega)$ exclude $(-1, 0)$ for all frequencies ω. When the modelling error is described in terms of a multiplicative uncertainty as in (5), robust stability is guaranteed if and only if a nominal system with $p(s) = \tilde{p}(s) \in \Pi$ is stable and

$$|\tilde{h}(i\omega)|l(\omega) < 1, \quad \forall\,\omega \tag{11}$$

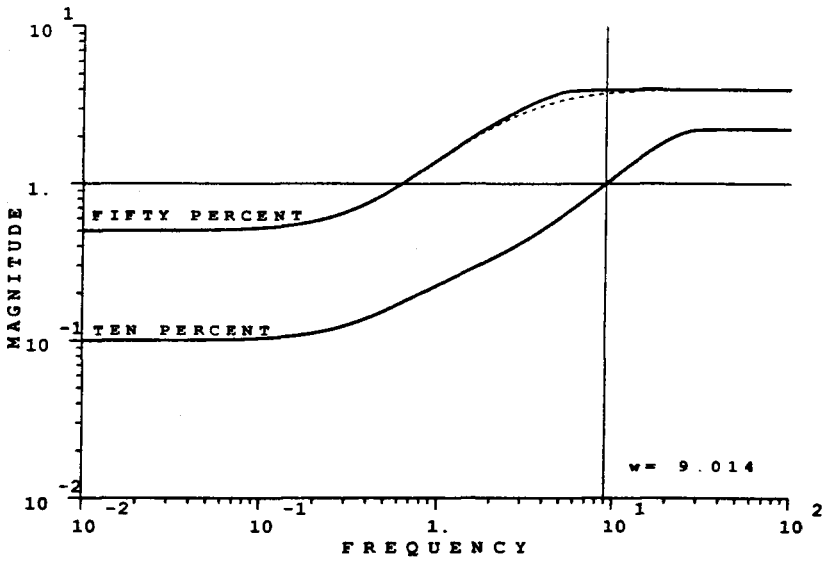

Figure 2. The bound $l(\omega)$ on the magnitude of the multiplicative uncertainty is shown for both 10 per cent parameter uncertainty and 50 per cent parameter uncertainty in model (6). At a frequency of 9·014 rad s^{-1} the bound $l(\omega) = 1{\cdot}0$ for the case of 10 per cent parameter uncertainty. The dashed curve is the magnitude of the rational function

$$l_m(s) = 1{\cdot}5\left(\frac{s+1}{0{\cdot}5s+1}\right)\left(\frac{1+0{\cdot}25s}{1-0{\cdot}25s}\right) - 1$$

used to approximate the bound $l(\omega)$ for SSV-optimal controller synthesis.

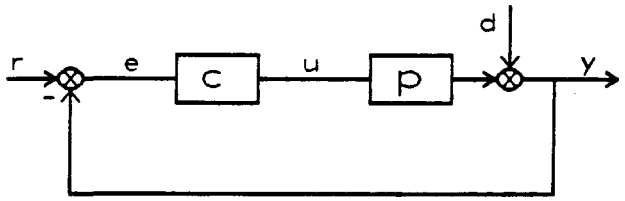

Figure 3. The standard feedback control structure with commands $r(s)$, disturbances $d(s)$, outputs $y(s)$, control actions $u(s)$ and errors $e(s)$.

where the nominal complementary sensitivity function $\tilde{h}(i\omega)$ is given by

$$\tilde{h}(i\omega) = \frac{\tilde{p}(i\omega)c(i\omega)}{1 + \tilde{p}(i\omega)c(i\omega)}$$

Condition (11) is equivalent to the condition that the disc-shaped regions with radius $|\tilde{p}(i\omega)c(i\omega)|l(\omega)$ centred at $\tilde{p}(i\omega)c(i\omega)$ exclude $(-1, 0)$ for all frequencies ω.

3.2. *Robust performance*

In addition to robust stability, 'good' command-following and disturbance-rejection are required of the control structure in Fig. 3. If the error signal $e(t) = r(t) - y(t)$ is kept 'small' for all inputs $r(t) - d(t)$, these performance objectives can be met. The errors are related to the inputs as shown in (12).

$$\frac{e(i\omega)}{r(i\omega) - d(i\omega)} = \frac{1}{1 + p(i\omega)c(i\omega)} \tag{12}$$

In this study robust performance will be defined mathematically by placing a bound on the magnitude of the sensitivity function $s(i\omega) = [1 + p(i\omega)c(i\omega)]^{-1}$.

$$|s(i\omega)| = \left|\frac{1}{1 + p(i\omega)c(i\omega)}\right| < \left|\frac{1}{w_2(i\omega)}\right|, \quad \forall\, \omega, \forall\, p(s) \in \Pi \tag{13}$$

Usually only small steady-state errors are acceptable so the magnitude of the performance weight $|w_2(i\omega)|$ is specified to be large at low frequencies and small at high frequencies. The inverse of a typical weight is shown in Fig. 4. For convenience (13) can be written as:

$$|1 + p(i\omega)c(i\omega)| > |w_2(i\omega)|, \quad \forall\, \omega, \forall\, p(s) \in \Pi \tag{14}$$

Since all plants $p(s) \in \Pi$ are restricted to lie within region $\pi(\omega)$ at frequency ω, the requirement (14) can be met by ensuring that the distance of regions $\pi(\omega)c(i\omega)$ from $(-1, 0)$ is greater than $|w_2(i\omega)|$.

When $p(i\omega) = \tilde{p}(i\omega)[1 + l_m(i\omega)]$, $|l_m(i\omega)| < l(\omega)$, (14) can be written in terms of the nominal complementary sensitivity function $\tilde{h}(i\omega) = 1 - \tilde{s}(i\omega)$ as follows:

$$\sup_{\omega} |\tilde{h}(i\omega)|l(\omega) + |(1 - \tilde{h}(i\omega))w_2(i\omega)| < 1 \tag{15}$$

Given nominal stability, both robust stability and robust performance of the control system are guaranteed if and only if condition (15) is satisfied. Condition (15) represents an additional performance specification for the complementary sensitivity function $\tilde{h}(i\omega)$ beyond the small gain theorem requirement (11) for robust stability alone.

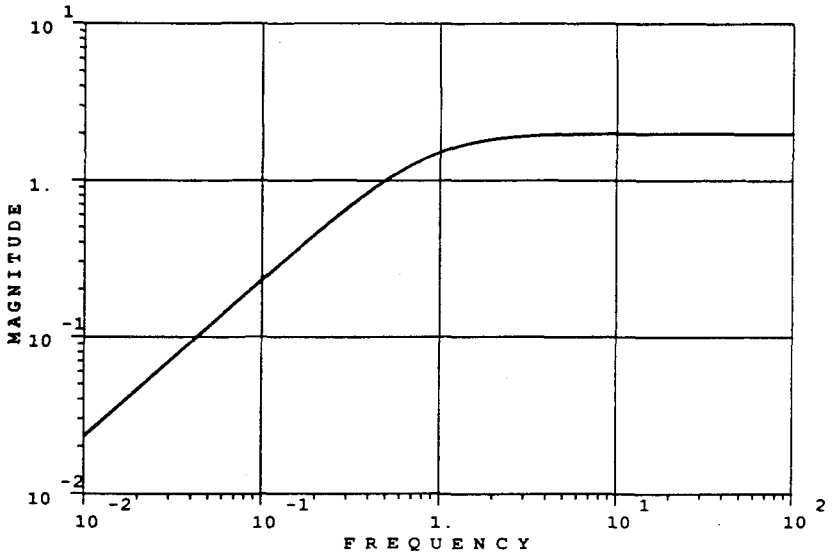

Figure 4. The inverse of the performance weight $w_2(s) = (1{\cdot}162s + 1)/2{\cdot}324s$ used for experiment 1 in Table 5. The worst-case sensitivity function must lie below this curve to satisfy the robust performance specification.

Requirement (15) is equivalent to a special case of the robust performance condition derived by Doyle (1982). Doyle defines the 'structured singular value' to be the supremum in (15).

3.3. *A performance weight for the Smith predictor problem*

Performance requirement (13) indicates that the weight $w_2(s)$ specifies a bound on the maximum peak of the sensitivity function. It is useful to examine the functional form of the H_2-optimal nominal sensitivity function for the expected inputs before selecting a performance weight for a particular problem. An expression for the H_2-optimal nominal sensitivity function for general inputs is given by the theorem in § 4.2 of this paper. If the process were known exactly the weight $w_2(s)$ could be selected to be just less than the inverse of the nominal sensitivity function. This would lead to a structured singular value for the system of just less than one; the system would pass the robust performance test.

For the special case of first-order with time-delay systems (3) the H_2-optimal nominal sensitivity function for step inputs is:

$$\tilde{s}_{\text{opt}}(i\omega) = 1 - \exp(-\bar{\theta}i\omega) \tag{16}$$

If a first-order Padé approximation is used for the time-delay in (16) equation (17) results.

$$\tilde{s}_{\text{opt}}(i\omega) \approx \frac{\bar{\theta}i\omega}{\frac{\bar{\theta}}{2}i\omega + 1} \tag{17}$$

Equation (17) suggests the following functional form for the weight $w_2(i\omega)$:

$$w_2(i\omega) = b\frac{ai\omega + 1}{ai\omega} \tag{18}$$

Note expressions (17) and (18) are inverses of one another when $a = \bar{\theta}/2$ and $b = 1/2$. The weight $w_2(i\omega)$ in (18) requires that the bandwidth of the closed-loop system be at least $1/a$ and that the maximum peak in the sensitivity function be less than $1/b$. Parameter a would be increased and parameter b decreased to allow for degradation in closed-loop performance due to modelling errors. The inverse of the weight $w_2(i\omega)$ used for experiment 1 in Table 5 with $a = 1{\cdot}162$ and $b = 0{\cdot}5$ is sketched in Fig. 4. The worst-case (largest magnitude) sensitivity function generated by the set of models Π must lie below this curve to satisfy the robust performance specification. The controller is typically designed to push the worst-case sensitivity function as far below this curve as possible over the entire frequency range.

4. Designing the controller

4.1. *Smith predictor structure*

In order to construct the Smith predictor control structure shown in Fig. 1 it is necessary to select a process model $\tilde{p}(s) = \tilde{p}^0(s) \exp(-\tilde{\theta}s)$ and to design the controller $g(s)$. Usually $g(s)$ is selected to be a conventional P, PI or PID controller. The controller $g(s)$ must be designed so that the system is robust with respect to errors between the actual process $p^0(s) \exp(-\theta s)$ and the model $\tilde{p}^0(s) \exp(-\tilde{\theta}s)$.

The Smith predictor control structure can be considered to be a particular parameterization of the more general feedback control structure. The relationship between $g(s)$ and the standard feedback controller $c(s)$ in Fig. 3 is given by (19).

$$c(s) = \frac{g(s)}{1 + g(s)\tilde{p}^0(s)[1 - \exp(-\tilde{\theta}s)]} \tag{19}$$

Unfortunately, the Smith predictor structure does not provide much insight into the design of controller $g(s)$. The effect of the level of model uncertainty on the choice of controller parameters is not clear. A systematic method for designing robust Smith predictors can be developed by considering an alternate parameterization of the controller.

4.2. *Internal model control parameterization of the Smith predictor*

An alternate parameterization of $c(s)$ is the internal model control (IMC) structure shown in Fig. 5. It has been shown that the IMC structure leads to a Smith predictor controller for open-loop stable processes with time-delay (Brosilow 1979, Holt 1984, Rivera *et al.* 1985). An advantage of the IMC structure is that the system is guaranteed to be nominally stable if both $\tilde{p}(s)$ and $q(s)$ are stable (Garcia and Morari 1982). Moreover, since any transfer function (e.g. $\tilde{h}(s) = \tilde{p}(s)q(s)$) relating inputs to outputs is

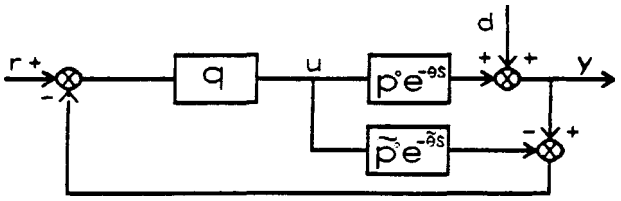

Figure 5. The internal model control (IMC) parameterization of the Smith predictor controller.

affine in the IMC controller the restrictions placed on $q(s)$ by robustness requirements (11) and (15) are clear. Usually only a single tuning parameter λ is required. Adjusting λ to meet stability and performance requirements is straightforward.

The IMC design procedure involves two steps:

(1) a controller $\tilde{q}(s)$ is designed to be H_2-optimal for the nominal model and the expected input to the system; and

(2) the controller is 'detuned' by the addition of a low-pass filter $f(s)$ to meet robustness requirements.

The resulting IMC controller is given by $q(s) = \tilde{q}(s)f(s)$.

Morari *et al.* (1987) derived the following theorem for the H_2-optimal controller $\tilde{q}(s)$ when $\tilde{p}(s)$ is stable.

Theorem

Consider the IMC structure shown in Fig. 5 with process model $\tilde{p}(s)$ and controller $q(s)$. The nominal model $\tilde{p}(s)$ is factored into an allpass portion $\tilde{p}_A(s)$ and a minimum phase portion $\tilde{p}_M(s)$

$$\tilde{p}(s) = \tilde{p}_A(s)\tilde{p}_M(s)$$

so that $\tilde{p}_A(s)$ includes all the right-half-plane zeros and delays of $\tilde{p}(s)$ and

$$|\tilde{p}_A(i\omega)| = 1, \quad \forall\, \omega$$

The expected disturbance input $d(s)$ is factored similarly

$$d(s) = d_A(s)d_M(s)$$

The controller $\tilde{q}(s)$ that minimizes the two-norm of the error is then given by

$$\tilde{q}(s) = (\tilde{p}_M(s)d_M(s))^{-1}[\tilde{p}_A^{-1}(s)d_M(s)]_* \tag{20}$$

where the operator $[\,\cdot\,]_*$ denotes that after a partial fraction expansion of the operand all terms involving the poles of $\tilde{p}_A^{-1}(s)$ are omitted. The H_2-optimal sensitivity function $\tilde{s}(i\omega)$ is given by

$$\tilde{s}(i\omega) = 1 - \tilde{p}(i\omega)q(i\omega) = 1 - \tilde{p}_A(i\omega)d_M^{-1}(i\omega)[\tilde{p}_A^{-1}(i\omega)d_M(i\omega)]_*$$

The filter form is selected to ensure that the controller $q(s)$ is proper and that the closed-loop system has the appropriate asymptotic tracking properties. For asymptotic tracking of step inputs $f(s)$ can be chosen of the form

$$f(s) = \frac{1}{(\lambda s + 1)^n}$$

where n is large enough to make $q(s)$ proper and λ is the IMC filter tuning parameter. (Filter forms for other inputs can be found in Morari *et al.* 1987.) Usually a single tuning parameter is used. A small value for λ yields faster system response whereas a large λ detunes the system and results in greater stability margins. If robust performance is specified in terms of a weight like $w_2(i\omega)$ in (18) with both bandwidth and maximum peak (MP) requirements, it may not be possible to meet both requirements with a single tuning parameter. When confronted with this situation the filter form can be changed to incorporate more tuning parameters as in

$$f(s) = \frac{1}{(\lambda_1 s + 1)(\lambda_2 s + 1)}$$

or an alternative constant performance weight $w_2' = 1/MP$ without a bandwidth constraint can be selected. If the alternative weight is selected the controller is designed so that the maximum magnitude of the sensitivity function is equal to $1/w_2' = MP$. Designing the controller so that the worst-case sensitivity function is as far below $1/w_2' = MP$ has no meaning since the absence of a bandwidth requirement in w_2' would allow complete detuning of the controller ($\lambda = \infty$ and $c(s) = 0$).

The relationship between the IMC controller $q(s)$ and the standard feedback controller $c(s)$ is given by (21).

$$c(s) = \frac{q(s)}{1 - q(s)\tilde{p}^0(s)\exp(-\tilde{\theta}s)} \tag{21}$$

The particular example of controller design for first-order with time-delay systems clarifies the relationship between the IMC parameterization and the Smith predictor. Consider the set of process models (6) with $p' = 1$. Select the nominal model as in (7) with all parameters at their mean values. The H_2-optimal controller $\tilde{q}(s)$ for step disturbances is given by $\tilde{q}(s) = (\bar{\tau}s + 1)/\bar{k}$. The appropriate filter is $f(s) = 1/(\lambda s + 1)$, resulting in the IMC controller

$$q(s) = \frac{\bar{\tau}s + 1}{\bar{k}(\lambda s + 1)} \tag{22}$$

Substituting the IMC controller (22) and the nominal model (7) into the expression (21) for the conventional feedback controller results in

$$c(s) = \frac{\bar{\tau}s + 1}{\bar{k}(\lambda s + 1 - \exp(-\bar{\theta}s))} \tag{23}$$

Note that (23) is equivalent to the Smith predictor controller (19) when $\tilde{p}^0(s) = \bar{k}/(\bar{\tau}s + 1)$ and $g(s)$ is the PI controller $g(s) = (\bar{\tau}s + 1)/\bar{k}\lambda s$.

5. Tuning the controller for robust performance

In this section five alternative methods are presented for designing robust controllers for systems with time-delay. The first four methods result in Smith predictor controllers; the fifth, in the structured-singular-value-optimal controller. The methods differ in their numerical complexity, in the type of uncertainty description they consider, and in the robust performance guarantee they offer. The more numerically complex methods introduce less conservativeness into the controller design. In selecting an appropriate design method the required system performace is of paramount importance. If performance requirements are mild then the 'quick design' procedure should suffice. Moderate performance requirements might necessitate the robustness test that considers actual parameter uncertainties rather than a multiplicative error approximation. More demanding performance requirements might require optimizing all parameters in the Smith predictor controller. Only the toughest performance requirements would justify synthesis of the structured-singular-value-optimal controller.

The IMC design procedure and tuning methods presented here are applicable to all open-loop stable processes that can be modelled by (1) or (2). The methods are illustrated with controller designs for the particularly useful first-order with time-delay model. Three recommended tuning methods were compared by examining controller designs for twenty-four families of process models (3) with $p'(s) = 1$. All

possible combinations of 10 per cent and 50 per cent uncertainty in gain, time-constant and time-delay were investigated at each of three levels of the ratio $\bar{\tau}/\bar{\theta}$. Tuning method A was used to design controllers for an even greater range of the parameter uncertainties and the ratio $\bar{\tau}/\bar{\theta}$. The results of the different IMC filter-tuning techniques are presented in Tables 1–5. Details of each of the tuning techniques are outlined below.

Experiment	$dk/\bar{k}$	$d\tau/\bar{\tau}$	$d\theta/\bar{\theta}$	λ robust stability	For MP = 2·0		
					λ_A	λ_B	λ_C
1	0·1	0·1	0·1	0·080	0·525	0·661	0·313
2	0·1	0·5	0·1	0·230	1·109	1·647	1·425
3	0·5	0·1	0·1	0·107	1·199	1·498	0·495
4	0·1	0·1	0·5	0·401	1·136	1·648	1·594
5	0·1	0·5	0·5	0·737	1·412	2·547	2·895
6	0·5	0·5	0·1	0·627	1·833	2·677	3·135
7	0·5	0·1	0·5	0·537	2·012	2·256	2·367
8	0·5	0·5	0·5	1·091	2·312	3·477	4·541

Table 1. Filter parameters resulting from tuning methods A–C. λ from robust stability condition is shown for comparison. In experiments 1–8 the ratio $\bar{\tau}/\bar{\theta} = 1{\cdot}0$.

Experiment	$dk/\bar{k}$	$d\tau/\bar{\tau}$	$d\theta/\bar{\theta}$	λ robust stability	For MP = 2·0		
					λ_A	λ_B	λ_C
9	0·1	0·1	0·1	0·080	0·454	0·632	0·316
10	0·1	0·5	0·1	0·185	0·758	1·172	0·923
11	0·5	0·1	0·1	0·107	1·115	1·344	0·496
12	0·1	0·1	0·5	0·399	1·104	1·608	1·562
13	0·1	0·5	0·5	0·611	1·189	2·087	2·208
14	0·5	0·5	0·1	0·367	1·293	1·872	1·733
15	0·5	0·1	0·5	0·529	1·998	2·120	2·202
16	0·5	0·5	0·5	0·823	2·125	2·704	3·194

Table 2. Filter parameters resulting from tuning methods A–C. λ from robust stability condition is shown for comparison. In experiments 9–16 the ratio $\bar{\tau}/\bar{\theta} = 0{\cdot}5$.

Experiment	$dk/\bar{k}$	$d\tau/\bar{\tau}$	$d\theta/\bar{\theta}$	λ robust stability	For MP = 2·0		
					λ_A	λ_B	λ_C
17	0·1	0·1	0·1	0·080	0·594	0·661	0·311
18	0·1	0·5	0·1	0·415	1·703	2·905	3·316
19	0·5	0·1	0·1	0·106	1·309	1·787	0·489
20	0·1	0·1	0·5	0·400	1·267	1·637	1·576
21	0·1	0·5	0·5	0·971	2·391	3·757	5.141
22	0·5	0·5	0·1	1·688	2·714	5·617	8·790
23	0·5	0·1	0·5	0·535	2·200	2·476	2·478
24	0·5	0·5	0·5	2·090	3·677	6·356	10·066

Table 3. Filter parameters resulting from tuning methods A–C. λ from robust stability condition is shown for comparison. In experiments 17–24 the ratio $\bar{\tau}/\bar{\theta} = 3{\cdot}0$.

			Values for the filter parameter λ for these ratios of $\bar{\tau}/\bar{\theta}$						
$dk/\bar{k}$	$d\tau/\bar{\tau}$	$d\theta/\bar{\theta}$	0·05	0·1	0·5	1·0	3·0	10·0	30·0
0·0	0·0	0·0	0·000	0·000	0·000	0·000	0·000	0·000	0·000
0·0	0·1	0·0	0·030	0·062	0·196	0·245	0·277	0·283	0·285
0·1	0·0	0·0	0·265	0·266	0·266	0·265	0·265	0·265	0·266
0·0	0·0	0·1	0·192	0·192	0·196	0·192	0·192	0·192	0·192
0·0	0·1	0·1	0·199	0·203	0·268	0·339	0·399	0·415	0·418
0·1	0·1	0·0	0·267	0·271	0·360	0·417	0·457	0·468	0·469
0·1	0·0	0·1	0·400	0·400	0·400	0·400	0·400	0·400	0·400
0·1	0·1	0·1	0·403	0·410	0·454	0·525	0·594	0·612	0·617
0·1	0·5	0·1	0·433	0·447	0·758	1·109	1·703	2·041	2·157
0·5	0·1	0·1	1·097	1·102	1·115	1·199	1·309	1·342	1·349
0·1	0·1	0·5	1·100	1·106	1·104	1·136	1·267	1·338	1·355
0·1	0·5	0·5	1·130	1·155	1·189	1·412	2·391	3·102	2·318
0·5	0·5	0·1	1·128	1·161	1·293	1·833	2·714	3·226	3·395
0·5	0·1	0·5	1·977	1·987	1·998	2·012	2·200	2·292	2·319
0·5	0·5	0·5	2·020	2·059	2·125	2·312	3·677	4·666	5·017
0·0	0·0	0·0	0·000	0·000	0·000	0·000	0·000	0·000	0·000
0·1	0·1	0·1	0·403	0·410	0·454	0·525	0·594	0·612	0·617
0·2	0·2	0·2	0·777	0·784	0·799	0·959	1·179	1·267	1·292
0·3	0·3	0·3	1·166	1·185	1·166	1·403	1·860	2·099	2·164
0·4	0·4	0·4	1·573	1·607	1·621	1·855	2·674	3·189	3·349
0·5	0·5	0·5	2·020	2·059	2·125	2·312	3·667	4·666	5·017
0·6	0·6	0·6	2·485	2·538	2·664	2·765	4·884	6·724	7·498
0·7	0·7	0·7	2·974	3·053	3·215	3·216	6·341	9·819	11·478
0·8	0·8	0·8	3·499	3·595	3·837	3·659	8·152	14·892	18·926
0·9	0·9	0·9	4·051	4·166	4·479	4·280	10·192	24·200	37·169

Table 4. Controller parameters resulting from tuning method A. The ratio $\bar{\tau}/\bar{\theta}$ varies allowing the control system designer to interpolate between values for λ in the table to arrive at an acceptable tuning parameter.

Experiment	$dk/\bar{k}$	$d\tau/\bar{\tau}$	$d\theta/\bar{\theta}$	λ_A	λ_D	a	sup (15)	K	τ	θ
1	0·1	0·1	0·1	0·998	0·998	1·162	1·026	0·969	0·989	1·005
2	0·1	0·5	0·1	1·225	1·225	1·512	1·120	0·923	0·733	0·962
3	0·5	0·1	0·1	1·310	1·310	2·312	1·082	0·994	0·887	0·992
4	0·1	0·1	0·5	2·121	1·899	1·794	0·982	1·051	1·234	0·965
5	0·1	0·5	0·5	2·460	2·460	2·194	1·030	0·863	0·986	0·953
6	0·5	0·5	0·1	1·870	1·870	2·874	1·104	0·937	0·575	0·977
7	0·5	0·1	0·5	2·207	1·976	3·212	1·013	1·080	0·949	1·004
8	0·5	0·5	0·5	2·395	2·395	3·397	1·122	0·857	0·684	0·992

Table 5. Controller parameters resulting from optimization method D. The ratio $\bar{\tau}/\bar{\theta} = 1{\cdot}0$. Parameter a in the performance weight and λ from tuning method A are included for comparison. The structured singular value μ is shown for the system with the controller resulting from the optimization.

5.1. *Method A: tuning with actual uncertainty regions*

The first IMC filter-tuning method utilizes the loop transfer-function uncertainty regions $\pi(\omega)c(i\omega)$ to test for robust performance. Real parameter uncertainties in (1) are treated *exactly*. Once a filter parameter λ has been selected the sensitivity function with largest magnitude at each frequency given by

$$|s^*(\omega)| = \max_{p(i\omega)\in\Pi} \left| \frac{1}{1 + p(i\omega)c(i\omega)} \right| \tag{24}$$

is determined by locating the point closest to $(-1, 0)$ on each uncertainty region $\pi(\omega)c(i\omega)$. The filter parameter is adjusted until the robust performance requirement (14) has been satisfied. Increasing λ reduces the maximum peak in $|s^*(\omega)|$ and decreases the bandwidth of the system.

For the first-order with time-delay examples, the weight $w_2' = 1/MP = 1/2$ was used to specify performance requirements. Controller (23) was designed following the IMC procedure after selecting the nominal model (7). The IMC filter parameter λ was adjusted and regions $\pi(\omega)c(i\omega)$ located until the maximum peak in the sensitivity function $|s^*(\omega)|$ was determined to be 2. Values of λ leading to this result are listed in Tables 1–4. As expected, the filter parameter increases as the level of parameter uncertainty increases—less aggressive control action is required for robustness with respect to large modelling errors. The filter parameter increases slightly as a function of the ratio $\bar{\tau}/\bar{\theta}$.

5.2. *Method B: tuning with multiplicative error*

In the second IMC filter-tuning method the real parameter uncertainties in (1)–(3) are approximated by a multiplicative perturbation $l_m(i\omega)$ for the purposes of robustness analysis. The approximation is discussed in § 2.2 above. After the IMC controller has been designed and the filter form selected the IMC tuning parameters λ_i are implicitly defined by condition (15) for robust performance. If a performance weight $w_2' = 1/MP$ is selected filter parameters are adjusted iteratively until

$$\sup_{\omega} |\tilde{h}(i\omega)| l(\omega) + \frac{1}{MP} |(1 - \tilde{h}(i\omega))| = 1 \tag{25}$$

If the performance requirements are too severe it may not be possible to find values for the λ_i such that (15) is satisfied. When this situation is encountered it is possible that the less conservative tuning method based on the actual parameter uncertainties will lead to an acceptable design. If not, either the performance requirements must be relaxed or a different IMC filter form must be selected.

For the first-order with time-delay examples and performance weight $w_2' = 1/MP = 1/2$, condition (25) can be rewritten to yield an implicit expression for the filter paramater λ in controller (23):

$$\sup_{\omega} \frac{l(\omega)}{|\lambda i\omega + 1|} + \frac{1}{MP} \frac{|\lambda i\omega + 1 - \exp(-\bar{\theta} i\omega)|}{|\lambda i\omega + 1|} = 1 \tag{26}$$

Condition (26) represents the robust performance specification on the filter parameter λ. The robust stability requirement (11) is rewritten in terms of the filter parameter in (27) for comparison.

$$\sup_{\omega} \frac{l(\omega)}{|\lambda i\omega + 1|} < 1 \tag{27}$$

Values of λ leading to equality in (26) and (27) are listed in Tables 1–3 for each level of parameter uncertainty. Filter parameters required for robust performance are significantly larger than those required for robust stability in all of the examples. The same general trends are observed in the filter parameters for robust performance as in tuning method A. Note, however, that the values of λ from method B are slightly larger than those from method A. Conservativeness that entered the design procedure when parameter uncertainties were approximated by multiplicative uncertainty resulted in less aggressive control action.

5.3. *Method C: a quick design method*

At the frequency where the magnitude of the multiplicative uncertainty is equal to one condition (11) indicates that $\tilde{h}(i\omega)$ must already be rolled-off to prevent instability. This observation motivates a 'quick design' procedure for selecting the filter parameters λ_i. At the frequency ω' where $l(\omega') = 1$ the filter parameters can be implicitly defined by a conservative bound as follows:

$$|\tilde{h}(i\omega')|l(\omega') + |(1 - \tilde{h}(i\omega'))w_2(i\omega')| \leqslant |\tilde{h}(i\omega')|l(\omega') + (1 + |\tilde{h}(i\omega')|)w_2(i\omega')| = 1 \qquad (28)$$

With $l(\omega') = 1$ and the choice of $w_2(i\omega') = 1/MP$ equation (28) becomes:

$$|\tilde{h}(i\omega')| = \frac{MP - 1}{MP + 1} \qquad (29)$$

Equation (29) allows quick calculation of the IMC filter parameters λ_i once the frequency ω' at which $l(\omega') = 1$ has been located. Bound 1 enables quick calculation of ω' when simultaneous uncertainties in gain, time-constant, and time-delay are encountered. For example, see Fig. 4 where $\omega' = 9{\cdot}014$ rad s^{-1} for ten per cent uncertainty in k, τ and θ.

For the first-order with time-delay examples and the controller (23), at ω' the nominal complementary sensitivity function is given by $\tilde{h}(i\omega') = 1/(\lambda i\omega' + 1)$. Then equation (29) can be rewritten explicitly for λ as follows:

$$\lambda = \frac{\left[\left(\dfrac{MP + 1}{MP - 1}\right)^2 - 1\right]^{1/2}}{\omega'} \qquad (30)$$

where MP is the desired maximum magnitude of the sensitivity function and ω' is the frequency at which $l(\omega') = 1$. Equation (30) with $MP = 2$ was used to calculate filter parameters shown in Tables 1–3. Although the filter parameters compare favourably with those obtained by the two methods discussed above the quick design method does *not* guarantee that the maximum peak in the sensitivity function will be less than MP. No such guarantee can be made since the quick design method considers only one frequency ω'. In fact, the filter parameters calculated using (30) for the examples with high levels of gain uncertainty lead to maximum peaks greater than 2. For those cases where gain uncertainty dominates (where the quick design method is least accurate) it is straightforward to tune the controller based on simple gain-margin arguments. Nevertheless, the data indicate that the quick design method will be useful for a wide range of uncertainty in model parameters. The filter parameter obtained via this method can certainly be used as a first guess for either of the more rigorous iterative methods A or B discussed above.

5.4. *Alternate nominal models*

The Smith predictor controller (21) resulting from the IMC design procedure contains more adjustable parameters than the λ_i in the IMC filter. All the parameters fixed by the choice of a nominal model also appear in the controller. Since the Smith predictor given by (20) with $\lambda = 0$ is known to be optimal for the processes (1)–(3) when there is no parameter uncertainty, the recommended IMC design method seems appropriately justified. Chen (1984), however, indicated that the nominal model with all parameters at their mean values does not always lead to an optimal control system design when the uncertainties are considered. Certainly it seems logical to fix nominal model parameters at their mean values when confronted by the process description (1)–(3). In order to evaluate the performance lost as a result of this selection another set of controller designs was performed for the first-order with time-delay examples in which all four controller parameters $\bar{k}$, $\bar{\tau}$, $\bar{\theta}$ and λ in (23) were optimized.

A control-relevant identification technique developed by Rivera and Morari (1986) was used to optimize all four parameters in the Smith predictor (23). Inputs to the optimization procedure include a nominal model, the magnitude of the multiplicative uncertainty, a performance weight w_2, and the structure of the model to be identified. The input nominal model was specified to be the centre of the smallest disk containing all models in the set (3). The optimization procedure selects a new nominal model and IMC filter parameter λ so as to reduce the structured singular value (15). Note that through the IMC design procedure selecting a new nominal model and filter parameter is tantamount to selecting new values for the parameters in the Smith predictor controller (11).

Table 5 lists the controller parameters selected by the optimization procedure for the same eight levels of uncertainty as in Table 1. The mean value for the three model parameters is 1·0 for all eight levels of uncertainty. In most cases the controller parameters in Table 5 do not differ significantly from 1·0. The weight w_2 in (18) with $b = 1/2$ and the parameter a indicated in Table 5 was input to the optimization procedure for each example. It can be verified using tuning method A that this is the best level of robust performance achievable with nominal model parameters at their mean values as in (7)—the system would fail the robust performance test (14) if parameter a had a value less than that indicated in Table 5. The optimization procedure attempted to reduce the supremum in (15) using a multiplicative error approximation for the actual parameter uncertainties. Values of the supremum for the eight designs are shown in Table 5. In the designs where the supremum is greater than one the additional conservativeness introduced by the multiplicative error approximation outweighted any benefit from optimizing all four parameters in the controller. These designs would not be considered robust based on the test involving the multiplicative error approximation. Results of this study indicate that selection of a nominal model with gain, time-constant, and time-delay at their mean values will, in most cases, lead to an acceptable Smith predictor controller.

5.5. *Structured-singular-value-optimal controller*

The structured-singular-value-optimal (SSV-optimal) controller is the controller that minimizes the supremum in (15). In this section the Smith predictor is compared with SSV-optimal controllers. The comparison illustrates how system performance might be effected by selecting the form of the controller to be that of the Smith predictor. The comparison also highlights differences in the SSV-optimal controllers

that result when process uncertainty is modelled with a single multiplicative uncertainty or with multiple real parameter uncertainties.

Both Smith predictor and SSV-optimal controllers were designed for the system modelled by (3). The nominal values of gain, time-constant and time-delay were all unity. The case of 50 per cent uncertainty in each of the three parameters was studied. Performance requirements were expressed in terms of the weight $w_2(i\omega)$ in (18) with $a = 3{\cdot}397$ and $b = 0{\cdot}5$. Recall that this level of robust performance was possible using a Smith predictor based on the nominal model and the tuning method in § 5.1 (see Table 5). The Smith predictor controller is given by (23) with $\lambda = 2{\cdot}395$.

The SSV-optimal controllers for the system were synthesized following the methods outlined in Chu *et al.* (1986) and Doyle (1982). Model uncertainty was represented by a single multiplicative uncertainty for synthesis of the first SSV-optimal controller. Figure 6 (*a*) shows the control structure with uncertainty and performance requirements written in terms of blocks Δ_1 and Δ_2 with norm $\|\Delta_i\|_2 \leqslant 1$. The structure 6 (*a*) can be rearranged into that shown in Fig. 7 (*a*). The SSV-optimal controller is then given by the stabilizing K which solves

$$\min_{D,K} \|DF_l(G; K)D^{-1}\|_\infty$$

where

$$F_l(G; K) = G_{11} + G_{12}K(I - G_{22}K)^{-1}G_{21}$$

and

$$D = \text{diag}\,(d_1, d_2, \ldots, d_n)$$

with n being the number of blocks in

$$\Delta = \text{diag}\,(\Delta_1, \Delta_2, \ldots, \Delta_0)$$

The HONEYX† computer software used to synthesize the SSV-optimal controller requires rational approximations of all irrational transfer functions appearing in the block structure. Hence, a fourth-order Padé approximation was substituted for the time-delay in $\tilde{p}$; a first-order Padé approximation, for the time-delay in the bound (8) for L_m (see the dashed curve in Fig. 2).

For synthesis of the second SSV-optimal controller model uncertainty was represented by individual parameter uncertainties. Figure 6 (*b*) shows individual uncertainties in gain, time-constant and time-delay written in terms of three blocks Δ_1, Δ_2 and Δ_3. Note that the block structure represents a first-order Padé approximation for the time-delay. Figure 7 (*b*) illustrates the equivalent interconnection structure for that in Fig. 6 (*b*). The HONEYX software assumes each Δ_i is a complex perturbation with $\|\Delta_i\|_2 \leqslant 1$ even though they represent real parameter variations.

The magnitude and phase of the two SSV-optimal controllers are shown in Fig. 8. The controller resulting when a single multiplicative uncertainty was used (labelled 2 in Fig. 8) was 18th order. The controller resulting when multiple parameter uncertainties were used (labelled 3 in Fig. 8) was 19th order. Note in Fig. 8 that both SSV-optimal controllers have slightly lower gain than the Smith predictor (labelled 1) for frequencies below one. The magnitude of model uncertainty is low over this

† Developed by Honeywell Systems and Research Center, Minneapolis, Minnesota, U.S.A.

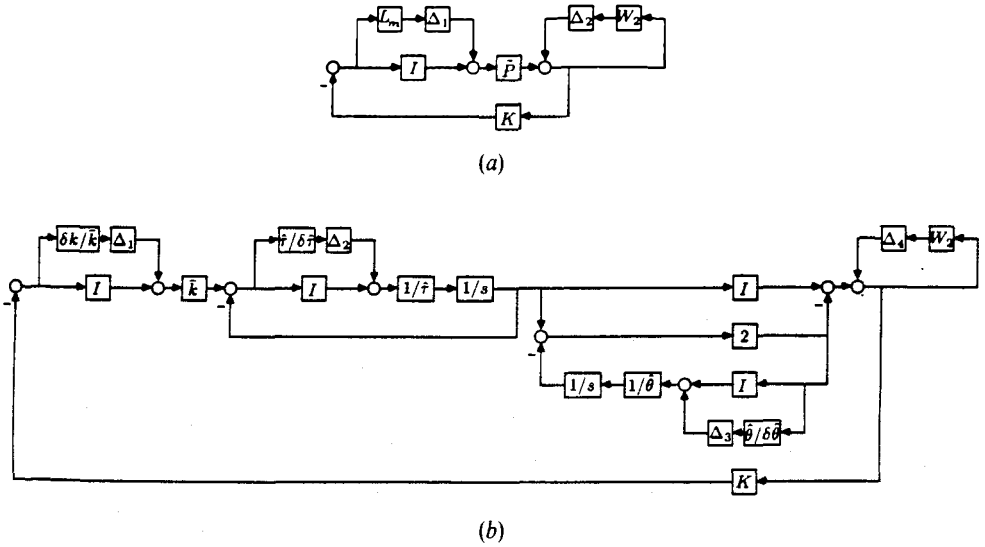

Figure 6. Feedback control structures incorporating a single multiplicative uncertainty (*a*) and individual gain, time-constant and time-delay uncertainty (*b*) are shown. In (*b*) a first-order Padé approximation is used to represent time-delay. Since the inverse of τ and θ appear in (*b*) the following variables are used to define real parameter variations: $1/\hat{\tau} = (1/2\tau_{min}) + (1/2\tau_{max})$, $1/\hat{\theta} = (1/2\theta_{min}) + (1/2\theta_{max})$, $1/\delta\hat{\tau} = (1/\hat{\tau}) - (1/\tau_{max})$, $1/\delta\hat{\theta} = (1/\hat{\theta}) - (1/\theta_{max})$.

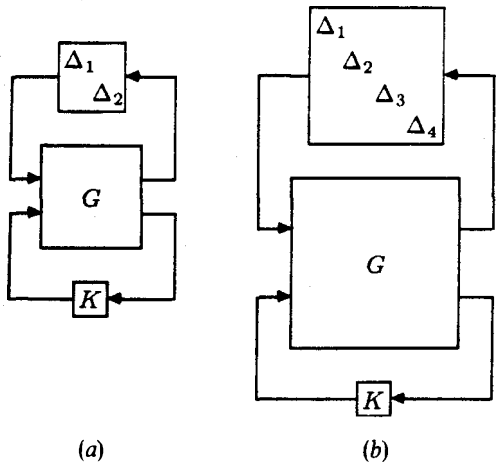

Figure 7. The two feedback structures in Fig. 6 can be rewritten as shown with interconnection matrix G, norm-bounded matrix Δ and controller K.

frequency range; hence the controller shape is largely determined by the performance weight w_2. At higher frequencies the SSV-optimal controllers employ higher gain than the Smith predictor. The higher gain causes oscillation in the nominal sensitivity function in the high frequency range as shown in Fig. 9. The SSV-optimal controllers reduce the structured singular value (see Fig. 10) at frequencies near 0·3 where the performance requirement is tight and increase it at higher frequencies where the performance requirement allows additional gain. Note that there is little difference

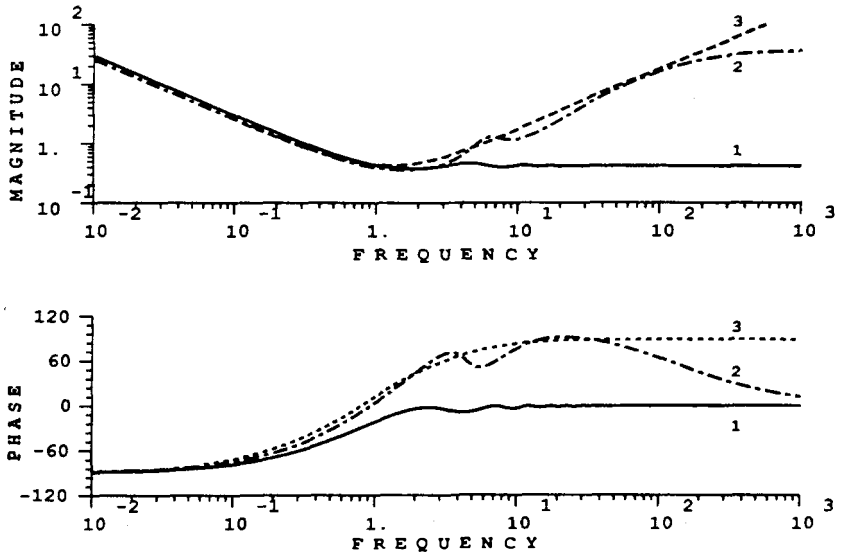

Figure 8. The Bode plots of SSV-optimal and Smith predictor controllers are quite similar in the low frequency range. Curve 1 is the Smith predictor. The SSV-optimal controllers synthesized using multiplicative uncertainty and parameter uncertainty are curves 2 and 3, respectively.

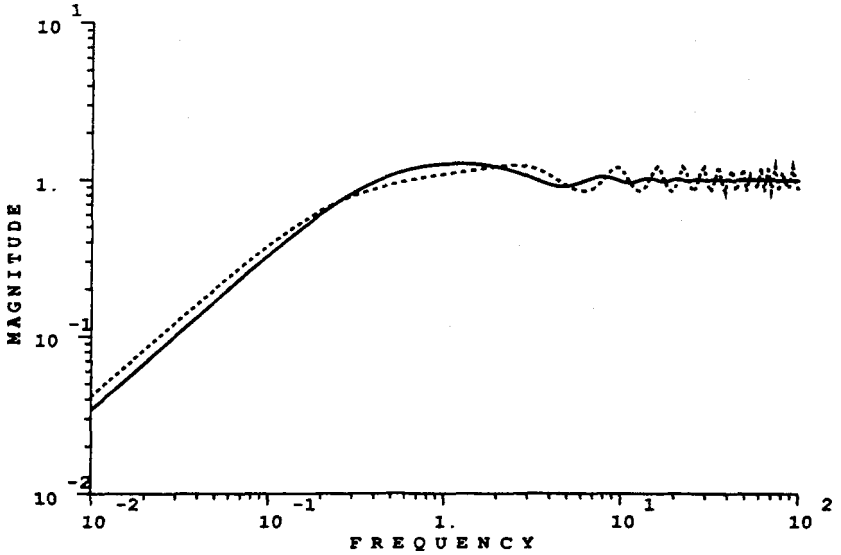

Figure 9. The sensitivity function for the system with SSV-optimal controller (dashed curve) has larger amplitude oscillations in the high frequency range than does that with the Smith predictor controller (solid line). The sensitivity functions with the two SSV-optimal controllers are indistinguishable from one another.

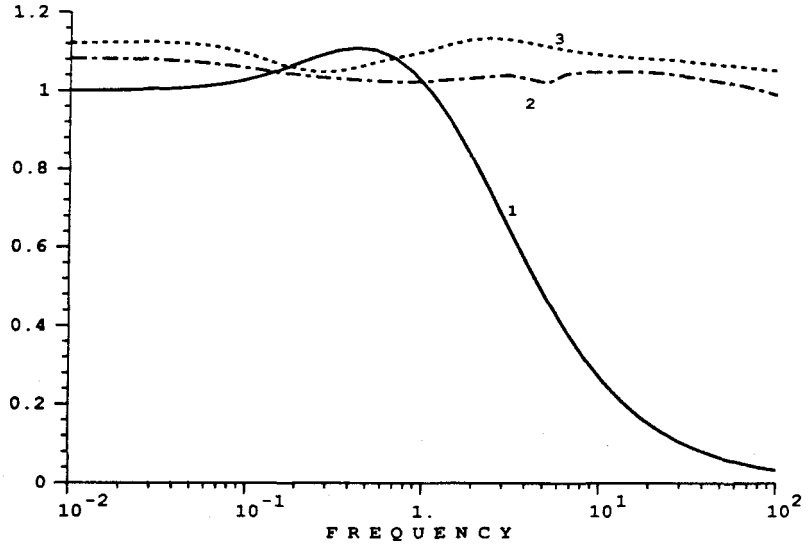

Figure 10. The structured singular values for the control system with SSV-optimal controllers (2 and 3) and Smith predictor controller (1) are compared here. Structured singular values with SSV-optimal controllers synthesized using multiplicative uncertainty and parameter uncertainty are on curves 2 and 3, respectively.

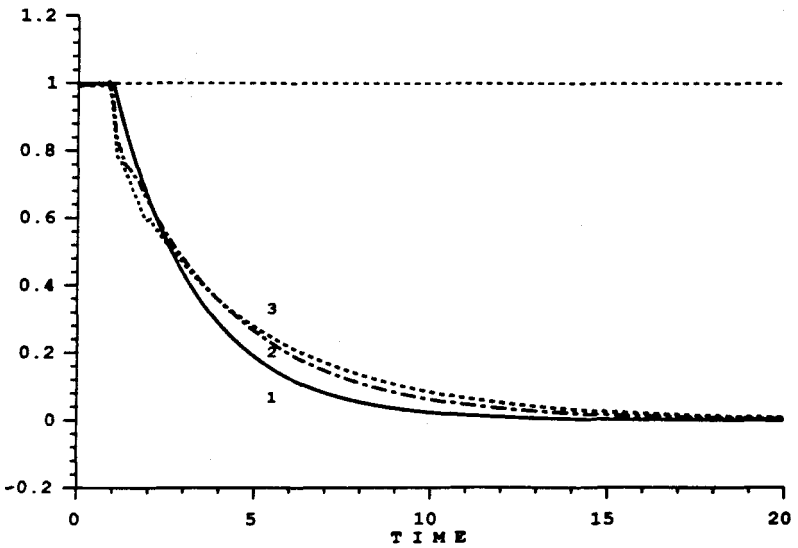

Figure 11. Responses to step disturbances are quite similar for the system with Smith predictor (1), with SSV-optimal controller synthesized using multiplicative uncerta nty (2), and with the SSV-optimal controller synthesized using parameter uncertainties (3).

between the two SSV-optimal controllers in Figs. 8 and 10, indicating that relatively little conservativeness entered the design when the Δ_i representing real parameters were assumed to be complex. This outcome may be limited to this example, however, since such an assumption can in general be quite conservative. All structured singular values in Fig. 10 are greater than one, indicating that the performance requirement w_2 would have to be relaxed in order for the system to pass the robust performance test based on the norm-bounded blocks Δ_i. Recall that the robust performance test based on the actual uncertainty regions can be passed using the same requirement w_2 used in Fig. 10.

Figure 11 shows the nominal system response to step disturbances with Smith predictor and SSV-optimal controllers. There is relatively little difference in nominal system response despite the complexity of the SSV-optimal controllers.

6. Discussion and conclusions

The internal model control structure provides a useful framework for the design and tuning of robust Smith predictor controllers for systems with time-delay. Results of this study offer several alternatives to the control system designer confronted with the task of designing robust controllers for processes modelled by transfer-functions with real-parameter uncertainties. An H_2-optimal IMC controller can easily be designed for the nominal model and expected disturbance using the results of § 4. Augmenting the controller with a filter can ensure robust performance despite parameter uncertainties. The IMC filter can be tuned following the methods outlined in § 5 or the model can be non-dimensionalized (see § 6.1) allowing the use of tabulated filter-tuning constants. The Smith predictor that results from the IMC design procedure compares favourably with the SSV-optimal controller for systems with time-delay. Simultaneous parameter uncertainties can be considered exactly when testing for robust performance, or they can be approximated by a single multiplicative uncertainty for mathematical convenience. Bound 1 in § 2.2 gives an exact expression for the magnitude of multiplicative uncertainty that can be used to approximate simultaneous uncertainties in gain, time-constant and time-delay. Use of Bound 1 in SSV-optimal controller synthesis was demonstrated.

6.1. *Non-dimensionalizing the model*

When confronted with a stable process described by (6) the control designer can non-dimensionalize the model enabling use of tuning parameter data in Table 4. Model (6) with $p'(s) = 1$ can be rewritten as follows:

$$p^*(s^*) = \frac{p(s)}{k} = \frac{(1 + \delta k^*) \exp(-(1 + \delta\theta^*)s^*)}{(1 + \delta\tau^*)\frac{\bar{\tau}}{\bar{\theta}}s^* + 1}$$

where dimensionless parameters are defined by

$$s^* = s\bar{\theta}, \quad dk^* = \frac{\delta k}{\bar{k}}, \quad \delta\tau^* = \frac{\delta\tau}{\bar{\tau}}, \quad \delta\theta^* = \frac{\delta\theta}{\bar{\theta}}$$

Note that the following bounds are implied for the dimensionless parameters:

$$|\delta k^*| < 1, \quad |\delta\tau^*| < 1, \quad |\delta\theta^*| < 1, \quad 0 < \frac{\bar{\tau}}{\bar{\theta}} < \infty$$

A dimensionless IMC controller $q^*(s^*)$ can be designed for $p^*(s^*)$ with the appropriate filter parameter λ^* found by interpolating between values listed in Tables 1–4.

The real controller $q(s)$ is related to its dimensionless counterpart as follows:

$$q(s) = \frac{q^*(s\bar{\theta})}{\bar{k}}$$

The real controller $q(s)$ will have an IMC filter parameter given by

$$\lambda = \lambda^* \bar{\theta}$$

6.2. *Simulating the worst case response*

The time-domain behaviour of the system can be investigated by simulating the response of the 'worst case' sensitivity function to selected disturbances. When the regions $\pi(\omega)c(i\omega)$ are located the closest point on each region to $(-1, 0)$ defines the sensitivity function $s^*(\omega)$ as in (24). The magnitude of $s^*(\omega)$ at each frequency will be greater than or equal to the magnitude of any sensitivity function resulting from a model in (4). The response of $s^*(\omega)$ to different types of disturbances can be determined by inverse Fourier transform. If the process model is accurate, the integral square error in the response of the real system to each of these disturbances will be less than that in the response of $s^*(\omega)$ to the same disturbance. The shape of the response of $s^*(\omega)$, however, may not resemble the real system response since different models in Π contribute to $s^*(\omega)$ at different frequencies. Nevertheless, $s^*(\omega)$ can provide a useful measure of the system's disturbance rejection capability.

Responses of $s^*(\omega)$ to step disturbances are shown in Fig. 12 for 10 per cent and 50 per cent uncertainty in each of the three parameters k, τ and θ in the first-order with

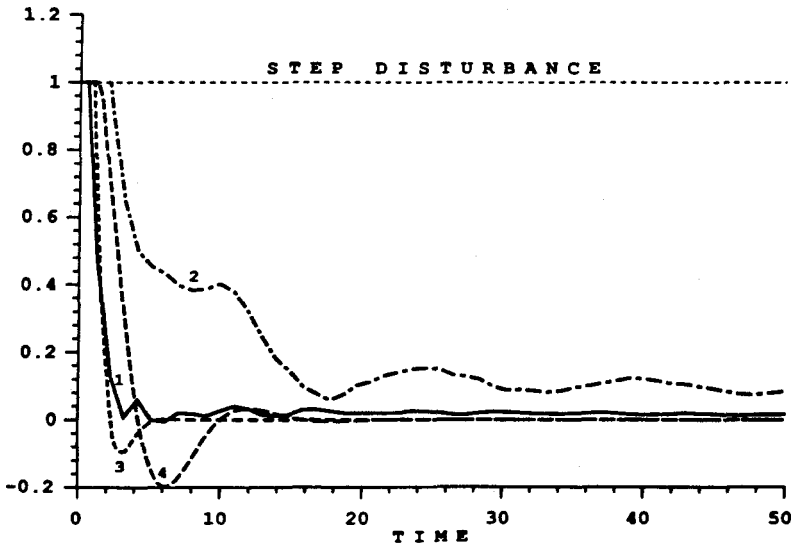

Figure 12. Using the Smith predictors resulting from tuning method A, the responses of $s^*(\omega)$ to step disturbances are shown for 10 per cent parameter uncertainty (curve 1) and 50 per cent parameter uncertainty (curve 2) in model (6). Responses of the model $p(s) = k \exp(-\theta s)/(\tau s + 1)$ with $k = \bar{k} + \Delta k$, $\tau = \bar{\tau} + \Delta\tau$ and $\theta = \bar{\theta} + \Delta\theta$ are shown using the same controllers for 10 per cent parameter uncertainty (curve 3) and 50 per cent parameter uncertainty (curve 4).

time-delay model. The worst case integral-square-error $\|e(t)\|_2^2$ for these two examples was calculated to be 2·258 and 6·425, respectively. A real system response to the step disturbance is shown for comparison at each of the two levels of uncertainty. The three parameters were specified to be at their highest values in the model used for the real system response: $k = \bar{k} + \Delta k$, $\tau = \bar{\tau} + \Delta\tau$ and $\theta = \bar{\theta} + \Delta\theta$. For 10 per cent parameter uncertainty and 50 per cent parameter the integral-square-error in the response of the real system to the step disturbance was calculated to be 1·304 and 2·335 for 10 per cent parameter uncertainty and 50 per cent parameter uncertainty, respectively. The integral-square-error in the response of the real first-order with time-delay system is less than that of $s^*(\omega)$. This is to be expected since $s^*(\omega)$ is the worst combination of parameter values at each frequency (an ∞-norm bound on the magnitude of the sensitivity function) rather than one particular first-order with time-delay model. The extent to which $s^*(\omega)$ gives a conservative estimate of the two-norm of the error emphasizes the inherent conservativeness introduced when transfer functions with real parameter uncertainties are represented by uncertainty regions on the complex plane—the parametric structure of the process model is lost. It also emphasizes the lack of clarity in the relationship between ∞-norm performance requirements and the eventual time-domain behaviour of the system.

6.3. *Additional applications*

Bound 1 and Bound 2 (see the Appendix) provide particularly useful links between parameter uncertainties and multiplicative error for simple process models. The bounds can be applied to higher order models if uncertainty can be accurately represented by variations in three parameters: gain, time-delay and one pole location or gain, time-delay and one zero location. In MIMO systems where low-order dynamics $g_{ii}(s)$ with parameter uncertainties can be factored out along the diagonal of the matrix transfer-function as shown below, the bounds can be applied to approximate the parameter uncertainties by multiplicative perturbations.

$$\begin{bmatrix} p_{11}(s) & p_{12}(s) \\ p_{21}(s) & p_{22}(s) \end{bmatrix} = \begin{bmatrix} \tilde{f}_{11}(s) & \tilde{f}_{12}(s) \\ \tilde{f}_{21}(s) & \tilde{f}_{22}(s) \end{bmatrix} \begin{bmatrix} g_{11}(s) & 0 \\ 0 & g_{22}(s) \end{bmatrix}$$

$$= \begin{bmatrix} \tilde{f}_{11}(s) & \tilde{f}_{12}(s) \\ \tilde{f}_{21}(s) & \tilde{f}_{22}(s) \end{bmatrix} \begin{bmatrix} \tilde{g}_{11}(s) & 0 \\ 0 & \tilde{g}_{22}(s) \end{bmatrix} \left(\begin{bmatrix} 1 & 0 \\ 0 & 1 \end{bmatrix} + \begin{bmatrix} l_{m_{11}}(s) & 0 \\ 0 & l_{m_{22}}(s) \end{bmatrix} \right)$$

Certain types of actuator uncertainty and input uncertainty are accurately described in this manner (see Skogestad and Morari 1986 for a distillation column example). Representing MIMO modelling error with different multiplicative uncertainties in each input direction can be less conservative than representing it with a single multiplicative perturbation to the whole matrix transfer-function. Approximating the parameter uncertainties in the MIMO transfer-function matrix with multiplicative uncertainties $l_{m_{11}}(s)$ and $l_{m_{22}}(s)$ also allows convenient application of structured singular value analysis for robust performance.

Appendix

Definition of variables

The description (6) for a set of process models can be rewritten as follows:

$$p(s) = p'(s)\frac{(\bar{k}+\delta k)}{(\bar{\tau}+\delta\tau)s+1}\exp\left[-(\bar{\theta}+\delta\theta)s\right]$$

$$p(s) = p'(s)\frac{\bar{k}}{\bar{\tau}s+1}\exp(-\bar{\theta}s)\left[1+\left(\frac{\bar{k}+\delta k}{\bar{k}}\right)\left(\frac{\bar{\tau}s+1}{(\bar{\tau}+\delta\tau)s+1}\right)\exp(-\delta\theta s)-1\right] \quad \text{(A 1)}$$

$$p(s) = \tilde{p}(s)[1+l_m(s)] \quad \text{(A 2)}$$

From equations (A 1) and (A 2) we can identify expressions for $\tilde{p}(s)$ and $l_m(s)$.

$$\tilde{p}(s) = \frac{\bar{k}}{\bar{\tau}s+1}\exp(-\bar{\theta}s) \quad \text{(A 3)}$$

$$l_m(s) = \left(\frac{\bar{k}+\delta k}{\bar{k}}\right)\left(\frac{\bar{\tau}s+1}{(\bar{\tau}+\delta\tau)s+1}\right)\exp(-\delta\theta s)-1 \quad \text{(A 4)}$$

Bound 1 gives the smallest bound $l(\omega)$ such that $|l_m(i\omega)| \leqslant l(\omega)$ for all δk, $\delta\tau$ and $\delta\theta$. The proof will be approached from the perspective of determining the greatest distance of $l_m(s)+1$ from the point (1, 0). Clearly this distance will be the bound $l(\omega)$. With $|\delta k| \leqslant \Delta k$, $|\delta\tau| \leqslant \Delta\tau$ and $|\delta\theta| \leqslant \Delta\theta$ all possible values for $l_m(s)+1$ at one frequency $s = i\omega$ can be located inside the boundary *ABCDEF* sketched in Fig. 13 (Laughlin *et al.* 1986). Along curve *AB* $\delta k = \Delta k$, $\delta\tau = -\Delta\tau$ and $\delta\theta$ varies. Along curve *BC* $\delta k = \Delta k$, $\delta\theta = -\Delta\theta$ and $\delta\tau$ varies. Along curve *CD* $\delta\tau = \Delta\tau$, $\delta\theta = -\Delta\theta$ and δk varies. Along curve *DE* $\delta k = -\Delta k$, $\delta\tau = \Delta\tau$ and $\delta\theta$ varies. Along curve *EF*, $\delta k = -\Delta k$, $\delta\theta = \Delta\theta$ and $\delta\tau$ varies. Along curve *FA*, $\delta\tau = -\Delta\tau$, $\delta\theta = \Delta\theta$ and δk varies. Equation (10) specifies the frequency ω^* when arg $[A] = \pi$. Bound 1 claims that point *A* on Fig. 13 is farther from (1, 0) than any other point on the boundary of the region *ABCDEF* for frequencies less than ω^*. Proving this claim is possible by considering the individual contributions of gain, time-constant and time-delay uncertainty to $l_m(s)+1$.

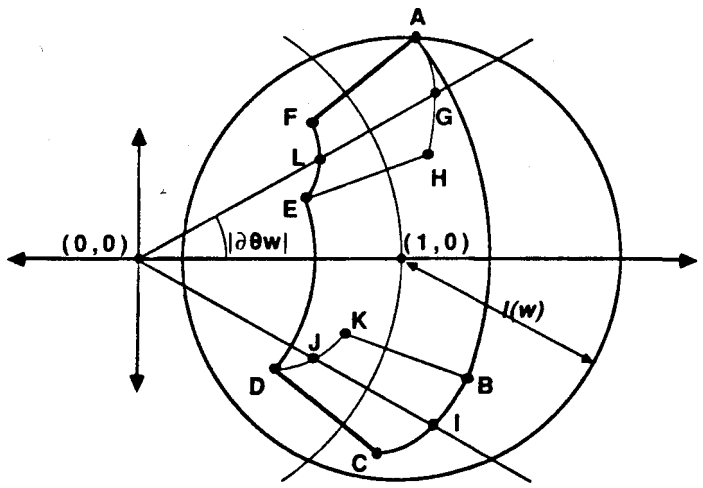

Figure 13. All possible values for $l_m(s)+1$ at one frequency $s = i\omega$ can be located inside the boundary *ABCDEF* given the parameter uncertainties in (6). The bound $l(\omega)$ on the magnitude of the multiplicative uncertainty is equal to the radius of the smallest disk centred at (1, 0) that contains the region boundary.

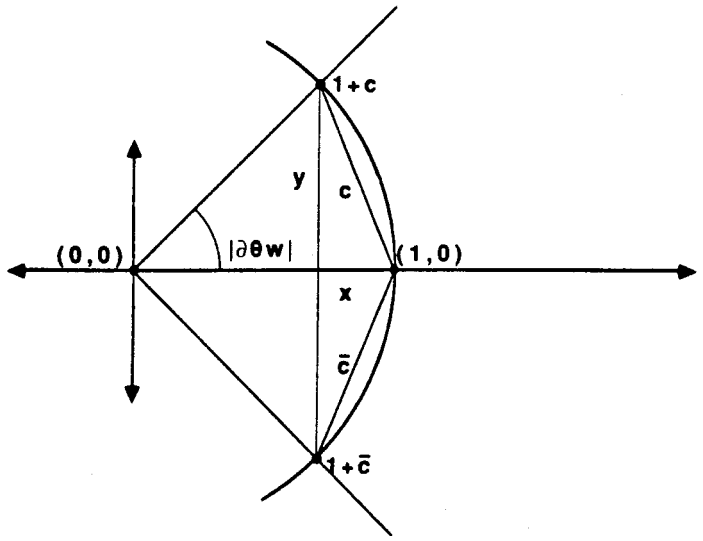

Figure 14. The contribution of time-delay uncertainty to $l_m(s)+1$.

Figure 14 represents the contribution of time-delay uncertainty to $l_m(s)+1$; that is, $\exp(+|\delta\theta|s) = 1+c$ and $\exp(-|\delta\theta|s) = 1+\bar{c}$. Restrict $|\delta\theta|\omega \leqslant \pi$ to define positive $x = 1-\cos(|\delta\theta|\omega)$ and positive $y = \sin(|\delta\theta|\omega)$. Then $c = -x+iy$ and it is easily verified that

$$-2x + x^2 + y^2 = 0 \tag{A 5}$$

The contribution of gain uncertainty to $l_m(s)+1$ is $(\bar{k}+|\delta k|)/\bar{k} = 1+r$ and $(\bar{k}-|\delta k|)/\bar{k} = 1-r$ where positive $r = |\delta k|/\bar{k}$.

Figure 15 represents the contribution of a left-half plane pole uncertainty to $l_m(s)+1$; that is $(\bar{\tau}s+1)/((\bar{\tau}-|\delta\tau|)s+1) = 1+b$ and $(\bar{\tau}s+1)/((\bar{\tau}+|\delta\tau|)s+1) = 1+d$

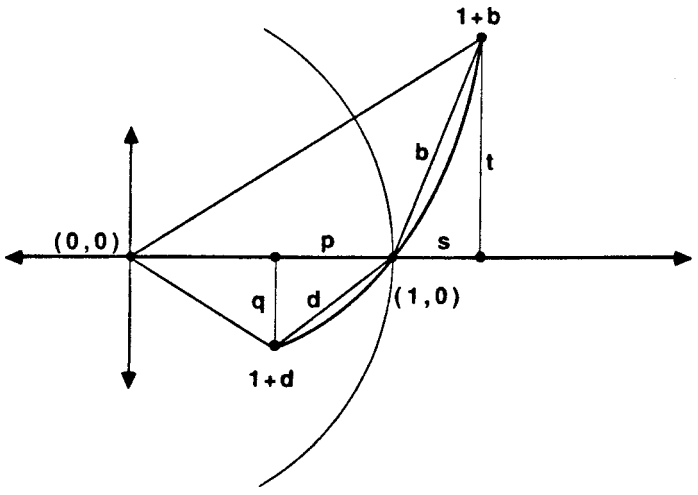

Figure 15. The contribution of left-half-plane pole uncertainty to $l_m(s)+1$.

where $b = s + it$, $d = -p - iq$, and positive s, t, p and q are defined below.

$$s = \frac{|\delta\tau|(\bar{\tau} - |\delta\tau|)\omega^2}{1 + (\bar{\tau} - |\delta\tau|)^2\omega^2}$$

$$t = \frac{|\delta\tau|\omega}{1 + (\bar{\tau} - |\delta\tau|)^2\omega^2}$$

$$p = \frac{|\delta\tau|(\bar{\tau} + |\delta\tau|)\omega^2}{1 + (\bar{\tau} + |\delta\tau|)^2\omega^2}$$

$$q = \frac{|\delta\tau|\omega}{1 + (\bar{\tau} + |\delta\tau|)^2\omega^2}$$

Since $|b| \geqslant |d|$ for all values of ω, $\bar{\tau} > 0$, and $|\delta\tau| \leqslant \bar{\tau}$ the following inequalities are easily verified:

$$s^2 + t^2 - p^2 - q^2 \geqslant 0 \tag{A 6}$$

$$t - q \geqslant 0 \tag{A 7}$$

$$s^2 + t^2 + p^2 + q^2 + s - p = |\delta\tau|\bar{\tau}\left(\frac{1}{1 + (\bar{\tau} - |\delta\tau|)^2\omega^2} - \frac{1}{1 + (\bar{\tau} + |\delta\tau|)^2\omega^2}\right) \geqslant 0 \tag{A 8}$$

The following lemmas will be used in the proof of Bound 1. For brevity they are presented here without proof. The reader can easily establish their validity via simple geometrical arguments.

Lemma 1

Consider a circle centered at the origin. Let XY be an arc of the circle passing through the positive real axis having endpoints X and Y. If $|\arg[X]| \leqslant \pi$ and $|\arg[Y]| \leqslant \pi$ then the point on XY with maximum distance from $(1, 0)$ is X if $|\arg[X]| > |\arg[Y]|$ or Y if $|\arg[Y]| > |\arg[X]|$.

Lemma 2

Consider a ray originating from $(0, 0)$. Let XYZ be a line segment on the ray with midpoint Y on or outside the unit circle and endpoint X nearest the origin. The point on XYZ with maximum distance from $(1, 0)$ is endpoint Z farthest from the origin.

Lemma 3

Consider a ray originating from $(0, 0)$. Let XYZ be a line segment on the ray with midpoint Y inside the unit circle and endpoint X nearest the origin. The point on XYZ with maximum distance from $(1, 0)$ is either endpoint X or endpoint Z.

Proof of Bound 1

Consider Fig. 13 illustrating the region containing possible values for $l_m(i\omega) + 1$ when $\bar{\tau} > 0$. The following arguments prove that of all points on boundary $ABCDEF$, point A is at the maximum distance from $(1, 0)$ at frequencies below ω^*.

(i) $|A - 1|$ is greater than or equal to the distance from $(1, 0)$ to any point on arc AB (Lemma 1).

(ii) $|A-1|$ is greater than or equal to the distance from (1, 0) to any point on segment FA (Lemma 2).

(iii) The distance from (1, 0) to any point on BI is less than or equal to the distance from (1, 0) to a corresponding point on AG (Lemma 1).

(iv) The distance from (1, 0) to any point on FL is less than or equal to the distance from (1, 0) to a corresponding point on AG (Lemma 2).

(v) The distance from (1, 0) to any point on EL is less than or equal to the distance from (1, 0) to a corresponding point on DJ (Lemma 1).

(vi) $|E-1|$ is greater than or equal to the distance from (1, 0) to any point on arc DE (Lemma 1).

(vii) $|A-1|$ is greater than the distance from (1, 0) to any other point on AG because AG lies outside the unit circle and both magnitude and argument of A are greater than those of any other point on AG.

(viii) Either $|C-1|$ or $|D-1|$ is greater than or equal to the distance from (1, 0) to any other point on CD (Lemma 3).

(ix) $|A-1| \geqslant |C-1|$ since

$$|A-1|^2-|C-1|^2=(1+2r+r^2)(s^2+t^2-p^2-q^2)+2y(1+r)(t-q)+2x(1+r)(p+s)+2r(s+p)+2pr^2\geqslant 0$$

(Equations (A 5)–(A 8) with r, s, t, p, q, x and y all positive.)

(x) $|A-1| \geqslant |D-1|$ since

$$|A-1|^2-|D-1|^2=(1+r^2)(s^2+t^2-p^2-q^2)+2r(s^2+t^2+p^2+q^2+s-p)+2px(1-r)+2y(t-q)+2ry(t+q)+2sx(1+r)+2pr^2+4rx+2r^2s\geqslant 0$$

(Equations (A 5)–(A 8) with r, s, t, p, x, and y all positive.)

(xi) Points on DJ and CI are not farther from (1, 0) than point A because arguments (vii)–(x) can be applied with smaller $\delta\tau$.

Therefore $l(\omega)=|A-1|$ for $\omega \leqslant \omega^*$.

For $\omega > \omega^*$ Bound 1 follows from the triangle inequality and the fact that the model described by the extremes of gain, time-constant, and time-delay in Bound 1 is a member of the set described by (6).

The region containing all possible values for $l_m(i\omega)+1$ when $\bar{\tau}<0$ is the mirror image of that in Fig. 13 across the real axis. The same arguments apply for the proof in this case with $s=-i\omega$, hence the change of signs in Bound 1 when $\bar{\tau}<0$. □

The proof of Bound 1 motivates a similar bound on the magnitude of the multiplicative error when simultaneous parameter uncertainties in process gain, zero location and time-delay are encountered.

Bound 2: gain, time-delay and zero uncertainty

Consider the following set of process models:

$$p(s)=p'(s)(\bar{k}+\delta k)((\bar{z}+\delta z)s+1)\exp\left[-(\bar{\theta}+\delta\theta)s\right] \tag{A 9}$$

where $p'(s)$ does not contain parameter uncertainties and $\bar{k}$, $\bar{z}$, $\bar{\theta}$, δk, δz and $\delta\theta$ are defined by:

$$\bar{k} = \frac{k_{\min} + k_{\max}}{2}, \quad \bar{z} = \frac{z_{\min} + z_{\max}}{2}, \quad \bar{\theta} = \frac{\theta_{\min} + \theta_{\max}}{2}$$

$$|\delta k| \leqslant \Delta k = |k_{\max} - \bar{k}| < |\bar{k}|, \quad |\delta z| \leqslant \Delta z = |z_{\max} - \bar{z}| < |\bar{z}|$$

$$|\delta\theta| \leqslant \Delta\theta = |\theta_{\max} - \bar{\theta}| < |\bar{\theta}|$$

Define a nominal model $\tilde{p}(s)$ with gain, zero and time-delay at their mean values:

$$\tilde{p}(s) = p'(s)\bar{k}(\bar{z}s + 1)\exp(-\bar{\theta}s) \tag{A 10}$$

The smallest possible bound $l(\omega)$ on the multiplicative error $l_m(s)$ such that all models in (A 9) are contained in the set $p(s) = \tilde{p}(s)[1 + l_m(s)]$ is given by:

$$l(\omega) = \left|\left(\frac{|\bar{k}| + \Delta k}{|\bar{k}|}\right)\left(\frac{(\bar{z} \pm \Delta z)i\omega + 1}{\bar{z}i\omega + 1}\right)\exp(\pm\Delta\theta i\omega) - 1)\right|, \quad \forall\,\omega < \omega^{**} \tag{A 11}$$

$$l(\omega) = \left|\left(\frac{|\bar{k}| + \Delta k}{|\bar{k}|}\right)\left(\frac{(\bar{z} \pm \Delta z)i\omega + 1}{\bar{z}i\omega + 1}\right)\right| + 1, \quad \forall\,\omega \geqslant \omega^{**} \tag{A 12}$$

where ω^{**} is defined implicitly by:

$$\pm\Delta\theta\omega^{**} + \arctan\left[\frac{\pm\Delta z\omega^{**}}{1 + \bar{z}(\bar{z} \pm \Delta z)\omega^{**2}}\right] = \pm\pi, \quad \frac{\pi}{2} \leqslant \Delta\theta\omega^{**} \leqslant \pi \tag{A 13}$$

Bound 2 applies to both left- and right-half-plane zeros in (A 3). Top signs are selected in (A 11)–(A 13) if $\bar{z}$ is positive, indicating a left-half-plane zero. Bottom signs are selected in (A 11)–(A 13) if $\bar{z}$ is negative, indicating a right-half-plane zero.

The similarity between Bound 1 for simultaneous uncertainties in gain, pole location and time-delay and Bound 2 for simultaneous uncertainties in gain, zero location and time-delay can be seen by examining $l_m(s)$. The description (A 9) for a set of process models can be rewritten as follows:

$$p(s) = p'(s)(\bar{k} + \delta k)((\bar{z} + \delta z)s + 1)\exp[-(\bar{\theta} + \delta\theta)s]$$

$$p(s) = p'(s)\bar{k}(\bar{z}s + 1)\exp(-\bar{\theta}s)\left[1 + \left(\frac{\bar{k} + \delta k}{\bar{k}}\right)\left(\frac{(\bar{z} + \delta z)s + 1}{\bar{z}s + 1}\right)\exp(-\delta\theta s) - 1\right] \tag{A 14}$$

$$p(s) = \tilde{p}(s)[1 + l_m(s)] \tag{A 15}$$

From equations (A 14) and (A 15) we can identify (A 10) as the expression for the nominal model $\tilde{p}(s)$ and the following expression as $l_m(s)$:

$$l_m(s) = \left(\frac{\bar{k} + \delta k}{\bar{k}}\right)\left(\frac{(\bar{z} + \delta z)s + 1}{\bar{z}s + 1}\right)\exp(-\delta\theta s) - 1 \tag{A 16}$$

Figure 16 represents the contribution of a left-half plane zero uncertainty to $l_m(s) + 1$; that is, $((\bar{z} + |\delta z|)s + 1)/(\bar{z}s + 1) = 1 + a$ and $((\bar{z} - |\delta z|)s + 1)/((\bar{z}s + 1) = 1 - a$ where $a = u + iv$ with positive u and v defined below.

$$u = \frac{|\delta z|\bar{z}\omega^2}{1 + \bar{z}^2\omega^2}$$

$$v = \frac{|\delta z|\omega}{1 + \bar{z}^2\omega^2}$$

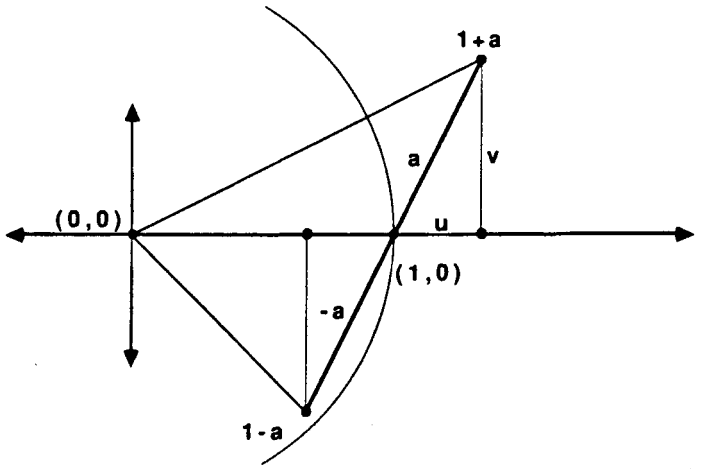

Figure 16. The contribution of left-half-plane zero uncertainty to $l_m(s) + 1$.

Proof of Bound 2 uses the same arguments used to prove Bound 1. The only modification required is that the zero uncertainty replace the pole uncertainty by setting $s = p = u$ and $t = q = v$ in the proof for the case $\bar{z} < 0$. Subsequently set $s = -i\omega$ in the proof for the case $\bar{z} > 0$. The substitution $s = -i\omega$ necessitates the change of signs in (6)–(8) for the case $\bar{z} > 0$.

References

Åström, K. J., 1977, *Int. J. Control*, **26**, 307.
Bhaya, A., and Desoer, C. A., 1985, *Int. J. Control*, **41**, 813.
Brosilow, C. B., 1979, The structure and design of Smith predictors from the viewpoint of inferential control. *Joint American Control Conf.*, Denver.
Callender, A., Hartree, D. R., and Porter, A., 1936, *Phil. Trans. R. Soc.*, **235**, 415.
Chen, S., 1984, Control system design for multivariable uncertain processes. Ph.D. thesis, Case Western Reserve University.
Chu, C. C., Doyle, J. C., and Lee, E. B., 1986, *Int. J. Control*, **44**, 565.
Cohen, G. H., and Coon, G. A., 1953, *Trans. Am. Soc. mech. Engrs*, July, 827.
Doyle, J. C., 1982, *Proc. Instn elect. Engrs*, Pt D, **129**, 242.
East, D. J., 1981, *Int. J. Control*, **34**, 731; 1982, *Ibid.*, **35**, 891.
Garcia, C. E., and Morari, M., 1982, *I. & E.C. Process Des. Dev.*, **21**, 308.
Holt, B. R., 1984, The assessment of dynamic resilience: the effect of non-minimum phase elements. Ph.D. thesis, University of Wisconsin–Madison.
Horowitz, I., 1983, *Int. J. Control*, **38**, 977.
Ioannides, A. C., Rogers, G. J., and Latham, V., 1979, *Int. J. Control*, **29**, 557.
Jerome, N. F., and Ray, W. H., 1986, *A.I.Ch.E. Jl*, **32**, 914.
Laughlin, D. L., Jordan, K. G., and Morari, M., 1986, *Int. J. Control*, **44**, 1675.
Morari, M., Zafirou, E., and Economou, C., 1987, *Robust Process Control* (Berlin: Springer-Verlag).
Ogunnaike, B. A., Lemaire, J. P., Morari, M., and Ray, W. H., 1983, *A.I.Ch.E. Jl*, **29**, 632.
Owens, D. H., and Raya, A., 1982, *Proc. Instn elect. Engrs*, Pt D, **129**, 298.
Palmor, Z. J., 1980, *Int. J. Control*, **32**, 937; 1985, *A.I.Ch.E. Jl*, **31**, 215.
Palmor, Z. J., and Shinnar, R., 1981, *A.I.Ch.E. Jl*, **27**, 793.
Rivera, D. E., and Morari, M., 1987, *Int. J. Control*, **46**, 505.
Rivera, D. E., Morari, M., and Skogestad, S., 1985, *I. & E.C. Process Des. Dev.*, **25**, 252.
Smith, O. J. M., 1957, *Chem. Engng Prog.*, **53**, 217.
Skogestad, S., and Morari, M., 1986, Control of ill-conditioned plants: high purity distillation. *A.I.Ch.E. Ann. Meeting*, Miami, Florida, U.S.A.

CHAPTER V: ROBUST PERFORMANCE OF CROSS-DIRECTIONAL BASIS-WEIGHT CONTROL IN PAPER MANUFACTURING

ROBUST PERFORMANCE OF CROSS-DIRECTIONAL BASIS-WEIGHT CONTROL IN PAPER MANUFACTURING

Daniel L. Laughlin and Manfred Morari

Abstract

The cross-machine-direction (CD) control problem in paper manufacturing is analyzed from the viewpoint of robust performance. The objective of robust performance is to maintain control-system stability and to satisfy a bound on the maximum singular value of the closed-loop sensitivity function despite modelling error. Characteristics common to all CD response control problems including paper basis-weight control are identified. The response of an important actuator for basis-weight control, the paper machine slice, is described by a single, dimensionless, design parameter that provides considerable insight about the CD response control problem. Methods for incorporating CD response characteristics and modelling error into accurate process models are presented. Interactions in typically large-dimension (many inputs and outputs) CD response problems are represented by three standard matrix forms: centrosymmetric, Toeplitz symmetric, and circulant symmetric matrices. Special properties of the three forms relevant to the CD control problem are identified. The properties enable development of controller design procedures to meet the robust performance objective despite model interaction uncertainties. The design procedure results in desirable diagonal and banded controllers. Sufficient conditions allowing design of the robust diagonal and banded controllers are developed. Stability, performance, and failure-tolerance properties of the controllers are proven.

1. Introduction

The cross-machine-direction (CD) control problem in paper manufacturing is aimed at maintenance of flat profiles of paper sheet properties across the paper machine. Basis-weight, or paper weight per unit area, is an example of one important sheet property. Variations in CD basis-weight can result in paper that will not lie flat. Successful control of CD paper sheet properties can mean significant reductions in raw material consumption. For example, Eastman Kodak reported a 2.4 percent reduction in fiber usage as a result of CD control [Carey et al., 1975]. Minimal variation in CD sheet properties enables operators to produce thinner paper closer to the target caliper. Additional motivations cited for better CD control in the paper manufacturing industry include: increasing demand for greater production rates; improving product quality despite a high turnover rate in the work force resulting in inexperienced operators; eliminating breaks, rewinds, and rejects; and reducing energy consumption [Wallace, 1981].

1.1. Control System Robustness Objective

The purpose of this paper is to analyze the CD response control problem from the perspective of robust performance. In this section the objective of robust performance is mathematically defined. The formulation is done in a manner consistent with the new theory by Doyle [1982, 1987]. First, a set of possible models Π is used to express uncertainty in knowledge of the physical system to be controlled. Control system requirements are then proposed – two universal requirements for the control system illustrated in Figure 1 are stability and acceptable attenuation of the disturbance in the output. If a controller satisfies these requirements for the whole set Π, it is said to exhibit robustness with respect to the modelling errors. Exactly what is meant by stability and acceptable attenuation of disturbances is defined in the following two sections.

1.1.1 Robust Stability

Nominal stability of the control system in Figure 1 for one process model $\tilde{P}(s) \in \Pi$ and robust stability for the whole set Π are defined as follows:

Definition 1 – Nominal Stability: The control system in Figure 1 with controller $C(s)$ and process $\tilde{P}(s)$ is stable if and only if all of its closed-loop poles are in the left-half plane.

Definition 2 – Robust Stability: The control system in Figure 1 with controller $C(s)$ and process $P(s) \in \Pi$ is robustly stable if and only if it is stable for all $P(s) \in \Pi$.

1.1.2. Robust Performance

Before defining robust performance, it is necessary to define what is meant by performance of the control system in Figure 1. The performance of a control system is defined in terms of a weight $W(s)$ restricting the magnitude of the closed-loop, sensitivity function $\left[I + P(s)C(s)\right]^{-1}$.

Definition 3 – Nominal Performance: The control system in Figure 1 with controller $C(s)$ and process $P(s) = \tilde{P}(s)$ exhibits performance if and only if it is nominally stable and

$$\sup_{s=i\omega} \sigma_{max}\left(W(s)\left[1 + P(s)C(s)\right]^{-1}\right) < 1. \tag{1}$$

Since the sensitivity function relates system outputs $y(s)$ to disturbances $d(s)$, it is desirable that it have low magnitude. It is convenient to select a weight $W(s)$ equal to scalar $w(s)$ times identity as in Equation 2, with parameter $0 < b < 1$ and parameter $a > 0$.

$$w(s) = b\frac{as + 1}{as} \tag{2}$$

If a control system satisfies the performance requirement 1 with weight $w(s)$ given by 2, it will have a bandwidth of at least $1/a$. The magnitude of a weight $|w(s)|$ with $b = 1/2$ and $a = 4$ is illustrated in Figure 2. The concept of robust performance now follows from that of nominal performance.

Definition 4 – Robust Performance: The control system in Figure 1 with controller $C(s)$ and process $P(s) \in \Pi$ exhibits robust performance if and only if it is nominally stable and the bound 1 is satisfied for all $P(s) \in \Pi$.

The supremum of the maximum singular value in 1 over all frequencies and over all process models $P(s) \in \Pi$ is Doyle's "structured singular value" μ for weighted sensitivity function problems. In this work the symbol $\mu(\omega)$ will denote the supremum of the maximum singular value in 1 over all process models as a function of frequency.

1.2. Controller Design Strategy

Design procedures are presented in Section 6, which result in desirable diagonal and banded controllers for CD response control systems with typically large dimensions (large numbers of inputs and outputs). In Sections 4 and 5 it is shown that the eigenvalues of useful CD response models can be bounded on a segment of the positive real axis. The segment is then interpreted as gain uncertainty in a SISO process model of the form $p(s)$ given in Equation 3.

$$\pi = \left\{ p(s) \middle| p(s) = k\left[\frac{a_j n_j(s) + \ldots + a_1 n_1(s) + a_0 n_0(s)}{b_l d_l(s) + \ldots + b_1 d_1(s) + b_0 d_0(s)}\right] e^{-\theta s} \right\} \qquad (3)$$

$$a_j \in [a_{j_{min}}, a_{j_{max}}],\ b_l \in [b_{l_{min}}, b_{l_{max}}]$$

$$k \in [k_{min}, k_{max}],\ \theta \in [\theta_{min}, \theta_{max}]$$

In Equation 3 the terms $n_j(s)$, and $d_l(s)$ are exact functions, while real numerator coefficients a_j, denominator coefficients b_l, gain k, and time-delay θ are bounded by minimum and maximum values. Since the real parameters in Equation 3 are inexactly known, π in Equation 3 represents a set of process models. Laughlin et al. [1986] have developed a procedure for designing SISO controllers $c(s)$ that exhibit robust performance in control systems with processes $p(s) \in \pi$. These controllers are modified in an appropriate manner to develop robust MIMO controllers for CD response control systems.

Analysis tests used to ensure that SISO controllers $c(s)$ exhibit robust performance are based on regions $\pi(i\omega)$ on the complex plane containing all possible $p(i\omega)$ in Equation 3. A method for locating these regions can be found in Laughlin et al. [1986]. Once these regions are located, a convenient test for SISO robust stability based on the familiar Nyquist stability test can be applied.

Nyquist Stability Test – SISO Nominal Stability: The SISO system in Figure 1 with controller $c(s)$ and nominal model $\tilde{p}(s)$ is stable if and only if the number of clockwise (positive) encirclements of $(-1,0)$ by $p(s)c(s)$, as s encircles (clockwise) the Nyquist contour (the right-half plane excluding singularities on the imaginary axis), is equal to the negative of the number of open-loop unstable poles.

Analysis Test 1 – SISO Robust Stability: The SISO system in Figure 1 with controller $c(s)$ and model $p(s) \in \pi$ is robustly stable if and only if the system is nominally stable for one $\tilde{p}(s) \in \pi$ and regions $\pi(i\omega)c(i\omega)$ exclude $(-1,0)$ for all frequencies ω.

Regions $\pi(i\omega)$ located for the SISO robust stability test are used in the SISO robust-performance test. The performance objective 1 requires that regions $\pi(i\omega)c(i\omega)$ be at greater than a specified distance from $(-1,0)$.

Analysis Test 2 – SISO Robust Peformance: The SISO system in Figure 1 with controller $c(s)$ and model $p(s) \in \pi$ exhibits robust performance if and only if the system is nominally stable for one $\tilde{p}(s) \in \pi$ and the distance of regions $\pi(i\omega)c(i\omega)$ from $(-1,0)$ exceeds $|w(i\omega)|$ for all frequencies ω.

Conditions for robust stability and robust performance of the MIMO CD response control system are developed from these SISO analysis tests in Sections 7 and 8. In addition to satisfying robust-performance requirements, the proposed controller-design procedure results in controllers that exhibit robust performance in remaining loops when one or more actuators fail.

1.3. Synopsis

The analysis presented in this paper is based on a process model including three factors always present in CD control problems: actuator dynamics, interactions, and time-delay. Most importantly, since knowledge of these three factors may be incomplete, methods for incorporating uncertainty in the process model are also presented. Characteristics of the CD sheet response model that cause difficulties in controller design are examined. The slice on the paper machine headbox is often selected to be the actuator for CD basis-weight control. Considerable insight about interactions in the response of CD sheet properties is gained by calculating the deflection of the slice caused by a single screw adjustment. A dimensionless parameter in the model used for this calculation offers an opportunity to influence interactions through slice design. Propagation of interactions introduced at the slice down the Fourdrinier wire is discussed. Analysis of continuous control systems without constraints is given here – issues of constraints and discretization are not addressed. Usually these issues can be resolved following design and analysis of a continuous control strategy.

Sections 2 – 9 of this paper are organized as follows:

2) A CD response model is developed and compared with literature models.

3) Control strategies reported in the literature are cited and discussed.

4) Properties of special matrix forms related to CD control are examined.

5) Singular value bounds are derived for CD response models despite real parameter interaction uncertainties.

6) Theorem 2 states a robust stability result for systems with controllers.

7) Theorem 3 states a robust performance result for systems with diagonal controllers.

8) Theorem 4 states an actuator-failure-tolerance result for systems with diagonal controllers.

9) Synthesis methods for robust diagonal, banded, and model-inverse-based CD response controllers are presented.

Following Section 9, conservativeness and application of the proposed controller design procedure are discussed. An slice-actuator design to enhance the quality of CD basis-weight control is examined. Proofs of theorems presented in this paper are given in the Appendix.

2. Model Development for Cross-Directional Response

Models relating the response of CD paper sheet properties to actuator adjustments are required before control strategies can be developed for the paper machine. One distinctive characteristic of all such models is that they are of large dimension. Typically, a beta ray gauge or a caliper sensor traverses the paper, measuring basis-weight or thickness at n points across the sheet. These data are used to calculate n actuator adjustments to be made upstream of the measurements. Such systems require an $n \times n$ matrix transfer-function relating CD sheet properties to actuator adjustments. Beecher and Bareiss [1970] report a 240 inch wide machine with 40 actuators spaced 6 inches apart across the slice. Up to 50 slice actuators are

reported by Karlsson [Karlsson et al., 1982]. Paper machines requiring response models as large as 100 × 100 are referenced in the literature [Wilhelm and Fjeld, 1983]. Moreover, an established trend is for new machines to become wider and faster, increasing the dimension of the system and making control more difficult [Wallace, 1981].

In this paper it will be assumed that the response of CD paper sheet properties to actuator adjustments is stable; that is, the CD sheet profile settles, following actuator adjustment to a point where successive measurements are nearly identical. This is a reasonable assumption for most paper machines, though Devries studied a machine for which successive CD basis-weight measurements were widely different [DeVries et al., 1977]. He attributed the instablility to turbulence and disturbances in the stock distribution system that propagated through the headbox. Wrist [1961] also identifies this type of instability in basis-weight caused by turbulent vortices in the headbox. He recommends correct headbox design with improved distribution of flow as the solution to the problem. Requirements for headbox design can be found in the article by Egelhof [1986]. It will be assumed here that the headbox design ensures a stable CD profile.

2.1. Actuator Dynamics, Time-Delay, and Interactions

Features common to all CD response models are actuator dynamics, time-delay, and interactions. A paper machine slice is designed so that it can be adjusted upward or downward by actuators at evenly spaced points along its length. Actuator spacing of 6 inches is standard, though spacings of 4.5 inches and 3.5 inches are reported for critical grades of paper [Ewald, 1987]. Mechanisms used to manipulate the slice include: motorized slice screws, thermal expansion of rods, thermal expansion of hydraulic fluid, and robots that travel between and adjust the slice screws [Wilkinson and Hering, 1983]. No matter what mechanism is used to manipulate the

slice, it is commonly assumed that every actuator along the slice can be modelled by the same dynamics [Wilhelm and Fjeld, 1983]. This means that scalar actuator dynamics (for example a first-order lag $p_a(s) = k_a/(\tau_a s + 1)$) multiplies the entire matrix transfer-function used to model CD response. Since basis-weight, moisture or caliper measurements are taken some distance down machine-direction from the slice, time passing before actuator manipulations are sensed must be included in the CD response model as delay $p_d(s) = e^{-\theta s}$. The importance of this delay in CD response models varies from machine to machine as production speeds vary from a few hundred feet of paper per minute to several thousand feet per minute.

When one actuator is manipulated, CD sheet properties invariably change for some distance either side of the position directly downstream from the actuator. These observed interactions are incorporated into the CD response model for n actuators through a constant matrix $P_{CD}^{n,m}$. It is usually assumed that interactions are the same for all actuator locations across the paper machine. Moreover, interactions are assumed to be symmetric about each actuator location. These assumptions cause matrix $P_{CD}^{n,m}$ to take on a "banded symmetric" structure as indicated in Equation 4. Matrix $P_{CD}^{n,m}$ can therefore be identified by measuring the CD sheet response to changes made at a single actuator – saving huge experimental effort when the slice has as many as 100 actuators.

$$P_{CD}^{n,m} = \underbrace{\begin{pmatrix} p_1 & p_2 & \cdots & p_m & 0 & \cdots & \cdots & 0 \\ p_2 & p_1 & p_2 & \cdots & p_m & \ddots & \ddots & \vdots \\ \vdots & p_2 & p_1 & p_2 & \cdots & \ddots & \ddots & \vdots \\ p_m & \vdots & p_2 & \ddots & \ddots & \vdots & p_m & 0 \\ 0 & p_m & \vdots & \ddots & \ddots & p_2 & \vdots & p_m \\ \vdots & \ddots & \ddots & \cdots & p_2 & p_1 & p_2 & \vdots \\ \vdots & \ddots & \ddots & p_m & \cdots & p_2 & p_1 & p_2 \\ 0 & \cdots & \cdots & 0 & p_m & \cdots & p_2 & p_1 \end{pmatrix}}_{n \times n} \tag{4}$$

Occasionally, elements in $P_{CD}^{n,m}$ near the upper left and lower right corners are modified to represent slight differences in CD response near the edges of the paper machine. The overall dynamic model for CD response is given by the product of $p_a(s)$, $p_d(s)$, and $P_{CD}^{n,m}$. An example of one such model is given in Equation 5.

$$P_{CD}^{20,3}(s) = p_a(s)p_d(s)P_{CD}^{20,3} = \frac{k_a e^{-\theta s}}{\tau_a s + 1} \underbrace{\begin{pmatrix} p_1 & p_2 & p_3 & 0 & \dots & 0 \\ p_2 & p_1 & p_2 & \ddots & \ddots & \vdots \\ p_3 & p_2 & \ddots & \ddots & \ddots & 0 \\ 0 & \ddots & \ddots & \ddots & p_2 & p_3 \\ \vdots & \ddots & \ddots & p_2 & p_1 & p_2 \\ 0 & \dots & 0 & p_3 & p_2 & p_1 \end{pmatrix}}_{20\times 20} \tag{5}$$

2.2. Model Parameter Uncertainties

Model uncertainty is inevitable in CD response. During normal operation, a paper machine experiences changes in speed, vacuum, and other wet, end process conditions that affect CD response in both magnitude and shape [Richards, 1982]. Headbox hydraulics are complicated and are subject to change with changing pulpwood characteristics. Time-delay can vary significantly: Beecher and Bareiss [1970] report production speeds from 150 to 750 feet per minute on a single paper machine – creating a potential 67 percent uncertainty in the time-delay θ. These and other uncertainties in the physical process are included in the set of process models $\Pi_{CD}^{n,m}$ defined by

$$\Pi_{CD}^{n,m} = \left\{ P_{CD}^{n,m}(s) \middle| \begin{matrix} P_{CD}^{n,m}(s) = p(s)P_{CD}^{n,m} \\ p(s) \in \pi \end{matrix} \right\}, \tag{6}$$

where real elements p_i in the interaction matrix $P_{CD}^{n,m}$ are bounded as in

$$p_i \in [p_{i_{min}}, p_{i_{max}}],$$

and the set π is given by Equation 3. For example, consider first-order actuator dynamics with time-delay:

$$\pi = \{p(s) | p(s) = p_a(s)p_d(s) = \frac{k_a e^{-\theta s}}{\tau_a s + 1}\} \tag{7}$$
$$k_a \in [k_{a_{min}}, k_{a_{max}}],\ \tau_a \in [\tau_{a_{min}}, \tau_{a_{max}}],\ \theta \in [\theta_{min}, \theta_{max}].$$

Each real parameter in the scalar dynamics in Equation 7 is allowed to vary between the specified upper and lower bound independent of the other real parameters. Note that other scalar dynamics in Equation 7 are possible, though the choice of first-order-with-time-delay dynamics is often appropriate for the CD paper sheet response model. Uncertainty in actuator dynamics is represented by the bounds for k_a and τ_a; time-delay uncertainty, by the bounds for θ.

Uncertainty in the CD interaction matrix $P_{CD}^{n,m}$ is conveniently expressed by $p_i \in [p_{imin}, p_{imax}]$ in model 4. This type of correlated coefficient uncertainty in $P_{CD}^{n,m}$ can naturally reflect observed deviations in experimentally measured CD response interactions. McFarlin [1983] cites ignorance of such interaction uncertainty as a probable cause of instability in CD response control systems.

2.3. Reported Models

The proposed or experimental models in Table 1 of interactions in CD basis-weight response to a change at actuator p_1 are reported in the literature. Models 1)–13) have been normalized so that response at position p_1 is 1.0.

Table 1

Reported CD Response Downstream from Actuator Positions

	p_1	p_2	p_3	p_4	p_5	p_6	p_7	p_8	p_9	p_{10}
1)*	1.0	1.2	0.6	−0.4	−0.9	−0.2	−0.2			
2)	1.0	0.4	−0.5	0.05						
3)	1.0	0.4								
4)	1.0	−0.15	0.03	−0.01						
5)	1.0	0.2								
6)	1.0	0.4								
7)	1.0	0.5	−0.5							
8)*	1.0	0.1	−0.3							
9)*	1.0	1.3	0.8	−0.6	−0.3	0.0	−0.1			
10)*	1.0	0.9	0.7	0.8	1.0	0.6	−0.5	−0.4	−0.2	−0.2
11)*	1.0	0.45	−0.55							
12)*	1.0	0.4	−0.2	−0.4	−0.2					
13)*	1.0	0.2	−0.1	−0.1						

Models marked with * appear to be actual process data.

Sources:

1) from "Sweden Research Labs" [Wallace, 1981]

2) [Wilkinson and Hering, 1983]

3) [Boyle, 1978]

4) from actuator model [Tong, 1976]

5) , 6), 7) [Wilhelm and Fjeld, 1983]

8) , 9), 10) newsprint, sack paper, and paper board, respectively from Karlsson et al. [1983] discretized here at 20 cm actuator spacing

11) [Richards, 1982]

12) [Cuffey, 1957]

13) change in slice opening only [Cuffey, 1957]

The CD responses in Table 1 correspond to elements in interaction matrix $P_{CD}^{n,m}$ labelled with p_i of the corresponding actuator position. Indicated numerical values are available in the references by Tong [1976], and Wilhelm and Fjeld [1983]; those for other models are based on values read from low resolution plots and are therefore approximate. Data from Tong [1976] were taken from the center of his CD response model – he employed slightly different numerical values to model interactions near the edge of the paper machine.

2.4. Properties of the Cross-Directional Model

The extent of interaction in CD response varies considerably among the models reported in the literature. The data from Karlsson et al. [1982] indicate that there is some correlation between thicker product and interactions extending over a greater number of actuator positions on the slice. Negative CD response elements can be found in many of the models reflecting the observation that efforts to increase the basis-weight downstream from one actuator position may actually decrease it on either side of that position. Strong interactions lead to large positive and negative off-diagonal elements in matrix P_{CD}^{n} in the response model. What has been reported is that such strong interactions cause difficulties in the control of CD response.

A measure of the severity of expected control difficulty is the condition number γ of the CD response model given by Equation 3.

$$\gamma\left(P_{CD}^{n,m}\right) = \frac{\sigma_{max}\left(P_{CD}^{n,m}\right)}{\sigma_{min}\left(P_{CD}^{n,m}\right)} \tag{8}$$

That high condition number processes can be difficult to control is well understood – Skogestad and Morari [1986] discuss the effects of high condition number processes at length. High condition number of the CD response model means that strong control action is required to attenuate disturbances entering the process in the direction of the minimum singular vector. Strong control action taken in the wrong

direction, however, can lead to instability or poor performance. It is therefore difficult or impossible to design an acceptable controller based on CD response models with high condition number, when input uncertainty or uncorrelated interaction-element uncertainty is also present. Efforts must be taken to avoid these types of model uncertainty descriptions when they are not physically motivated, so that a controller with good performance can be designed.

In the limit of $\gamma \rightarrow \infty$, the CD response model $P_{CD}^{n,m}$ is singular. If this is the case, CD response is uncontrollable because upstream actuator positions causing measured downstream response profiles cannot be determined. That strong enough interactions could result in a singular CD response model was recognized by Wilhelm and Fjeld [1983]. Paper machines must be constructed to have nonsingular $P_{CD}^{n,m}$ so that CD control is possible.

For CD interactions $P_{CD}^{n,m}$ as given by Equation 4, the condition number γ is a function of both interaction and dimension. Figure 3 illustrates the condition number of $P_{CD}^{n,m}$ with elements $p_1 = 1.0$, $p_2 = r$, and $p_3 = -r$ for $0 \leq r \leq 0.5$ as a function of model dimension n. The plot has been truncated at $\gamma = 50.0$ to improve scale – γ increases to ∞ above each of the "flat" peaks in the plot. For values of r greater than 0.25, models of all dimensions $6 \leq n \leq 20$ have at least one singularity. Values of r at which singularities occur change dramatically as the dimension of the system changes. Given the level of interaction $r = 0.424$, for example, a 7×7 system has relatively low condition number $\gamma = 6.77$, while a 14×14 system is singular. Building a paper machine twice the width of one on which CD control is easily accomplished can result in CD response that is impossible to control.

The behavior of CD response models illustrated in Figure 3 is easily explained by locating the eigenvalues of $P_{CD}^{n,m}$. Since $P_{CD}^{n,m}$ is symmetric, it has real eigenvalues distributed along some segment of the real axis. For values of $r < 0.25$, the segment of the real axis containing the eigenvalues excludes the origin for all dimensions n ($P_{CD}^{n,m}$ is positive-definite for these values of r). For larger values of r, the origin

can be between minimum and maximum eigenvalues on the real axis – for certain dimensions n it is an eigenvalue and $P_{CD}^{n,m}$ is singular.

In Section 5 of this paper, conditions are derived for which a CD response model with given interactions is positive-definite. When it can be proven that all eigenvalues of $P_{CD}^{n,m}$ are positive, a synthesis procedure in Section 6 results in a diagonal controller that robustly stabilizes the system. In the following section a parameter in a slice actuator model is identified that can guide slice design so that the CD response model is positive-definite.

2.5. *Slice Actuator Design to Influence Interactions*

The design of the paper machine slice has a significant effect on the interactions in CD response. The actuators must be located near enough to one another so that narrow uneven streaks in the paper can be eliminated. However, each actuator-slice junction can behave as a fulcrum, causing negative elements in the CD response model [Cuffey, 1957]. Wilhelm states that strong interaction in the CD response model is the result of poor choice of actuator spacing [Wilhelm and Fjeld, 1983]. Interactions introduced at the slice propagate down the paper machine and can often be exacerbated by subsequent processing steps. The nature of interactions introduced and the balance between design parameters are explained by developing a model for the slice.

The slice can be modelled as a beam supported by springs equally spaced at actuator locations. If the beam is assumed to be made of a linearly elastic material (linear moment-curvature relationship) and only small deflections are anticipated (linear curvature-deflection relationship), a linear equation relates the deflection along the beam to the moment acting along the beam. These assumptions agree with normal slice operation. Under the same assumptions the principle of superposition of solutions to linear equations can be used to calculate the deflection resulting from many forces acting on the beam (many actuators) as the sum of deflections

resulting from single forces (one actuator at a time) acting on the beam. Under these assumptions the symmetrical deflection can be easily calculated when a step displacement is introduced at the center of the slice. The result of this calculation has important implications for slice-actuator design. The example analysis that follows is a discrete version of the standard Winkler foundation problem discussed in the reference by Scott [1981], where deflection $\delta(x)$ of an infinitely long beam resting on a foundation with uniform spring constant per unit length k_s/a, caused by a force F acting at the center, is given by:

$$\delta(x) = \frac{F\lambda_w a}{2k_s}\big(cos(\lambda_w x) + sin(\lambda_w x)\big)e^{-\lambda_w x};\ x > 0.$$

The parameter λ_w in the expression above is called the Winkler spring constant.

Since the slice is symmetric about the center of the paper machine, half of it can be modelled as a cantilever beam acted on by both a moment and a force at $(0,0,0)$ in Figure 4. The expression for the deflection of the beam $\delta(x)$ caused by one force F_a acting at a a distance $x = a$ from the origin in Figure 4 is given by Equation 9 [Crandall et. al., 1978].

$$\delta(x) = \frac{F_a}{6EM}\big(\lfloor x-a\rfloor^3 - x^3 + 3x^2a\big) \tag{9}$$

The expression $\lfloor\cdots\rfloor$ in Equation 9 is a "singularity" function indicating a value of zero when the argument is negative. Constant E is the elastic modulus of the beam; constant M is the moment of inertia of the beam cross section about the z-axis in Figure 4. The deflection caused by n forces F_{ia} acting at distances $x = ia$ from the origin is therefore given by:

$$\delta_n(x) = \frac{1}{6EM}\sum_{i=1}^{n} F_{ia}\big(\lfloor x-ia\rfloor^3 - x^3 + 3x^2ia\big). \tag{10}$$

Equation 10 can be evaluated at positions $x = ia$ to yield the following expression for the displacement at each actuator position:

$$\underbrace{\begin{pmatrix} \delta_n(1a) \\ \delta_n(2a) \\ \vdots \\ \delta_n(na) \end{pmatrix}}_{\vec{\delta}_n} = \frac{a^3}{6EM} Q \underbrace{\begin{pmatrix} F_{1a} \\ F_{2a} \\ \vdots \\ F_{na} \end{pmatrix}}_{\vec{F}_n}. \tag{11}$$

Matrix $Q \in \Re^{n \times n}$ is symmetric with elements given by $Q_{ij} = 3i^2 j - i^3$ for $j \geq i$. The vector of forces $\vec{F}_n$ is related to the vector of displacements $\vec{\delta}_n$ by

$$\begin{aligned} \vec{F}_n &= k_s(\vec{\delta}_o - \vec{\delta}_n) \\ &= k_s(\vec{\delta}_o - \frac{a^3}{6EM} Q \vec{F}_n) \end{aligned} \tag{12},$$

where k_s is the spring constant of each actuator and $\vec{\delta}_o$ is a vector $\in \Re^n$ with each element equal to the displacement δ_o at the center actuator. Solving for $\vec{F}_n$ in Equation 12 results in

$$\vec{F}_n = (I + \frac{k_s a^3}{6EM} Q)^{-1} k_s \vec{\delta}_o. \tag{13}$$

Now the slice displacement at distances x from the center of the slice can be written in dimensionless form by

$$\frac{\delta_n(x)}{\delta_o} = \frac{k_s a^3}{6EM} \sum_{i=1}^{n} F_{ia} \left(\left| \frac{x}{a} - i \right|^3 - \left(\frac{x}{a} \right)^3 + 3 \left(\frac{x}{a} \right)^2 i \right), \tag{14}$$

where F_{ia} are elements in $\vec{F}_n$ given by Equation 13. The displacement of the slice at the actuator positions is given in dimensionless form by

$$\frac{\vec{\delta}_n}{\delta_o} = \frac{k_s a^3}{6EM} Q (I + \frac{k_s a^3}{6EM} Q)^{-1} \vec{1}, \tag{15}$$

where $\vec{1}$ is a vector $\in \Re^n$ with each element equal to one. Note the appearance of the dimensionless slice actuator design parameter $D_a = k_s a^3 / 6EM$ in Equations 14 and 15. Parameter D_a is related to the Winkler spring constant through $D_a = \frac{2}{3} \lambda_w^4 a^4$. The limiting behavior of slice displacement for extreme values of D_a is easy to

interpret physically and mathematically from Equation 15. For $D_a = 0$, the slice is perfectly rigid and level; for $D_a = \infty$, the actuator springs are perfectly rigid, causing the slice to bend between their fixed endpoints. This behavior and other slice displacements for intermediate values of D_a are illustrated in Figure 5, generated by using Equation 14 with $n = 10$. Note that deflection of the slice is negative for certain actuator positions on either side of center – this accounts for negative elements in the CD response model.

Tong proposed that the slice be modelled as a beam in simple bending between rigid actuators – such a model corresponds to the limit $D_a \rightarrow \infty$ in Equation 15. Interactions labelled 4 in Table 1 were calculated from his model [Tong, 1976]. The extension of such a model to allow for compressible actuators provides insight about how the slice might be designed to suppress interactions. McFarlin [1983] states that in at least one application the stiff slice rod was replaced with "a tubular rod with stiffness similar to that of the slice lip ... like a stiff spring ... thereby protecting the slice lip from excessive bending."

Earlier in this century slices were commonly made of brass, 6 to 12 inches wide and about one-half inch thick [Witham, 1942]. Modern slices are usually made of type 316 stainless steel to avoid excessive corrosion. More exotic materials are sometimes used; for example, Carey et al. [1975] report a titanium slice. Modern slice cross sections are thicker in the middle to resist machine direction shear while maintaining flexibility [Velguth, 1987]. Figure 6 shows the cross section of two slices now available from the Beloit Corporation (courtesy of the Beloit Corporation, Beloit, Wisconsin U.S.A.). In practice, the deflection of the slice must be limited to protect it from damage. McFarlin [1983] reports that a maximum force of 11,121 Newtons can be applied to a Beloit Converflo slice with a maximum deviation between adjacent actuators of 0.038 mm. Headbox manufacturers supply these figures. See Wrist [1961] for a discussion of additional slice-design considerations:

controlling the orientation of fibers in the jet, controlling angle of impact of the jet on the wire, raising the velocity of the jet to that of the wire, etc.

2.7. Wave Propagation on the Fourdrinier

Slice deflection alone cannot account for the magnitude of some of the larger negative off-diagonal elements in CD response models in Table 1. Bernoulli's Equation applied to flow under the slice results in velocity proportional to the slice opening. If no further effects are taken into account, CD response models with small negative off-diagonal elements like 4) from Tong [1976] result. Water waves on the Fourdrinier wire can propagate interactions introduced by the slice even further along the cross-machine-direction. Wrist [1961] reports a study showing that radioactively marked fibers traveled 6 inches in the cross-machine-direction through the wet end of a newsprint machine producing paper at a rate of 1600 feet per minute. Behavior of the water waves is similar to that of a wake behind a ship – waves propagate in a "V" formation downstream from the location where an actuator is adjusted. The expression for velocity v of a small surface wave of height δy propagating into still shallow water of depth y is given by White [1979] as

$$v = \sqrt{gy\left(1 + \frac{\delta y}{y}\right)\left(1 + \frac{\frac{1}{2}\delta y}{y}\right)}. \tag{16}$$

Constant g in Equation 16 is acceleration that is due to gravity. Equation 16 indicates that higher waves will travel faster in the cross-machine direction on the Fourdrinier wire than will lower waves. The effect of this is to flatten the peak of the wave exiting at the center of the slice opening in Figure 5. Since interactions in CD response elements are normalized so that the center response is one, the off-diagonal elements become proportionately larger. The magnitude of this effect is, of course, dependent on machine speed, product caliper, fluid properties of the furnish fiber suspension, speed of deposition of fibers on the Fourdrinier wire, length of the wire, mechanical shake applied to the wire, etc.

3. Reported Control Strategies

Control systems for regulation of CD paper sheet properties have been on line in paper mills for some time. Beecher and Bareiss [1970] reported motorized slice control at St. Regis in 1970. They reported a 60 percent reduction in deviation from a standard basis weight profile on a 92 inch machine with 16 actuators after implementation of an analog, PI-based control system. Eastman Kodak implemented CD control at their Rochester N.Y. mill in 1973 [Carey et al., 1975]. Two control schemes are reported in the literature for CD response control in paper manufacturing: linear-quadratic-optimal (LQ) and model inverse-based control. The following researchers report using LQ controller-design methods minimizing quadratic cost functions penalizing both deviations in paper sheet properties and slice position: Wilhelm and Fjeld [1983], Tong [1976], Boyle [1978], Richards [1982] and Wilkinson [1983]. Mostly steady-state models are proposed – interaction matrices $P_{CD}^{n,m}$. New control actions are often taken only after steady state is reached. In model inverse-based controllers the inverse of $P_{CD}^{n,m}$ is used to define control actions [Wilkinson, 1983]. Often $P_{CD}^{n,m}$ is identified on-line and is used in some type of adaptive control scheme. Additional review of control methods applied to the paper manufacturing industry can be found in the article by Dumont [1986].

One weakness of reported controller design techniques is that they do not address the issue of robustness with respect to errors in the CD response model. In light of the many difficult-to-model process characteristics, for example, wave propagation on the Fourdrinier wire, such modelling errors are inevitable. A more satisfactory controller design technique would guarantee system stability and performance despite modelling errors. Another weakness of both model-inverse-based controller-design methods and LQ controller-design methods is that they lead to complicated control algorithms for large-dimension systems. The inverse of a band diagonal CD interaction model $P_{CD}^{n,m}$ is in general a full matrix – a 100×100 system would lead to a controller with 10,000 elements. A more desirable controller

structure would be itself diagonal or band-diagonal, so that paper sheet properties at one point could be controlled by manipulating a few actuators on either side. In Section 9 of this paper, robust controller-design procedures are developed that result in these more desirable controller structures.

4. Special Models for Cross-Directional Sheet Properties

Special properties of three models for CD response enable convenient robust controller design despite correlated parameter uncertainties in response interactions. The models are centrosymmetric, Toeplitz symmetric, and circulant symmetric matrices. General examples and selected properties of the three special CD interaction matrices are given in this section. Nomenclature for these matrix forms is standard in the mathematics literature – additional properties of the three forms can be found in the works by Davis [1979], Bellman [1970], and Aitken [1954]. Transformations relating the three forms are presented that allow development of tight bounds on CD response-model eigenvalues despite parameter uncertainties. The bounds establish that with similar interactions the three forms closely resemble one another for large-dimension systems. This result enables development of convenient robust controller-design techniques in Section 9.

4.1. Model Structures

The three special model structures, centrosymmetric, Toeplitz symmetric and circulant symmetric, imply certain assumptions about the nature of CD response interactions. Assumptions that accompany each form are given in the following three sections of this paper. It is important to consider the appropriateness of these

assumptions for a particular CD control problem. Whether or not the assumptions are accurate can mean success or failure of the control-system design based on one of the models.

4.1.1 Centrosymmetric

Centrosymmetric models have elements that are symmetric about the center of the matrix. If a paper machine were constructed to be symmetric with respect to a vertical plane through the center of the sheet, then the physical CD response would be exactly centrosymmetric. Centrosymmetric models can represent edge effects observed in the CD response, that is, slight differences in response observed at different distances from the center of the sheet. An example of a centrosymmetric matrix $P_{CS}^{n,m}$ is given by Equation 17.

$$P_{CS}^{n,m} = \underbrace{\begin{pmatrix} p_{11} & p_{12} & \cdots & p_{1m} & 0 & \cdots & \cdots & \cdots & \cdots & 0 \\ p_{21} & p_{22} & p_{23} & \cdots & p_{2m} & 0 & \ddots & \ddots & \ddots & \vdots \\ \vdots & p_{32} & \ddots & \ddots & \cdots & \ddots & \ddots & \ddots & \ddots & \vdots \\ p_{m1} & \vdots & \ddots & p_{mm} & \ddots & \cdots & \ddots & \ddots & \ddots & \vdots \\ 0 & p_{m2} & \vdots & \ddots & \ddots & \ddots & \vdots & \ddots & 0 & \vdots \\ \vdots & 0 & \ddots & \vdots & \ddots & \ddots & \ddots & \vdots & p_{m2} & 0 \\ \vdots & \ddots & \ddots & \ddots & \cdots & \ddots & p_{mm} & \ddots & \vdots & p_{m1} \\ \vdots & \ddots & \ddots & \ddots & \ddots & \cdots & \ddots & \ddots & p_{32} & \vdots \\ \vdots & \ddots & \ddots & \ddots & 0 & p_{2m} & \cdots & p_{23} & p_{22} & p_{21} \\ 0 & \cdots & \cdots & \cdots & \cdots & 0 & p_{1m} & \cdots & p_{12} & p_{11} \end{pmatrix}}_{n \times n} \tag{17}$$

If it is further assumed that the effect of actuator adjustment at position i on response at position j is the same as that at position j on response at position i, then $P_{CS}^{n,m}$ is centrosymmetric symmetric. When $P_{CS}^{n,m}$ is symmetric it is denoted by $P_{CSS}^{n,m}$ in this paper.

4.1.2 Toeplitz Symmetric

In Toeplitz symmetric models the same element is repeated along each diagonal of the matrix. The assumption, that changes observed downstream from one actuator caused by adjustments at the nearest neighboring actuators is independent of position across the machine, leads to a Toeplitz symmetric model. The CD response model $P_{CD}^{n,m}$ in Equation 4 is Toeplitz symmetric – this is the CD response model most often found in the literature. Toeplitz symmetric CD response models are denoted by $P_{CD}^{n,m} = P_{T}^{n,m}$ in this paper.

4.1.3. Circulant Symmetric

A circulant symmetric structure $P_{C}^{n,m}$ is given by Equation 18.

$$P_C^{n,m} = \underbrace{\begin{pmatrix} p_1 & p_2 & \cdots & p_m & 0 & \cdots & 0 & p_m & \cdots & p_2 \\ p_2 & p_1 & p_2 & \cdots & p_m & 0 & \cdots & \ddots & \ddots & \vdots \\ \vdots & p_2 & p_1 & p_2 & \cdots & p_m & \ddots & \ddots & \ddots & p_m \\ p_m & \vdots & p_2 & p_1 & p_2 & \cdots & \ddots & \ddots & \vdots & 0 \\ 0 & p_m & \vdots & p_2 & \ddots & \ddots & \vdots & p_m & 0 & \vdots \\ \vdots & 0 & p_m & \vdots & \ddots & \ddots & p_2 & \vdots & p_m & 0 \\ 0 & \vdots & \ddots & \ddots & \cdots & p_2 & p_1 & p_2 & \vdots & p_m \\ p_m & \ddots & \ddots & \ddots & p_m & \cdots & p_2 & p_1 & p_2 & \vdots \\ \vdots & \ddots & \ddots & \cdots & 0 & p_m & \cdots & p_2 & p_1 & p_2 \\ p_2 & \cdots & p_m & 0 & \cdots & 0 & p_m & \cdots & p_2 & p_1 \end{pmatrix}}_{n \times n} \tag{18}$$

For simplicity, $P_{C}^{n,m}$ is often written $circ(p_1, p_2, ..., p_m, 0, ..., 0, p_m, ..., p_2)$. Circulant symmetric matrices are both Toeplitz symmetric and centrosymmetric. They possess the additional property $P_{C}^{n,m} = QP_{C}^{n,m}Q^{-1}$, where $Q = circ(0, ..., 0, 1)$ is an $n \times n$ "permutation" matrix. As such, $P_{C}^{n,m}$ represents CD response interactions of

a paper machine without edge effects similar to the truncated infinite-dimensional model cited by Wilhelm and Fjeld [1983]. Circulant matrices commute with one another – the eigenvalues of the product of two circulant matrices are equal to the product of the eigenvalues of the two matrices. Circulant matrices lend valuable insight about properties of related CD response models, because their eigenvalues and eigenvectors can be determined by inspection. Eigenvalues λ_i and corresponding eigenvectors $\vec{v}_i$ of circulant matrices are given by Equations 19.

$$\lambda_i\big(\ circ(p_1, p_2, p_3 ..., p_n)\big) = p_1 + w_i p_2 + w_i^2 p_3 + ... + w_i^{n-1} p_n \tag{19}$$

$$\vec{v}_i = \begin{pmatrix} 1 \\ w_i \\ w_i^2 \\ \vdots \\ w_i^{n-1} \end{pmatrix},$$

where w_i is one of the n roots of $w^n = 1$ (for proof see Bellman [1970]). Equation 19 is a powerful tool for bounding the eigenvectors of $P_C^{n,m}$ despite correlated element uncertainties given by $p_i \in [p_{imin}, p_{imax}]$. For circulant symmetric matrices $P_C^{n,m}$ Equation 19 simplifies to

$$\lambda_i\big(\ circ(p_1, p_2, ..., p_m, 0, ..., 0, p_m, ..., p_2)\big)$$

$$= p_1 + 2Re\big[w_i\big] p_2 + 2Re\big[w_i^2\big] p_3 + ... + 2Re\big[w_i^{m-1}\big] p_m. \tag{20}$$

Evaluating 20 is straightforward even when uncertain p_i are bounded on the real axis – addition of uncorrelated line segments is all that is required.

4.2. Transformations Relating Special Models

Transformations given in this section relate the special models $P_{CSS}^{n,m}$ and $P_T^{n,m}$ to the circulant symmetric model $P_C^{n,m}$. The transformations and subsequent eigenvalue bounds will demonstrate that the three models closely approximate one another for large dimensions n – the large system dimensions usually encountered in CD paper response control. The transformations are of the form $B = R^T AR$, where nonsquare matrices R are defined so that $R^T R = I^{n\times n}$. Matrix A from which $P_T^{n,m}$ and $P_{CSS}^{n,m}$ are derived is the circulant symmetric matrix $P_C^{n,m}$.

4.2.1 Circulant Symmetric to Toeplitz Symmetric

Transformation 1: The transformation from the circulant symmetric matrix $P_C^{n+2(m-1),m}$ to the Toeplitz symmetric matrix $P_T^{n,m}$ is given by

$$P_T^{n,m} = \left(R_{C\to T}^{n,m}\right)^T P_C^{n+2(m-1),m} R_{C\to T}^{n,m}, \tag{21}$$

where

$$\left(R_{C\to T}^{n,m}\right)^T = \left(0^{n\times(m-1)} \quad I^{n\times n} \quad 0^{n\times(m-1)}\right) \in \Re^{n\times n+2(m-1)}.$$

4.2.2 Toeplitz Symmetric to Centrosymmetric Symmetric

Transformation 2: The transformation from the Toeplitz symmetric $P_T^{n,m}$ defined in Transformation 1 above to the centrosymmetric symmetric matrix $P_{CSS}^{n,m}$ is given by

$$P_{CSS}^{n,m} = \left(S_{CSS}^{n,m}\right)^{\frac{1}{2}} P_T^{n,m} \left(S_{CSS}^{n,m}\right)^{\frac{1}{2}}, \tag{22}$$

where

$$S_{CSS}^{n,m} = diag(s_1, s_2, ..., s_x, ..., s_2, s_1) \in \Re^{n \times n},\ s_i > 0$$

is a diagonal centrosymmetric matrix with $x = n/2$ for even n or $x = (n+1)/2$ for odd n. (Scalar s_x appears twice for even n.)

5. Singular Value and Eigenvalue Bounds for Special Models

In this section, bounds on singular values (and hence bounds on eigenvalues for positive-definite $P_{CD}^{n,m}$) of CD response interaction models $P_{CD}^{n,m}$ are derived. All eigenvalues of $P_T^{n,m}$ and appropriately scaled $P_{CSS}^{n,m}$ are found on the same segment of the real axis as are those of a corresponding matrix $P_C^{n+2(m-1),m}$. The bounds form the basis for robust-stability, robust-performance, and robust-failure-tolerance results in Sections 6–8, in which this segment of the real axis is treated as if it were gain uncertainty in a SISO model.

5.1 Bounds from Singular Values of $P_C^{n+2(m-1),m}$

Lemma 1 is established before proof of Theorem 1, bounding singular values of positive-definite symmetric $P_T^{n,m}$ and $P_{CSS}^{n,m}$ by those of positive-definite symmetric $P_C^{n+2(m-1),m}$.

Lemma 1: The singular values of matrix A bound the singular values of matrix B, when $A \in \Re^{q \times q}$ is a real symmetric matrix and $B \in \Re^{n \times n}$ $(n < q)$ is equal to $R^T A R$, where $R \in \Re^{q \times n}$ is such that $R^T R = I^{n \times n}$:

$$\sigma_{min}(A) \leq \sigma_{min}(B) \leq \sigma_{max}(B) \leq \sigma_{max}(A).$$

Since matrices $P_T^{n,m}$ and $P_{CSS}^{n,m}$ result from transformations

$$\left(S^{n,m}\right)^{1/2} R^T A R \left(S^{n,m}\right)^{1/2},$$

where matrix A is $P_C^{n+2(m-1),m}$ Lemma 1 can be used to bound their singular values by those of the circulant symmetric matrix.

Theorem 1: If $P_C^{q+2(m-1),m}$ is positive definite symmetric, then $P_T^{n,m}$ and $P_{CSS}^{n,m}$ defined by Transformations 1 and 2 are positive-definite symmetric and singular values of $P_C^{q+2(m-1),m}$ bound the singular values of matrices $P_T^{n,m}$ and $P_{CSS}^{n,m}$ as follows for all dimensions $n \leq q$:

$$\sigma_{min}\left(P_C^{q+2(m-1),m}\right) \leq \sigma_i\left[P_T^{n,m}\right] \leq \sigma_{max}\left(P_C^{q+2(m-1),m}\right)$$

$$\sigma_{min}\left(P_C^{q+2(m-1),m}\right) \leq \sigma_i\left[\left(S_{CSS}^{n,m}\right)^{-\frac{1}{2}} P_{CSS}^{n,m}\left(S_{CSS}^{n,m}\right)^{-\frac{1}{2}}\right] \leq \sigma_{max}\left(P_C^{q+2(m-1),m}\right).$$

Theorem 1 exploits the knowledge that Toeplitz symmetric matrices are cut out of the center of a larger dimension circulant symmetric matrix through Transformation 1. Lemma 1 then guarantees that eigenvalues of positive-definite $P_C^{q+2(m-1),m}$ will bound those of $P_T^{n,m}$ for all dimensions n less than or equal to q. Since centrosymmetric matrices $P_{CSS}^{n,m}$ are derived from Toeplitz symmetric matrices through Transformation 2, their eigenvalues can be bounded by those of a higher dimension circulant symmetric matrix as well.

5.2 Alternative Bounds

The Gershgorin bounds (see, for example, MacFarlane [1970]) on the eigenvalues (and hence on the singular values for positive-definite symmetric matrices) of matrices of $P_T^{n,m}$, $P_C^{n,m}$, and $P_{CSS}^{n,m}$ are easily calculated. Gershgorin's Theorem states that the eigenvalues of a matrix $P = [p_{ij}]$ will lie within the union of i disks centered at p_{ii} with radius $\Sigma|p_{ij}|$; $j \neq i$. Given their banded structure, Gershgorin bounds can be determined by inspection for Toeplitz symmetric, centrosymmetric, and circulant symmetric interaction matrices of all dimensions.

The relative tightness of alternative bounds on eigenvalues of CD interaction matrices is of importance, since the segment of the real axis containing the eigenvalues is treated as gain uncertainty in the following controller design procedures –

tighter bounds result in a less conservative controller design. Bounds on CD interaction matrices based on those of the circulant symmetric matrix $P_C^{n,m}$ are tighter than Gershgorin bounds. This is clearly the case because eigenvalues of $P_C^{n,m}$ are themselves inside the same Gershgorin bounds. Moreover, for correlated interaction parameter uncertainties in the model 6 the Gershgorin bounds will be excessively conservative. Gershgorin bounds ignore correlation between parameters p_i on either side of the main diagonal in the model.

6. Robust Stability Result

Robust stability of MIMO CD response-control systems with diagonal controllers is guaranteed when the conditions of Theorem 2 are satisfied.

Theorem 2: If the SISO control system with loop-transfer function $kp(s)c(s)$ is robustly stable for all $p(s) \in \pi$ and all $k \in \left[\sigma_{min}\left(P_C^{q+2(m-1),m}\right), \sigma_{max}\left(P_C^{q+2(m-1),m}\right)\right]$, where $P_C^{q+2(m-1),m}$ is positive-definite symmetric, then the MIMO control systems with the loop transfer-functions

$$\left[P_C^{n,m}p(s)\right]\left\{c(s)\right\}$$

$$\left[P_T^{n,m}p(s)\right]\left\{c(s)\right\}$$

$$\left[P_{CSS}^{n,m}p(s)\right]\left\{c(s)\left(S_{CSS}^{n,m}\right)^{-1}\right\},$$

are robustly stable for all $p(s) \in \pi$ for all dimensions $n \leq q$. Note that the above formulae are expressed in the form $[\ MIMO\ process\ ]\ \{\ MIMO\ controller\ \}$.

7. Robust Performance Result

Robust performance of MIMO CD response-control systems with diagonal controllers is guaranteed when the conditions of Theorem 3 are satisfied.

Theorem 3: If the SISO control system with loop-transfer function $kp(s)c(s)$ exhibits robust performance in the sense that $\left|w(\omega)\left(1+kp(i\omega)c(i\omega)\right)^{-1}\right| < 1$ for all ω, for all $p(s) \in \pi$, and for all $k \in \left[\sigma_{min}\left(P_C^{q+2(m-1),m}\right), \sigma_{max}\left(P_C^{q+2(m-1),m}\right)\right]$, where $P_C^{q+2(m-1),m}$ is positive-definite symmetric, then the MIMO control systems with the loop transfer-functions given in Theorem 2 exhibit robust performance for all dimensions $n \leq q$ in the sense that

$$\sigma_{max}\left[w(s)\left(I + \left[P_C^{n,m}p(s)\right]\left\{c(s)\right\}\right)^{-1}\right] < 1 \ \forall\omega$$

$$\sigma_{max}\left[w(s)\left(I + \left[P_T^{n,m}p(s)\right]\left\{c(s)\right\}\right)^{-1}\right] < 1 \ \forall\omega$$

$$\sigma_{max}\left[w(s)\left(I + \left[P_{CSS}^{n,m}p(s)\right]\left\{c(s)\left(S_{CSS}^{n,m}\right)^{-1}\right\}\right)^{-1}\right] < 1 \ \forall\omega$$

for all $p(s) \in \pi$.

8. Robust Failure Tolerance Result

Not only can robust stability and robust performance of properly designed MIMO CD response control systems be guaranteed, but robust failure tolerance can be guaranteed as well. That is, both robust stability and robust performance requirements of the remaining system will be satisfied when one or more sensors and actuators are taken out of the control loop. Actuator/sensor failure is equivalent to premultiplication and postmultiplication of the loop transfer-function by R^T and R, respectively, where $R \in \Re^{n\times r}$ is a matrix ($r < n$) such that $R^TR = I^{r\times r}$. Matrix R^T is such that R^TP eliminates rows of P where sensors fail. Matrix R is such that CR eliminates columns of C where actuators fail. Robust failure tolerance of MIMO CD response control systems with diagonal controllers is guaranteed when the conditions of Theorem 4 are satisfied.

Theorem 4: Let $R \in \Re^{n\times r}$ be a matrix ($r < n$) such that $R^T A$ eliminates rows of A with $R^T R = I^{r\times r}$. If the SISO control system with loop-transfer function $kp(s)c(s)$ exhibits robust performance in the sense that $\left|w(\omega)\left(1 + kp(i\omega)c(i\omega)\right)^{-1}\right| < 1$ for all ω, for all $p(s) \in \pi$, and for all $k \in \left[\sigma_{min}\left(P_C^{q+2(m-1),m}\right), \sigma_{max}\left(P_C^{q+2(m-1),m}\right)\right]$, where $P_C^{q+2(m-1),m}$ is positive-definite symmetric, then the MIMO control systems with the loop transfer-functions given in Theorem 2 premultiplied by R^T and post-multiplied by R exhibit robust failure tolerance for all dimensions $r < n \leq q$ in the sense that the systems are robustly stable and

$$\sigma_{max}\left[w(s)\left(I + R^T\left[P_C^{n,m}p(s)\right]\{c(s)\}R\right)^{-1}\right] < 1 \;\forall\omega$$

$$\sigma_{max}\left[w(s)\left(I + R^T\left[P_T^{n,m}p(s)\right]\{c(s)\}R\right)^{-1}\right] < 1 \;\forall\omega$$

$$\sigma_{max}\left[w(s)\left(I + R^T\left[P_{CSS}^{n,m}p(s)\right]\{c(s)\left(S_{CSS}^{n,m}\right)^{-1}\}R\right)^{-1}\right] < 1 \;\forall\omega$$

for all $p(s) \in \pi$.

9. Controller Synthesis Methods

In this section three design methods utilizing results in Theorems 1–4 are presented for CD response control. The design methods lead to diagonal, banded, and full matrix transfer-function controller structures. The proposed methods enable design of CD response controllers for robust performance, where previous design methods cannot be successfully applied.

Prior to this work, two alternatives existed that could theoretically address the problem of designing CD response controllers for robust performance. The first alternative involves iterations between controller selection (by any means) and the structured-singular-value analysis of Doyle [1987]. This alternative is not practical for design of CD response controllers because of the large number of inputs/outputs

and the many required repeated real scalar parameter uncertainties. Consider, for example, a CD response model with d inputs and outputs, x parameter uncertainties in the scalar dynamics, and z interaction parameter uncertainties. In Doyle's analysis, the structured singular value of a $d(x + z + 1) \times d(x + z + 1)$ matrix would have to be calculated with respect to $x + z$ repeated real scalar perturbation blocks of dimension $d \times d$ and one full $d \times d$ performance block. These dimensions exceed the capabilities of existing software for CD response models with few inputs and outputs. Moreover, the analysis can be quite conservative when repeated scalar perturbation blocks are required. The second alternative is the decentralized controller-design method for robust performance proposed by Skogestad and Morari [1987]. Like the first alternative, this alternative is also not practical for design of CD response controllers. In order to calculate the bounds used in the design of a CD response controller with d inputs and outputs, yet another $d \times d$ uncertainty block structure is added to the structured-singular-value analysis problem described above.

The proposed design methods can be easily applied to CD response-control problems with many inputs and outputs. Large numbers of parameter uncertainties in the scalar dynamics and interaction parameter uncertainties can also be accommodated.

9.1. Decentralized Controller Design

It has been demonstrated that the eigenvalues of positive-definite CD response interaction matrices $P_{CD}^{n,m}$ can be conveniently bounded on the real axis. By treating this segment on the real axis as uncertainty in gain k, it is possible to design a robust diagonal controller $c(s)\left(S^{n,m}\right)^{-1}$ for the MIMO process $P_{CD}^{n,m}(s) = p(s)P_{CD}^{n,m}$ by designing a robust controller $c(s)$ for the SISO process $kp(s)$. The gain k can reflect CD interaction uncertainty through bounded parameters p_i in Equation 20.

Interaction uncertainty and more severe CD response interactions leads to eigenvalues on a slightly different/larger segment of the real axis. Most importantly, by treating interaction uncertainty in this way, robust performance of the MIMO system is implied by robust performance of the SISO system. Theorem 2 in Section 6 proves that the diagonal controller will robustly stabilize the system. Theorem 3 in Section 7 states that the system will satisfy the robust-performance requirement. Theorem 4 in Section 8 states that robust failure tolerance of the system is guaranteed.

9.1.1. Synthesis Method

For a CD response model with interactions given by $P_T^{n,m}$ or $P_{CSS}^{n,m}$, the diagonal controller synthesis method is outlined as follows:

Diagonal Controller Synthesis Method:

1) Determine the circulant symmetric matrix $P_C^{n+2(m-1),m}$ corresponding to the model $P_T^{n,m}$ or $P_{CSS}^{n,m}$ from transformations 1–2.
2) Model uncertainty in SISO dynamics $p(s) = p_a(s)p_d(s)$ as in Equation 7.
3) Calculate $\lambda_{min}\left(P_C^{n+2(m-1),m}\right)$ and $\lambda_{max}\left(P_C^{n+2(m-1),m}\right)$.
4) If $\lambda_i\left(P_C^{n+2(m-1),m}\right) > 0 \ \forall i$ continue – scalar times diagonal integral control is possible only for positive-definite matrices $P_C^{n+2(m-1),m}$.
5) Select a performance weight $w(s)$ as in Equation 2.
6) Design a controller $c(s)$ for robust performance for the SISO process $kp(s)$ with $p(s) \in \pi$, where $k \in \left[\lambda_{min}\left(P_C^{n+2(m-1),m}\right), \lambda_{max}\left(P_C^{n+2(m-1),m}\right)\right]$.
7) Scale MIMO controller $C(s) = c(s)I^{n\times n}$ with the appropriate matrix $\left(S^{n,m}\right)^{-1}$ for robust performance of the MIMO system (see Theorem 2).

Alternative methods exist for the SISO robust performance problem in step 6). The Internal Model Control (IMC) design method presented by Laughlin et al. [1986]

for robust performance despite model parameter uncertainties solves this problem. In the IMC design method, the feedback controller $c(s)$ is parameterized in terms of a stable controller $q(s) = \tilde{q}(s)f(s)$, and a nominal model $\tilde{p}(s)$ as shown in Figure 7. The feedback controller $c(s)$ is related to $q(s)$ through $c(s) = q(s)/[1 - \tilde{p}(s)q(s)]$. First, an H_2 optimal controller $\tilde{q}(s)$ is designed for a particular disturbance $d(s)$. Then $\tilde{q}(s)$ is detuned for robustness by filter $f(s)$. Usually only a single filter parameter ϵ in $f(s) = 1/(\epsilon s + 1)$ is adjusted with a transparent tradeoff between performance and robustness. Several tables of recommended filter parameters for processes with time-delay (as in Equation 7) can be found in the paper discussing design of Smith predictors by Laughlin et al. [1987]. The robust performance test used to determine acceptable filter parameters is the region-mapping method of analysis test 2.

9.1.2. Example 1

The first example problem is design of a diagonal controller for the system $P_{CD}^{20,3}(s)$ in Equation 5, with interactions $P_{CD}^{20,3} = P_T^{20,3}$ defined as follows:

$$p_1 = 1.0 \ ; \ p_2 \in [0.1, 0.2] \ ; \ p_3 \in [-0.1, -0.05]. \tag{23}$$

Uncertain first-order actuator dynamics with time-delay are given by

$$p(s) = \frac{k_a e^{-\theta s}}{\tau_a s + 1} \tag{24}$$

$$k_a \in [0.9, 1.1] \ ; \ \theta \in [0.8, 1.2] \ ; \ \tau \in [0.7, 1.3].$$

Minimum and maximum eigenvalues of $P_C^{24,3}$ are given by Equation 20 as follows:

$$\lambda_{min}\left(P_C^{24,3}\right) = 0.4$$

$$\lambda_{max}\left(P_C^{24,3}\right) = 1.3 \ .$$

For comparison, Gershgorin bounds on the eigenvalues of $P_T^{n,3}$ are $0.4 \leq \lambda_i(P_T^{n,3}) \leq 1.6$. A less conservative design results from the bounds based on $\lambda_i[P_C^{24,3}]$.

Since $P_C^{24,3}$ is positive-definite, the design procedure applies. The performance weight $w(s)$ is selected to assure a bandwidth of at least 0.25 rad/sec. as in Equation 2 (and in Figure 2) with $b = 1/2$ and $a = 4$. Next a SISO controller is designed for $kp(s)$ with $k \in [0.4, 1.3]$ following the IMC design procedure of Laughlin et al. [1986]. The design procedure is based on a nominal model $kp(s)$, with all parameters k_a, τ_a, k, and θ equal to their mean values. The IMC controller is $q(s) = \tilde{q}(s)f(s)$, where $\tilde{q}(s)$ (H_2 optimal for step disturbances) and $f(s)$ are given by:

$$\tilde{q}(s) = \frac{s+1}{0.85}$$

$$f(s) = \frac{1}{2s+1}.$$

The standard feedback controller $c(s)$ (a Smith predictor) is therefore given by:

$$c(s) = \frac{1}{0.85}\frac{s+1}{2s+1-e^{-s}}. \tag{25}$$

Figure 8 is the region Nyquist plot for this example. Since none of the regions $\pi(i\omega)$ contain $(-1,0)$, the SISO system is robustly stable. The solid curve in Figure 9 is $\mu(\omega)$ for this example, where $\mu(\omega)$ is the supremum of $|w(i\omega)[1+p(i\omega)c(i\omega)]^{-1}|$ over all $p(s) \in \pi$. Since $\mu(\omega) < 1$ for all ω, sufficient conditions in Theorem 3 for robust performance of the MIMO system are satisfied.

An attempt was made to calculate $\mu(\omega)$ for this example (with controller c(s), interaction uncertainties, parameter uncertainties in the scalar dynamics, and performance requirement all remaining the same), utilizing structured-singular-value analysis. The size of the problem exceeded capabilities of existing software for CD response models having more than seven inputs and outputs. The $\mu(\omega)$ result labelled "repeated complex" in Figure 9 was successfully calculated for a seven-input/seven-output example, when all real perturbations were approximated by

complex perturbations. Theorems 1–4 can be used to show that the theoretical $\mu(\omega)$ curve for the seven-input/seven-output model with real perturbations lies below the solid curve in Figure 9. Not only is the structured singular value analysis limited to a CD response model with few inputs and outputs, but it is conservative as well.

The resulting MIMO controller for this example is simply $c(s)$ times a 20×20 identity matrix, since no scaling matrix $S^{n,m}$ is required for problems with Toeplitz symmetric models. Response of the closed-loop system to step disturbances is illustrated in Figure 10. Parameters in the process model used for the simulation given by

$$p(s) = \frac{1.1e^{-0.8s}}{0.7s+1} \begin{pmatrix} 1.0 & 0.2 & -0.1 & 0 & \dots & 0 \\ 0.2 & 1.0 & -0.1 & \ddots & \ddots & \vdots \\ -0.1 & 0.2 & \ddots & \ddots & \ddots & 0 \\ 0 & \ddots & \ddots & \ddots & 0.2 & -0.1 \\ \vdots & \ddots & \ddots & 0.2 & 1.0 & 0.2 \\ 0 & \dots & 0 & -0.1 & 0.2 & 1.0 \end{pmatrix} \tag{26}$$

are far from their mean values to demonstrate controller robustness. The three step disturbances used in the simulations enter the system in different directions. Disturbances for Figures 10a, 10b, and 10c are given as follows:

$$d_{10a} = (1, .8, .4, -.4, -.8, -1, -.8, -.4, .4, .8, 1, .8, .4, -.4, -.8, -1, -.8, -.4, .4, .8)$$

$$d_{10b} = (1, -1, 1, -1, 1, -1, 1, -1, 1, -1, 1, -1, 1, -1, 1, -1, 1, -1, 1, -1)$$

$$d_{10c} = (1, .9, .7, .4, 0, -1, 1, -1, -.7, -.3, .3, .7, 1, -1, 1, 0, -.4, -.7, -.9, -1).$$

Note that the response to disturbance d_{10b} is more sluggish than that to d_{10a}. Disturbance d_{10b} enters with a large component in the direction of the vector corresponding to the minimum singular value and is therefore difficult to reject. This behavior could have been predicted by calculating the vector $\vec{v}_i$ corresponding to the

minimum eigenvalue (and hence singular value) of the circulant symmetric matrix $P_C^{20,3} = circ(1, 0.2, -0.1, 0, ..., 0, -0.1, 0.2)$, with $w_i = -1$ in Equation 19. Disturbance d_{10a} enters in a more favorable direction. The response to disturbance d_{10c} displays elements of both favorable and unfavorable directions. For a more detailed discussion of the effects of disturbance direction, see the articles by Skogestad and Morari [1986].

9.1.3. Example 2

The second example problem is determination of eigenvalue bounds for CD response model $P_T^{20,3}$ with interactions defined by:

$$p_1 = 1.0 \; ; \; p_2 \in [0.3, 0.5] \; ; \; p_3 \in [0.1, 0.2].$$

Minimum and maximum eigenvalues of the corresponding $P_C^{24,3}$ are

$$\lambda_{min}(P_C^{24,3}) = 0.2$$

$$\lambda_{max}(P_C^{24,3}) = 2.4,$$

placing bounds on eigenvalues of $P_T^{20,3}$ given by $0.2 \leq \lambda_i(P_T^{20,3}) \leq 2.4$. Gershgorin bounds on the eigenvalues of $P_T^{20,3}$ are $-0.4 \leq \lambda_i(P_T^{20,3}) \leq 2.4$ by comparison. Since the lower Gershgorin bound is negative, the Gershgorin bounds are useless for designing a diagonal controller by the proposed method – a negative lower bound results in more than 100 percent uncertainty in gain k that cannot be accommodated by the SISO design procedure. The lower eigenvalue bound based on $P_C^{24,3}$ is greater than zero. Bounds based on $P_C^{24,3}$ can therefore be used in the diagonal controller-design procedure – 85 percent uncertainty in the gain k is required. The eigenvalue bounds based on $P_C^{24,3}$ apply to matrices $P_T^{n,3}$ of all dimensions $n \leq 20$.

9.2. Banded Controller Design

The similarity between CD response models $P_{CSS}^{n,m}$, $P_T^{n,m}$, and $P_C^{n,m}$ for large dimensions n motivates the following design procedure for a banded controller based on $P_C^{n,m}$. Stability, performance, and failure-tolerance results in Sections 6, 7, and 8 apply for the system only if the process and controller are circulant symmetric. Since the CD response model of a real paper machine is never circulant symmetric, an engineering "leap of faith" must be taken to apply the resulting controller to a real system. Whether or not sufficient conditions for robust performance are satisfied with the actual model can be determined through structured-singular-value analysis. However, as stated earlier, the large number of inputs/outputs and large number of repeated real perturbations in the CD response model can make application of structured-singular-value analysis impractical, or can lead to unacceptable conservativeness.

9.2.1. Synthesis Method

The product of a circulant symmetric process $P_C^{n,mp}$ and a circulant symmetric controller $C_C^{n,mc}$ is the circulant symmetric matrix $G_C^{n,mp+mc-1}$. Bounds on the eigenvalues of $G_C^{n,mp+mc-1}$ are given by Equation 20. In this design procedure, the objective is to minimize an upper bound on the condition number of positive-definite G_C before proceeding with the design of diagonal $C(s)$ as described above. As a result, the gain uncertainty and requisite detuning in the required SISO design are minimized. Performance of the resulting MIMO system with controller $C_T^{n-2(mc-1),mc}C(s)$ and process $P_T^{n-2(mp-1),mp}$ is improved. For example, consider the interaction matrix $G_C^{n,4}$ given by Equation 27.

$$
\begin{aligned}
G_C^{n,4} &= P_C^{n,3} C_C^{n,2} \\
&= circ(1, a, b, 0, ..., 0, b, a) \times circ(1, c, 0, ..., 0, c) \\
&= circ(1 + 2ac, a + c + bc, b + ac, bc, 0, ..., 0, bc, b + ac, a + c + bc)
\end{aligned} \tag{27}
$$

The optimum controller parameter c is that which yields a positive definite $G_C^{n,4}$ and solves

$$
\min_c \gamma\left[G_C^{n,4}\right] \tag{28}
$$

$$
= \min_c \gamma\left[\, circ(1 + 2ac, a + c + bc, b + ac, bc, 0, ..., 0, bc, b + ac, a + c + bc)\right]
$$

$$
\leq \min_c \left[\frac{\max_i \left((1 + 2ac) + 2Re\left[\omega_i\right](a + c + bc) + 2Re\left[\omega_i^2\right](b + ac) + 2Re\left[\omega_i^3\right]bc\right)}{\min_i \left((1 + 2ac) + 2Re\left[\omega_i\right](a + c + bc) + 2Re\left[\omega_i^2\right](b + ac) + 2Re\left[\omega_i^3\right]bc\right)} \right]
$$

from Equation 20, where the ω_i are roots of $\omega_i^n = 1$. The upper bound on the objective function 28 can be solved when $P_C^{n,mp}$ contains parameter uncertainties as in 23. Neither numerator terms nor denominator terms in 28 are bilinear (or worse) in $P_C^{n,mp}$ coefficients – a result that holds for arbitrary mp. As a result, both numerator and denominator in 28 can be evaluated without introducing any conservativeness. Their ratio, however, may be conservative, because $P_C^{n,mp}$ coefficients need not have the same value in numerator and denominator when their respective maximums and minimums are achieved – hence the less than or equal sign in 28.

9.2.2. Example

Consider design of banded controller with interaction matrix $C_T^{20,2}$ for the process interaction model $P_T^{20,3}$. Let the process model interaction parameters be defined by 23. Then the parameters n, a, and b in Equation 28 are given by 26, p_2, and p_3, respectively. Figure 11 illustrates the upper bound on condition number γ

of positive-definite matrix $G_C^{26,4}$ as a function of parameter c in $C_C^{26,2}$. From Figure 11, the optimum parameter c for this example is given by $c = -0.21$, resulting in an upper bound on the condition number given by $\gamma = 1.80$.

From eigenvalue bounds calculated in Section 9.1.2, an upper bound on the condition number of $P_C^{24,3}$ is 3.25. The upper bound on the condition number calculated for the optimized product $G_C^{26,4} = P_C^{26,3}C_C^{26,2}$ (and hence for $P_C^{24,3}C_C^{24,2}$) is 1.80. This represents a reduction in required gain uncertainty k for the SISO controller design from 53 percent to 29 percent with a banded controller.

The process model $P_T^{20,3}$ and controller $C_T^{20,2}$ with the same interactions might represent real paper machine interactions. Since the product $P_T C_T$ is in general neither Toeplitz symmetric nor centrosymmetric symmetric, the bounds based on circulant symmetric matrices developed in this paper cannot be applied. Gershgorin bounds can, of course, be used, but they are likely to be very conservative. The same model interaction parameter uncertainties appear in several off-diagonal elements in $P_T C_T$ – Gershgorin bounds treat each appearance as an independent rather than a correlated uncertainty. Robust performance analysis of the MIMO system with Toeplitz symmetric controller and uncertain Toeplitz symmetric interactions fits within the framework of structured-singular-value analysis by Doyle [1982]. Available techniques for computing the result of structured-singular-value analysis for this application yield only a conservative upper bound, because an $n \times n$ repeated real perturbation block is required for each uncertain p_i in $P_T^{n,m}$. The recommended engineering "leap of faith" based on the similarity of $P_C^{n,m}$ and $P_T^{n,m}$ for large n may be required.

9.3. Model Inverse-Based Controller Design

The diagonal and banded controller-design procedures above are not applicable to systems with CD response models that are not positive-definite or that

cannot be postmultiplied by a banded matrix C_C (as in Equation 27) to become positive-definite. For such systems, the following full-matrix, model-inverse-based, controller-design procedure is a viable alternative when interaction uncertainty is negligible. The IMC design procedure of Laughlin et al. [1986] can be used to design controllers given by Equation 29 for systems with CD response modelled by the set $\Pi_{CD}^{n,m}$ in Equation 6.

$$C(s) = c(s)\left(\tilde{P}_{CD}^{n,m}\right)^{-1}, \tag{29}$$

where scalar $c(s) = q(s)/[1 - \tilde{p}(s)q(s)]$, and $q(s)$ is detuned for robustness with respect to scalar dynamic uncertainty (usually with a single tuning parameter) as in the diagonal controller-design procedure above.

The model-inverse-based, controller-design procedure applied to the system with CD response model $P_{CD}^{20,3}(s)$, with exact interactions $\tilde{P}_{CD}^{20,3} = \tilde{P}_{T}^{20,3}$ defined by mean values in 23, scalar dynamics defined by 24, performance requirement $w(s)$ defined by Equation 2 with $b = 1/2$ and $a = 4$, leads to the controller with IMC filter parameter $\epsilon = 1$ given by

$$C(s) = \frac{s+1}{\epsilon s + 1 - e^{-1}}\left(\tilde{P}_{T}^{20,3}\right)^{-1}. \tag{30}$$

Morari et al. [1988] have shown that controller 30 is the H_2-optimal controller for step disturbances when $\epsilon = 0$. Detuning of the controller with $\epsilon = 1$ is required to satisfy the sufficient conditions for robust performance despite parameter uncertainties in the scalar dynamics. The $\mu(\omega)$ plot for this system is illustrated in Figure 9, indicating that the robust-performance objective has been met.

When CD response interaction uncertainty is significant, the above design procedure does not apply. Unless structured-singular-value analysis is used to evaluate robust performance with respect to interaction uncertainties and real parameter uncertainties in the scalar dynamics, the only alternative is to detune the controller

for robust performance with respect to a conservative norm-bounded multiplicative uncertainty $1 + L_m(s)$ with $\sigma_{max}[L_m(s)] \leq |l_m(s)|$ given by

$$1 + l_m(s) = \big(1 + l_d(s)\big)\big(1 + l_i(s)\big)$$

$$|l_m(s)| = |l_i| + |l_d(s)| + |l_i||l_d(s)|, \tag{31}$$

where l_i is the multiplicative error representing interaction parameter uncertainties, and $l_d(s)$ is the multiplicative error representing scalar dynamic uncertainties. For example, consider the uncertain interaction parameters in model $P_T^{20,3}$, given by 23, written in the form $P_T^{20,3} = \tilde{P}_T^{20,3}\big[I + \big(\tilde{P}_T^{20,3}\big)^{-1} E_T^{20,3}\big]$ with nominal $\tilde{P}_T^{20,3}$ given by mean values in 23 and norm-bounded elements e_i in additive interaction error $E_T^{20,3}$ given by $|e_1| = 0$, $|e_2| \leq 0.05$, and $|e_3| \leq 0.025$. Let $E_C^{24,3}$ be the circulant matrix that would result in $E_T^{20,3}$ through Transformation 1. The maximum singular value of $E_C^{24,3}$ is equal to 0.15 (from Equation 19). Since $\sigma_{max}[E_T^{20,3}] \leq \sigma_{max}[E_C^{24,3}]$, an upper bound on the magnitude of multiplicative interaction error $|l_i| = \sigma_{max}\big[\big(\tilde{P}_T^{n,m}\big)^{-1} E_T^{20,3}\big]$ is easily calculated as follows:

$$|l_i| \leq \sigma_{max}\big[\big(\tilde{P}_T^{20,3}\big)^{-1}\big]\sigma_{max}\big[E_C^{24,3}\big] = 1.8 \times 0.15 = 0.27.$$

The magnitude of multiplicative error $|l_d(s)|$ representing scalar dynamic uncertainties in 24 (by $p(s) = \tilde{p}(s)[1 + l_d(s)]$) is given by a formula in Laughlin et al. [1987]. Magnitude of the resulting $l_m(s)$ in Equation 31 is displayed in Figure 12. The IMC filter parameter required to detune the controller in 30 for robust performance with respect to perturbation $L_m(s)$ and the performance weight $w(s)$ defined by Equation 2 with $b = 1/2$ and $a = 4$ is $\epsilon = 2.6$. When the indicated nominal model and single multiplicative perturbation $L_m(s)$ are considered in this example, $\mu(\omega)$ is easily calculated because the nominal loop transfer function is scalar $p(s)c(s)$ times identity. The plot of $\mu(\omega)$ for this design is displayed in Figure 9.

10. Discussion of Conservativeness and Application

In designing a diagonal controller for CD response control, the desirable simplicity of the controller and actuator failure tolerance are achieved at the cost of some performance. Robustness with respect to interaction parameter uncertainties requires detuning of the controller. Some insight about the price paid for the robust diagonal controller can be evaluated by comparing performance of a robust diagonal controller with that of a robust (with respect to uncertain scalar dynamics only) model-inverse-based controller. Consider the system with CD response model $P_{CD}^{20,3}(s)$ with interactions $P_{CD}^{20,3} = P_T^{20,3}$ defined by 23, model dynamics defined by 24, actual process dynamics defined by Equation 25 and performance requirement $w(s)$ defined by Equation 2 with $b = 1/2$ and $a = 4$. The diagonal controller 26 provides robust performance with respect to both uncertain scalar dynamics and uncertain interaction parameters. The model-inverse-based controller 30 (with $\epsilon = 1$ and $\left(\tilde{P}_T^{20,3}\right)^{-1}$ equal to the inverse of interactions in 25 provides robust performance with respect to only uncertain scalar dynamics. The system responses at one actuator position to a step set point change are illustrated in Figure 13. The response with diagonal controller, labelled 1 in Figure 13, is for a step change in the direction of the maximum singular vector of $P_T^{20,3}$. The response with diagonal controller, labelled 3 in Figure 13, is for a step change in the direction of the minimum singular vector. Since the model-inverse-based controller fully decouples the system without interaction uncertainties, there is no unfavorable direction and the speed of response to step changes in all directions is the same as that labelled 1. Note that there is little difference in response to a set point change (and hence to a disturbance) in a favorable direction but significant difference in an unfavorable direction. This is the nature of conservativeness introduced when a robust diagonal controller is specified – conservativeness that is more severe for high condition number processes.

Consider CD response interactions in Table 1 to be elements in $P_T^{20,m}$, where m is the appropriate integer. Eigenvalue bounds for the models calculated from $P_C^{20+2(m-1),m}$ are displayed in Table 2. The ratios $\lambda_{max}/\lambda_{min}$ equal to condition numbers for positive-definite models are listed in Table 2 as well.

Table 2

Condition Numbers and Eigenvalue Bounds

for CD Response Models in Table 1

	λ_{min}	λ_{max}	γ
1)*	−1.2	2.44	
2)	−0.9	1.16	
3)	0.20	1.80	9.00
4)	0.74	1.38	1.86
5)	0.60	1.40	2.33
6)	0.20	1.80	9.00
7)	−1.0	1.25	
8)*	0.20	1.01	5.05
9)*	0.19	3.26	17.2
10)*	−0.4	6.40	
11)*	−1.0	1.18	
12)*	0.20	1.19	5.95
13)*	0.60	1.13	1.88

Models marked with * appear to be actual process data.

Table 2 indicates that the diagonal controller-design procedure developed in this paper can be applied to eight of the models reported in the literature (those that are positive-definite). The banded or model-inverse-based controller-design procedure would have to be used for models that are not positive-definite.

11. Conclusions

The procedure presented in this paper enables design of robust, large-dimension, diagonal and banded controllers for CD response in paper manufacturing. Robust performance is addressed in the spirit of the new structured-singular-value theory by Doyle [1982]. Robust performance of a particular SISO control-system design based on singular value bounds of the CD interaction matrix implies robust performance of the corresponding MIMO system despite interaction parameter uncertainties. Moreover, the control system based on such a design exhibits robust actuator/sensor failure tolerance.

The robust controller-design procedure developed in this paper is applicable to cross-machine-direction control problems other than paper basis-weight control. Similar interaction models result, regardless of the CD response being controlled or the actuator selected. Other candidate CD control systems in the paper manufacturing industry include: water sprays immediately downstream of the slice for CD basis-weight control [Wallace, 1981]; hot and cold air showers on calender stack for CD caliper control [Wilhelm and Fjeld, 1983]; sectionalized steam boxes or steam showers for CD moisture control [Wallace, 1981]. Applications outside the paper manufacturing industry include plastic sheet fabrication and thin-film coating operations. Whenever wide flat sheets of uniform products are manufactured, a similar control problem might be encountered.

It was shown that the paper machine slice actuator has a significant effect on interactions in the CD response model. The CD basis-weight response model

can be tailored to improve controllability with the aid of the dimensionless slice-design parameter D_a and slice-actuator model. Cross-machine-direction response models can be calculated as direct functions of D_a if basis-weight is assumed to be proportional to the area under the slice in Figure 5 (this assumption corresponds to an infinitely fast machine with no CD wave propagation on the Fourdrinier wire). Eigenvalues and condition number bounds based on $P_C^{20+2(m-1)}$ for the resulting CD response models $P_T^{20,m}$ are plotted as functions of D_a in Figure 14. Recall that in the proposed controller-design procedures large condition numbers translate into large gain uncertainty – hence the sufficient conditions for robust performance require highly detuned controllers. Robust diagonal controllers with good performance are therefore possible on paper machines with slices described by large values of D_A. Since elimination of narrow, uneven streaks in paper requires narrow actuator spacing, more flexible slices are necessary to maintain large D_A if a diagonal or banded controller is desired. In his review of the application of control methods to the pulp and paper industry, Dumont [1986] recognizes, that because the industry is old, many mills were not designed with concern for their controllability. Upgrading slice actuators with CD control in mind may well be required.

12. Appendix

Proofs of the theorems presented in this paper will be given here.

Proof of Lemma 1

Since matrix A is symmetric, $A = A^{\frac{1}{2}}A^{\frac{1}{2}}$ where $A^{\frac{1}{2}}$ is symmetric. Since $R^T \in \Re^{n\times q}$, the range of R is a subset of $\Re^q$. Then by definition

$$\sigma_{max}(A^{\frac{1}{2}}) = \max_{\vec{x}\in\Re^q\neq 0} \frac{||A^{\frac{1}{2}}\vec{x}\,||_2}{||\vec{x}\,||_2} \geq \max_{\vec{x}\in\ Range(R)\neq 0} \frac{||A^{\frac{1}{2}}\vec{x}\,||_2}{||\vec{x}\,||_2},$$

because the maximization occurs over a smaller set $\vec{x} \in\ Range(R) \subset \Re^q$. Since $R\vec{y}$ is nontrivial for all nontrivial $\vec{y}$:

$$\max_{\vec{x}\in\ Range(R)\neq 0} \frac{||A^{\frac{1}{2}}\vec{x}\,||_2}{||\vec{x}\,||_2} = \max_{\vec{y}\in\Re^n\neq 0} \frac{||A^{\frac{1}{2}}R\vec{y}\,||_2}{||R\vec{y}\,||_2}.$$

Since $B = R^TAR$ is symmetric when A is symmetric, the following equalities hold:

$$\begin{aligned}
\max_{\vec{y}\neq 0} \frac{||A^{\frac{1}{2}}R\vec{y}\,||_2}{||R\vec{y}\,||_2} &= \max_{\vec{y}\neq 0}\left[\frac{\vec{y}^{\,T}R^TA^{\frac{1}{2}^T}A^{\frac{1}{2}}R\vec{y}}{\vec{y}^{\,T}R^TR\vec{y}}\right]^{\frac{1}{2}} \\
&= \max_{\vec{y}\neq 0}\left[\frac{\vec{y}^{\,T}R^TAR\vec{y}}{\vec{y}^{\,T}\vec{y}}\right]^{\frac{1}{2}} \\
&= \max_{\vec{y}\neq 0}\left[\frac{\vec{y}^{\,T}B\vec{y}}{\vec{y}^{\,T}\vec{y}}\right]^{\frac{1}{2}} \\
&= \max_{\vec{y}\neq 0}\left[\frac{\vec{y}^{\,T}B^{\frac{1}{2}^T}B^{\frac{1}{2}}\vec{y}}{\vec{y}^{\,T}\vec{y}}\right]^{\frac{1}{2}} \\
&= \max_{\vec{y}\neq 0}\frac{||B^{\frac{1}{2}}\vec{y}\,||_2}{||\vec{y}\,||_2} \\
&= \sigma_{max}(B^{\frac{1}{2}}) \quad .
\end{aligned}$$

Therefore, $\sigma_{max}(A^{\frac{1}{2}}) \geq \sigma_{max}(B^{\frac{1}{2}})$ and $\sigma_{max}(A) \geq \sigma_{max}(B)$ when A is symmetric. The same analysis with *max* replaced by *min* and $\geq$ replaced by $\leq$ leads to $\sigma_{min}(A^{\frac{1}{2}}) \leq \sigma_{min}(B^{\frac{1}{2}})$ and $\sigma_{min}(A) \leq \sigma_{min}(B)$ when A is symmetric.

Further, if A is positive-definite, then

$$\langle R\vec{y}, AR\vec{y}\rangle = \langle \vec{y}, R^T AR\vec{y}\rangle = \langle \vec{y}, B\vec{y}\rangle > 0 \ \forall \vec{y} \neq 0,$$

so B is positive-definite.

QED.

Proof of Theorem 1

Matrix $P_C^{q+2(m-1),m}$ from which matrices $P_T^{n,m}$ and $P_{CSS}^{n,m}$ are derived in transformations 1 and 2 is symmetric. Let $P_C^{q+2(m-1),m}$ be positive-definite as well. By definition $R^T R = I^{n\times n}$ in transformation 1. Also by definition, matrix $S_{CSS}^{n,m}$ in transformation 2 is real positive-definite diagonal. Therefore Lemma 1 proves the bounds on singular values of $P_T^{n,m}$ and $P_{CSS}^{n,m}$ and that $P_T^{n,m}$ and $P_{CSS}^{n,m}$ are positive-definite for all dimensions $n \leq q$.

QED.

Proof of Theorem 2

If $P_C^{q+2(m-1),m}$ is positive definite symmetric, then by Theorem 1 the following matrices with $n \leq q$ are positive-definite symmetric with eigenvalues $\lambda_i \in \left[\sigma_{min}\left(P_C^{q+2(m-1),m}\right), \sigma_{max}\left(P_C^{q+2(m-1),m}\right)\right]$:

$$P_C^{n+2(m-1),m}$$

$$P_T^{n,m}$$

$$\left(S_{CSS}^{n,m}\right)^{-\frac{1}{2}} P_{CSS}^{n,m} \left(S_{CSS}^{n,m}\right)^{-\frac{1}{2}}.$$

Each of the symmetric matrices above can be expressed as $U\Lambda U^T$, where U is unitary, and $\Lambda = diag(\lambda_i)$. Since the SISO control system with loop-transfer function $kp(s)c(s)$ is robustly stable for all $p(s) \in \pi$ and for all $k = \lambda_i$, the fully diagonal MIMO control system with loop transfer-function $\Lambda p(s)c(s)$ is robustly stable for all dimensions $n \leq q$. (Robust stability for a fully diagonal system is equivalent

to robust stability of all individual loops.) Premultiplication of the loop-transfer function by U and postmultiplication by $U^T = U^{-1}$ do not change the robust stability of the system. Therefore, the MIMO control system with loop transfer-function $U\Lambda p(s)c(s)U^T$ is robustly stable. Since $p(s)$ and $c(s)$ are scalars, the control system with loop transfer-function $U\Lambda U^T p(s)c(s)$ is robustly stable. Now $U\Lambda U^T$ is equal to $\left(S_{CSS}^{n,m}\right)^{-\frac{1}{2}} P_{CSS}^{n,m} \left(S_{CSS}^{n,m}\right)^{-\frac{1}{2}}$ for the third matrix above, where $S_{CSS}^{n,m}$ is either scalar times identity or centrosymmetric diagonal. Premultiplication of $\left(S_{CSS}^{n,m}\right)^{-\frac{1}{2}} P_{CSS}^{n,m} \left(S_{CSS}^{n,m}\right)^{-\frac{1}{2}}$ by $\left(S_{CSS}^{n,m}\right)^{\frac{1}{2}}$ and postmultiplication by $\left(S_{CSS}^{n,m}\right)^{-\frac{1}{2}}$ and the fact that diagonal matrices commute with one another prove the robust stability results.

QED.

Proof of Theorem 3

If $P_C^{q+2(m-1),m}$ is positive-definite symmetric, then by Theorem 1 the three matrices highlighted in the proof of Theorem 2 are positive-definite symmetric with eigenvalues $\lambda_i \in \left[\sigma_{min}\left(P_C^{q+2(m-1),m}\right), \sigma_{max}\left(P_C^{q+2(m-1),m}\right)\right]$. Therefore, each of the matrices can be expressed as $U\Lambda U^T$ where U is unitary, and $\Lambda = diag(\lambda_i)$. Since the SISO control system with loop-transfer function $kp(s)c(s)$ exhibits robust performance in the sense that $\left|w(\omega)\left(1 + kp(i\omega)c(i\omega)\right)^{-1}\right| < 1$ for all ω, for all $p(s) \in \pi$, and for all $k = \lambda_i$, the fully diagonal MIMO control system with loop transfer-function $\Lambda p(s)c(s)$ exhibits robust performance in the sense that

$$\sigma_{max}\left[w(\omega)\left(I + \Lambda p(s)c(s)\right)^{-1}\right] < 1 \ \forall\omega$$

for all $p(s) \in \pi$. (The maximum singular value of a diagonal matrix is equal to the magnitude of the largest diagonal element.) The maximum singular value is invariant to unitary transformation, so

$$\sigma_{max}\left[w(\omega)\left(I + U\Lambda p(s)c(s)U^T\right)^{-1}\right] < 1 \ \forall\omega.$$

Since $p(s)$ and $c(s)$ are scalars,

$$\sigma_{max}\left[w(\omega)\left(I + U\Lambda U^T p(s)c(s)\right)^{-1}\right] < 1 \ \forall\omega.$$

Now $U\Lambda U^T$ is equal to $\left(S_{CSS}^{n,m}\right)^{-\frac{1}{2}} P_{CSS}^{n,m} \left(S_{CSS}^{n,m}\right)^{-\frac{1}{2}}$ in the third matrix listed in the proof of Theorem 2 above, where $S_{CSS}^{n,m}$ is centrosymmetric diagonal. Premultiplication of

$$\left[w(\omega)\left(I + U\Lambda U^T p(s)c(s)\right)^{-1}\right]$$

by $\left(S_{CSS}^{n,m}\right)^{\frac{1}{2}}$ and postmultiplication by $\left(S_{CSS}^{n,m}\right)^{-\frac{1}{2}}$ do not change its maximum singular value σ_{max} when $S_{CSS}^{n,m}$ is centrosymmetric diagonal. This establishes the robust performance results.

QED.

Proof of Theorem 4

If $P_C^{q+2(m-1),m}$ is positive-definite symmetric, then by Theorem 1 the three matrices listed in the proof of Theorem 2 are positive-definite symmetric with eigenvalues $\lambda_i \in \left[\sigma_{min}\left(P_C^{q+2(m-1),m}\right), \sigma_{max}\left(P_C^{q+2(m-1),m}\right)\right]$. Actuator/sensor failure is equivalent to premultiplication and postmultiplication of these three matrices by R^T and R, respectively, where $R \in \Re^{n\times r}$ is a matrix $r < n$) such that $R^T R = I^{r\times r}$. By Lemma 1 the eigenvalues of

$$R^T[X]R,$$

where X is one of the three matrices listed in the proof of Theorem 1 above, are bounded on the real axis by $\sigma_{min}\left(P_C^{q+2(m-1),m}\right)$ and $\sigma_{max}\left(P_C^{q+2(m-1),m}\right)$. Therefore, Theorems 2 and 3 with the fact that $S^{n\times n}R^{n\times r} = R^{n\times r}S^{r\times r}$ for diagonal matrices S (appropriate rows and columns of $S^{n\times n}$ are eliminated in $S^{r\times r}$) prove the robust stability and robust performance results for actuator/sensor failure.

QED.

References

Aitken, A. C., *Determinants and Matrices* (Interscience Publishers, Inc.: New York), 1954, pp. 121–125.

Althoff, J., Personnal Communication, Beloit Inc., Beloit, WI, November 3, 1987.

Beecher, A. E., and R. A. Bareiss, "Theory and Practice of Automatic Control of Basis Weight Profiles," *Tappi*, 53, May 1970, pp. 847–852.

Bellman, R., *Introduction to Matrix Analysis* (McGraw Hill Co.: New York), 1970, pp. 231–248.

Boyle, T. J., "Practical Algorithms for Cross-Direction Control," *Tappi*, 61, June 1978, pp. 77–80.

Carey, E. W., with C. R. Bietry and H. W. Stoll, "Performance Factors Associated with Profile Control of Basis Weight on a Paper Machine," *Tappi*, 58, June 1975, pp. 75–78.

Crandall, S. H., with N. C. Dahl and T. J. Lardner, *An Introduction to the Mechanics of Solids* (McGraw-Hill, Inc.: New York), 2nd Ed., 1978, pp. 511–576.

Cuffey, W. H., "Some Factors Involved in Basis Weight Uniformity," *Tappi*, 40, June 1957, pp. 190A–197A.

Davis, P. J., *Circulant Matrices* (John Wiley & Sons: New York), 1979.

DeVries, W. R., with S. M. Pandit and S. M. Wu, "Evaluation of the Stability of Paper Basis-Weight Profiles Using Multivariate Time Series," *IEEE Transactions on Automatic Control*, AC-22, 1977, pp. 590–594.

Doyle, J. C., "A Review of μ for Case Studies in Robust Control," *IFAC World Congress*, Munich, July 1987.

Doyle, J. C., "Analysis of Feedback Systems with Structured Uncertainties," *Proc. Inst. Elect. Engrs.*, Pt. D, 129, 1982, pp. 242–250.

Dumont, G. A., "Application of Advanced Control Methods in the Pulp and Paper Industry – A Survey," *Automatica*, 22, 1986, pp. 143–153.

Egelhof D., "The Influence of the Headbox on Asymmetry in Paper," *Das Papier*, No. 7, 1986, pp. 313–318.

Karlsson, H., with I. Lundqvist and T. Ostman, "Principles and Potentials of CD-Basis Weight Control," *Proceedings of the EUCEPA Symposium on Control Systems in the Pulp and Paper Industry*, Stockholm, Sweden, May 11-14, 1982, pp. 238–243.

Karlsson, H., and L. Haglund, "Optimal Cross-Direction Basis Weight and Moisture Profile Control on Paper Machines," *Proceedings of the 3rd International Pulp and Paper Process Control Symposium*, Vancouver, B. C., Canada, May 2-4, 1983, pp. 139–145.

Laughlin, D. L. with K. G. Jordan and Manfred Morari, "Internal Model Control and Process Uncertainty: Mapping Uncertainty Regions for SISO Controller Design," *International Journal of Control*, 44, 1986, pp. 1675–1698.

Laughlin, D. L. with D. E. Rivera and Manfred Morari, "Smith Predictor Design for Robust Performance," *International Journal of Control*, 46, 1987, pp. 477–504.

MacFarlane, A. G. J., "Return-Difference and Return-Ratio Matrices and Their Use in Analysis and Design of Multivariable Feedback Control Systems," *Proc. Instn. Elect. Engrs.*, 117, 1970, pp. 2037–2049.

McFarlin, D. A., "Control of Cross-Machine Sheet Properties on Paper Machines," *Proceedings of the 3rd International Pulp and Paper Process Control Symposium*, Vancouver, B. C., Canada, May 2-4, 1983, pp. 49–54.

Morari, M., with E. Zafirou and C. Economou, *Robust Process Control*, Springer Verlag, to be published, 1988.

Richards, G. A., "Cross Direction Weight Control" *Japan Pulp and Paper*, November 1982, pp. 41–53.

Scott, R. F., *Foundation Analysis* (Prentice-Hall, Inc.: New Jersey), 1981, pp. 119–201.

Skogestad, S., and M. Morari, "Control of Ill-Conditioned Plants: High Purity Distillation," *AICHE Annual Meeting*, paper 74a, Miami Beach, Florida, November 1986.

Skogestad, S., and M. Morari, "Implications of Large RGA-Elements on Control Performance," *AICHE Annual Meeting*, paper 6d, Miami Beach, Florida, November 1986.

Skogestad, S., and M. Morari, "Robust Peformance of Decentralized Control Systems by Independent Designs," Automatica, submitted January, 1987.

Tong, R. M., "Automatic Control of Grammage Profile on a Paper Machine," *Proceedings of the 3rd IFAC PRP Conference*, Brussels, Belgium, 1976, pp. 289–298.

Velguth, J., Personnal Communication, Voith Inc., Appleton, WI, November 2, 1987.

Wallace, B. W., "Economic Benefits Offered by Computerized Profile Control of Weight, Moisture, and Caliper," *Tappi*, 64, July 1981, pp. 79–83.

White, F. M., *Fluid Mechanics* (McGraw-Hill, Inc.: New York), 1979, pp. 597–601.

Wilhelm, R. G., Jr., and M. Fjeld, "Control Algorithms for Cross Directional Control: the State of the Art," *Preprints of the 5th IFAC PRP Conference*, Antwerp, Belgium, October 11-13, 1983, pp. 139–150.

Wilkinson, A. J., and A. Hering, "A New Control Technique for Cross Machine Control of Basis Weight," *Preprints of the 5th IFAC PRP Conference*, Antwerp, Belgium, October 11-13, 1983, pp. 151–155.

Witham, G. S., *Modern Pulp and Paper Making: A Practical Treatise* (Reinhold Publishing Co.: New York), 2nd Ed., 1942.

Wrist, P. E., "Dynamics of Sheet Formation on the Fourdrinier Machine," *Oxford Symposium on Formation and Structure*, 1961, pp. 839–899.

FIGURES FOR CHAPTER V

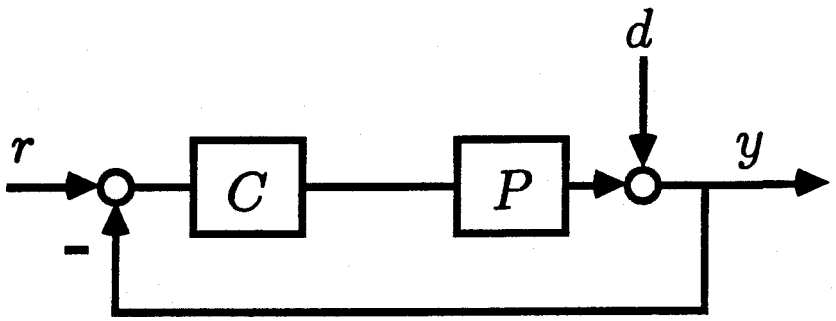

Figure 1: Standard feedback control system with process $P(s)$, controller $C(s)$, set-point $r(s)$, disturbances $d(s)$, and output $y(s)$.

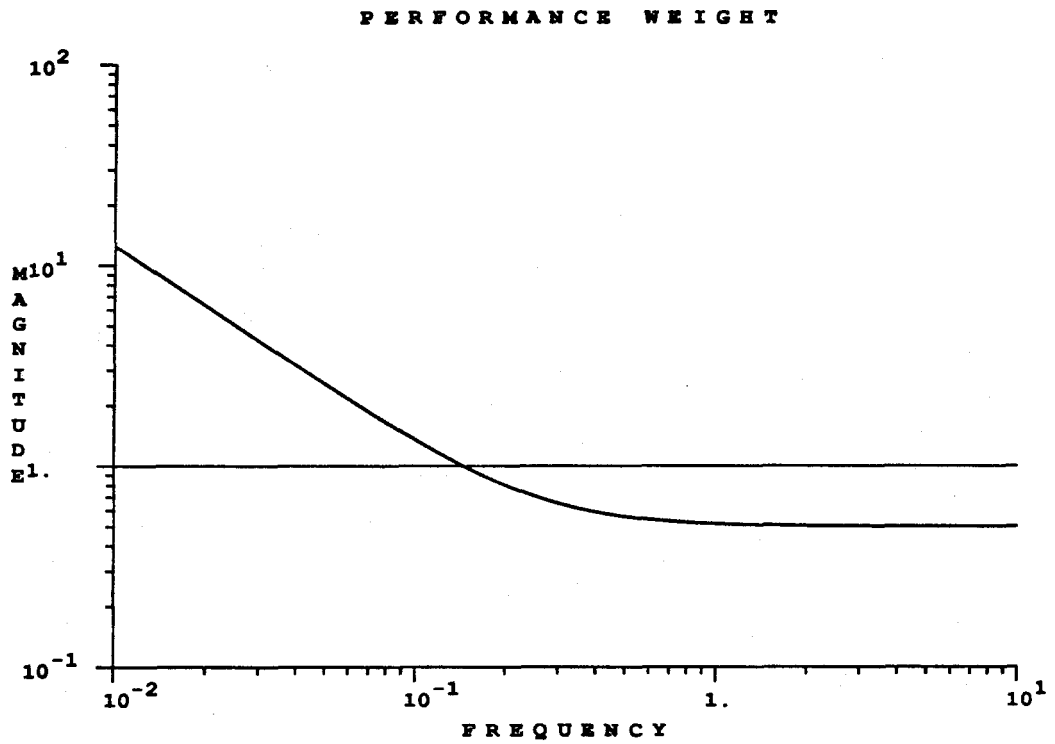

Figure 2: Magnitude of the performance weight specifying acceptable bandwidth and magnitude of the sensitivity function: $w(s) = (4s + 1)/8s$.

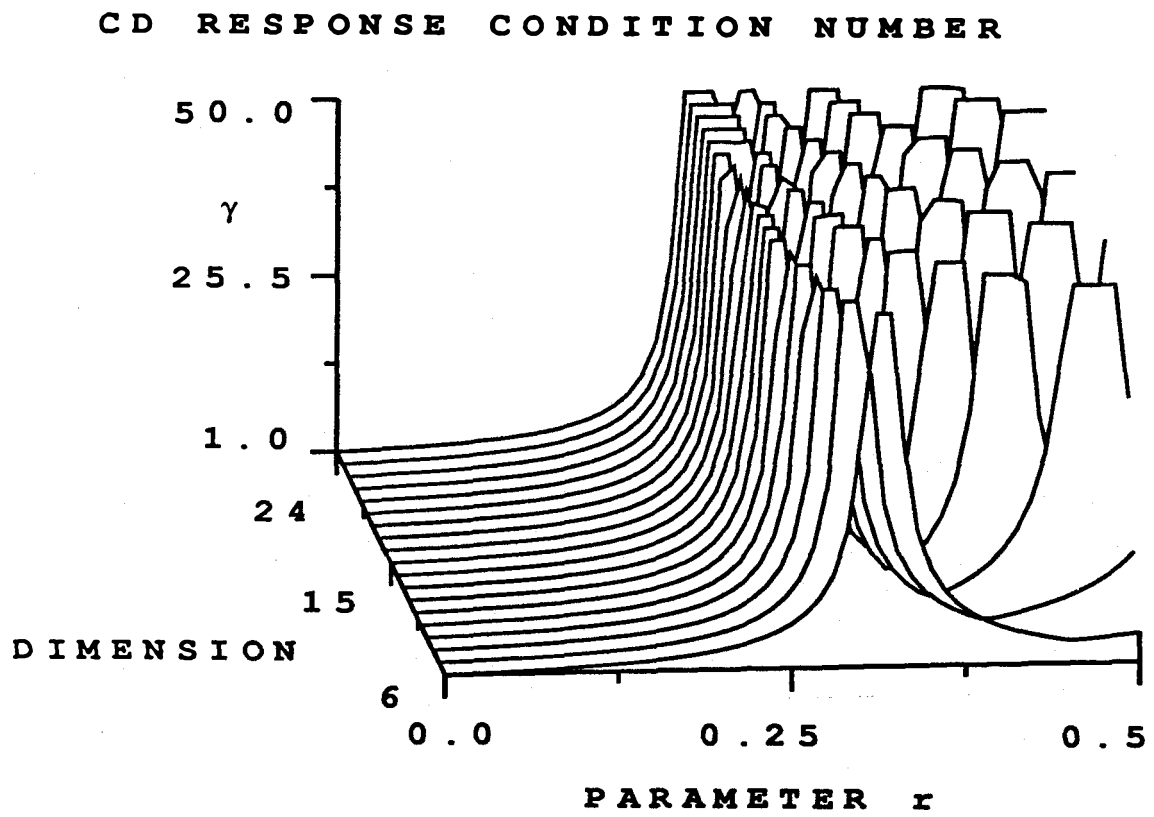

Figure 3: Condition number of $P_{CD}^{n,3}$ with $p_1 = 1$, $p_2 = r$, and $p_3 = -r$ in Equation 4 as a function of parameter r and dimension n. (Truncated at $\gamma = 50$ to improve scale.)

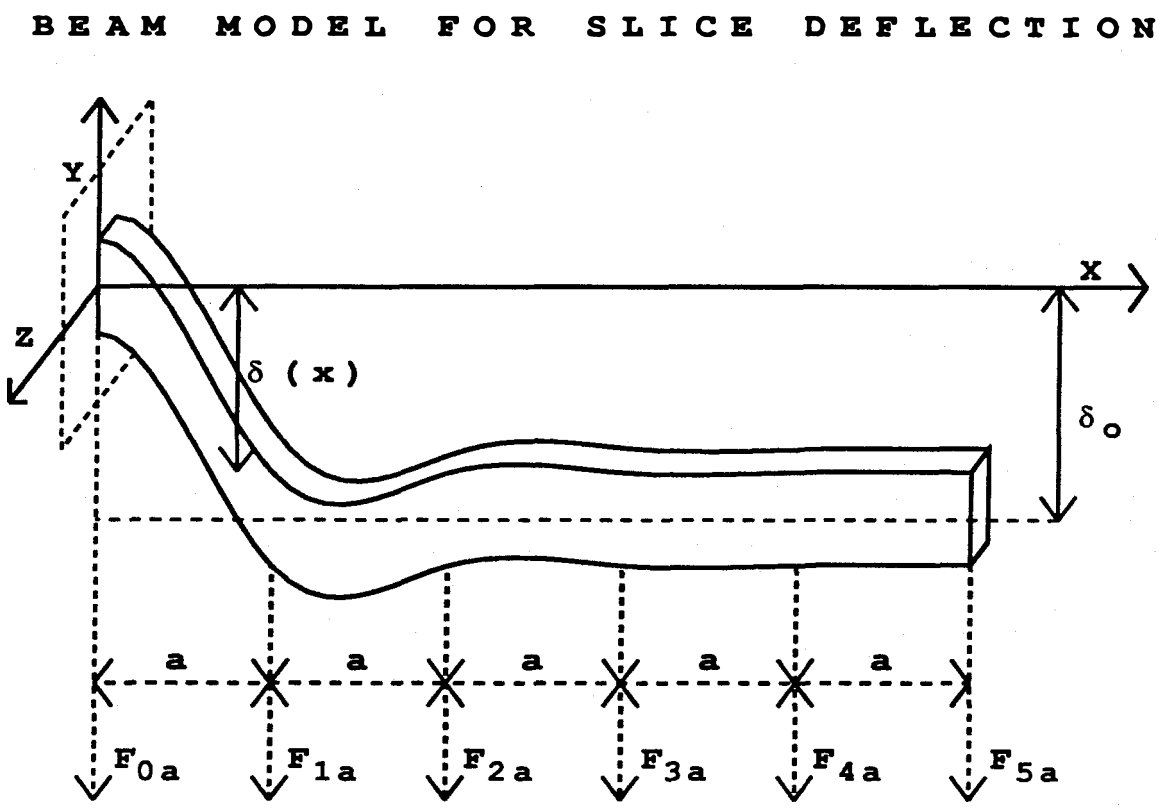

Figure 4: Slice modelled as a beam supported by springs at actuator locations. The springs exert forces F_n on the slice at distances na from the center $(0,0,0)$.

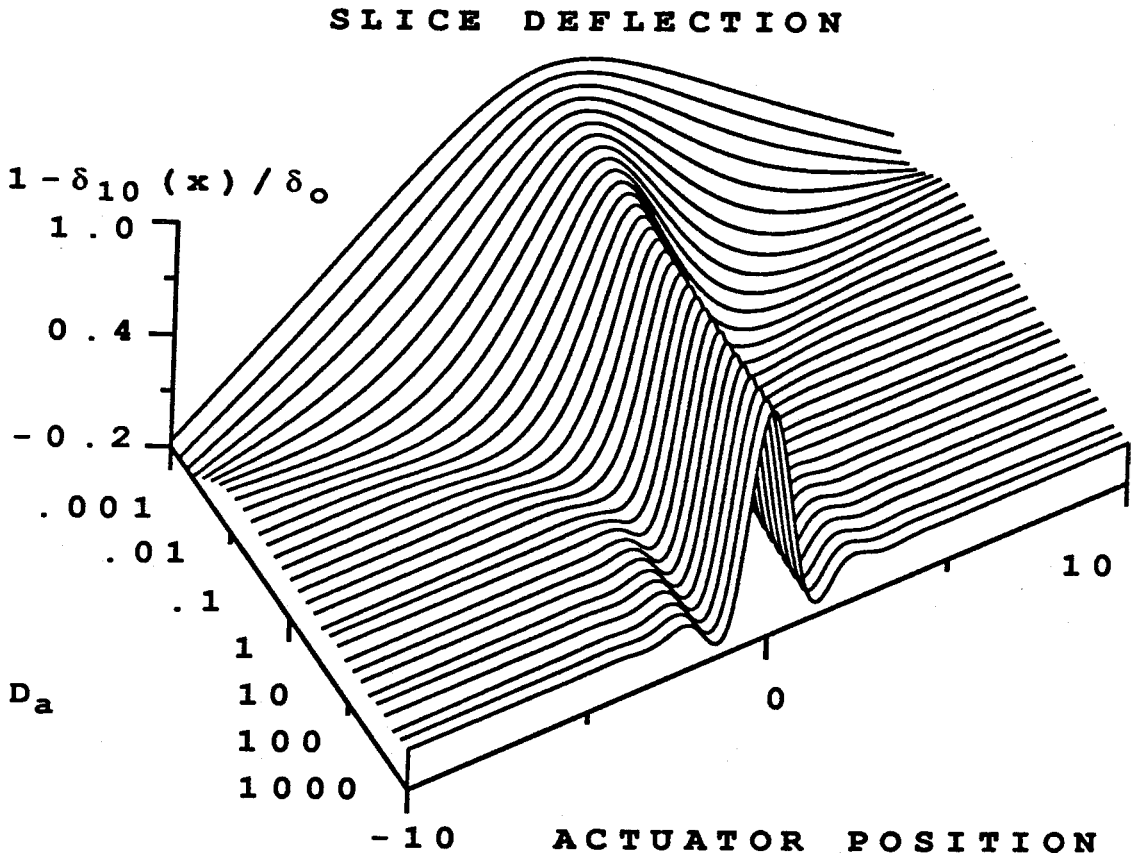

Figure 5: Deflection of the slice actuator as a function of the dimensionless design parameter D_a.

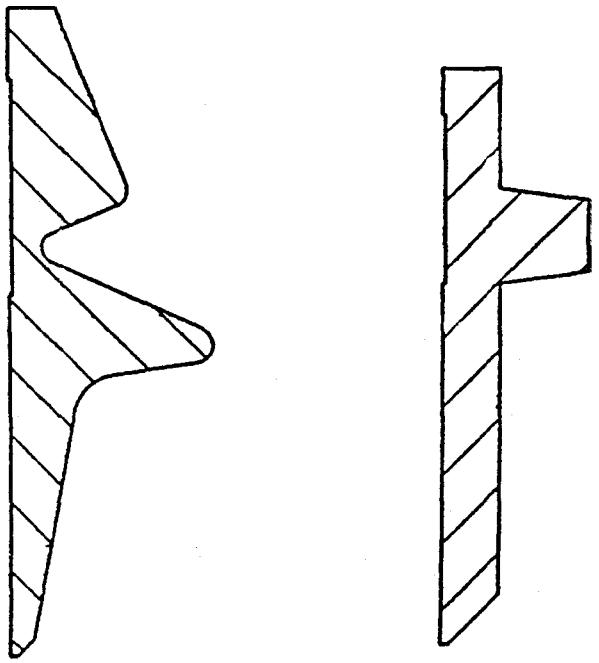

Figure 6: Cross sections of two slices currently available from Beloit Corporation. Note that the slices are thicker in the middle to resist machine direction shear while maintaining flexibility.

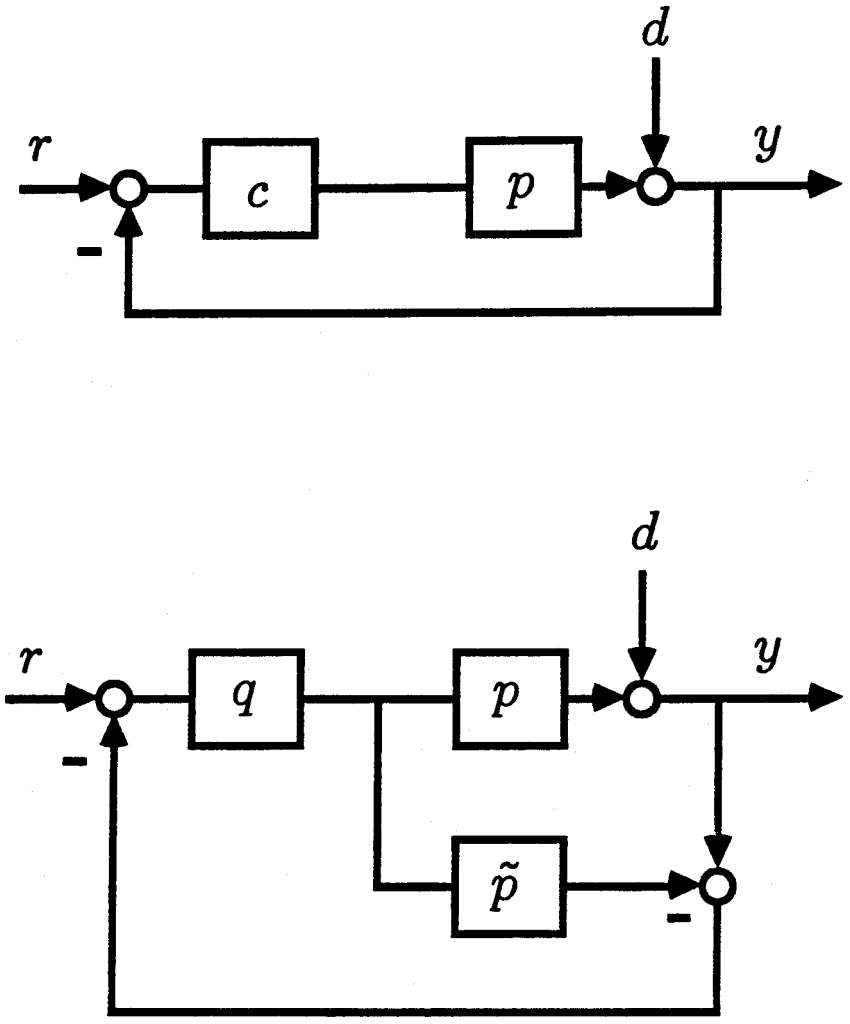

Figure 7: Internal Model Control (IMC) parameterization of feedback controller has process $p(s)$, model $\tilde{p}(s)$, controller $q(s)$, set point $r(s)$, disturbances $d(s)$ and output $y(s)$.

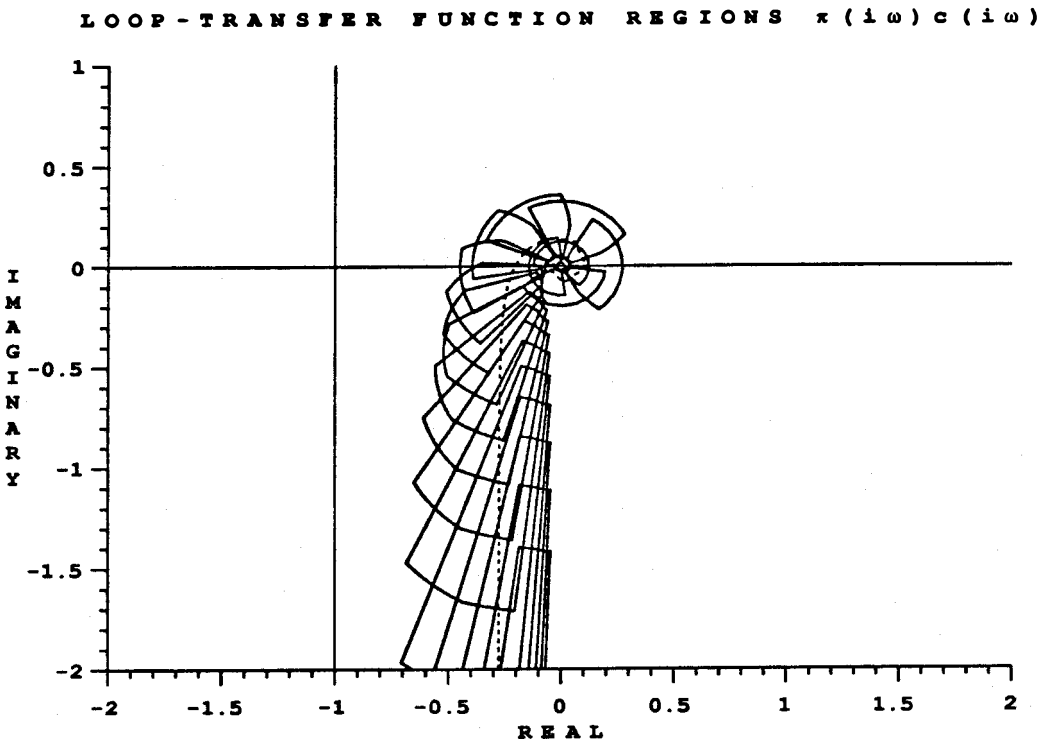

Figure 8: Nyquist plot illustrating robust stability of the system with loop transfer-function $kp(s)c(s)$ for all $p(s) \in \pi$ and for all $k \in [\lambda_{min}(P_C^{24,3}), \lambda_{max}(P_C^{24,3})]$. Since none of the regions $\pi(i\omega)c(i\omega)$ include $(-1,0)$ the system is robustly stable.

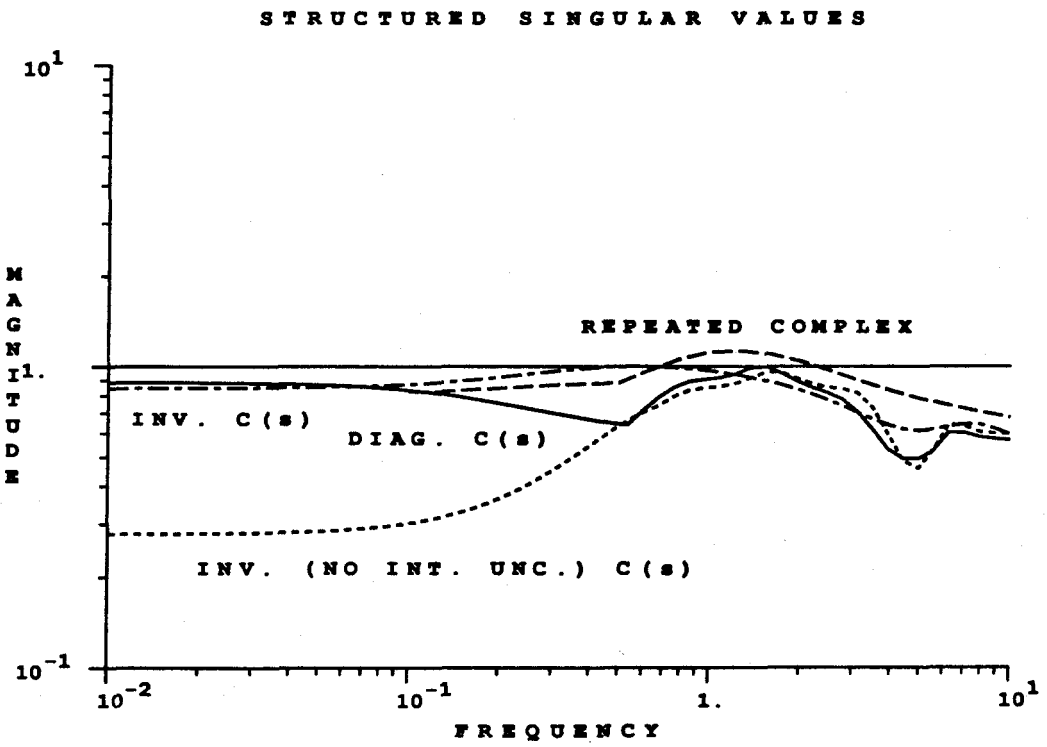

Figure 9: Plots of $\mu(\omega)$ for the CD response control systems designed in Sections 9.1.2 and 9.3. When $\mu(\omega)$ is less than one for all frequencies, robust performance is guaranteed.

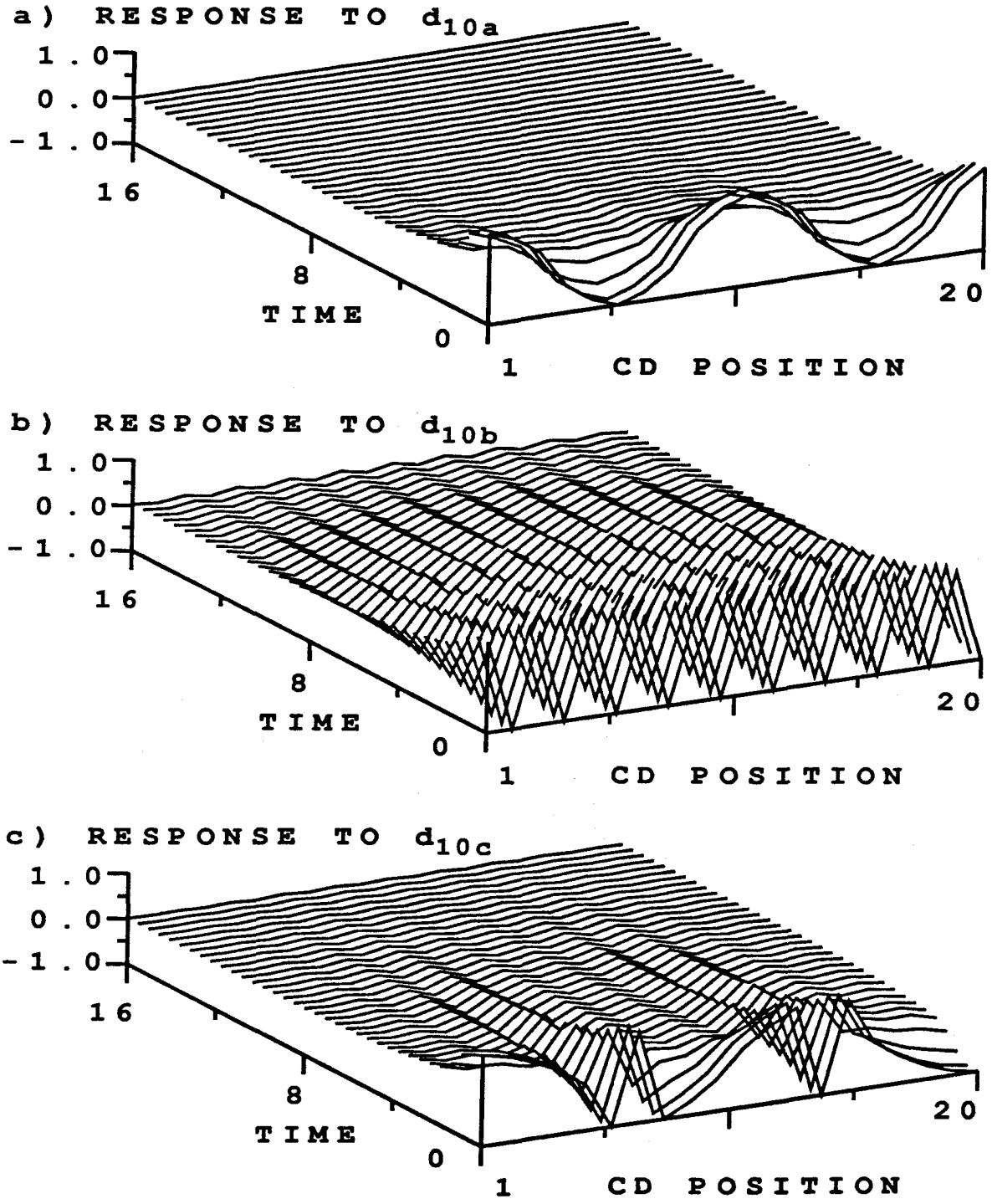

Figure 10: Simulations of CD response to step disturbances d_{10a}, d_{10b}, and d_{10c}. Note that response to d_{10b} in the direction of the vector corresponding to the minimum singular value is sluggish.

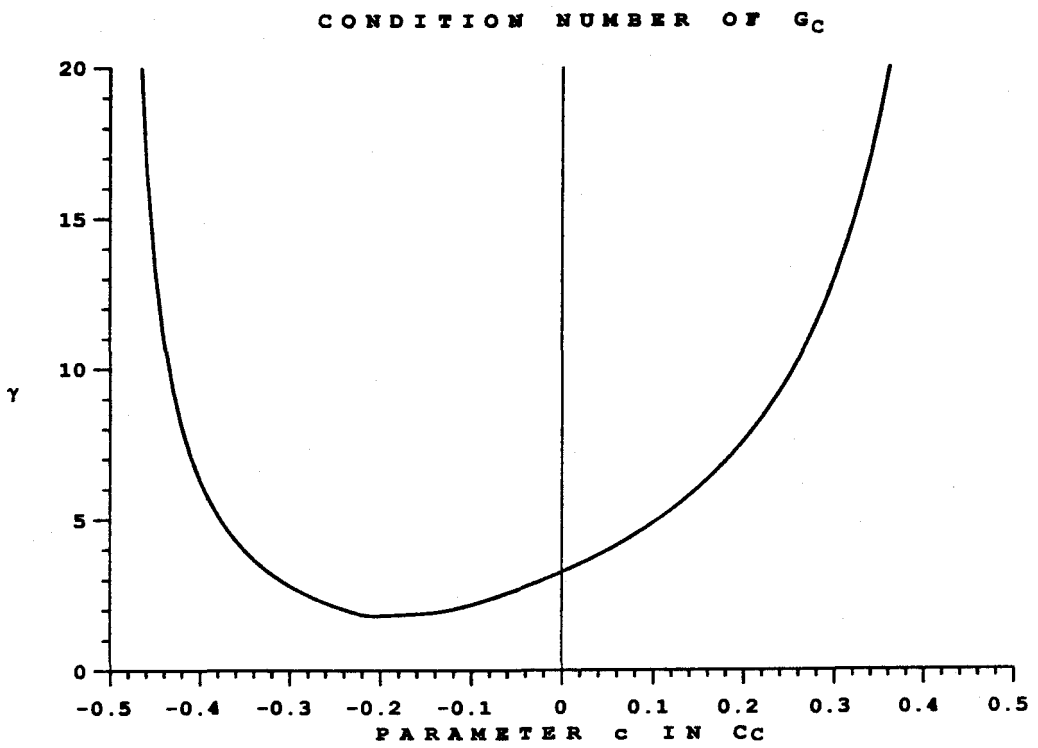

Figure 11: Condition number of positive definite $G_C^{26,4}$ as a function of parameter c in Equation 28. The optimal value of c is -0.21.

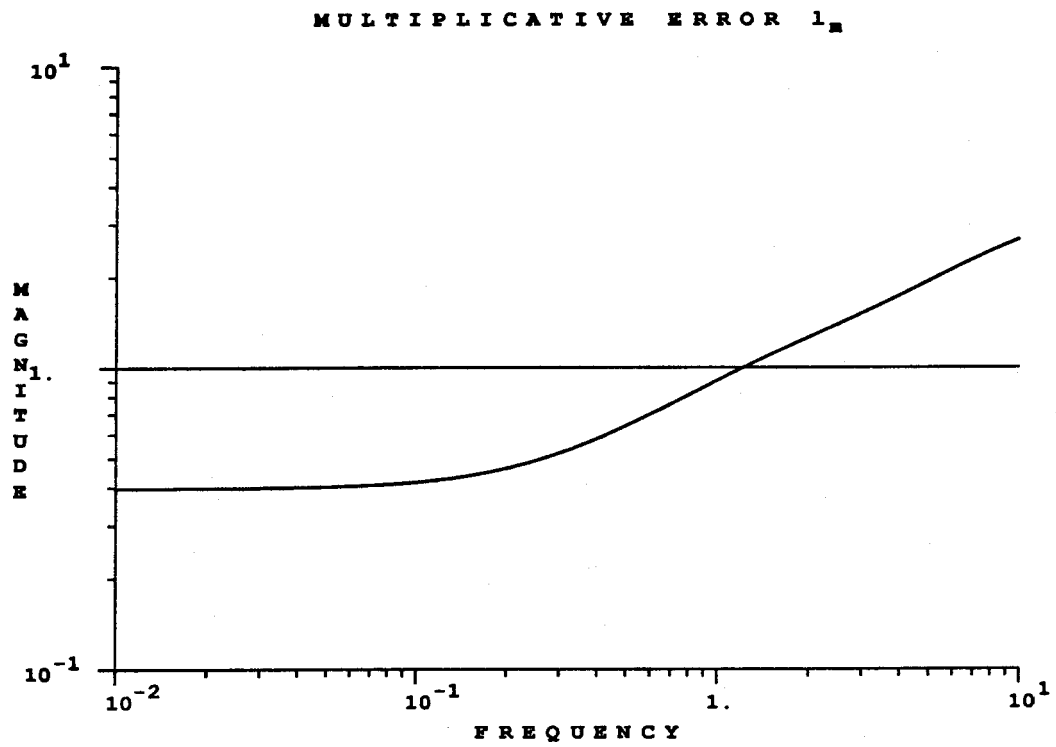

Figure 12: Magnitude of multiplicative error $l_m(s)$ used for the model-inverse-based design in section 9.3 with interaction parameter uncertainties.

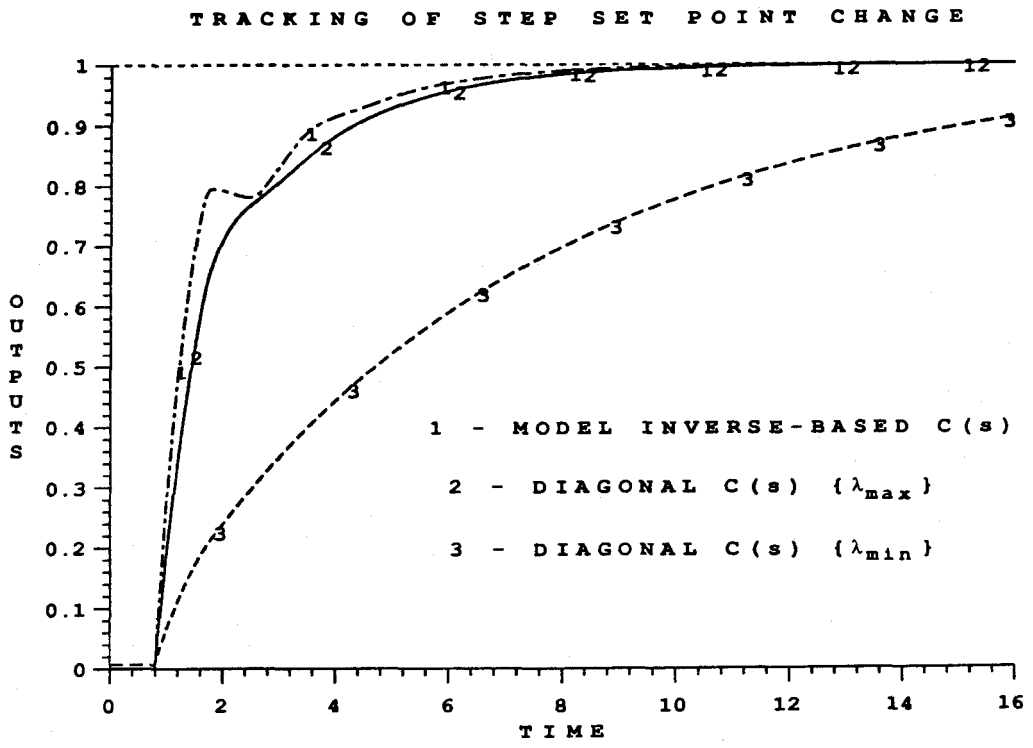

Figure 13: Responses at one actuator position to a step-change in set-point are shown for the system with diagonal controller in Section 9.1.2 and the model-inverse-based controller in Section 9.3 without interaction parameter uncertainties.

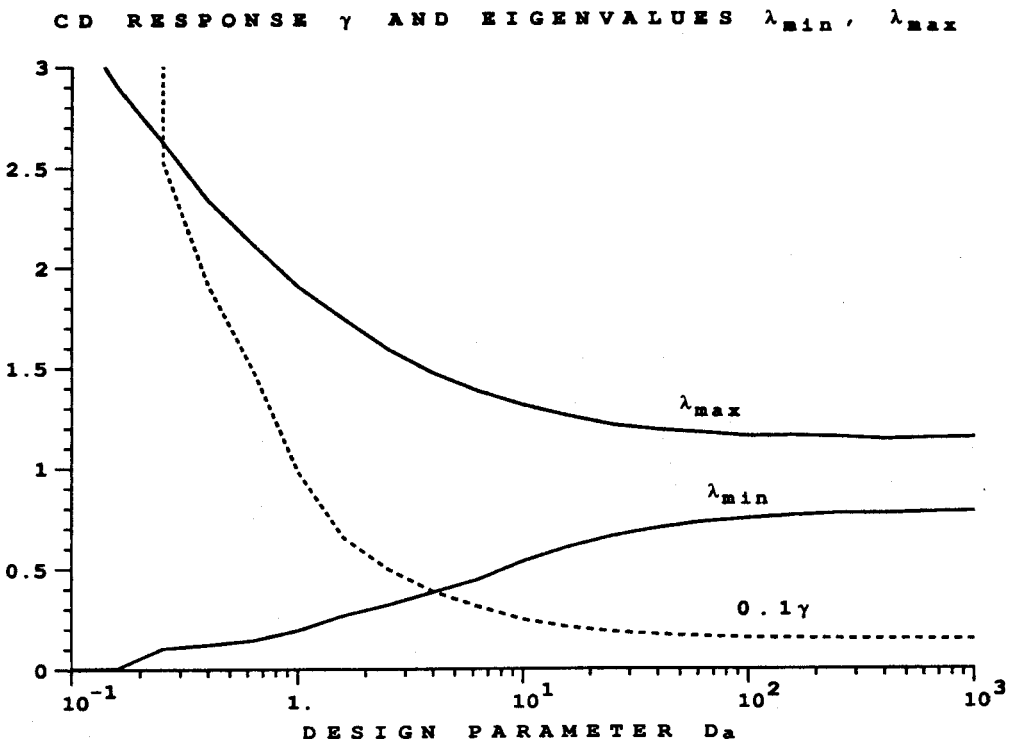

Figure 14: Eigenvalue and condition number bounds of CD response interactions model $P_T^{20,m}$ as functions of the dimensionless actuator design parameter D_a.

CHAPTER VI: STUDIES ON μ-SYNTHESIS OF DECENTRALIZED CONTROLLERS

STUDIES ON μ-SYNTHESIS OF DECENTRALIZED CONTROLLERS

Daniel L. Laughlin and Manfred Morari

Abstract

In this study, alternatives for synthesizing μ-optimal decentralized controllers are explored. The problem of synthesizing the controllers is approached by rearranging the general μ-synthesis interconnection structure or by augmenting the structure with uncertainties in such a way that magnitudes of off-diagonal controller elements are restricted. In the first two methods, successive iterations of μ-synthesis are employed to optimize a decentralized controller. In one design method, μ-synthesis is used to optimize individual decentralized controller blocks. In the second method, the magnitude of the difference between the controller to be synthesized and an estimate of the optimal decentralized controller are penalized. A third method is proposed for penalizing magnitudes of off-diagonal controller blocks that may enable direct μ-synthesis of n-block decentralized controllers. All known results for the three methods are summarized. Where appropriate, the three methods are illustrated by examples with widely different interactions. The best decentralized controller results are compared with full, multivariable, μ-optimal controller designs to illustrate robust performance forfeited by the constraint of a decentralized controller structure.

1. Introduction

Decentralized controllers are often cited as more desirable than full multivariable controllers for reasons of failure tolerance, relative simplicity, and straightforward tuning. Many methods are proposed in the literature for designing decentralized controllers – the most recent of these [Skogestad and Morari, 1987] presents sufficient conditions for independent loop designs that proved robust performance of the control system. The measure of control-system robust performance is the structured singular value μ proposed by Doyle [1982]. The μ-synthesis algorithm outlined in the reference by Doyle [1987] enables design of nearly μ-optimal full multivariable controllers. No algorithm exists currently for synthesis of the μ-optimal decentralized controller.

This work explores possibilities for utilizing the μ-synthesis algorithm for decentralized controller design. Three methods for synthesizing decentralized controllers presented here have not been proven to yield the μ-optimal controller. However, motivating properties of the methods lead to the reasonable assumption that the resulting controllers are nearly optimal. It is useful in the design of decentralized controllers to know exactly what level of control-system performance is forfeited by constraining the controller structure. Comparison of the nearly μ-optimal, decentralized controllers resulting from the proposed design methods with the full multivariable μ-optimal controller provides more accurate knowledge of the performance forfeited than was previously available.

Sections 1.1, 1.2, 1.3, and 1.4 briefly review control-system performance objectives, interaction measures for decentralized control, previous decentralized controller-design methods, and μ-synthesis, respectively. In Section 1.5, characteristics of illustrative examples are presented before moving ahead to the proposed decentralized controller synthesis methods. Proofs of theorems in this work are presented in the Appendix.

1.1. Control System Performance Objectives

Two universal control-system objectives are stability and acceptable disturbance attenuation (performance) despite modelling errors. Often as in Figure 1 modelling errors are written as a norm-bounded ($\sigma_{max}[\Delta_i] \leq 1;\ \forall\omega$), multiplicative perturbation $\Delta_i W_i(s)$ on a nominal model $\tilde{P}(s)$. Robust stability is the requirement that all the poles of the closed-loop system be in the left-half plane despite perturbations $\Delta_i W_i(s)$. Robust performance is expressed in terms of a bound on the maximum singular value of the weighted closed-loop sensitivity function as in $\sigma_{max}[W_p(s)(I + \tilde{P}(s)K(s))^{-1}] < 1$ for all frequencies and for all $P(s) = \tilde{P}(s)(I + \Delta_i W_i(s))$. A key insight of Doyle [1982] was recognition that robust performance of a feedback control structure is equivalent to robust stability of the structure in Figure 1 (for now neglect W_u), where the loop containing norm-bounded Δ_p connects the output with the disturbance. The structure in Figure 1 can always be rewritten as in the bottom of Figure 2, where $\Delta = diag[\Delta_i, \Delta_p]$. Doyle defines the structured singular value $\mu[M]$ in terms of the robust stability requirement for the structure in the bottom of Figure 2. The result is that robust performance of the system in Figure 1 is guaranteed if and only if the structure in the bottom of Figure 2 is robustly stable if and only if $\mu[M] < 1$, where

$$\frac{1}{\mu[M]} = \min_{\Delta}\left\{ \sigma_{max}(\Delta) \;\middle|\; det(I - M\Delta) = 0 \right\}. \tag{1}$$

The uncertainty matrix Δ has structure according to the number and type of uncertainties in Figure 1 – hence the name "structured" singular value for μ.

The techniques currently used to compute μ are upper bound calculation by the method of Doyle [1982] and lower bound calculation by the method of Fan and Tits [1986]. The method of Doyle is based on the bound

$$\mu[M] \leq \inf_{D} \sigma_{max}(DMD^{-1}), \tag{2}$$

where matrices D commute with Δ. Doyle [1982] has shown that, for three or fewer blocks along the diagonal of Δ, the equality in 2 holds.

1.2. Interaction Measures for Control System Design

Interaction measures are often used to predict the stability and performance of a system with a decentralized controller. One popular interaction measure is the relative gain array (RGA) defined by Bristol [1966]. Elements in the RGA for model $\tilde{P} = [p_{ij}]$ are given by Equation 3.

$$RGA_{ij} = p_{ij}\hat{p}_{ji}, \tag{3}$$

where $\hat{p}_{ji}$ is the (j,i)th element in $\tilde{P}^{-1}$. Elements in any row or any column of the RGA sum to one. As defined, an element in the RGA represents the ratio of gain in an individual open loop to the gain in the same loop when all other control loops are closed. The RGA is generally useful in determining measured-output/manipulated-variable pairings in decentralized control structures. Negative or large main diagonal RGA elements indicate poor pairings and interactions that may cause difficulties in control. Main diagonal RGA elements with values near one indicate good pairings and less severe interactions.

Grosdidier and Morari [1986] define the μ interaction measure (IM) as follows:

$$IM = \mu^{-1}[E_H] = \mu^{-1}[(\tilde{P}_f - \tilde{P}_d)\tilde{P}_d^{-1}], \tag{4}$$

where $\tilde{P}_d$ is the block diagonal part of the full nominal model $\tilde{P}_f$ corresponding to the structure of the desired decentralized controller, and μ is calculated with respect to the block structure of the controller. The μ interaction measure is the tightest possible bound on the maximum singular values of complementary-sensitivity-function blocks (corresponding to blocks in the decentralized controller),

such that the full decentralized control structure will be nominally stable. This μ interaction measure condition for nominal stability is given as follows:

IM Condition for Nominal Stability [Grosdidier and Morari, 1986]

If each loop in $\tilde{H}_d = \tilde{P}_d K_d \left(I + \tilde{P}_d K_d\right)^{-1}$ is stable and $\tilde{P}_f$ and $\tilde{P}_d$ have the same number of unstable poles then $\tilde{H}_f = \tilde{P}_f K_d \left(I + \tilde{P}_f K_d\right)^{-1}$ is stable if

$$\sigma_{max}\left(\tilde{H}_d\right) \leq \mu^{-1}\left[E_H\right];\ \forall\omega, \tag{5}$$

where μ is computed with respect to the block structure of K_d.

1.3. Previous Decentralized Controller Design Methods

Few existing methods for designing decentralized controllers address robustness with respect to modelling errors. The inverse Nyquist array method of Rosenbrock [1969] allows nominal stability of the multivariable systems with loop transfer-function $\left(\tilde{P}(s)K(s)\right)$ to be determined from stability of individual loops and a condition based on Gershgorin bounds for the location of eigenvalues of $\left(\tilde{P}(s)K(s)\right)$. For stable model $\tilde{P} = \left[\tilde{p}_{ij}\right]$ and controller $K = diag\left[k_{ii}\right]$, the multivariable system is guaranteed to be stable if single loops with loop transfer-functions $\tilde{p}_{ii}k_{ii}$ are stable and Gershgorin circles with centers $1 + \tilde{p}_{ii}(i\omega)k_{ii}(i\omega)$ and radii

$$\sum_{j \neq i} \left|\tilde{p}_{ij}(i\omega)k_{ii}(i\omega)\right|$$

do not contain the origin. Mayne [1973] presents an algorithm in which loops are closed sequentially in order to design a stabilizing controller with concern for acceptable nominal performance and failure tolerance. The IM condition for nominal stability presented above can be used to guide independent loop designs so that the multivariable system is nominally stable. Nett [1986] employs the μ interaction

measure in an algorithm for sequential loop closing to stabilize the nominal system. Bernstein [1987] presents a repeated sequential application of LQG controller design in which individual decentralized controller blocks are optimized to reduce a quadratic objective function. None of these methods addresses the objective of robust performance as defined in Section 1.1 above.

One existing decentralized controller-design method does address the objective of robust performance. Skogestad and Morari [1987] generalize the μ interaction measure by deriving sufficient conditions for robust performance of the multivariable system based on independent, single-block, controller designs. Their sufficient conditions for robust performance are the tightest possible bounds on $\sigma_{max}\left(\tilde{H}_d(s)\right)$ such that robust performance is guaranteed for the multivariable system. This independent design approach, when successful, results in desirable, failure-tolerant, decentralized control systems. However, the independent design approach is inherently limited because information about other control loops in the design is ignored when designing any given loop. Controller designs for illustrative examples *c* and *d* below demonstrate that stabilizing integral controllers can be designed for systems that fail the IM condition for nominal stability.

1.4. μ-Synthesis

A review of the μ-synthesis algorithm for controller design can be found in the article by Doyle [1987]. Only those aspects of the algorithm relevant to this work will be discussed here. The μ-synthesis algorithm locates a controller K that nearly optimizes the robust performance of the control structure in Figure 1 with respect to norm-bounded perturbations Δ_i. Partition the interconnection matrix transfer-function $G(s)$ in Figure 2 (equivalent to Figure 1) as follows:

$$G(s) = \begin{pmatrix} G_{11} & G_{12} \\ G_{21} & G_{22} \end{pmatrix}. \tag{6}$$

The objective of μ-synthesis is to design a stabilizing controller K for the system that minimizes $\mu\left[F_l(G,K)\right]$, where $F_l(G,K) = G_{11} + G_{12}K\left(I - G_{22}K\right)^{-1}G_{21}$ and μ is calculated with respect to the block structure Δ. The Youla parameterization [Youla et al., 1976] given by $K = F_l(K_o, Q)$ parameterizes all stabilizing controllers K in terms of one stabilizing controller K_o and any stable, proper, rational transfer-function Q. The Youla parameterization is such that $F_l(G,K) = T_{11} + T_{12}QT_{21}$ is stable and affine in Q. The objective function in μ-synthesis can, with the Youla parameterization, be rewritten as

$$\min_{Q} \left|\left| \begin{matrix} R_{11} - Q & R_{12} \\ R_{21} & R_{22} \end{matrix} \right|\right|_x, \tag{7}$$

where x is the μ-norm computed with respect to the block structure Δ. The μ-synthesis algorithm iterates between two steps in an attempt to reach a minimum in the objective function 7. The first step is to solve the H_∞ ($x = \infty$ in 7) problem, using methods in the reference by Chu et al. [1986]. The second step is to minimize the objective function

$$\min_{D} \left|\left| DF_l(G,K)D^{-1} \right|\right|_\mu \tag{8}$$

over scaling matrices D that commute with Δ. Optimal D scales are then fit by stable, proper, rational transfer-functions and incorporated into G in preparation for the next H_∞ iteration.

The software for μ-synthesis used in this work is the version in *HONEYX* developed by Honeywell Systems and Research Center, Minneapolis, MN. Practical computation of what will be called "μ-optimal" controllers in this work employed μ-synthesis in *HONEYX*, where an approximate solution to the H_∞ problem is solved. In the approximate solution, the Q that minimizes the objective function 7 is calculated using only R_{11} (assuming $R_{12} = R_{21} = R_{22} = 0$ in 7). A penalty W_u in Figure 1 requires finite controller gain at high frequencies – this to avoid

instability in the loop through Δ_p. As written in Figure 1, W_u modifies the performance objective such that it is no longer a purely weighted sensitivity function. An alternative that preserves the performance objective as described in Section 1.1 is to replace W_u by $\Delta_u W_u$ and to inject the signal exiting this block at the disturbance junction. The unfortunate result of this alternative is to increase computational complexity in 8. The structure in Figure 1 was therefore used as written to reduce required computation time. It is shown in Section 2 that a W_u can be selected to have minimal effect on the objective function.

For μ-synthesis of decentralized controllers, it would be extremely useful to have a stable parameterization of all stabilizing decentralized controllers. Currently, no such parameterization is available that includes only decentralized controllers and excludes other controller structures. Desoer and Gundes [1987] present a method for parameterizing only a subset of stabilizing diagonal controllers for 2×2 systems. As such, their parameterization is not useful in the context of μ-synthesis. Given this lack of a general parameterization for stabilizing decentralized controllers, a direct H_∞-optimal solution for decentralized controllers is not available at this time. The alluring alternative explored in this work is rearranging the block structure in Figure 1 or augmenting it with uncertainty structures so that the H_∞-optimal controller will be (nearly) decentralized.

1.5. Illustrative Examples

Four example systems are used when possible to illustrate interaction measures and decentralized controller-design methods discussed in this work. The four 2×2 process models have widely different steady-state interactions and condition numbers – as such they lead to control-system designs with markedly different robust performance results despite the same uncertainty description and performance specification. Characteristics of the four example systems are presented in the following sections.

1.5.1. *Nominal Models*

Nominal models for illustrative examples *a–d* are given as follows:

$$\tilde{P}^a(s) = \frac{1}{s+1}\begin{pmatrix} 1.0 & 1.0 \\ 1.0 & 1.1 \end{pmatrix} \tag{9}$$

$$\tilde{P}^b(s) = \frac{1}{s+1}\begin{pmatrix} 1.0 & 1.0 \\ -1.0 & 1.1 \end{pmatrix}$$

$$\tilde{P}^c(s) = \frac{1}{s+1}\begin{pmatrix} 1.0 & 2.0 \\ 1.0 & 1.1 \end{pmatrix}$$

$$\tilde{P}^d(s) = \frac{1}{s+1}\begin{pmatrix} 1.0 & 10.0 \\ 0.0 & 1.1 \end{pmatrix}.$$

1.5.2. *Uncertainty Description and Performance Weights*

In the four example problems, uncertainty weight $W_i(s)$ in Figure 1 is scalar $w_i(s)$ times identity given by Equation 10.

$$w_i(s) = 0.2\frac{1+1.1s}{1+0.1s} \tag{10}$$

Weight $w_i(s)$ represents 20 percent gain uncertainty at steady state in the nominal models 9, with uncertainty in dynamics increasing sharply in magnitude over the frequency range 1 to 10. The performance weight $W_p(s)$ in Figure 1 used for problems *a–d* is scalar $w_p(s)$ times identity given by Equation 11.

$$w_p(s) = \frac{1+5s}{0.001+10s} \tag{11}$$

Performance weight $w_p(s)$ places a bandwidth requirement of approximately $0.2 rad/sec$ on the closed-loop sensitivity function. The weight W_u in Figure 1 was given by scalar $w_u = 0.05$ times identity for examples *a–d*. Such a W_u penalizes the controller magnitude in that $\sigma_{max}\left[\left(W_p - W_u W_i K\right)\left(I + PK\right)^{-1}\right]$ must be less

than one for all frequencies for all models P to preserve stability of the Δ_p loop in Figure 1. Since W_i is relatively small at low frequencies, the penalty on controller magnitude is important only in the high frequency range. For high frequencies, the penalty as specified is approximately given by $\sigma_{max}[0.5 - 0.1K] < 1$. It will be clear from synthesis results for examples *a–d* that this penalty leads to controller element magnitudes of less than 10 or so at high frequencies.

1.5.3. Interaction Measures

The relative gain arrays of examples *a–d* are given as follows:

$$RGA^a = RGA[\tilde{P}^a(s)] = \begin{pmatrix} 11 & -10 \\ -10 & 11 \end{pmatrix} \tag{12}$$

$$RGA^b = RGA[\tilde{P}^b(s)] = \begin{pmatrix} 0.5238 & 0.4762 \\ 0.4762 & 0.5238 \end{pmatrix}$$

$$RGA^c = RGA[\tilde{P}^c(s)] = \begin{pmatrix} -1 & 2 \\ 2 & -1 \end{pmatrix}$$

$$RGA^d = RGA[\tilde{P}^d(s)] = \begin{pmatrix} 1 & 0 \\ 0 & 1 \end{pmatrix}.$$

Based on these RGA's, difficulty is expected in designing controllers for examples *a* and *c* relative to examples *b* and *d*. In particular, example *c* with negative RGA elements on the main diagonal represents poor measured-variable/manipulated-variable pairings for decentralized control. Based on the RGA, alone example *d* appears to be an ideal prospect for decentralized control. It is clear from results achieved in Section 4 that this appearance is misleading as a result of the strong interaction between input 2 and output 1 in $\tilde{P}^d$.

The μ-interaction measures for examples *a–d* are given as follows:

$$IM^a = \mu^{-1}(E_H^a) = \mu^{-1}\begin{pmatrix} 0.0 & 1.0/1.1 \\ 1.0 & 0.0 \end{pmatrix} = 1.0 \tag{13}$$

$$IM^b = \mu^{-1}(E_H^b) = \mu^{-1}\begin{pmatrix} 0.0 & 1.0/1.1 \\ -1.0 & 0.0 \end{pmatrix} = 1.0$$

$$IM^c = \mu^{-1}(E_H^c) = \mu^{-1}\begin{pmatrix} 0.0 & 2.0/1.1 \\ 1.0 & 0.0 \end{pmatrix} = 0.55$$

$$IM^d = \mu^{-1}(E_H^d) = \mu^{-1}\begin{pmatrix} 0.0 & 10.0/1.1 \\ 0.0 & 0.0 \end{pmatrix} = 0.11.$$

These IM's clearly indicate that integral decentralized controllers are not possible for examples c and d by independent loop designs. That stabilizing integral decentralized controllers are synthesized in Section 4 for these examples illustrates conservativeness of design methods based on the μ-interaction measure.

2. Full μ-Optimal Controller Designs

The version of μ-synthesis in $HONEYX$, incorporating the approximate solution to the H_∞-synthesis problem, was used to design controllers for examples a–d. The optimal structured singular values $\mu(\omega)$ were calculated for each example with both $w_u = 0.0$ and $w_u = 0.05$ in Figure 1. These structured singular values are displayed in Figure 3. Note that the non-zero w_u affects the structured singular value $\mu(\omega)$ only slightly over the frequency range where its maximum is reached. Bode plots of μ-optimal controllers for examples a–d are displayed in Figures 4–7.

It is interesting to interpret the results of full, multivariable μ-synthesis for examples a–d in light of the condition numbers for the examples. The condition numbers of models $\tilde{P}^a$–$\tilde{P}^d$ are given as follows:

$$\gamma^a = \gamma[\tilde{P}^a(s)] = 42.076 \tag{14}$$

$$\gamma^b = \gamma[\tilde{P}^b(s)] = 1.071$$

$$\gamma^c = \gamma[\tilde{P}^c(s)] = 6.854$$

$$\gamma^d = \gamma[\tilde{P}^d(s)] = 101.99.$$

Structured singular values in Figure 3 and condition numbers for examples *a–d* can be similarly ordered in increasing magnitude: *b*, *c*, *a*, *d*. This result illustrates the inherent difficulty encountered in designing controllers for high-condition-number models with input uncertainty as in Figure 1.

3. Diagonal Elements of μ-Optimal Controller Designs

The author's experience has been that the diagonal part of a full matrix μ-optimal controller (denoted by $DO\mu$) is often a stabilizing decentralized controller. This is not a surprising observation since μ-optimal controllers are, after all, designed to provide robust performance. The level of robust performance of a μ-optimal controller can be such that stability and performance objectives are met despite the perturbation introduced by eliminating off-diagonal controller elements. The $DO\mu$ controllers, if they are stabilizing, can be used as initial controllers K_d' in the optimization algorithms proposed in Sections 4 and 5. Alternatively, the $DO\mu$ controllers themselves can be used as decentralized controllers for the system if they satisfy robust-performance requirements.

3.1. $DO\mu$ Results for Illustrative Examples

The $DO\mu$ controllers containing the full-order diagonal elements of μ-optimal controllers presented in Section 2 were analyzed for nominal stability and robust performance for example systems *a–d*. The $DO\mu$ controllers for examples *a*, *b* and *d* stabilize systems with processes $\tilde{P}^a$, $\tilde{P}^b$ and $\tilde{P}^d$, respectively. Only the $DO\mu$ controller for example *c* failed to provide nominal stability. The structured singular values for system with stabilizing $DO\mu$ controllers are displayed in Figures 15 and 16.

3.2. Conditions for Stabilizing DOμ Controllers

Whether or not the diagonal part K_d of the full μ-optimal controller K_f is stabilizing can be determined directly by calculating the eigenvalues of the resulting closed-loop system. Alternatively, the closed-loop system with a $DO\mu$ controller is guaranteed to be stable if either of the bounds in Theorems 1 or 2 is satisfied. Although it could be argued that the bounds are superfluous, they may shed light on the feasibility of controller synthesis when the magnitude of the off-diagonal part K_o of the controller is in some way penalized (as in the two-block synthesis method presented in Section 5).

Theorem 1: Assume that the system with controller K_f (shown in the top of Figure 8) is stable and that K_f and K_d have the same unstable poles. The closed-loop system with K_d is stable if the following bound is satisfied:

$$\rho\left[\left(I+\tilde{P}K_f\right)^{-1}\tilde{P}K_o\right] < 1;\ \forall\omega. \tag{15}$$

In Figure 9 the off-diagonal part of the controller K_o is considered to be two different types of multiplicative perturbations on the full controller K_f. The smaller set of perturbations is indicated by the top figure with $|\delta| \leq 1$. The larger set is indicated by the bottom figure with $\sigma_{max}\left[\Delta_{ij}\right] \leq 1$. Theorem 1 gives the tightest possible bound such that closed-loop stability is maintained despite perturbations in the smaller set. Theorem 2 gives the tightest possible bound such that closed-loop stability is maintained despite perturbations in the larger set.

Theorem 2: Assume that the system with controller K_f (shown in the top of Figure 8) is stable and that K_f and K_d have the same unstable poles. The closed-loop system with K_d is stable if the following bound is satisfied:

$$\sigma_{max}\left[K_o\right] < \mu_{K_o}^{-1}\left[\left(I+\tilde{P}K_f\right)^{-1}\tilde{P}\right];\ \forall\omega, \tag{16}$$

where μ_{K_o} is calculated with respect to the following block structure (equal to the block structure in Figure 9 multiplied by a unitary matrix):

$$\Delta_{K_o} = \begin{pmatrix} \Delta_{12} & 0 \\ 0 & \Delta_{21} \end{pmatrix}.$$

3.3. Theorems Applied to Illustrative Examples

Theorems 1 and 2 were applied to examples *a–d* to evaluate whether or not results for $DO\mu$ controllers could have been predicted. The magnitude of terms in the bound given by Theorem 1 are displayed in Figures 10 and 11. Figures 12 and 13 display magnitudes of terms in Theorem 2 bounds for the examples. The figures illustrate that for examples *a* and *b* sufficient conditions of both Theorems 1 and 2 are satisfied for preserving nominal stability after deleting off-diagonal controller elements. Examples *c* and *d*, on the other hand, do not satisfy the sufficient conditions (although example *d* nearly satisfies sufficient conditions of Theorem 1). That the $DO\mu$ controller for example *d* preserves nominal stability despite the fact that sufficient conditions of the theorems are not satisfied illustrates conservativeness of the theorems.

4. Repeated Sequential μ-Synthesis Controller Designs

The controller block K in Figure 2 can be a single block in a decentralized controller when all other controller blocks are incorporated into the general interconnection matrix G. This flexibility of the general interconnection structure makes possible the following repeated sequential ($RS\mu$) algorithm for decentralized controller synthesis:

Repeated Sequential μ-Synthesis $RS\mu$ Algorithm

1) Select an initial stabilizing decentralized controller $K_d' = diag[K_i']$; $i = 1, n$. Calculate an initial structured singular value for the system μ'.
2) Form the interconnection matrix G in Figure 2 so that a single controller block K_i' is separated as matrix K.
3) Use μ-synthesis to design new controller block K_i'' resulting in $\mu'' \leq \mu'$.
4) Set $K_i' = K_i''$ and $\mu' = \mu''$.
5) Repeat steps 2–4 for all controller blocks $i = 1, n$.
6) Return to step 1 until a minimum in μ' is reached.

Bernstein [1987] used this type of repeated sequential algorithm to minimize a quadratic objective function using LQG controller-design methods. Use of the μ objective function and μ-synthesis controller-design method optimizes the decentralized controller for robust performance. Convergence of the $RS\mu$ algorithm is guaranteed by Theorem 3.

Theorem 3: Each iteration of the repeated sequential, μ-synthesis algorithm outlined above will reduce or leave unchanged the structured singular value μ for the system.

In practice, model reduction is required in each step of the repeated sequential μ-synthesis algorithm for decentralized control. Numerical problems are encountered in the available μ-synthesis software when the interconnection matrix transfer-function G in Figure 2 has too many states or is ill-conditioned. The states of each controller block K_i' are incorporated into G – leading to a new block K_i'' with even more states. Clearly, the number of states in G will grow to an unacceptably large number in relatively few iterations if model reduction is not applied to each K_i'. In the $RS\mu$ algorithm used for controller designs *a–d*, model reduction was performed by truncating the states of a balanced minimal realization for each

K_i. Each K_i' was reduced to fewer than ten states. The exact number of states was selected in such a way as to have minimal adverse effect on the structured singular value μ'.

4.1. RSμ Results for Illustrative Examples

The version of μ-synthesis in $HONEYX$ incorporating the approximate solution to the H_∞-synthesis problem was used to design controllers for examples *a–d* following the $RS\mu$ algorithm. Between 10 and 20 iterations were utilized in the examples with model reduction to fewer than 10 states after each iteration. Subsequent iterations resulted either in higher μ (because of model reduction) or in no significant improvement. The optimal structured singular values $\mu(\omega)$ for the systems (calculated with weight $W_u = 0$) are displayed in Figure 14. Bode plots of the $RS\mu$-optimal controllers for examples *a–d* are displayed in Figures 17–20.

4.2. Comparison with DOμ Controllers

The structured singular values of example systems *a–d* with μ-optimal controllers, stabilizing $DO\mu$ controllers, and $RS\mu$ controllers are compared in Figures 15 and 16. Bode plots of $DO\mu$ controllers and $RS\mu$ controllers are compared in Figures 17–20.

5. Simultaneous Two-Block μ-Synthesis Controller Designs

In this section an algorithm is proposed for optimizing elements of a two-block decentralized controller (though extension of the algorithm for more than two blocks may be useful). The basic idea is that magnitude of the off-diagonal part K_o of the controller K_f resulting from μ-synthesis can be limited by incorporating

appropriate penalties into the feedback control structure 1. For example, in Figure 21 the magnitude of $K_o = K_f - K_d$ must be small enough to prevent instability in the loop containing $\Delta_e W_e(s)$. If K_d is an estimate of the optimal, two-block, decentralized controller, it is reasonable to expect that the diagonal part of K_f synthesized for the structure in Figure 21 may be closer to the optimal. If so, the block diagonal part of K_f can be placed in the structure for an additional optimizing iteration. Magnitudes of off-diagonal elements in K_f can be influenced by the weight W_e. Steps in the proposed algorithm are given as follows:

Two-Block μ-Synthesis Algorithm ($TB\mu$)

1) Select a weight $W_e(s)$ penalizing the magnitude of off-diagonal controller blocks.
2) Select an initial stabilizing, two-block, decentralized controller $K_d' = diag[K_{11}', K_{22}']$. Calculate an initial structured singular value μ' for the system without the $\Delta_e W_e(s)$ loop.
3) Perform μ-synthesis with the two-block structure in 21 to design a full controller K_f that results in $\mu \leq \mu'$.
4) Eliminate the off-diagonal part K_o of controller K_f to form new controller K_d'', if nominal stability can be preserved.
5) Calculate structured singular value μ'' with the new decentralized controller K_d'' for the system without the $\Delta_e W_e(s)$ loop.
6) If $\mu'' \leq \mu'$ set $K_d' = K_d''$, set $\mu' = \mu''$ and repeat steps 3–6. If $\mu'' > \mu'$, go to step 7.
7) If the resulting controller K_d' is acceptable, then end. If it is not acceptable, return to step 1 and select a different weight $W_e(s)$.

That the algorithm has any hope of reaching the optimal decentralized controller is motivated by Theorem 4.

Theorem 4: Let $R_f \in C^{n\times m}$ be composed of four blocks $R_{11} \in C^{u\times v}$, $R_{12} \in C^{u\times(m-v)}$, $R_{21} \in C^{(n-u)\times v}$, and $R_{22} \in C^{(n-u)\times(m-v)}$ as follows:

$$R_f = \begin{pmatrix} R_{11} & R_{12} \\ R_{21} & R_{22} \end{pmatrix}.$$

Then the following is true of $\sigma_{max}[R_o]$, where $R_o = R_f - diag[R_{11}, R_{22}]$:

$$\begin{aligned} \sigma_{max}[R_o] &= \sigma_{max}\begin{pmatrix} 0 & R_{12} \\ R_{21} & 0 \end{pmatrix} \\ &= \min_{R_{11}} \sigma_{max}\begin{pmatrix} R_{11} & R_{12} \\ R_{21} & 0 \end{pmatrix} \\ &\leq \min_{R_{11}} \sigma_{max}\begin{pmatrix} R_{11} & R_{12} \\ R_{21} & R_{22} \end{pmatrix} \\ &\leq \sigma_{max}[R_f]. \end{aligned} \tag{17}$$

The result $\sigma_{max}[R_f - R_d] \leq \sigma_{max}[R_f]$ holds only for 2×2 block diagonal matrices R_d. An example of a 3×3 matrix R_f for which $\sigma_{max}[R_f - diag(R_f)] = 91.85$ and $\sigma_{max}[R_f] = 91.56$ was found by generating random matrices on a computer. The matrix R_f is given by:

$$Re[R_f] = \begin{pmatrix} -10.53533 & -32.37298 & -1.978634 \\ -23.12827 & 5.560493 & 31.54301 \\ -22.09775 & 39.16768 & 7.253468 \end{pmatrix}$$

$$Im[R_f] = \begin{pmatrix} 35.33086 & 30.86909 & 37.68517 \\ -45.81063 & -42.22833 & 44.02956 \\ 30.52077 & -27.55929 & -10.12934 \end{pmatrix}.$$

Theorem 4 enables proof of Theorem 5, stating what is known about convergence of steps in the $TB\mu$ algorithm for synthesis of decentralized controllers.

Theorem 5: The following can be said about the convergence of steps in the $TB\mu$ algorithm:

a) The controller K_f synthesized in step 3 of the algorithm will result in $\mu \leq \mu'$ for the system with penalty loop $\Delta_e W_e(s)$.

b) By setting $K_d' = K_d''$ in step 6, an upper bound on the structured singular value for the system with penalty loop $\Delta_e W_e(s)$ is reduced – the magnitude of the smallest destabilizing signal through the loop is increased.

No improvement over $RS\mu$ controllers was achieved by applying the $TB\mu$ algorithm to examples *a–d*. Since convergence of the $TB\mu$ algorithm has not been established, it is possible that such improvement will never be possible. However, since the $HONEYX$ software employed in these efforts locates only nearly optimal controllers, it is possible that better software will enable better results to be obtained. That the loop containing $\Delta_e W_e$ restricts the magnitude of off-diagonal controller blocks is illustrated by the following two examples. As in the $RS\mu$ algorithm, model reduction of the optimal controller estimate K_d is an important concern in the $TB\mu$ algorithm. An interesting result for the example in Section 5.1 is that a better two-state diagonal controller was synthesized with the algorithm than the one resulting from direct model reduction (truncating the states of a balanced minimal realization) of the $DO\mu$ controller.

5.1. An Example with Two SISO Blocks

The $TB\mu$ algorithm reduces the magnitude of SISO off-diagonal controller elements for the system in Figure 21 with the following parameters:

$$\tilde{P}^e(s) = \begin{pmatrix} \frac{1}{1+s} & \frac{0.5}{1+0.1s} \\ \frac{0.5}{1+0.1s} & \frac{1}{1+s} \end{pmatrix} \tag{18}$$

$$w_p(s) = \frac{1+2s}{0.001+4s}$$

$$w_i = 0.2$$

$$w_e = 0.1$$

$$w_u = 0.0.$$

The magnitude of μ-optimal controller elements for this example are displayed at the top of Figure 22. The magnitude of controller elements resulting from the two-block synthesis algorithm are displayed at the bottom of Figure 22. Note that the magnitudes of off-diagonal elements are reduced by a factor of approximately ten by the algorithm. The structured singular values for the example are presented in Figure 23, indicating that a better two-state diagonal controller was synthesized using the $TB\mu$ algorithm than the one that resulted from model reduction of the $DO\mu$ controller.

5.2. An Example with One SISO Block and One MIMO Block

The $TB\mu$ algorithm is applied here to the design of a decentralized controller with a SISO K_{11} block and a 2×2 K_{22} block. The $TB\mu$ algorithm results for this structure are denoted by $TB2\mu$ in the relevant figures. Similarly, the $DO2\mu$ controller is the diagonal part of the μ-optimal controller with the same structure. System parameters in Figure 21 for this example are given by 19.

$$\tilde{P}^f(s) = \begin{pmatrix} \frac{1}{1+s} & \frac{0.5}{1+0.5s} & \frac{0.5}{1+0.5s} \\ \frac{0.5}{1+0.5s} & \frac{1}{1+s} & \frac{0.5}{1+0.1s} \\ \frac{0.5}{1+0.5s} & \frac{0.5}{1+0.1s} & \frac{1}{1+s} \end{pmatrix} \tag{19}$$

$$w_p(s) = \frac{1+10s}{0.001+20s}$$

$$w_i = 0.2$$

$$w_e = 1.0$$

$$w_u = 0.0$$

The magnitude of μ-optimal controller elements for this example are displayed at the top of Figure 24. The magnitude of controller elements resulting from the two-block synthesis algorithm are displayed at the bottom of Figure 24. As in the previous example, the magnitudes of off-diagonal elements are reduced by the algorithm. Structured-singular-value results for this example are presented in Figure 25.

6. n-Block μ-Synthesis Controller Design

An uncertainty structure that appears promising for simultaneous n-block μ-synthesis of decentralized controllers is shown in Figure 26. Properties of the structure were studied independently by both the author and Smith [1987]. The idea for μ-synthesis of decentralized controllers with the structure is that for a specific uncertainty Δ_k the magnitude of only the off-diagonal controller elements is penalized. The μ-synthesis algorithm will preferentially select a decentralized controller from the set of stabilizing controllers to minimize the effect of penalties on off-diagonal blocks.

Uncertainty structures $\left(I + \Delta_k W_k(s)\right)$ and $\left(I + \Delta_k W_k(s)\right)^{-1}$ premultiplying and postmultiplying the controller K are designed in such a way as to commute with a decentralized controller with a desired structure. A repeated scalar block of dimension n is placed in $\left(I + \Delta_k W_k(s)\right)$ at positions corresponding to each $n \times n$ full block in the decentralized controller. These two $n \times n$ blocks therefore commute with one another. If the desired decentralized controller structure is given by $K_d = diag\left[K_1^{n1}, K_2^{n2}, \cdots, K_j^{nj}\right]$, where each K_j^{nj} is a $nj \times nj$ block, then the uncertainty structure must be given by $\Delta_k W_k = diag\left[w_{k1}\delta_1^{n1}, w_{k2}\delta_2^{n2}, \cdots, w_{kj}\delta_j^{nj}\right]$, where each $w_{kj}\delta_j^{nj}$ is scalar $w_{kj}\delta_j$ times an $nj \times nj$ identity matrix. For example, in a system with a 2×2 controller, the product of the uncertainty structures and the controller will be given by

$$\begin{pmatrix} 1 + w_{k1}\delta_1 & 0 \\ 0 & 1 + w_{k2}\delta_2 \end{pmatrix} \begin{pmatrix} k_{11} & k_{12} \\ k_{21} & k_{22} \end{pmatrix} \begin{pmatrix} (1 + w_{k1}\delta_1)^{-1} & 0 \\ 0 & (1 + w_{k2}\delta_2)^{-1} \end{pmatrix}$$

$$= \begin{pmatrix} k_{11} & (1 + w_{k1}\delta_1)k_{12}(1 + w_{k2}\delta_2)^{-1} \\ (1 + w_{k2}\delta_2)k_{21}(1 + w_{k1}\delta_1)^{-1} & k_{22} \end{pmatrix}. \qquad (20)$$

It is clear from 20 that, for decentralized controllers that commute with Δ_k, the uncertainty structures cancel one another. They do not contribute to instability of either Δ_i or Δ_p loops in the control structure. The Δ_k structures therefore have

the effect of penalizing only the magnitude of off-diagonal controller elements. If $|\delta| \leq 1$, it is clear that an infinitely large perturbation on the magnitude of an off-diagonal controller element can be specified when $w_{kj} = 1$.

It would, of course, be the objective in decentralized controller synthesis to employ a structure that drives the magnitude of off-diagonal controller elements to zero. This would require the perturbation on off-diagonal controller elements to be infinite (corresponding to weights w_{kj} equal to 1). Unfortunately, stabilization of the Δ_k feedback loop in Figure 26 imposes a lower bound on the structured singular value that can be calculated for the system. The lower bound is given by Theorem 6 (proven by Smith [1987] for 2×2 systems – proven here for arbitrary dimension).

Theorem 6: Consider the block structure in Figure 26 with uncertainty $\Delta_k W_k(s)$ selected to commute with any block diagonal controller K. Let weight $W_k(s)$ be scalar $w_k(s)$ times identity. A lower bound on the the structured singular value for the system is given by $\mu \geq |w_k(i\omega)|$.

The implication of Theorem 6 for simultaneous n-block μ-synthesis of decentralized controllers is that if $w_k = 1$ were selected in order to drive the magnitude of off-diagonal controller elements to zero, the lower bound on the structured singular value for the system will also be 1. An implication of the repeated Δ_k structure of Figure 26 on μ-synthesis in its current incarnation is that full matrix D scales in 8 would have to be fit by rational transfer-functions. Despite these shortcomings of the n-block structure, it still holds promise for decentralized controller synthesis. If $w_k < 1$ and there were a stabilizing decentralized controller K_d for the system that commuted with Δ_k and provided robust performance ($\mu < 1$ for the system), then a perfect μ-synthesis would locate K_d.

The result in Theorem 6 is clearly visible in μ-analysis results for example systems a and b with $RS\mu$ controllers in the n-block structure. The structured singular values of the example systems are plotted as functions of frequency in

Figures 27 and 28 for values of W_k equal to 0.5, 0.6, 0.7, 0.8, 0.9, and 0.95. Notice that the lower bound on μ given by Theorem 6 is clear for each curve.

7. Robust Performance of Full vs. Decentralized Controllers

Performance of the example control systems *a–d* is expected to be better with full multivariable controllers than with decentralized controllers. Simulations of step-disturbance rejection by example systems with nominal models in 9 illustrate levels of performance achieved with μ-optimal and $RS\mu$-optimal controllers. The responses to disturbances in individual channels and to simultaneous disturbances in both channels are displayed in Figures 29–36. Low levels of performance result with decentralized controllers in example systems *c* and *d*. The negative diagonal elements of RGA^c warned that this would be the case for example *c*. In example *d*, the poor performance results from the large off-diagonal element in $\tilde{P}^d$ despite favorable RGA^d. Performance degradation in examples *a* and *b* with decentralized controllers is not too severe.

Success of decentralized controller design via repeated sequential μ-synthesis suggests a definitive robust-performance interaction measure. It can be argued that the value of some existing interaction measures is that they allow the control-system designer to make decisions before computationally intensive syntheses are performed. The proposed interaction measure is available after synthesis of an optimal or near optimal decentralized controller. At some point, the superior insight available from interaction measure RPIM defined below and inevitable future improvements in μ-synthesis and computer hardware will outweigh motivation for avoiding the required synthesis.

Definition: Robust-Performance Interaction Measure

The robust-performance interaction measure $RPIM$ is defined as

$$RPIM(\omega) = \frac{\mu_D(\omega)}{\mu_O(\omega)}, \tag{21}$$

where $\mu_D(\omega)$ is the structured singular value for the system with decentralized controller and $\mu_O(\omega)$ is that for the system with full μ-optimal controller.

Naturally, $RPIM$ depends on the structure of the decentralized controller, on the model uncertainty description, and on the performance specification. The interaction measure $RPIM$ exactly characterizes the performance forfeited when a decentralized controller is specified. The RPIM accompanied by either curve μ_O or μ_D provides more information about the feasibility of decentralized controller design for some systems than is available from existing interaction measures. For example, the μ interaction measure of Grosdidier and Morari [1986] and the bounds for design of robust decentralized controllers by Skogestad and Morari [1987] apply to independent design of controller blocks. The independent design method cannot be used to design integral controllers for examples *c* and *d*, since sufficient conditions 5 for nominal stablilty are violated – nevertheless, integral $RS\mu$ controllers for examples *c* and *d* are stabilizing.

The value of $RPIM$ should never be less than one if the true optimal controllers required in 21 are calculated. The full μ-optimal controller without the constraint of decentralized structure will yield a lower structured singular value than the μ-optimal controller with the constraint. Exact calculation of $RPIM$ in 21 is, of course, limited by our ability to calculate the required optimal controllers. At this point in time, the "μ-optimal" controllers determined by $HONEYX$ result from approximate solution of the H_∞ design problem. Efforts to utilized $HONEYX$ μ-synthesis to improve repeated sequential decentralized controller designs via the two-block and *n*-block methods described above were not successful (though in the future they may). The $RS\mu$ controllers for examples *a–d* are the nearest-to-μ-optimal decentralized controllers yet designed for these systems. The best available estimate for RPIM is therefore the ratio of $\mu_{RS}(\omega)/\mu_{Opt}(\omega)$, where μ_{RS} is the best decentralized controller resulting from repeated sequential μ-synthesis and μ_{Opt} is

the best result of full controller μ-synthesis. This RPIM estimate is displayed in Figure 37 for examples *a–d*.

Figure 37 establishes that robust performance of systems with models $\tilde{P}^c$ and $\tilde{P}^d$ is more severely deteriorated by the constraint of a decentralized controller structure than is that of systems with models $\tilde{P}^c$ or $\tilde{P}^d$. That the value of $RPIM$ for example system *a* is less than one is clear evidence that the $HONEYX$ software did not yield the full μ-optimal controller for the example.

8. Conclusions

This study demonstrated successful use of μ-synthesis in designing decentralized controllers for robust performance. Repeated sequential application of available μ-synthesis software optimized blocks in decentralized controllers for four example systems with widely different interactions. Performance of these nearly optimal decentralized controllers was compared with that of full multivariable μ-optimal controllers. The deterioration in system performance with decentralized controllers was related to the severity of model interactions. Decentralized controllers designed for two of the example systems could not result from independent loop design methods. It was demonstrated that diagonal elements of the full μ-optimal controller can be stabilizing decentralized controllers providing reasonable levels of robust performance. Sufficient conditions were derived for the diagonal part of the μ-optimal controller to be stabilizing. Properties of two novel uncertainty structures with potential for simultaneous μ-synthesis of decentralized controller blocks were developed an illustrated with examples. As available μ-synthesis software improves, the decentralized controllers resulting from algorithms in this work will provide more exact knowledge of robust performance forfeited by constaining the controller structure.

9. Appendix

Proofs of the theorems presented in this paper will be given here.

Proof of Theorem 1

The return difference operator for the system at the bottom of Figure 8 can be rewritten as follows with $\delta = -1$:

$$\begin{aligned} I + \tilde{P}K_d &= I + \tilde{P}(K_f - K_o) \\ &= (I + \tilde{P}K_f) - \tilde{P}K_o \\ &= (I + \tilde{P}K_f)\left[I - (I + \tilde{P}K_f)^{-1}\tilde{P}K_o\right]. \end{aligned} \qquad (22)$$

Let p_o denote the number of open-loop unstable poles of $\tilde{P}K_f$. Since the system with controller K_f is assumed stable, the following is true of the number of encirclements of the origin by of $det(I + \tilde{P}(s)K_f(s))$ as s traverses the Nyquist contour D:

$$N\{0, det(I + \tilde{P}K_f), D\} = -p_o.$$

Since K_f and K_d have the same number of unstable poles, the following is true if and only if the system with controller K_d is stable:

$$N\{0, det(I + \tilde{P}K_d), D\} = -p_o.$$

From Equation 22 this is equivalent to

$$N\{0, det(I + \tilde{P}K_f), D\} + N\{0, det(I - [I + \tilde{P}K_f]^{-1}\tilde{P}K_o), D\} = -p_o.$$

Therefore, the closed-loop system with controller K_d will be stable if and only if

$$N\{0, det(I - [I + \tilde{P}K_f]^{-1}\tilde{P}K_o), D\} = 0.$$

This condition is satisfied if the characteristic loci of $-[I + \tilde{P}K_f]^{-1}\tilde{P}K_o$ do not encircle $(-1,0)$. The bound in Theorem 1 is a sufficient condition for this to be true (by the Small Gain Theorem).

QED.

Proof of Theorem 2

Clearly, the off-diagonal part of the controller K_o is an element of the following uncertainty set when $\sigma_{max}[\Delta_{ij}] \leq 1$:

$$K_o \in \begin{pmatrix} \Delta_{12} & 0 \\ 0 & \Delta_{21} \end{pmatrix} \begin{pmatrix} 0 & I \\ I & 0 \end{pmatrix} \sigma_{max}[K_o].$$

Since the system is assumed stable with controller K_f (the same as $\Delta_{ij} = 0$ in Figure 9), robust stability with respect to all perturbations $\sigma_{max}[\Delta_{ij}] \leq 1$ is guaranteed if and only if

$$\mu_{K_o}\left[\begin{pmatrix} 0 & I \\ I & 0 \end{pmatrix}[I + \tilde{P}K_f]^{-1}\tilde{P}\sigma_{max}[K_o]\right] < 1; \ \forall\omega,$$

where μ_{Ko} is calculated with respect to the block structure in Theorem 2. The condition in Theorem 2 follows, since $\mu[UMa] = a\mu[M]$ for unitary matrices U and scalars a (see Doyle [1982]).

QED.

Proof of Theorem 3

In each iteration of the repeated sequential μ-synthesis, the controller block K_i' is a stabilizing controller among the set of stabilizing controllers (parameterized by Youla et al. [1976]) from which the μ-optimal controller is selected. If K_i' is the μ-optimal controller, it will be selected as K_i'' by μ-synthesis and $\mu'' = \mu'$. If not, a superior K_i'' will be selected and $\mu'' < \mu'$. Each iteration in the repeated sequential

μ-synthesis for decentralized control reduces or leaves unchanged the structured singular value.

QED.

Proof of Theorem 4

Part a) The following equality is established:

$$\sigma_{max}\begin{pmatrix} 0 & R_{12} \\ R_{21} & 0 \end{pmatrix} = \min_{R_{11}} \sigma_{max}\begin{pmatrix} R_{11} & R_{12} \\ R_{21} & 0 \end{pmatrix}. \tag{23}$$

Theorem 4.2 in Chu et al. [1986] gives the R_{11} that minimizes

$$\min_{R_{11}} \sigma_{max}\begin{pmatrix} R_{11} & R_{12} \\ R_{21} & A \end{pmatrix}$$

as

$$R_{11} = -YA^*Z + \gamma_o(I - YY^*)^{\frac{1}{2}} W (I - Z^*Z)^{\frac{1}{2}},$$

where $\sigma_{max}[W] < 1$ and Y and Z solve the following two equations:

$$R_{12} = Y(\gamma_o^2 I - A^*A)^{\frac{1}{2}}$$

$$R_{21} = (\gamma_o^2 I - AA^*)^{\frac{1}{2}} Z.$$

The result $R_{11} = 0$ in (23) follows with $A = W = 0$.

Part b) The following bound is established:

$$\min_{R_{11}} \sigma_{max}\begin{pmatrix} R_{11} & R_{12} \\ R_{21} & 0 \end{pmatrix} \leq \min_{R_{11}} \sigma_{max}\begin{pmatrix} R_{11} & R_{12} \\ R_{21} & R_{22} \end{pmatrix}. \tag{24}$$

Theorem 3.5 in Chu et al. [1986] gives the following equality for the right side of 24:

$$\min_{R_{11}} \sigma_{max} \begin{pmatrix} R_{11} & R_{12} \\ R_{21} & R_{22} \end{pmatrix} = \max\left\{ \sigma_{max} \begin{pmatrix} R_{21} & R_{22} \end{pmatrix}, \sigma_{max} \begin{pmatrix} R_{12} \\ R_{22} \end{pmatrix} \right\}. \tag{25}$$

The result 24 follows from 25, since

$$\begin{aligned} \min_{R_{11}} \sigma_{max} \begin{pmatrix} R_{11} & R_{12} \\ R_{21} & 0 \end{pmatrix} &= \max\left\{ \sigma_{max} \begin{pmatrix} R_{21} & 0 \end{pmatrix}, \sigma_{max} \begin{pmatrix} R_{12} \\ 0 \end{pmatrix} \right\} \\ &\leq \max\left\{ \sigma_{max} \begin{pmatrix} R_{21} & R_{22} \end{pmatrix}, \sigma_{max} \begin{pmatrix} R_{12} \\ R_{22} \end{pmatrix} \right\}. \end{aligned}$$

Parts a and b of the proof establish the result in Theorem 4.

QED.

Proof of Theorem 5

Part a) Since K_d' is a stabilizing controller, it is among the set of stabilizing controllers (parameterized by Youla et al. [1976]) from which the μ-optimal controller is selected. If K_d' is the μ-optimal controller, it will be selected as K_f'' by μ-synthesis, $\mu'' = \mu'$, and the gain through the loop containing Δ_e will be zero. If not, a superior K_f'' will be selected and $\mu'' < \mu'$ despite a nonzero signal in the loop containing Δ_e.

Part b) Frequency dependence is deleted from notation for clarity in the proof that follows. In Figure 21 the largest gain δ in the loop around block Δ_e is

$$\delta = \sigma_{max}\left[W_e\left(K_f'' - K_d'\right)S_w\right], \tag{26}$$

where Δ_i and Δ_p are selected within their bounds such that S_w is the worst-case transfer-function

$$S_w = \left[I + \tilde{P}\left(I + \Delta_i W_i\right)K_f'' - \Delta_p\left(W_p - W_u W_i K_f''\right)\right]^{-1}.$$

The maximum singular value of the smallest destabilizing perturbation Δ_e in this loop will be δ^{-1}. By definition, the structured singular value μ for the system will be less than or equal to δ (depending on whether or not a smaller perturbation in Δ_i or Δ_p can be destabilizing). Theorem 4 proves that $\sigma_{max}\left[K_f'' - K_d''\right] \leq \sigma_{max}\left[K_f'' - K_d'\right]$ for block diagonal matrix transfer-functions K_d with two blocks. This fact and the familiar property of norms $|ab| \leq |a||b|$ lead to

$$\delta \leq |w_e|\sigma_{max}\left[K_f'' - K_d''\right]\sigma_{max}\left[S_w\right] \leq |w_e|\sigma_{max}\left[K_f'' - K_d'\right]\sigma_{max}\left[S_w\right].$$

Step 5 therefore reduces an upper bound on μ.

QED.

Proof of Theorem 6

In Figure 6 select perturbations $\Delta_i = 0$ and $\Delta_p = 0$. Clearly, the structured singular value for this system will be less than or equal to that for finite perturbations Δ_i and Δ_p. The interconnection matrix M_1 corresponding to the uncertainty structure $\Delta = diag\left[\Delta_k, \Delta_k\right]$ is given by

$$M_1(i\omega) = -w_k(i\omega)\begin{pmatrix} \tilde{S}(i\omega) & \tilde{S}(i\omega)\tilde{P}(i\omega) \\ K(i\omega)\tilde{S}(i\omega) & K(i\omega)\tilde{S}(i\omega)\tilde{P}(i\omega) \end{pmatrix}, \qquad (27)$$

where $\tilde{S}(i\omega) = \left[I + \tilde{P}(i\omega)K(i\omega)\right]^{-1}$ is the nominal sensitivity function. Now let K be exactly block diagonal such that it commutes with Δ_k. For such a block-diagonal K the uncertainty structures involving the Δ_k cancel with one another and cannot contribute to instability in either the Δ_i or Δ_p loop. Now $\mu\left[M_1\right]$ with M_1 given in Equation 27 is invariant to the transformation $D_1 M_1 D_1^{-1}$, where

$$D_1 = \begin{pmatrix} I & 0 \\ 0 & K^{-1}(i\omega) \end{pmatrix}$$

commutes with Δ.

The new matrix $M_2 = D_1 M_1 D_1^{-1}$ is given by Equation 28:

$$M_2(i\omega) = -w_k(i\omega) \begin{pmatrix} \tilde{S}(i\omega) & I - \tilde{S}(i\omega) \\ \tilde{S}(i\omega) & I - \tilde{S}(i\omega) \end{pmatrix}. \tag{28}$$

Now $\mu[M_2]$ with M_2 given in Equation 28 is invariant to the transformation $U_2 M_2 U_2^{-1}$, where

$$U_2 = \begin{pmatrix} I & -I \\ 0 & I \end{pmatrix}$$

is unitary. The new matrix $M_3 = U_2 M_2 U_2^{-1}$ is given by Equation 29.

$$M_3(i\omega) = -w_k(i\omega) \begin{pmatrix} 0 & 0 \\ \tilde{S}(i\omega) & I \end{pmatrix} \tag{29}$$

Trivially, $\rho[M_3] = |w_k(i\omega)|$. Since $\rho[M_3]$ is a lower bound for $\mu[M_3] = \mu[M_1]$, the structured singular value for the system in Figure 26 will be greater than or equal to $|w_k(i\omega)|$ for all frequencies ω.

QED.

References

Bernstein, D. S., "Sequential Design of Decentralized Dynamic Compensators Using the Optimal Projection Equations: An Illustrative Example Involving Interconnected Flexible Beams," *Proceedings of the American Control Conference*, Minneapolis, June 10–12, 1987, pp. 986–989.

Bristol, E. H., "On a New Measure of Interaction for Multivariable Process Control," *IEEE Transactions on Automatic Control*, AC-11, 1966, pp. 133–134.

Chu, C. C., with J. C. Doyle and E. B. Lee, "The General Distance Problem in H_∞ Synthesis," *International Journal of Control*, 44, 1986, pp. 565–596.

Desoer, C. A., and A. N. Gundes, "Linear Time-Invariant Controller Design for Two-Channel Decentralized Control Systems," *Proceedings of the American Control Conference*, Minneapolis, June 10–12, 1987, pp. 1703–1704.

Doyle, J. C., "Analysis of Feedback Systems with Structured Uncertainties," *Proc. Inst. Elect. Engrs.*, Pt. D, 129, 1982, pp. 242–250.

Doyle, J. C., "A Review of μ for Case Studies in Robust Control," *IFAC World Congress*, Munich, July 1987.

Fan, M. K., and A. L. Tits, "Characterization and Efficient Computation of the Structured Singular Value," *IEEE Transactions on Automatic Control*, AC-31, August 1986, pp. 734–743.

Grosdidier, P., and M Morari, "Interaction Measures for Systems Under Decentralized Control," *Automatica*, 22, 1986, pp. 309–319.

Mayne, D. Q., "The Design of Linear Multivariable Systems," *Automatica*, 9, 1973, pp. 201–207.

Nett, C. N., and J. A. Uthgenannt, "An Explicit Formula and an Optimal Weight for the 2-Block Structured Singular Interaction Measure," *IEEE Transactions on Automatic Control*, submitted September 1, 1986.

Rosenbrock, H. H., "Design of Multivariable Control Systems Using the Inverse Nyquist Array," *Proc. Inst. Elect. Engrs.*, 116, 1969, pp. 1929–1936.

Skogestad, S., and M. Morari, "Robust Performance of Decentralized Control Systems by Independent Designs," *Automatica*, submitted January, 1987.

Smith, R. S., Personnal Communication, California Institute of Technology, June 19, 1987.

Youla, D. C., with H. A. Jabr, and J. J. Bongiorno, Jr., "Modern Wiener-Hopf Design of Optimal Controllers: Part II," *IEEE Transactions on Automatic Control*, AC-21, 1976, pp. 319–338.

FIGURES FOR CHAPTER VI

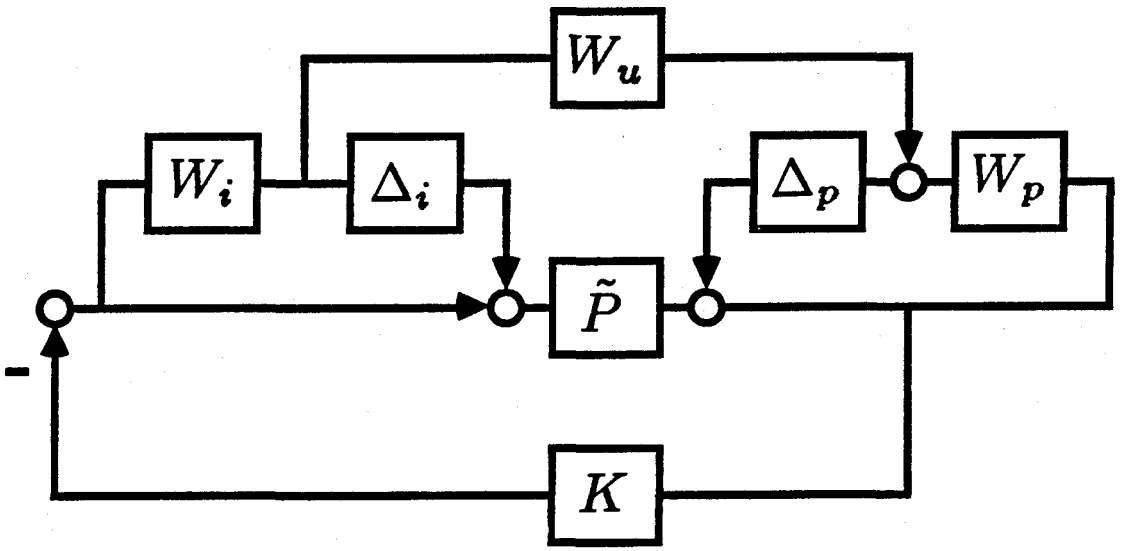

Figure 1: Feedback control system with nominal process $\tilde{P}(s)$, controller $K(s)$, weighted input uncertainty $\Delta_i W_i(s)$, performance weight $W_p(s)$, control action penalty $W_u(s)W_i(s)$, and performance block Δ_p.

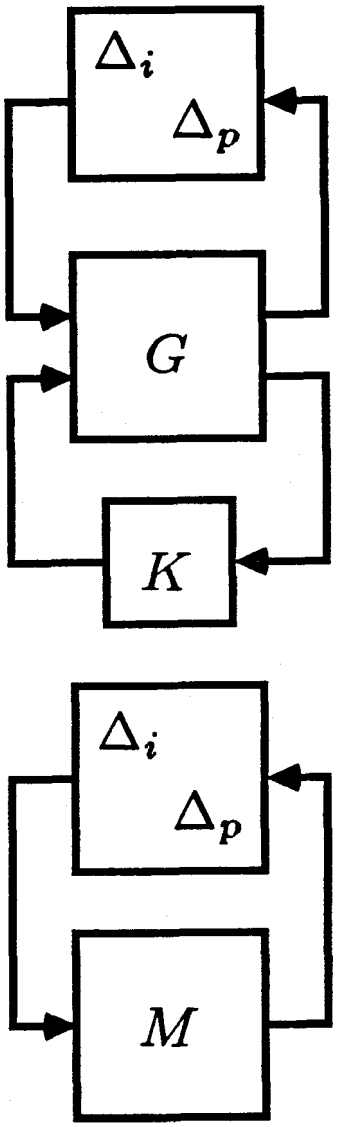

Figure 2: General interconnection structures for μ-synthesis and μ-analysis corresponding to the feedback control structure in Figure 1.

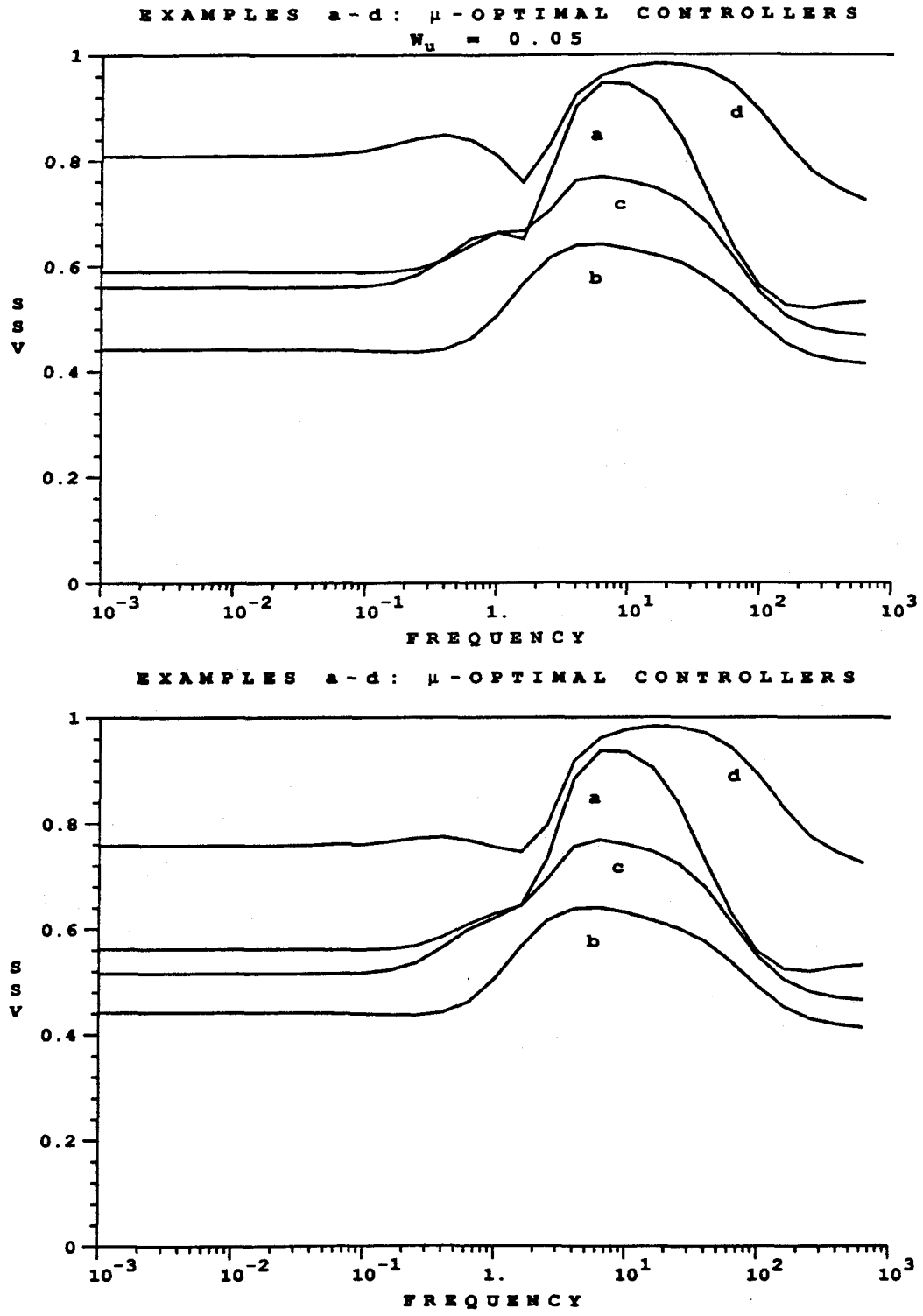

Figure 3: Structured singular values for systems with models *a-d* and full matrix μ-optimal controllers.

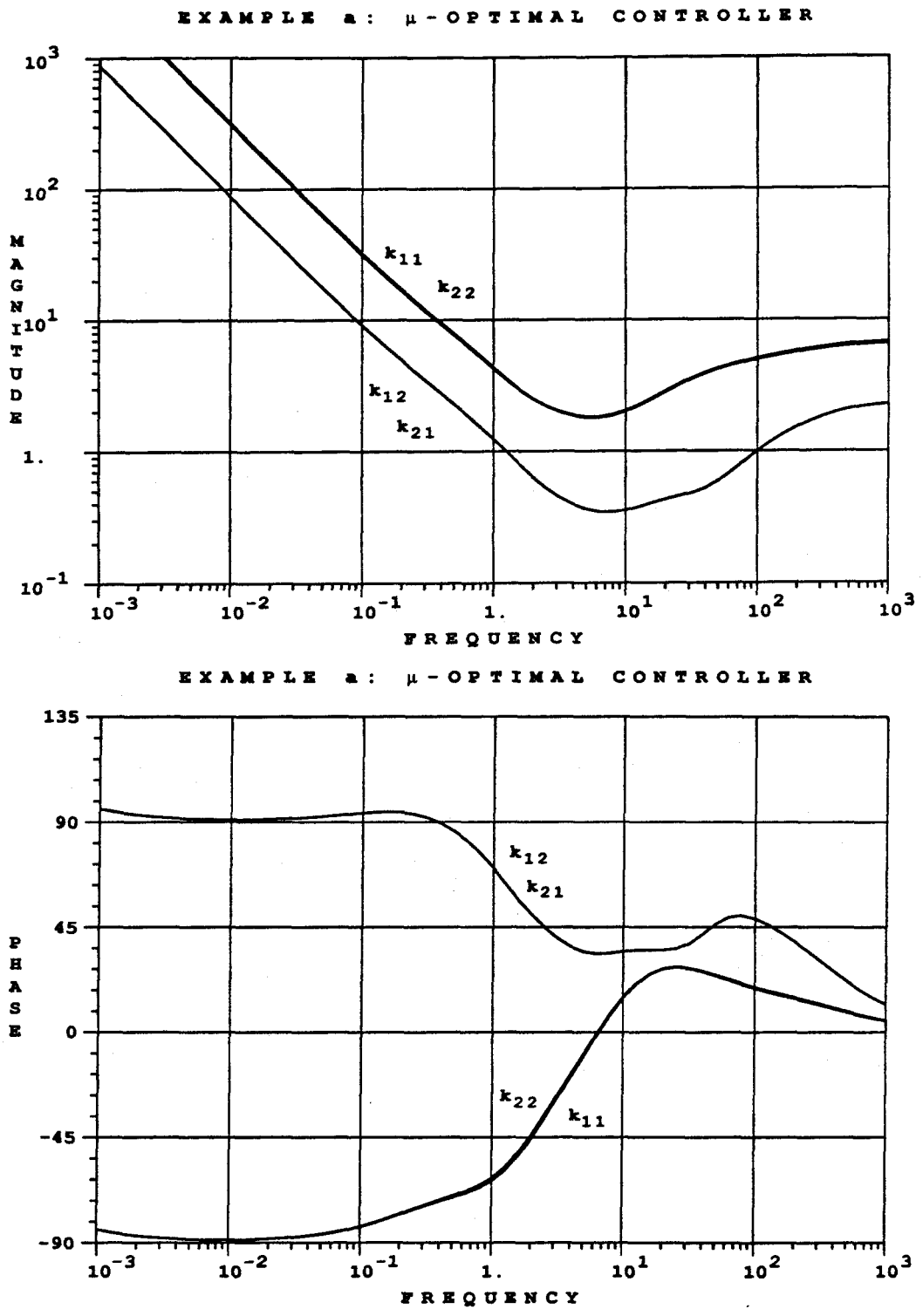

Figure 4: Bode plot for full matrix μ-optimal controller synthesized for example *a*.

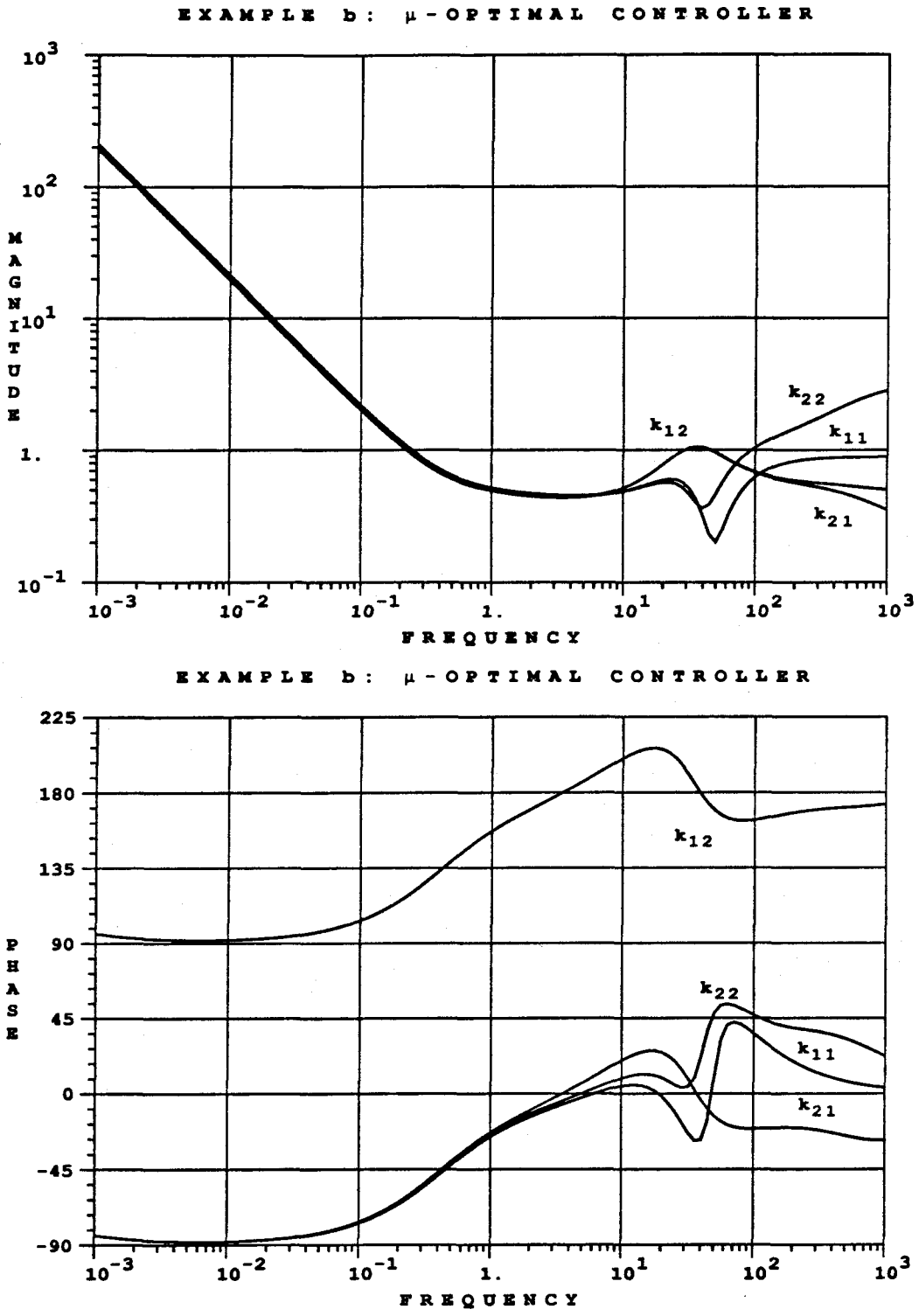

Figure 5: Bode plot for full matrix μ-optimal controller synthesized for example *b*.

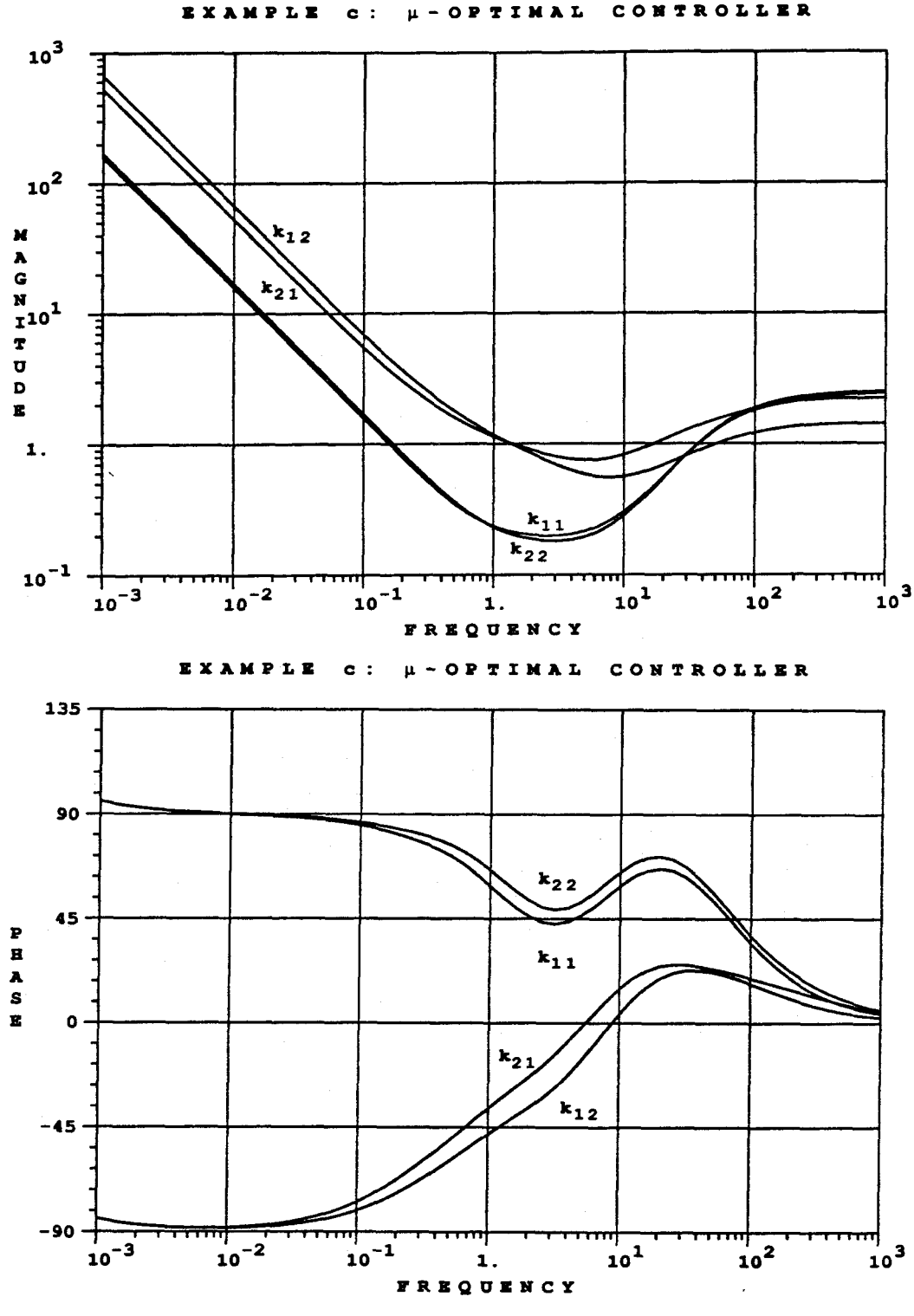

Figure 6: Bode plot for full matrix μ-optimal controller synthesized for example *c*.

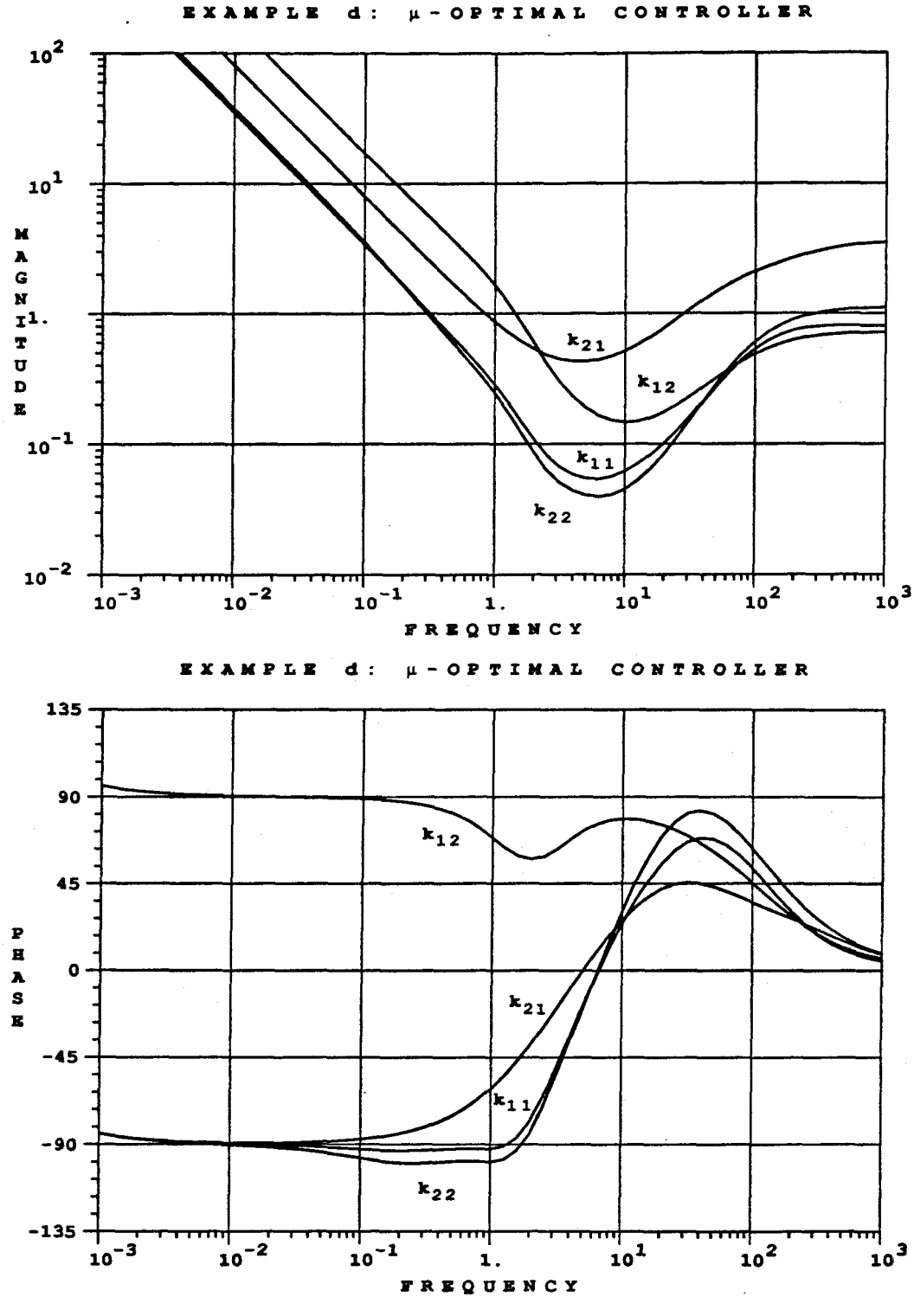

Figure 7: Bode plot for full matrix μ-optimal controller synthesized for example *d*.

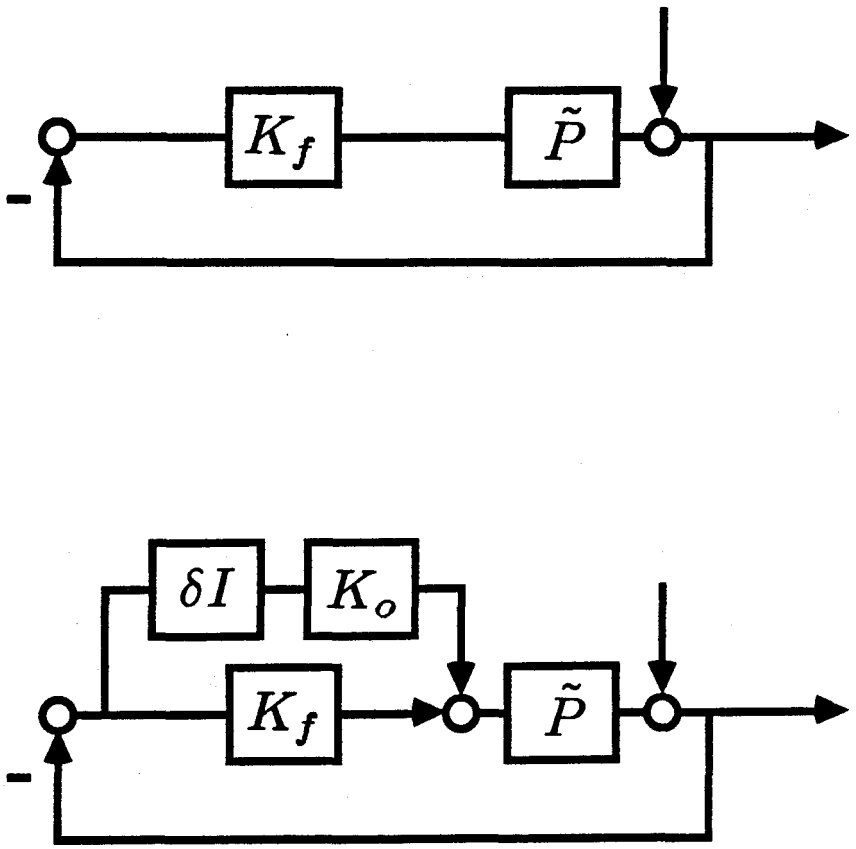

Figure 8: Feedback control structure with off-diagonal part K_o of the full controller K_f written as an additive perturbation to the controller.

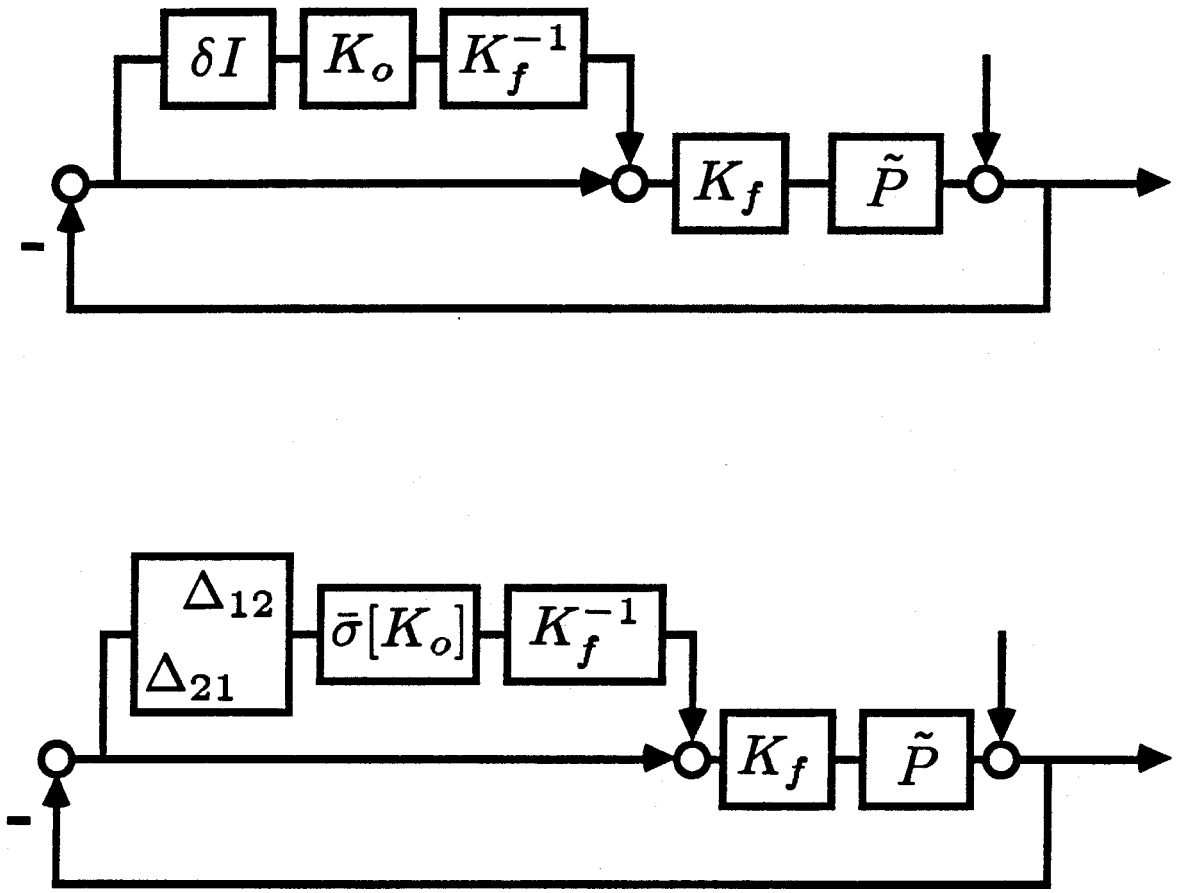

Figure 9: The off-diagonal part K_o of the full controller K_f is illustrated here as two types of norm-bounded multiplicative perturbations at the controller input.

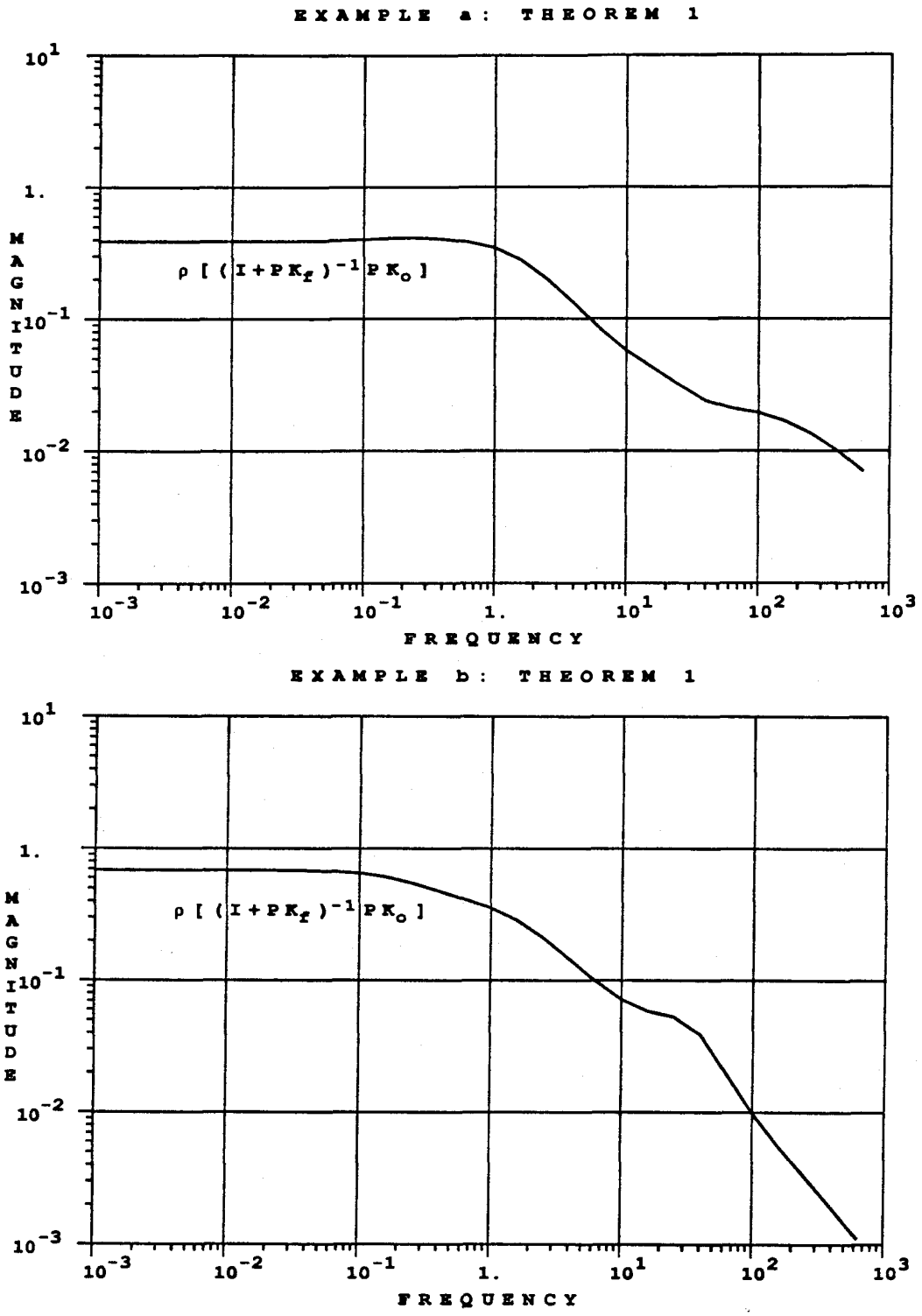

Figure 10: Theorem 1 applied to examples *a* and *b* showing that sufficient conditions are satisfied for both examples.

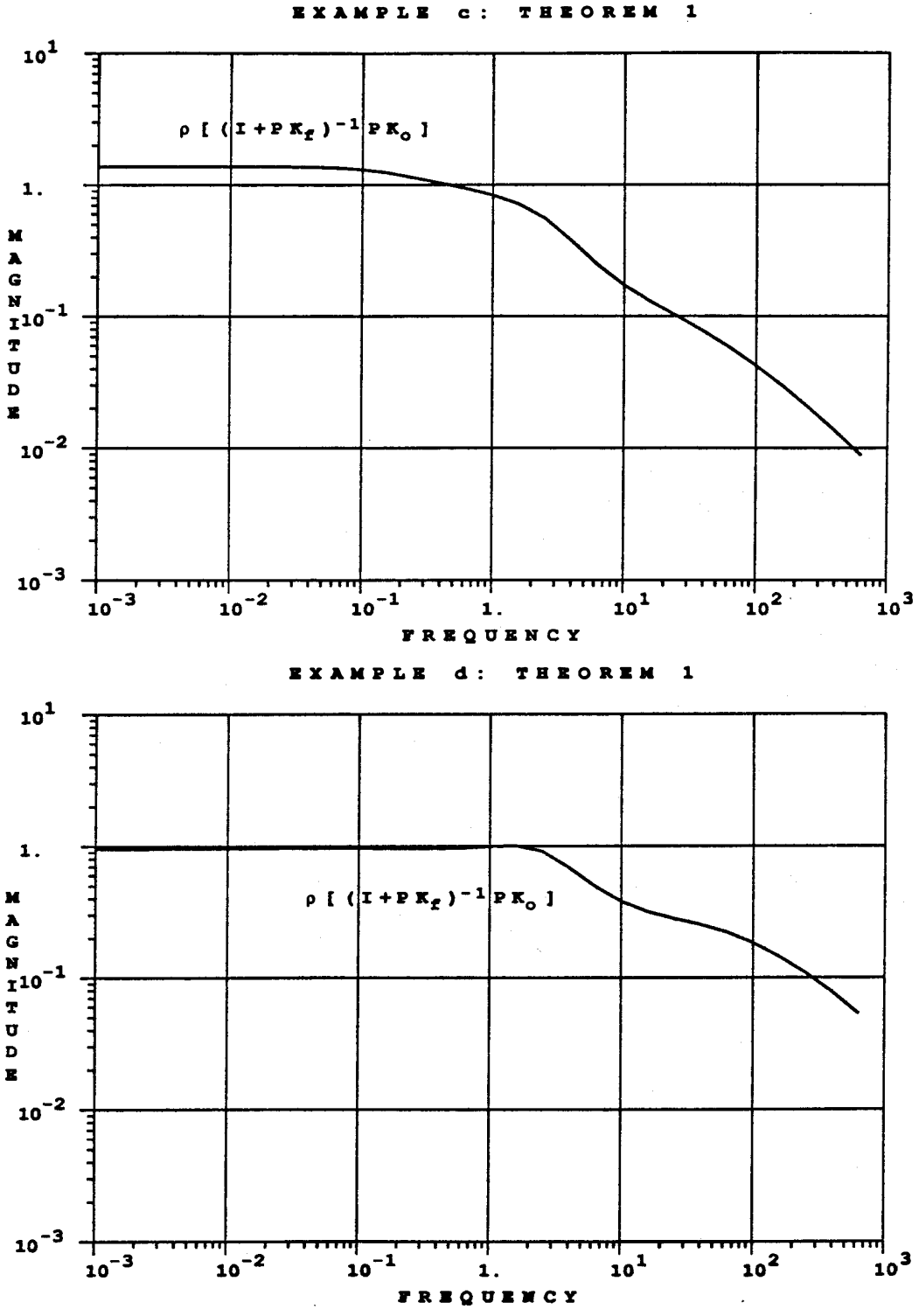

Figure 11: Theorem 1 applied to examples *c* and *d* showing that sufficient conditions are not satisfied for both examples.

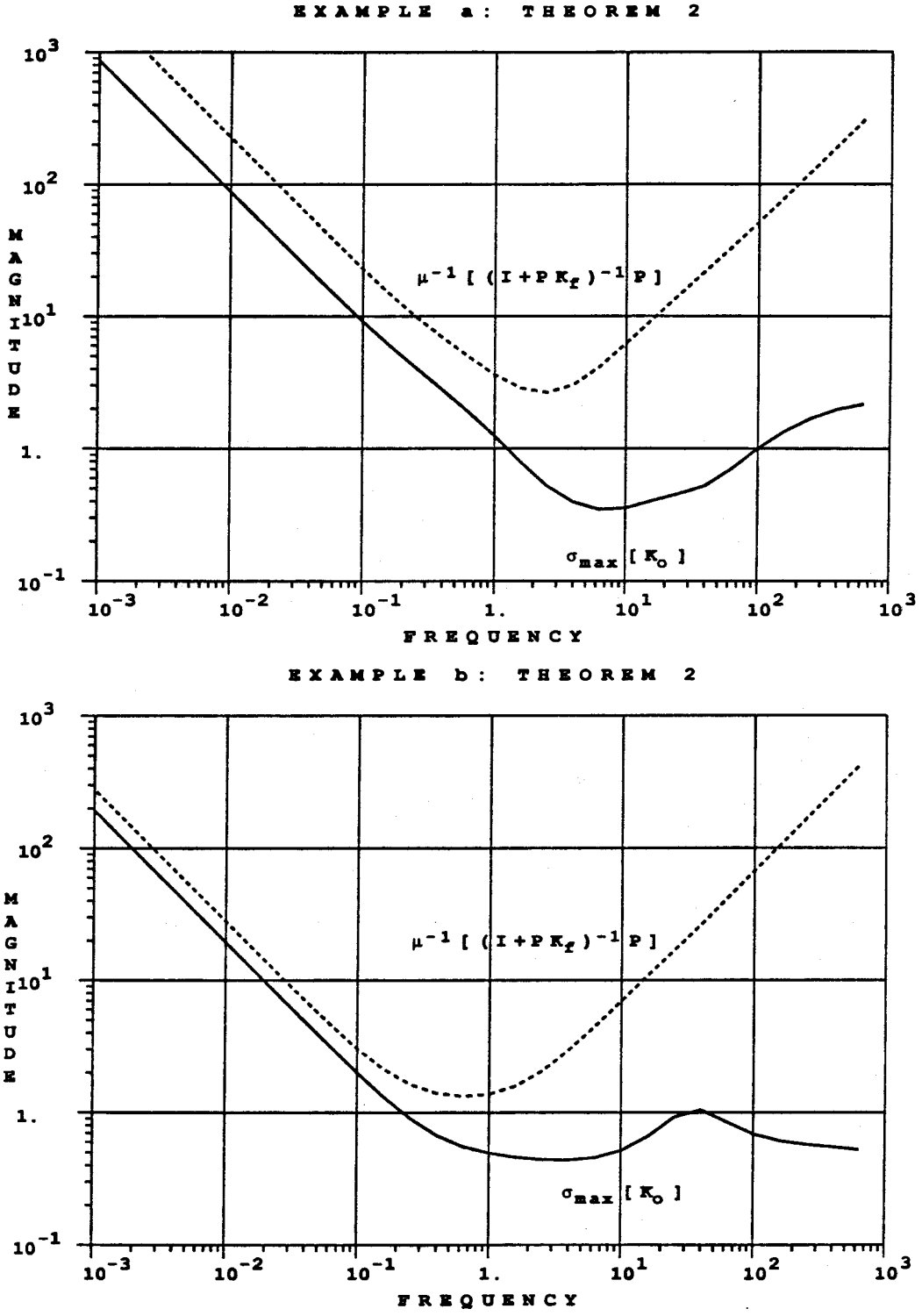

Figure 12: Theorem 2 applied to examples *a* and *b* showing that sufficient conditions are satisfied for both examples.

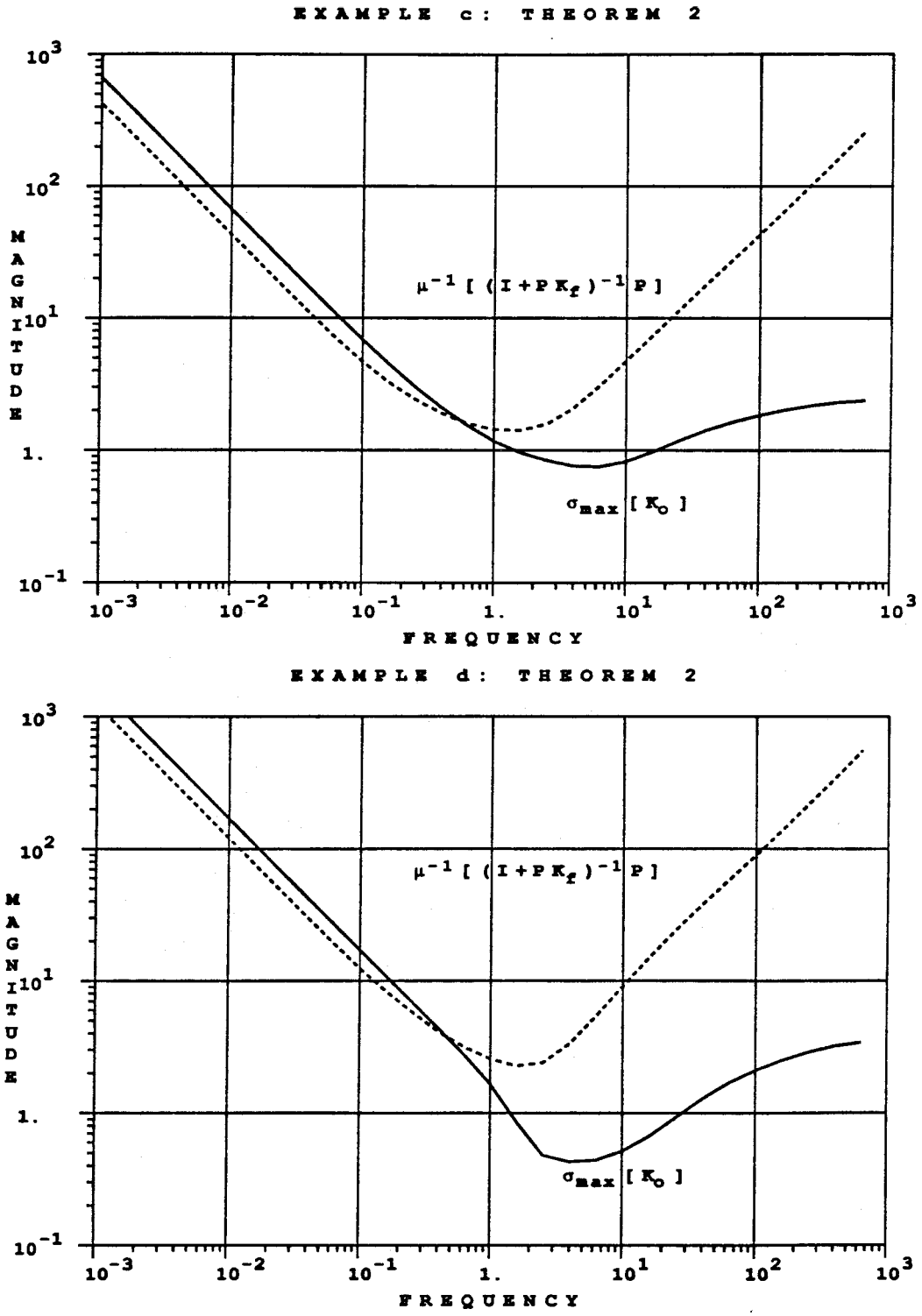

Figure 13: Theorem 2 applied to examples *c* and *d* showing that sufficient conditions are not satisfied for both examples.

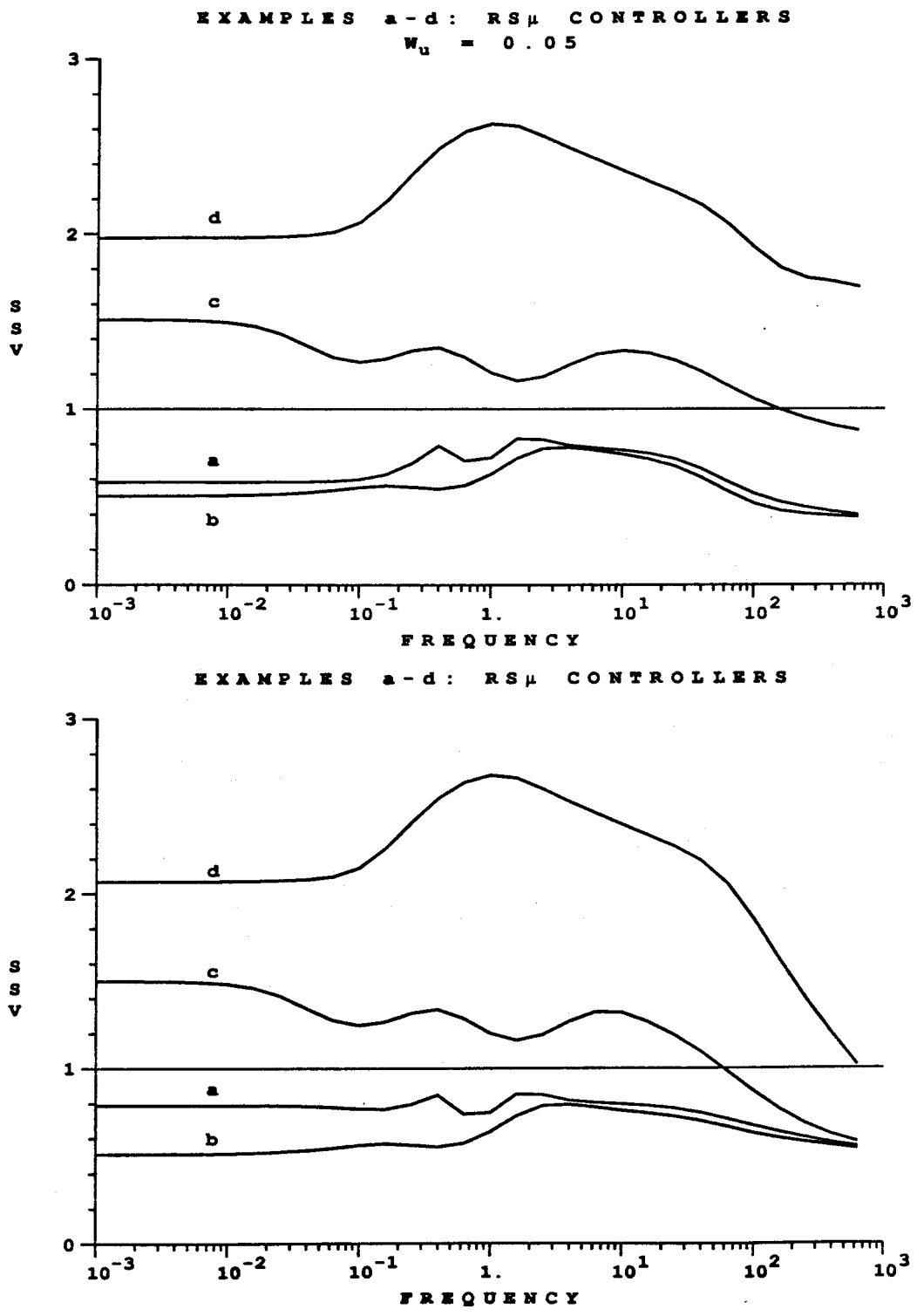

Figure 14: Structured singular values for systems with models *a–d* and repeated sequential $RS\mu$-optimal controllers.

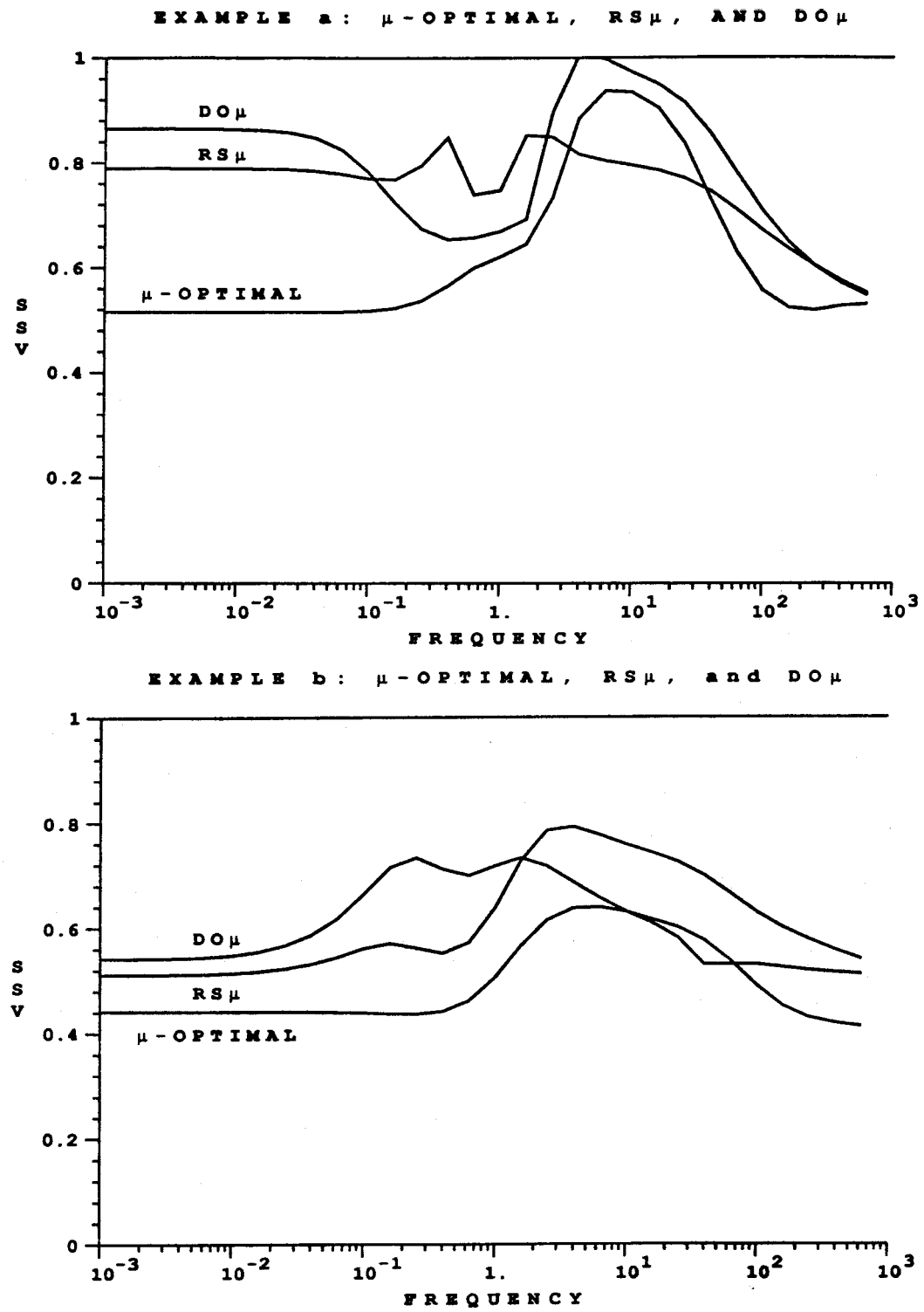

Figure 15: Comparison of structured singular values for systems with models a and b and μ-optimal, $DO\mu$, and $RS\mu$ controllers.

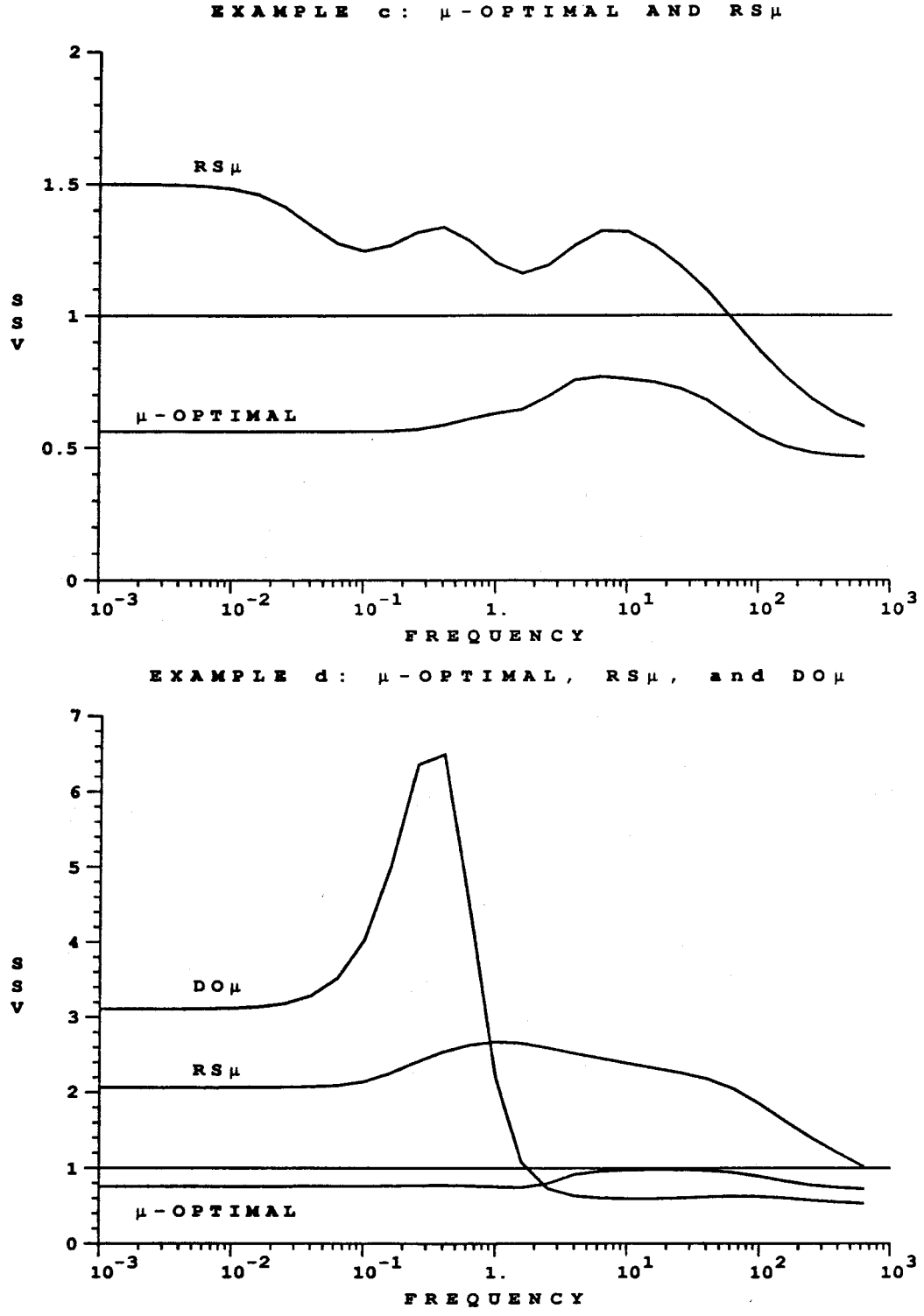

Figure 16: Comparison of structured singular values for systems with models c and d and μ-optimal, $DO\mu$, and $RS\mu$ controllers.

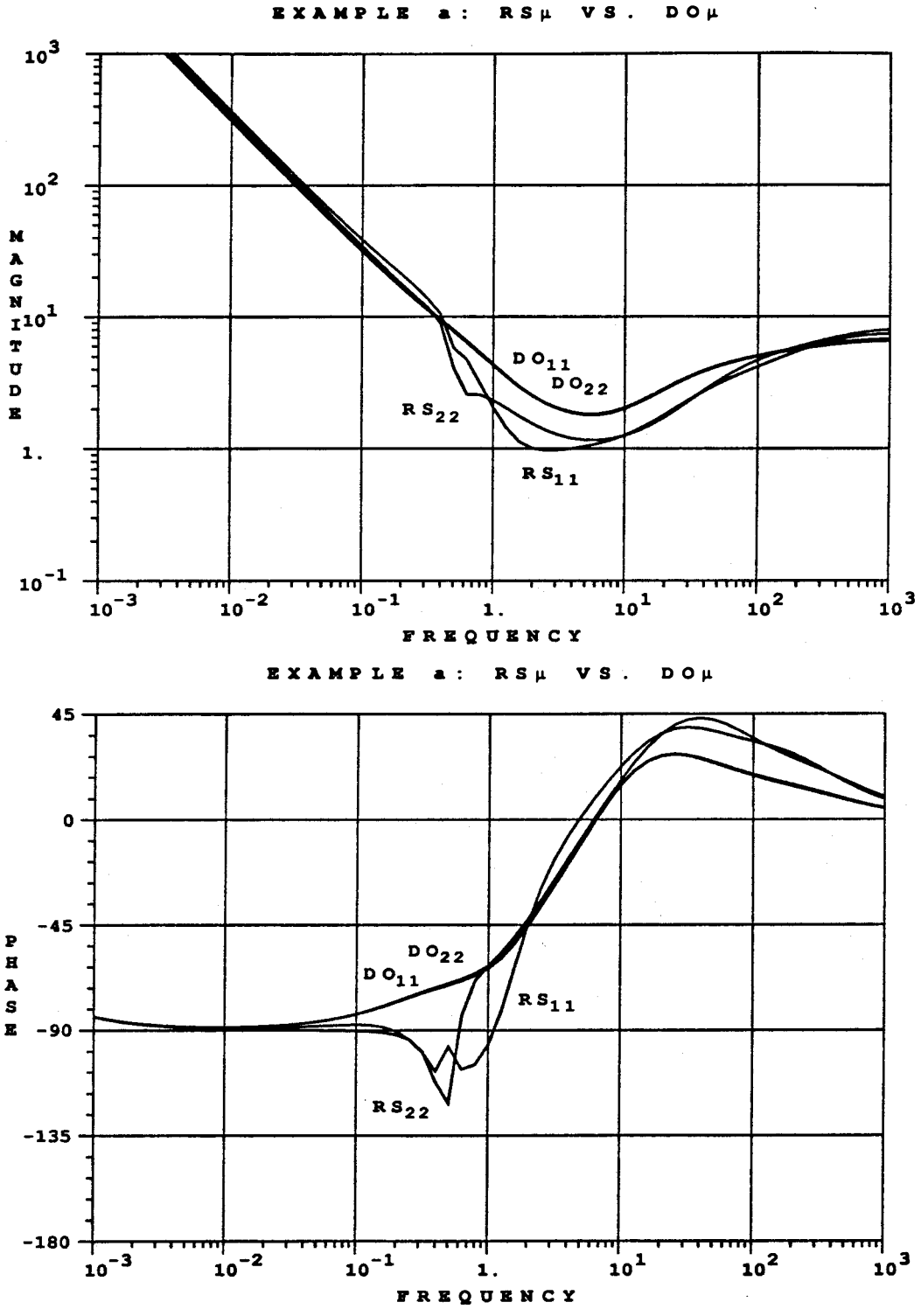

Figure 17: Comparison of Bode plots of controllers $DO\mu$ and $RS\mu$ for example a.

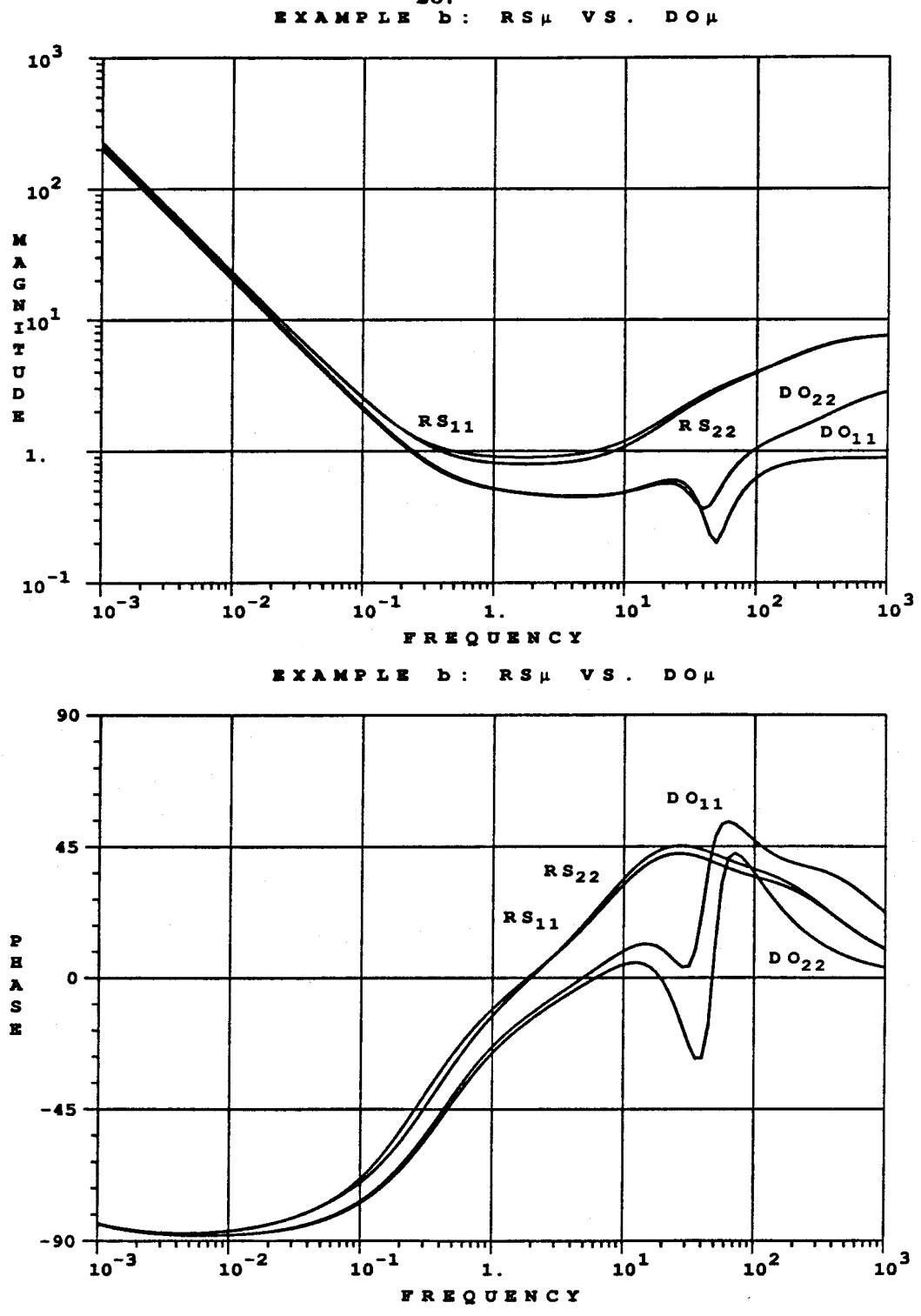

Figure 18: Comparison of Bode plots of controllers $DO\mu$ and $RS\mu$ for example *b*.

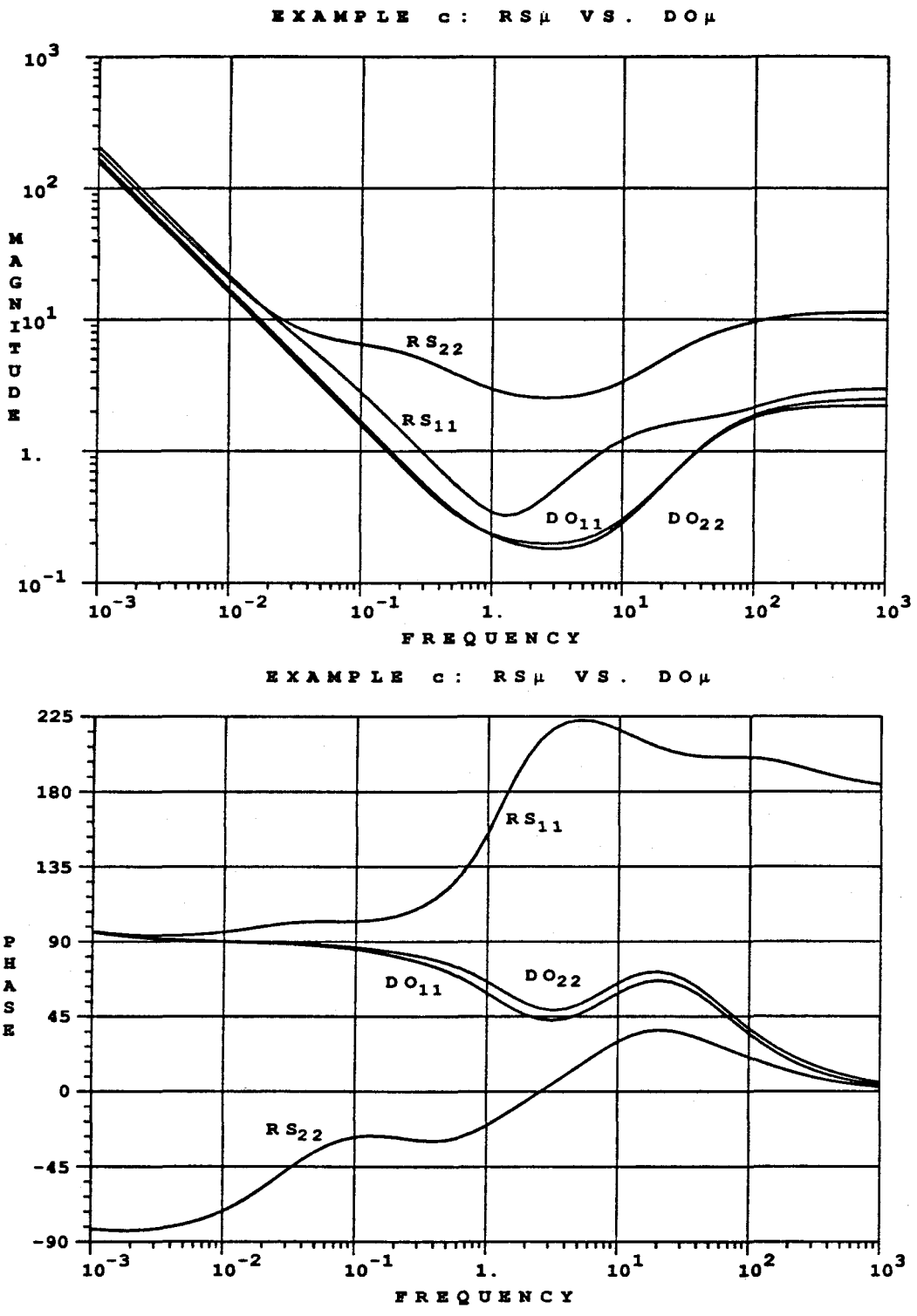

Figure 19: Comparison of Bode plots of controllers $DO\mu$ and $RS\mu$ for example *c*.

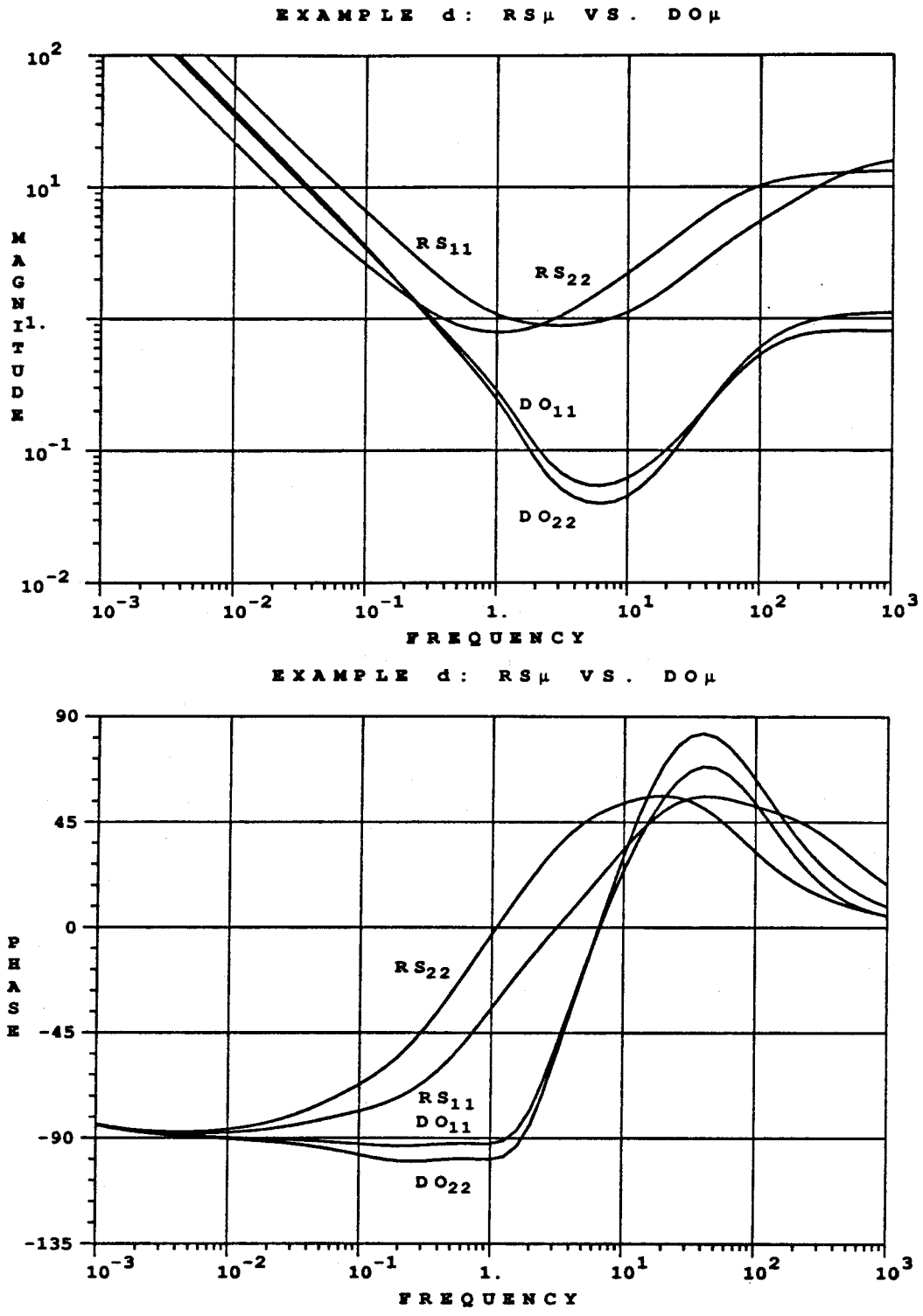

Figure 20: Comparison of Bode plots of controllers $DO\mu$ and $RS\mu$ for example *d*.

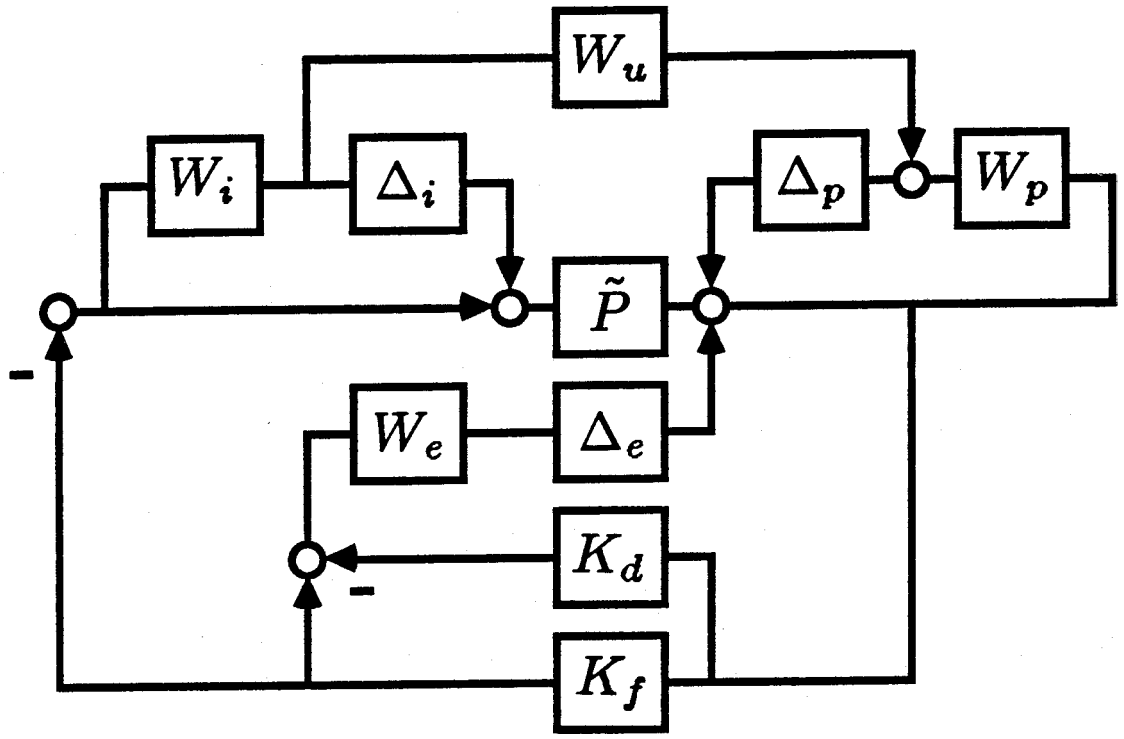

Figure 21: Block structure used for μ-synthesis of two-block decentralized controllers with penalty on off-diagonal controller elements $\Delta_e W_e(s)$.

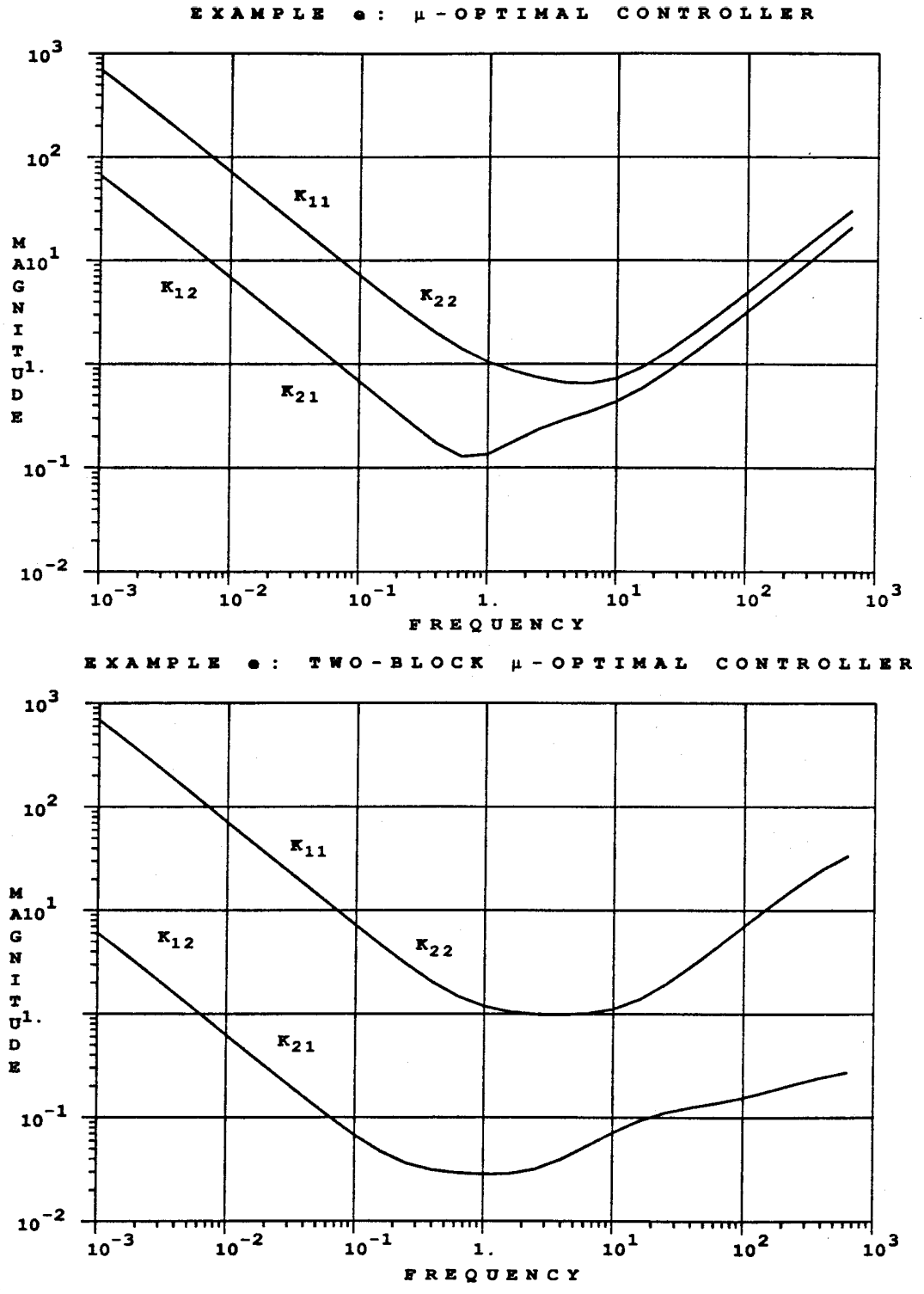

Figure 22: Bode plots for example e illustrating the effect of penalty $\Delta_e W_e(s)$ on the magnitude of off-diagonal controller elements.

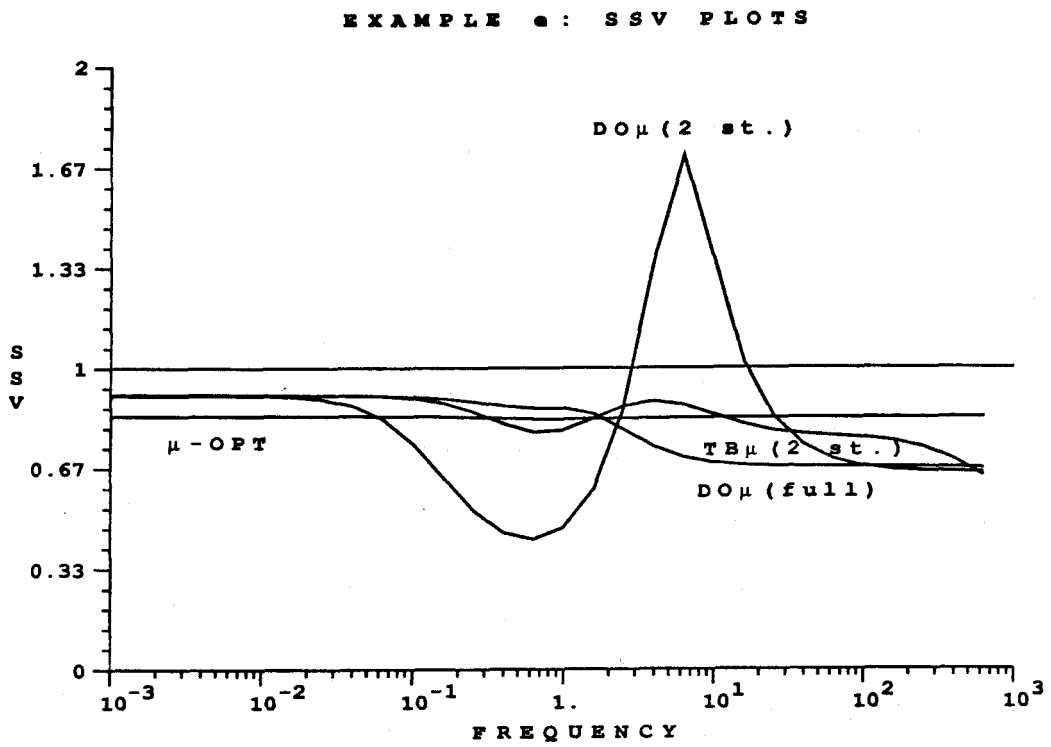

Figure 23: Structured Singular Value plots for example *e*. The diagonal part $DO\mu(full)$ of the μ-optimal controller loses much robust performance as a result of model reduction to two states $DO\mu(2st.)$. The two-block μ-synthesis leads to a much better two-state controller $TB\mu(2st.)$.

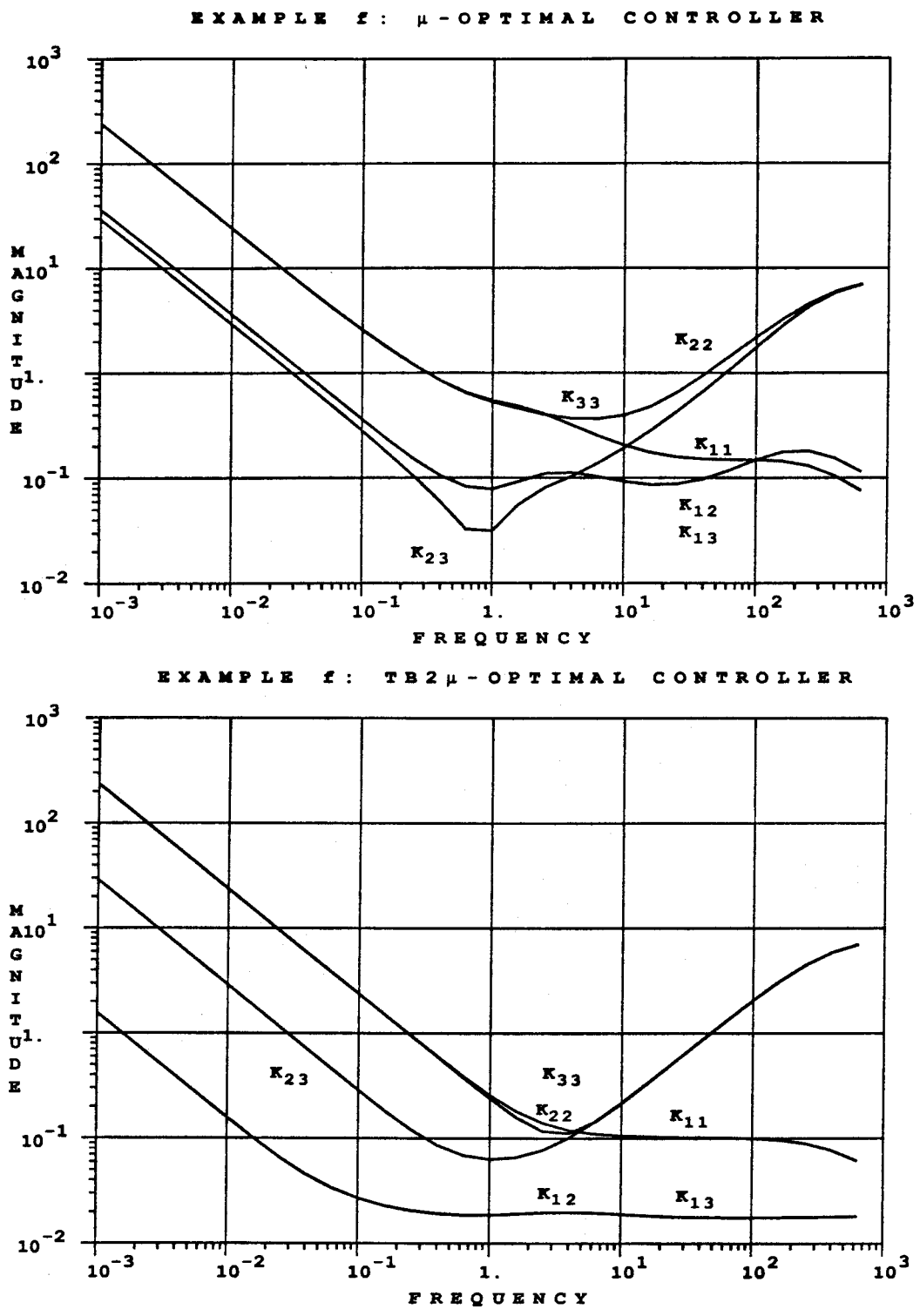

Figure 24: Bode plots for example f illustrating the effect of penalty $\Delta_e W_e(s)$ on the magnitude of off-diagonal controller elements.

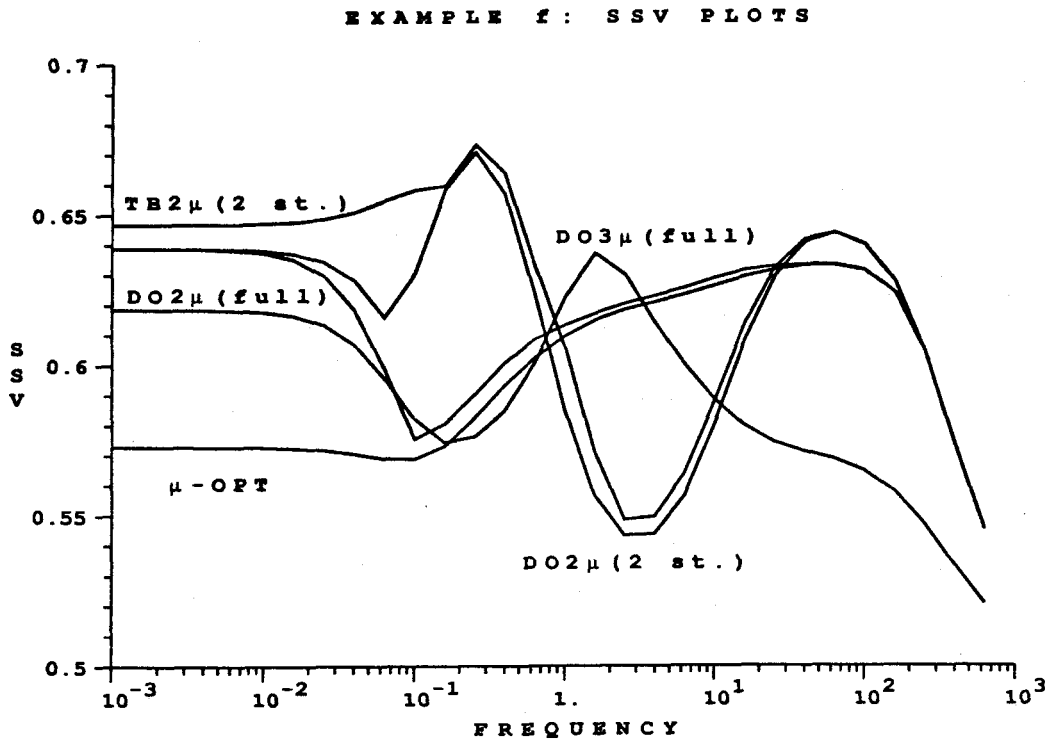

Figure 25: Structured singular values for example f. The fully decentralized part $DO3\mu(full)$ and two-block decentralized part $DO2\mu(full)$ of the μ-optimal controller both exhibit good levels of robust performance. Model reduction to two states of $DO2\mu(full)$ leads to $DO2\mu(2st.)$. Robust performance is little changed by the model reduction. The two-block μ-synthesis controller with two states $TB2\mu(2st.)$ is no improvement.

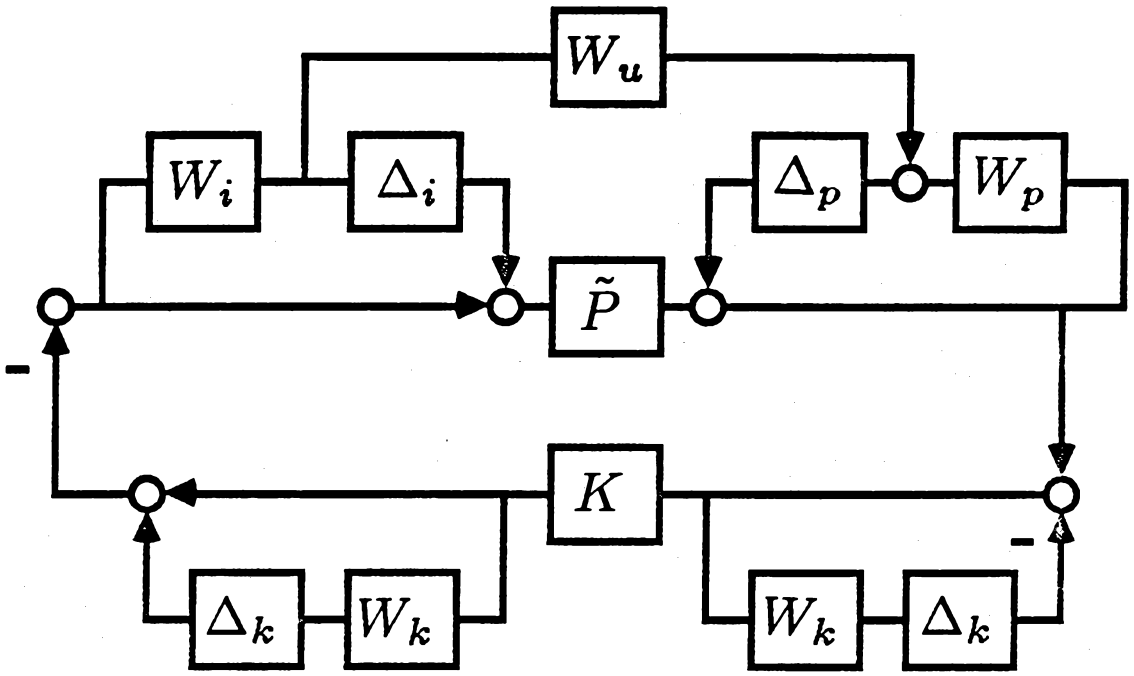

Figure 26: Block structure used for μ-synthesis of n-block decentralized controllers with penalties on off-diagonal controller elements $\left(I + \Delta_k W_k(s)\right)$ and $\left(I + \Delta_k W_k(s)\right)^{-1}$.

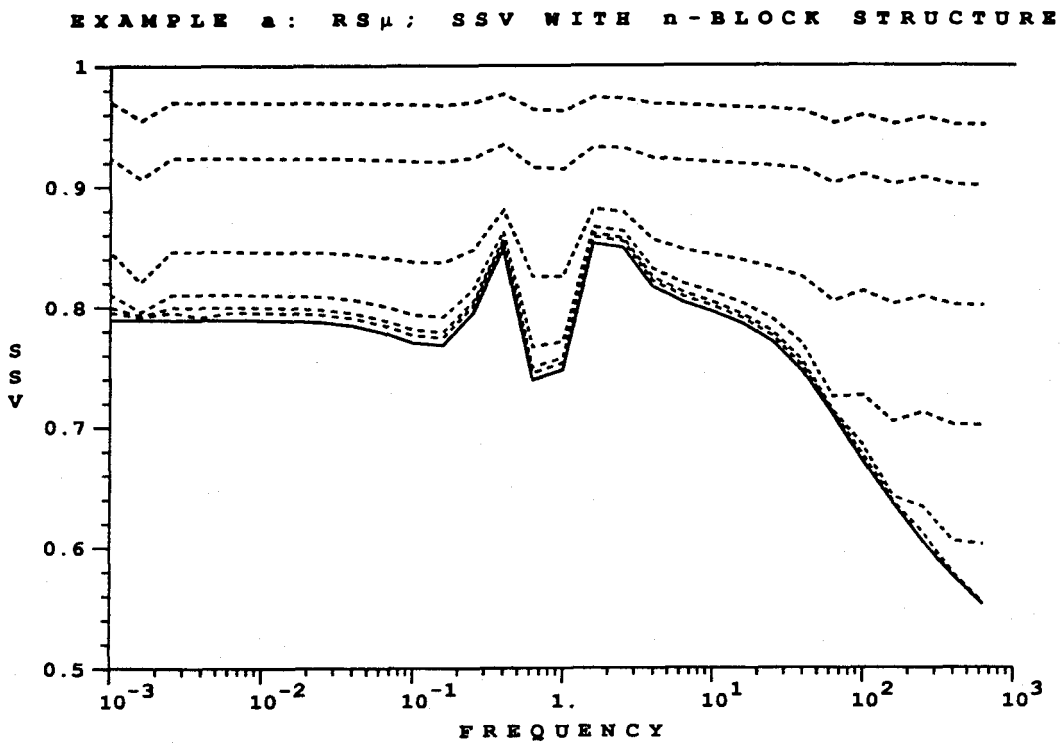

Figure 27: Structured singular values for example *a* with controller $RS\mu$. Solid curve is $\mu(\omega)$ without *n*-block penalty $W_k(s)$ on off-diagonal controller elements. Dashed curves correspond to values for $W_k(s)$ of 0.5, 0.6, 0.7, 0.8, 0.9, and 0.95 as magnitude of $\mu(\omega)$ increases.

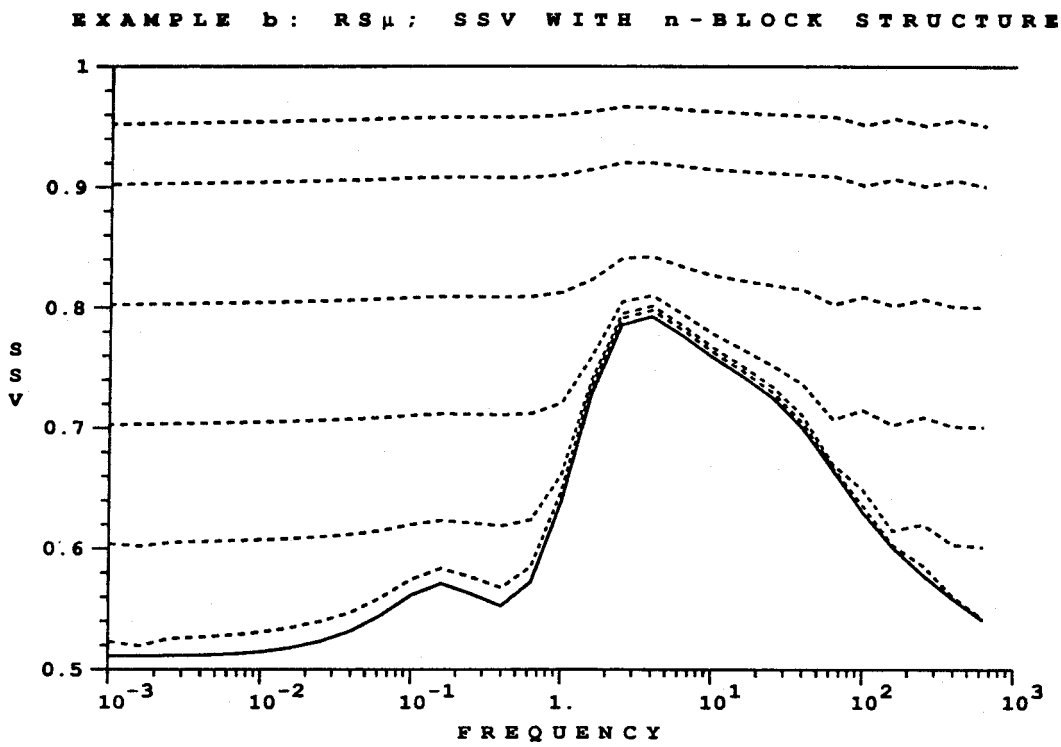

Figure 28: Structured singular values for example *b* with controller $RS\mu$. Solid curve is $\mu(\omega)$ without n-block penalty $W_k(s)$ on off-diagonal controller elements. Dashed curves correspond to values for $W_k(s)$ of 0.5, 0.6, 0.7, 0.8, 0.9, and 0.95 as magnitude of $\mu(\omega)$ increases.

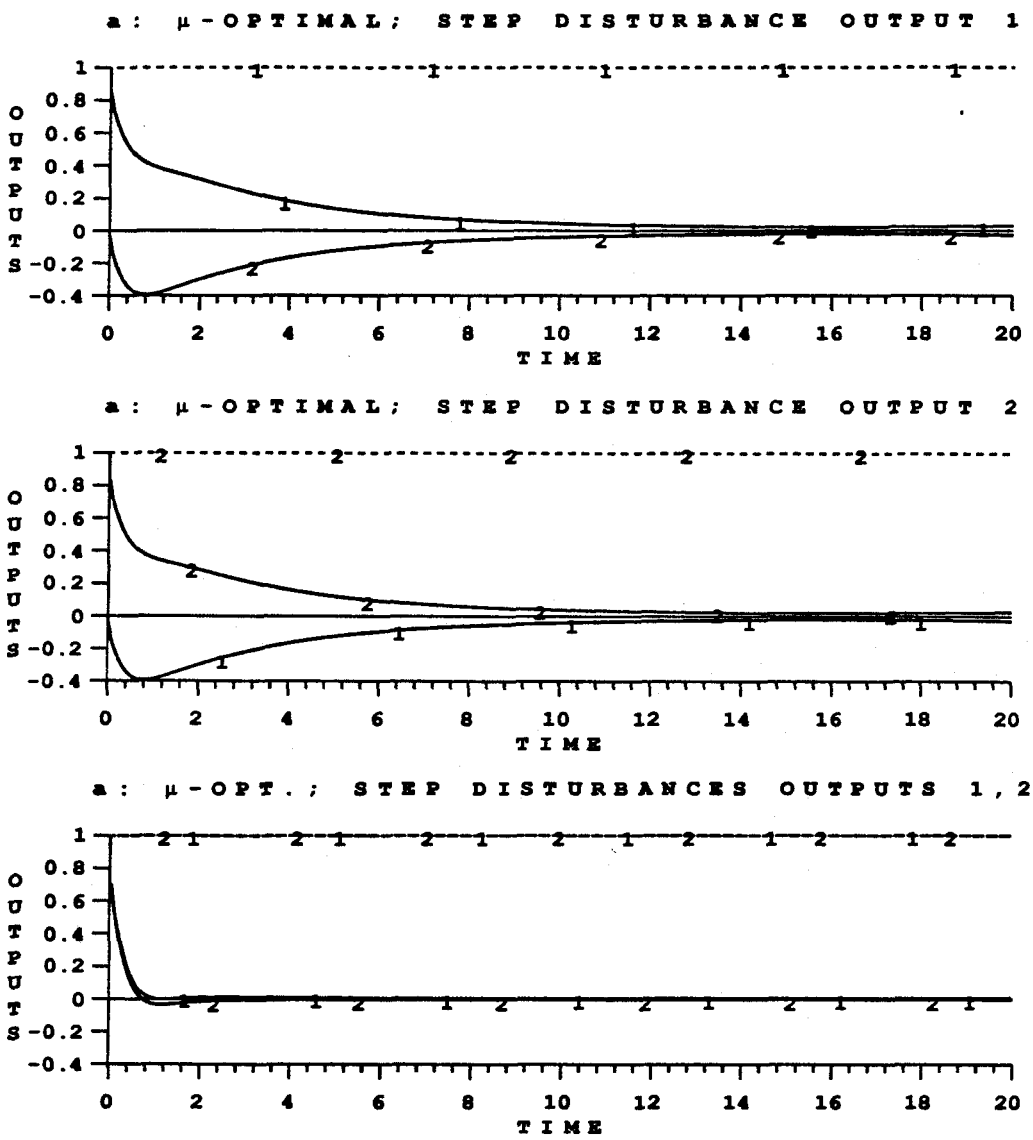

Figure 29: Responses to step disturbances for example a with full matrix μ-optimal controller.

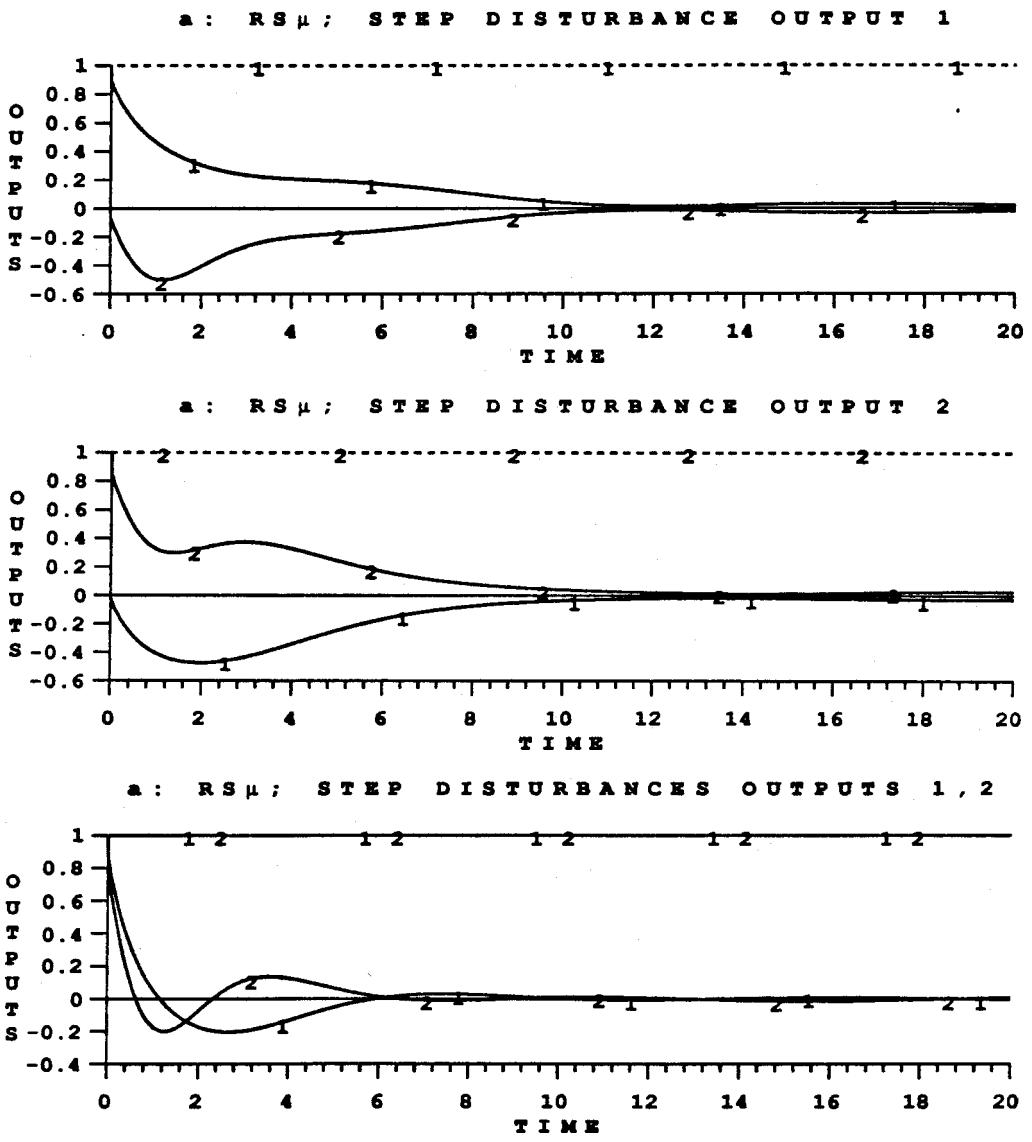

Figure 30: Responses to step disturbances for example a with diagonal controller from repeated sequential μ-synthesis.

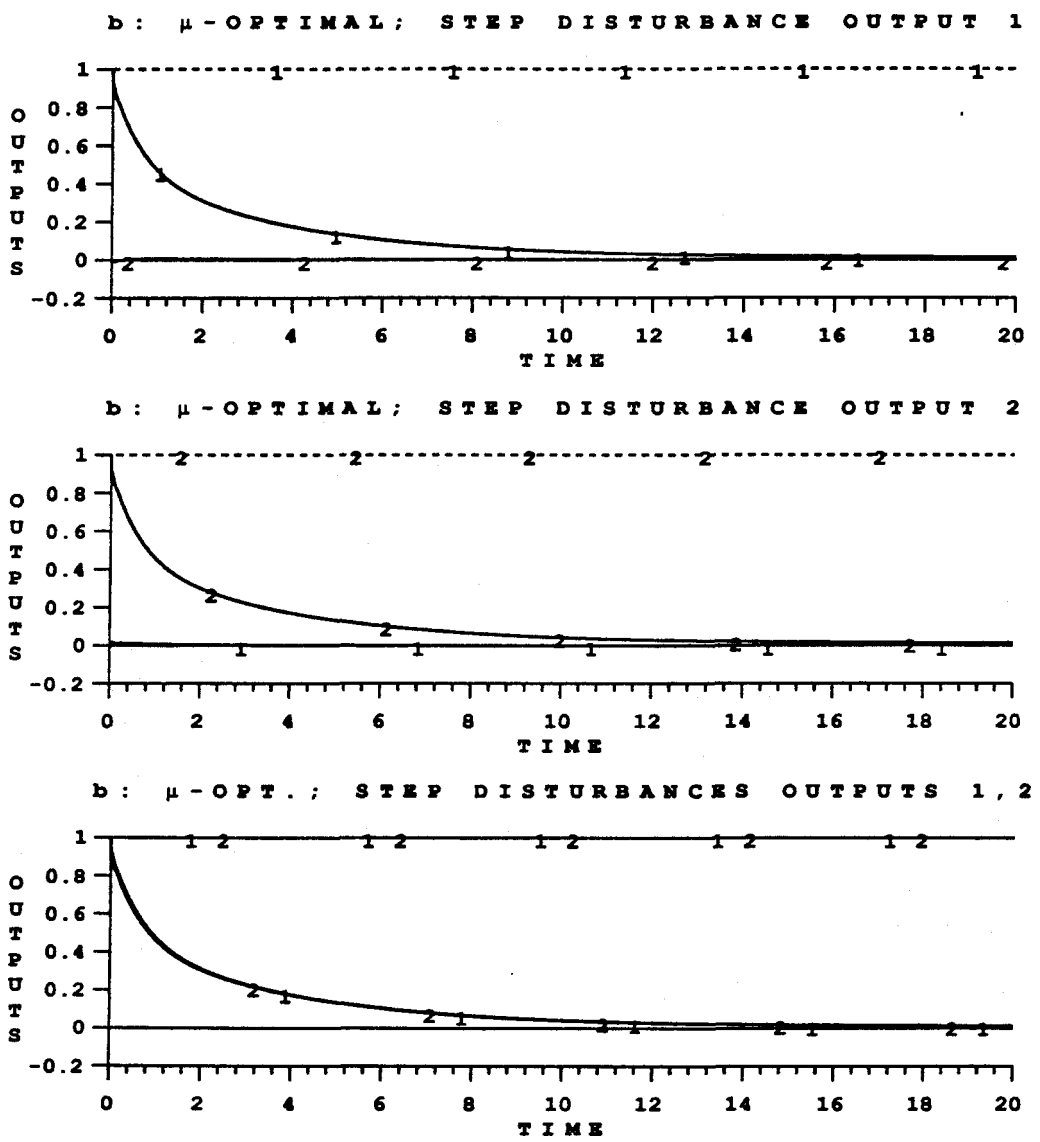

Figure 31: Responses to step disturbances for example b with full matrix μ-optimal controller.

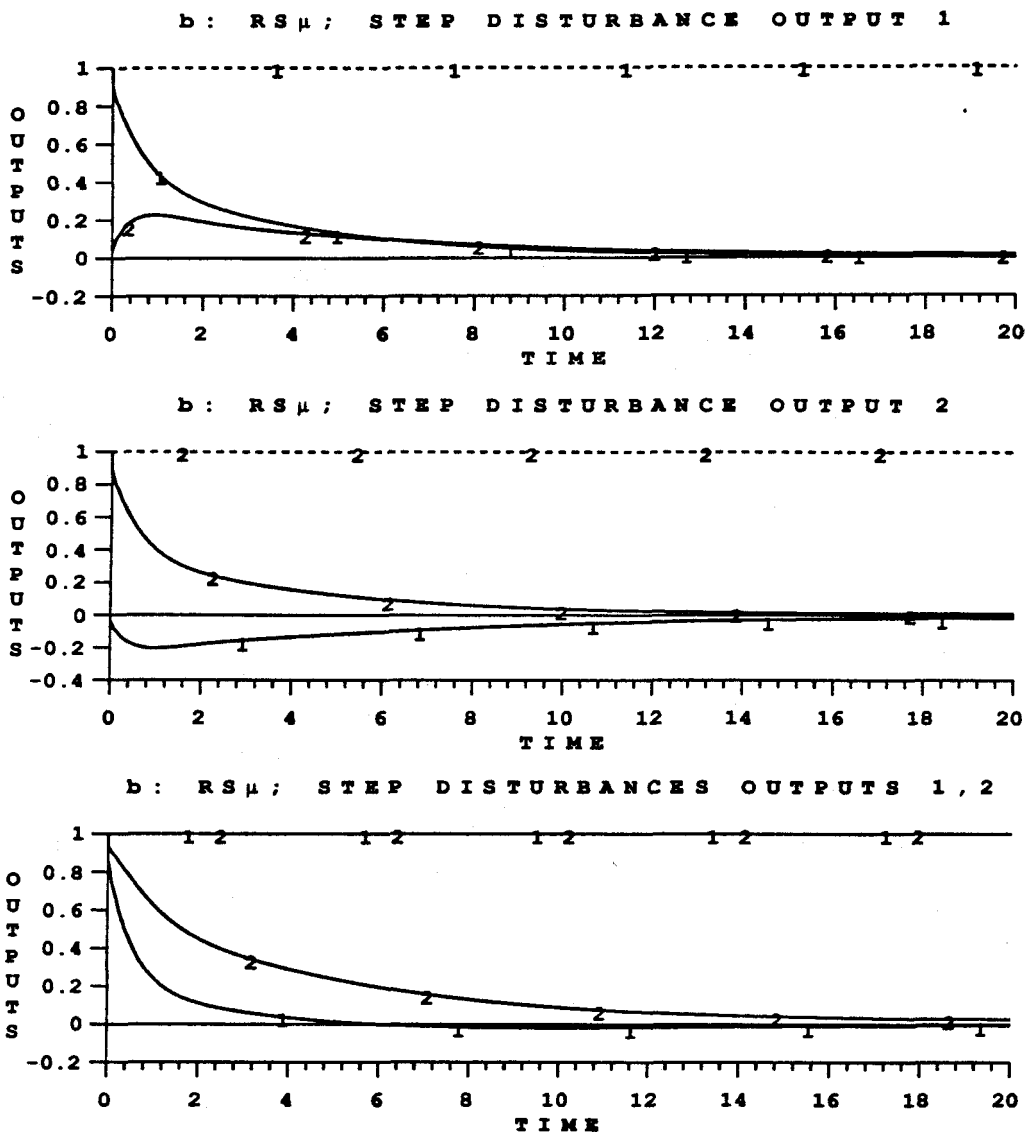

Figure 32: Responses to step disturbances for example *b* with diagonal controller from repeated sequential μ-synthesis.

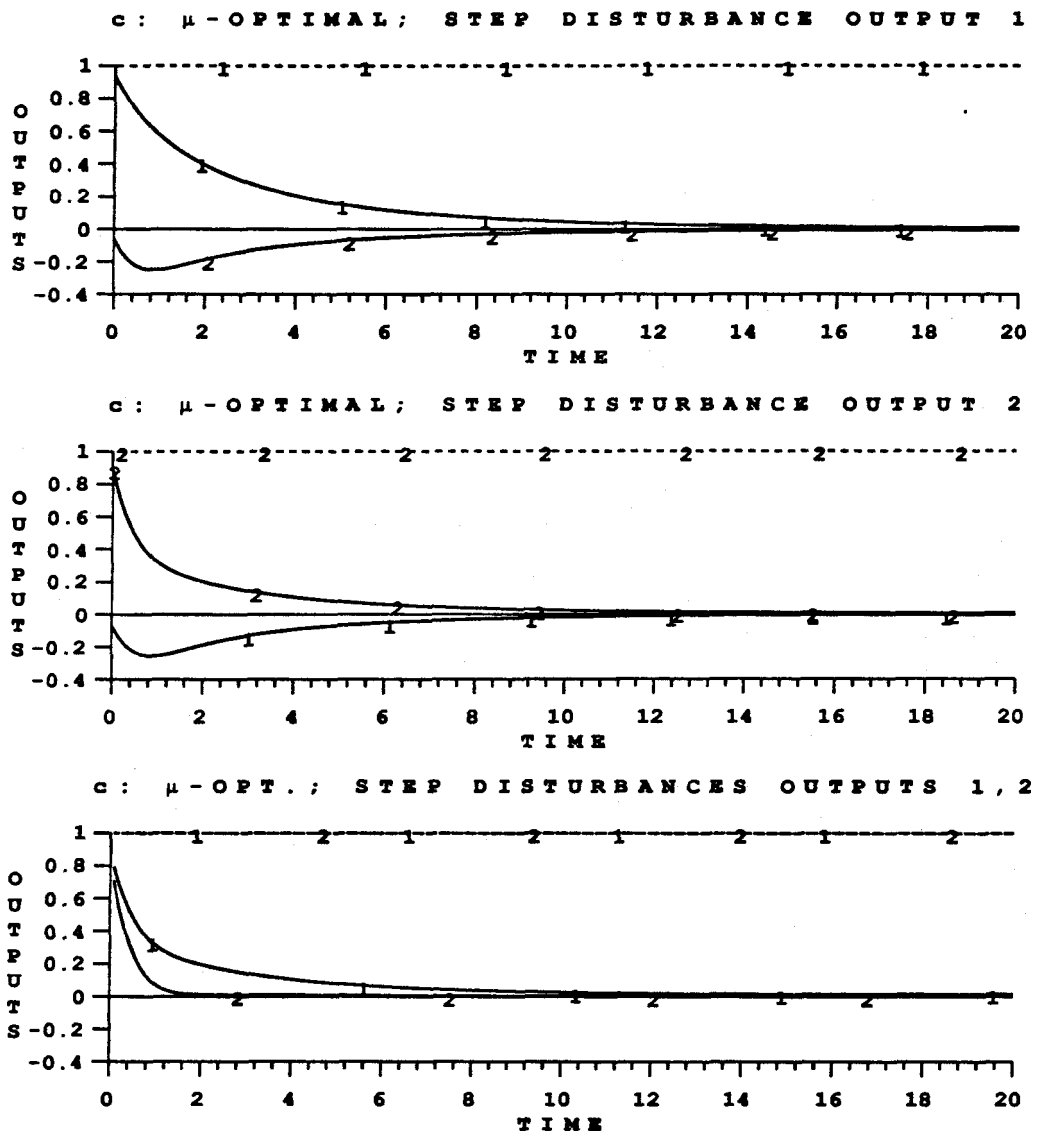

Figure 33: Responses to step disturbances for example c with full matrix μ-optimal controller.

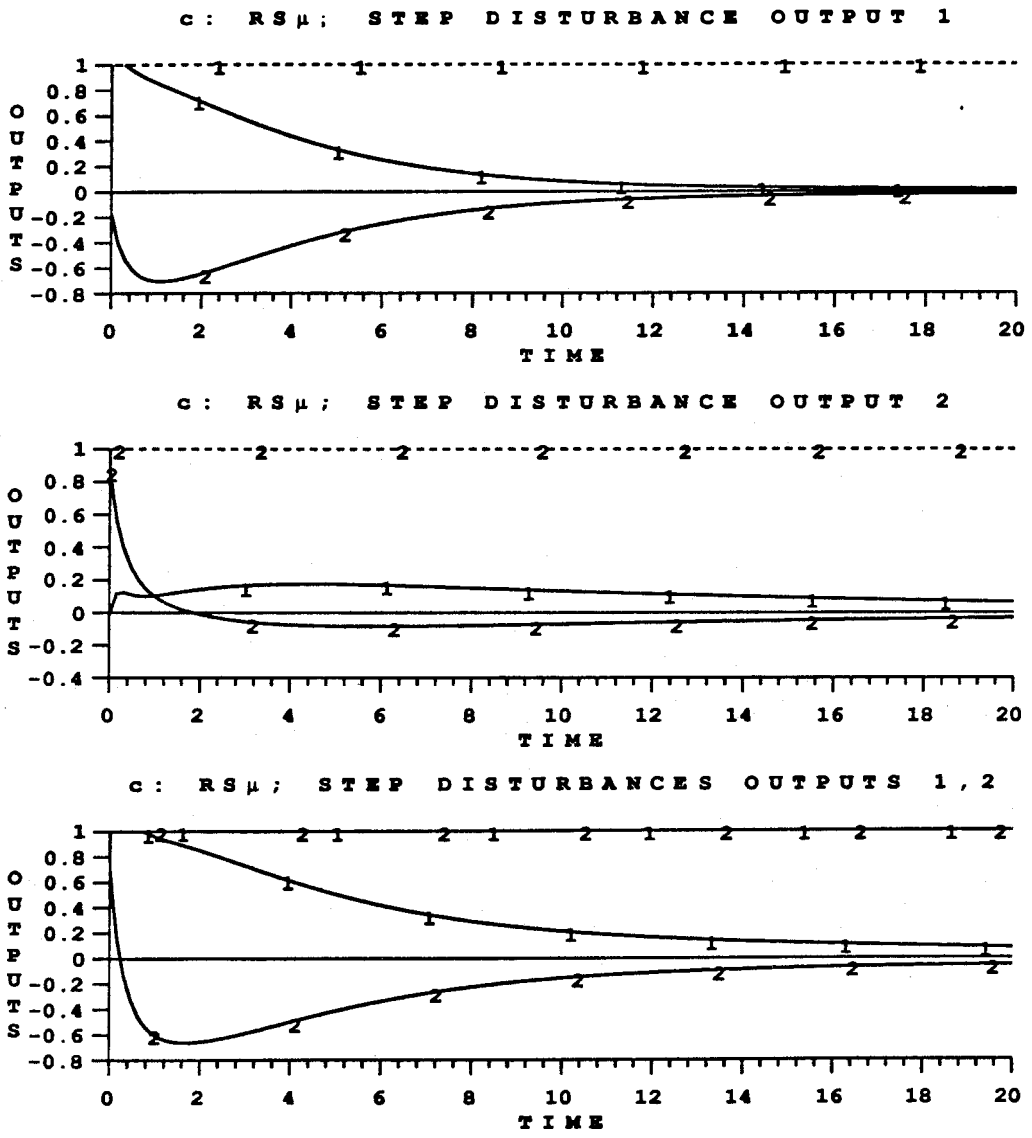

Figure 34: Responses to step disturbances for example c with diagonal controller from repeated sequential μ-synthesis.

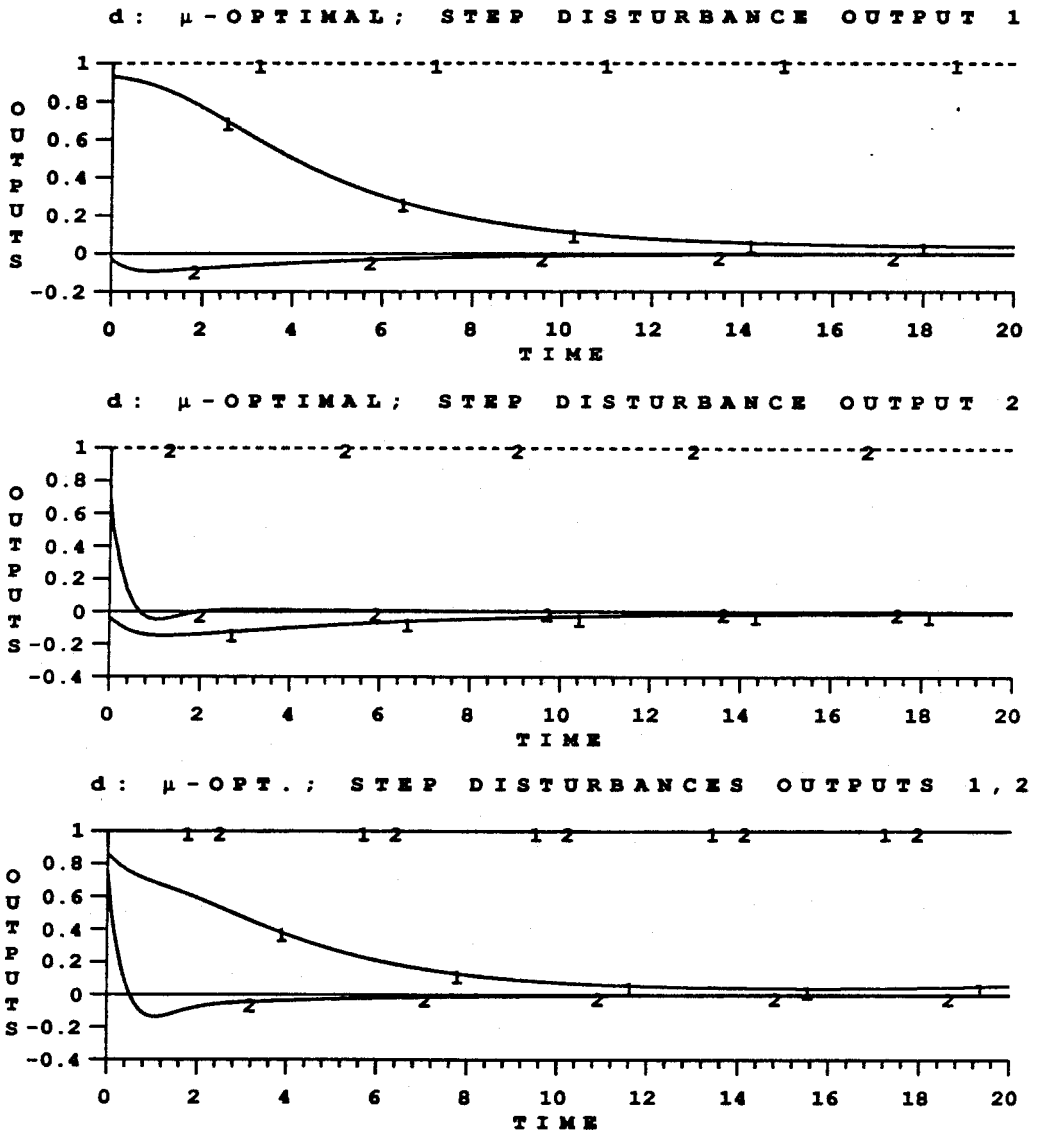

Figure 35: Responses to step disturbances for example d with full matrix μ-optimal controller.

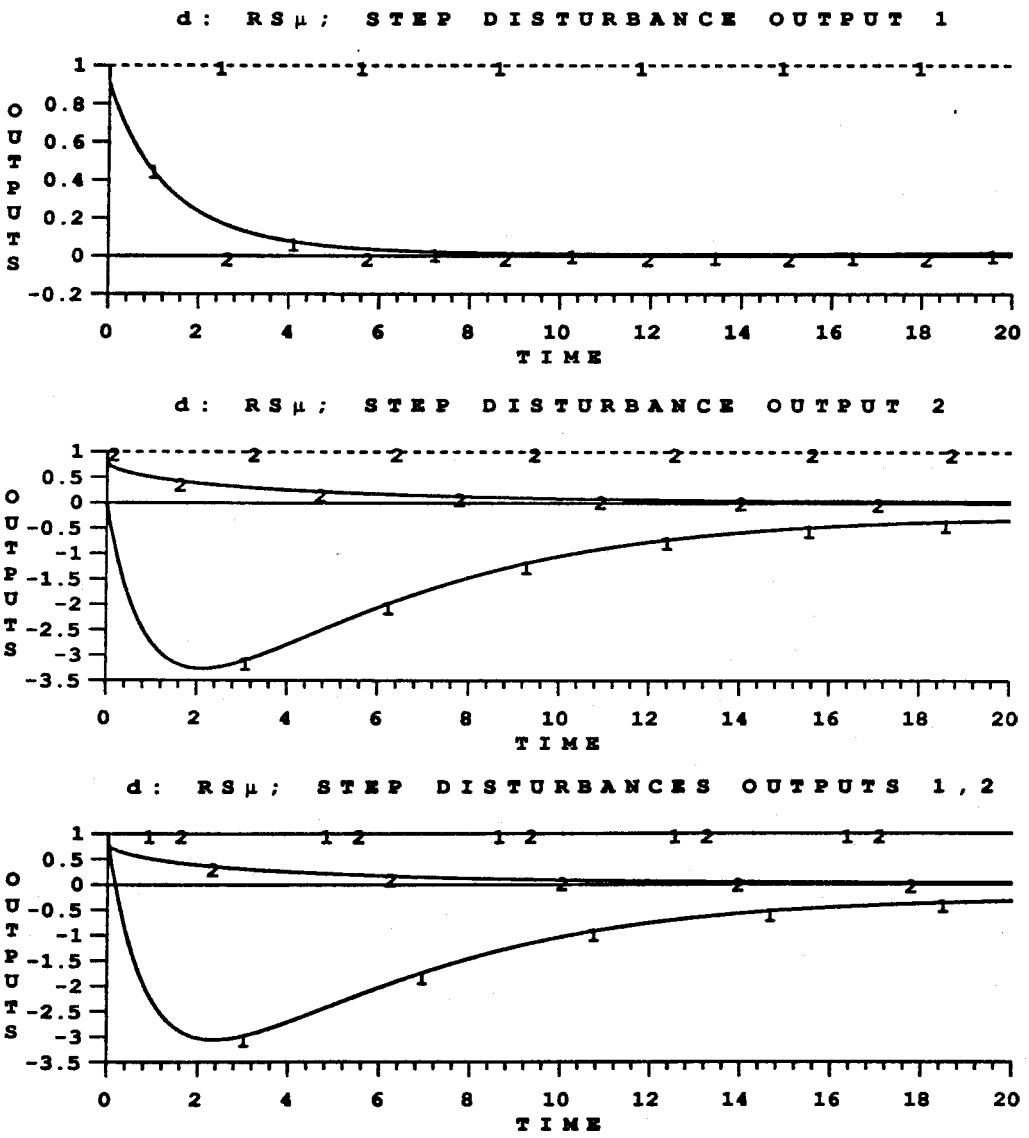

Figure 36: Responses to step disturbances for example *d* with diagonal controller from repeated sequential μ-synthesis.

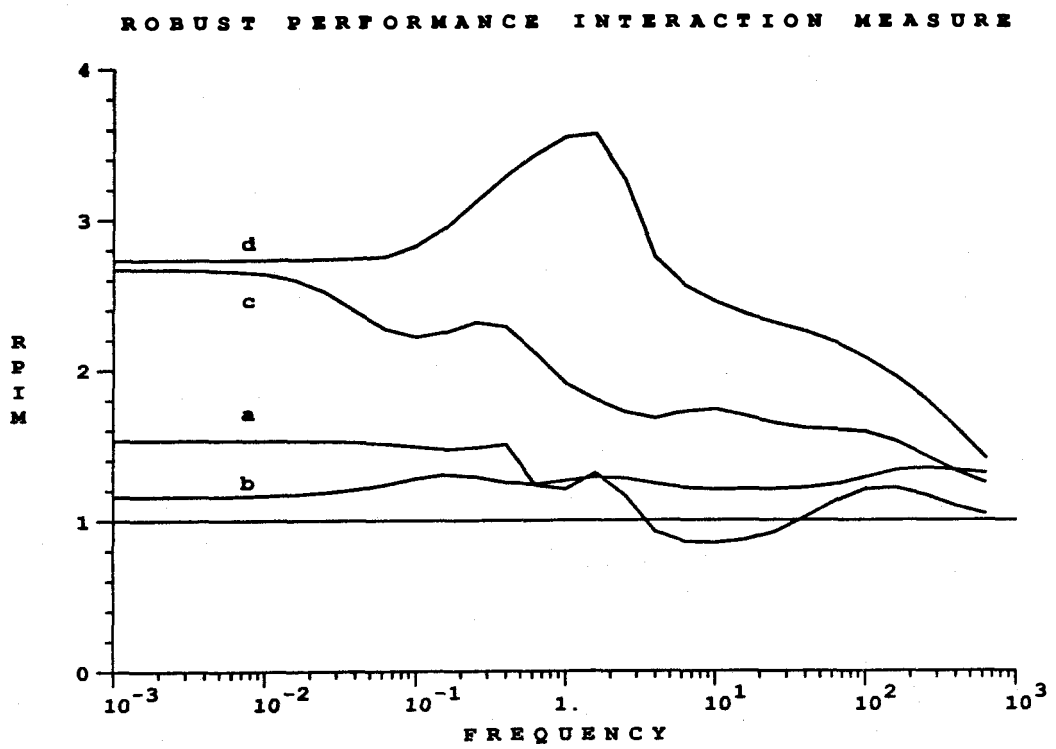

Figure 37: Robust performance interaction measures for systems *a–d* equal to the ratio $\mu_{RS}(\omega)/\mu_{Opt}(\omega)$.

CHAPTER VII: CONCLUSIONS AND RECOMMENDATIONS

CONCLUSIONS AND RECOMMENDATIONS

The new algorithm in this work for locating process uncertainty regions $\pi(i\omega)$ from model parameter uncertainties in 1 is superior to previous factorial and region-mapping methods. Deficiencies of the two previous methods have been corrected. The algorithm enables nonconservative evaluation of SISO control system robust performance despite model parameter uncertainties in the spirit of structured singular value analysis by Doyle [1982]. In Chapter II it was proven that the region boundaries located by the algorithm will contain the entire set 1 resulting from model parameter uncertainties. That the algorithm will converge to the exact set 1 as the resolution parameter r increases was also proven.

$$\pi = \left\{ p(s) | p(s) = x(s) + y(s)\ k \left[\frac{a_j n_j(s) + ... + a_1 n_1(s) + a_0 n_0(s)}{b_l d_l(s) + ... + b_1 d_1(s) + b_0 d_0(s)} \right] e^{-\theta s} \right\} \qquad (1)$$

$$a_j \in [a_{j_{min}}, a_{j_{max}}],\ b_l \in [b_{l_{min}}, b_{l_{max}}]$$

$$k \in [k_{min}, k_{max}],\ \theta \in [\theta_{min}, \theta_{max}]$$

Extension of the algorithm to enable calculation of regions containing the set of models in 2 may be a worthwhile investment of future effort. For such extension of the algorithm to be practical, it may be necessary to locate a superior routine for finding the union of overlapping regions on the complex plane. When the current implementation of the algorithm fails, it is inevitably inside the union-finding subroutine. As discussed in Chapter 2, the extension of the algorithm to sets of models in 2 will require locating the union of many more regions than are required by the current implementation.

$$g(s) = k\left[\frac{s+\alpha}{(s+\beta)(s+\gamma)}\right]e^{-\theta s} \tag{2}$$

$$\alpha \in [\alpha_{min}, \alpha_{max}],\ \beta \in [\beta_{min}, \beta_{max}],\ \gamma \in [\gamma_{min}, \gamma_{max}]$$

$$k \in [k_{min}, k_{max}],\ \theta \in [\theta_{min}, \theta_{max}]$$

Graphical, region-based analysis combines with IMC controller design to form a powerful, robust-controller-synthesis method. Specific advantages of the method include:

1) The IMC controller parameterization is stable.
2) IMC controllers resulting from the design procedure are typically of low order.
3) Few tuning parameters must be adjusted to achieve robust performance.
4) Robust-performance analysis is performed without conservativeness for SISO models with real parameter uncertainties.
5) Trade-offs between performance and robustness are transparent in the design procedure.

Unfortunately, the region-based robust-performance analysis is not generally applicable to MIMO systems. If an attempt were made to to bound the MIMO characteristic polynomial $det\left[I + PK\right]$ using region-mapping methods for the case of uncertain model elements (i.e. $P = \left[p_{ij}\right]$ with $p_{ij} \in \pi$), the result would be hopelessly conservative – correlation between p_{ij} appearing multiple times in the expansion of the determinant would be lost. Except in instances where special model structure can be exploited in robust performance analysis (as is the case for CD response control), μ-analysis is the only viable alternative.

The graphical robust-performance analysis test and related results in this work are of significant educational and practical utility. Transparency of the region-based analysis test for robust performance rendered it ideal for demonstrating the concept of robust controller design in the text by Morari et al. [1988]. The IMC design

method with region-based stability and performance analysis is used in ROBEX, an expert system for robust controller design [Lewin et al., 1987]. The method for translating parameter uncertainties into multiplicative error developed in chapter IV was useful in a laboratory process control problem [Smith et al., 1987]. As long as available μ-analysis and μ-synthesis algorithms work more effectively with norm-bounded complex perturbations (disks), the method for approximating real parameter uncertainties by disks will continue to be useful. The regions $\pi(i\omega)$ representing model uncertainty can be the starting point for the robust controller design technique based on conformal mapping developed by Sideris and Safonov [1985].

In chapter V a nontrivial problem was rigorously solved in the application of IMC controller design and region-based robust-performance analysis to decentralized CD response control. The large number of inputs and outputs in CD response models and the many required repeated real perturbations prevent existing μ-analysis and μ-synthesis from solving this problem. It was demonstrated that the value of the dimensionless slice actuator design parameter D_a can have a dramatic effect on the condition number of CD interaction response models. Since robust controllers can be designed more easily – and can provide better performance – for CD response models with low condition numbers, it may be necessary to redesign the slice to achieve better performance. Ziegler and Nichols [1943] long ago recognized the importance of designing processes with control in mind, as evidenced by their statement:

> In the application of automatic controllers, it is important to realize that controller and process form a unit; credit or discredit for results obtained are attributable to one as much as the other. A poor controller is often able to perform acceptably on a process which is easily controlled. The finest controller made,

when applied to a miserably designed process, may not deliver the desired performance.

Parameter D_a in the slice actuator model presented in this work can serve as a guide for development of better CD response control in paper manufacturing.

The bottom line on this is, of course, product quality improvement and preservation of precious natural resources through better control technology. In the paper manufacturing industry this can mean saving some 300 square miles of forest lands per year – wherein the author may be found from time to time.

REFERENCES

Aitken, A. C., *Determinants and Matrices* (Interscience Publishers, Inc.: New York), 1954, pp. 121–125.

Althoff, J., Personnal Communication, Beloit Inc., Beloit, WI, November 2, 1987.

Astrom, K. J., "Frequency Domain Properties of Otto Smith Regulators," *International Journal of Control*, 26, 1977, pp. 307–314.

Bass, L. J., and S. R. Schubert, "On Finding the Disc of Minimum Radius Containing a Given Set of Points," *Mathematical Computation*, 21, 1967, pp. 712–714.

Beecher, A. E., and R. A. Bareiss, "Theory and Practice of Automatic Control of Basis Weight Profiles," *Tappi*, 53, May 1970, pp. 847–852.

Bellman, R., *Introduction to Matrix Analysis* (McGraw Hill Co.: New York), 1970, pp. 231–248.

Bernstein, D. S., "Sequential Design of Decentralized Dynamic Compensators Using the Optimal Projection Equations: An Illustrative Example Involving Interconnected Flexible Beams," *Proceedings of the American Control Conference*, Minneapolis, June 10–12, 1987, pp. 986–989.

Bhaya, A., and C. A. Desoer, "Controlling Plants with Delay," *International Journal of Control*, 41, 1985, pp. 813–830.

Bolton, A. G., "Inverse Nyquist Design Using Region Algebra," *Int. J. Control*, 33, 1981, pp. 575–584.

Boyle, T. J., "Practical Algorithms for Cross-Direction Control," *Tappi*, 61, June 1978, pp. 77–80.

Bristol, E. H., "On a New Measure of Interaction for Multivariable Process Control," *IEEE Transactions on Automatic Control*, AC-11, 1966, pp. 133–134.

Brosilow, C. B., "The Structure and Design of Smith Predictors from the Viewpoint of Inferential Control," *JACC - Denver*, 1979.

Callender, A., with D. R. Hartree and A. Porter, "Time-Lag in a Control System," *Philosophical Transactions of the Royal Society of London*, 235, 1936, pp. 415–444.

Carey, E. W., with C. R. Bietry and H. W. Stoll, "Performance Factors Associated with Profile Control of Basis Weight on a Paper Machine," *Tappi*, 58, June 1975, pp. 75–78.

Chen, S., *Control System Design for Multivariable Uncertain Processes*, Ph.D. Thesis (Supervised by C. B. Brosilow), Case Western Reserve University, August 1984.

Chin, F., and C. Wang, "Optimal Algorithms for the Intersection and the Minimum Distance Problem Between Planar Polygons," *IEEE Transactions on Computers*, C-32, 1983, pp. 1203–1207.

Chu, C. C., with J. C. Doyle and E. B. Lee, "The General Distance Problem in H_∞ Synthesis," *International Journal of Control*, 44, 1986, pp. 565–596.

Churchill, R. V., with J. W. Brown and R. F. Verhey, *Complex Variables and Applications*, 3rd ed. (McGraw Hill, Inc.: New York), 1976, pp. 72–239.

Cohen, G. H., and G. A. Coon, "Theoretical Consideration of Retarded Control," *Transactions of the ASME*, July, 1953, pp. 827–834.

Cuffey, W. H., "Some Factors Involved in Basis Weight Uniformity," *Tappi*, 40, June 1957, pp. 190A–197A.

Crandall, S. H., with N. C. Dahl and T. J. Lardner, *An Introduction to the Mechanics of Solids* (McGraw-Hill, Inc.: New York), 2nd Ed., 1978, pp. 511–576.

Davis, P. J., *Circulant Matrices* (John Wiley & Sons: New York), 1979.

Desoer, C. A., and A. N. Gundes, "Linear Time-Invariant Controller Design for Two-Channel Decentralized Control Systems," *Proceedings of the American Control Conference*, Minneapolis, June 10–12, 1987, pp. 1703–1704.

DeVries, W. R., with S. M. Pandit and S. M. Wu, "Evaluation of the Stability of Paper Basis-Weight Profiles Using Multivariate Time Series," *IEEE Transactions on Automatic Control*, AC-22, 1977, pp. 590–594.

Doyle, J. C., "Analysis of Feedback Systems with Structured Uncertainties," *Proc. Inst. Elect. Engrs.*, Pt. D, 129, 1982, pp. 242–250.

Doyle, J. C., "A Review of μ for Case Studies in Robust Control," *IFAC World Congress*, Munich, July 1987.

Doyle, J. C., and A. Packard, "Uncertain Multivariable Systems from a State Space Perspective," *Proceedings of the American Control Conference*, Minneapolis, June 10-12, 1987, pp. 2147–2152.

Doyle, J. C., and G. Stein, "Multivariable Feedback Design: Concepts for a Classical/Modern Synthesis," *IEEE Transactions on Automatic Control*, AC-26, February 1981, pp. 4–16.

Dumont, G. A., "Application of Advanced Control Methods in the Pulp and Paper Industry – A Survey," *Automatica*, 22, 1986, pp. 143–153.

East, D. J., "A New Approach to Optimum Loop Synthesis," *International Journal of Control*, 34, 1981, pp. 731–748.

East, D. J., "On the Determination of Plant Variation bounds for Optimum Loop Synthesis," *International Journal of Control*, 35, 1982, pp. 891–908.

Edelsbrunner, H., with H. A. Maurer and D. G. Kirkpatrick, "Polygonal Intersection Searching," *Information Processing Letters*, 14, April 20, 1982, pp. 74–79.

Egelhof D., "The Influence of the Headbox on Asymmetry in Paper," *Das Papier*, No. 7, 1986, pp. 313–318.

Fan, M. K., and A. L. Tits, "Characterization and Efficient Computation of the Structured Singular Value," *IEEE Transactions on Automatic Control*, AC-31, August 1986, pp. 734–743.

Garcia, C. E., and M. Morari, "Internal Model Control: A Unifying Review and Some New Results," *I & EC Process Des. & Dev.*,21, 1982, pp. 308–323.

Graham, R. L., and F. F. Yao, "Finding the Convex Hull of a Simple Polygon," *Journal of Algorithms*, 4, 1983, pp. 324–331.

Grosdidier, P., and M Morari, "Interaction Measures for Systems Under Decentralized Control," *Automatica*, 22, 1986, pp. 309–319.

Henrici, P., *Applied and Computational Complex Analysis* (John Wiley & Sons: New York), 1, 1974.

Holt, B. R., and M. Morari, "Design of Resilient Processing Plants: The Effect of Deadtime on Dynamic Resilience," *Chem. Eng. Sci.*, 40, 1985, pp. 1229–1237.

Holt, B. R., and M. Morari, "Design of Resilient Processing Plants: The Effect of Right-half-plane Zeros on Dynamic Resilience," *Chem. Eng. Sci.*, 40, 1985, pp. 59–74.

Holt, B. R, *The Assessment of Dynamic Resilience: The Effect of Non-minimum Phase Elements*, Ph. D. Thesis, University of Wisconsin–Madison, 1984.

Horowitz, I. M., "Quantitative Feedback Theory," *IEE Proc.*, D-129, November 1982, pp. 215–226.

Horowitz, I. M., "Some Properties of Delayed Controls (Smith Regulator)," *International Journal of Control*, 38, 1983, pp. 977–990.

Ioannides, A. C., with G. J. Rogers and V. Latham, "Stability limits of a Smith Controller in Simple Systems Containing a Time Delay," *International Journal of Control*, 29, 1979, pp. 557–563.

Jerome, N. F., and W. H. Ray, "High-Performance Multivariable Control Strategies for Systems Having Time Delays," *AIChE Journal*, 32, 1986, pp. 914–931.

Jordan, K., *A Novel Analysis Technique for Processes With Uncertain Parameters*, M.S. Research Report, California Institute of Technology, 1985.

Karlsson, H., and L. Haglund, "Optimal Cross-Direction Basis Weight and Moisture Profile Control on Paper Machines," *Proceedings of the 3rd International Pulp and Paper Process Control Symposium*, Vancouver, B. C., Canada, May 2-4, 1983, pp. 139–145.

Karlsson, H., with I. Lundqvist and T. Ostman, "Principles and Potentials of CD-Basis Weight Control," *Proceedings of the EUCEPA Symposium on Control Systems in the Pulp and Paper Industry*, Stockholm, Sweden, May 11-14, 1982, pp. 238–243.

Krishnan, K. R., and A. Cruickshanks, "Frequency-domain design of feedback systems for specified insensitivity of time-domain response to parameter variation," *Int. J. Control*, 25, 1977, pp. 610–620.

Kurozumi, Y., and W. Davis, "Polygon Approximation by the Mini-max Method," *Computer Graphics and Image Processing*, 19, 1982, pp. 248–264.

Laughlin, D. L., with K. G. Jordan and Manfred Morari, "Internal Model Control and Process Uncertainty: Mapping Uncertainty Regions for SISO Controller Design," *International Journal of Control*, 44, 1986, pp. 1675–1698.

Laughlin, D. L., with D. E. Rivera and Manfred Morari, "Smith Predictor Design for Robust Performance," *International Journal of Control*, 46, 1987, pp. 477–504.

Lee, D. T., and F. P. Preparata, "Computational Geometry," *IEE Transactions on Computers*, C-33, December 1984, pp. 1072–1102.

Lewin, D. R., with R. E. Heersink, A. Skjellum, D. Laughlin, D. E. Rivera, and M. Morari, "ROBEX: Robust Control Synthesis via Expert System," *IFAC World Congress*, Munich, July 1987.

Longdon, L., and D. J. East, "A Simple Geometrical Technique for Determining Loop Frequency Response Bounds which Achieve Prescribed Sensitivity Specifications," *Int. J. Control*, 30, 1979, pp. 153–158.

MacFarlane, A. G. J., "Return-Difference and Return-Ratio Matrices and Their Use in Analysis and Design of Multivariable Feedback Control Systems," *Proc. Instn. Elect. Engrs.*, 117, 1970, pp. 2037–2049.

Mayne, D. Q., "The Design of Linear Multivariable Systems," *Automatica*, 9, 1973, pp. 201–207.

McFarlin, D. A., "Control of Cross-Machine Sheet Properties on Paper Machines," *Proceedings of the 3rd International Pulp and Paper Process Control Symposium*, Vancouver, B. C., Canada, May 2-4, 1983, pp. 49–54.

Morari, M., with E. Zafirou and C. Economou, *Robust Process Control*, Springer Verlag, to be published, 1988.

Morari, M., and S. Skogestad, "Effect of Model Uncertainty on Dynamic Resilience,"Proc. PSE 85, Cambridge, April 1985, IChE Symp. Ser., No. 92, 1985.

Nett, C. N., and J. A. Uthgenannt, "An Explicit Formula and an Optimal Weight for the 2-Block Structured Singular Interaction Measure," *IEEE Transactions on Automatic Control*, submitted September 1, 1986.

Nievergelt, J., and F. P. Preparata, "Plane-Sweeping Algorithms for Intersecting Geometric Figures," *Communications of the ACM*, 25, October 1982, pp. 739–747.

Ogunnaike, B. A., with J. P. Lemaire, M. Morari, and W. H. Ray, "Advanced Multivariable Control of a Pilot Plant Distillation Column," *AIChE Journal*, 29, 1983, pp. 632–640.

Owens, D. H., and A. Raya, "Robust Stability of Smith Predictor Controllers for Time Delay Systems," *Proc. Inst. Elect. Engrs.*, Pt. D, 129, 1982, p. 298.

Palmor, Z. J., and R. Shinnar, "Design of Advanced Process Controllers," *AIChE Journal*, 27, 1981, pp. 793–805.

Palmor, Z. J., "Improved Dead-Time Compensator Controllers," *AIChE Journal*, 31, 1985, pp. 215–221.

Palmor, Z. J., "Stability Properties of Smith Dead-Time Compensator Controllers," *International Journal of Control*, 32, 1980, pp. 937–949.

Preparata F. P., and S. J. Hong, "Convex Hulls of Finite Sets of Points in Two and Three Dimensions," *Communications of the ACM*, 20, February 1977, pp. 87–93.

Richards, G. A., "Cross Direction Weight Control," *Japan Pulp and Paper*, November 1982, pp. 41–53.

Rivera, D. E., with Manfred Morari and S. Skogestad, "Internal Model Control:PID Controller Design," *I & EC Process Design Development*, 25, 1985 pp. 252–265.

Rosenbrock, H. H., "Design of Multivariable Control Systems Using the Inverse Nyquist Array," *Proc. Inst. Elect. Engrs.*, 116, 1969, pp. 1929–1936.

Saeki, M., "A Method of Robust Stability Analysis with Highly Structured Uncertainties," *IEEE Transactions on Automatic Control*, AC-31, 1986, pp. 935–940.

Schwartz, J. T., "Finding the Minimum Distance Between Two Convex Polygons," *Information Processing Letters*, 13, 1981, pp. 168–170.

Scott, R. F., *Foundation Analysis* (Prentice-Hall, Inc.: New Jersey), 1981, pp. 119–201.

Sedgwick, R., *Algorithms* (Addison Wesley: London), 1983.

Sideris, A., and M. G. Safonov, "Design of Linear Control Systems for Robust Stability and Performance," *IFAC Workshop on Estimation and Control of Uncertain Systems*, Boston, MA, June 17-18, 1985.

Sideris, A., and R. R. E. de Gaston, "Multivariable Stability Margin Calculation with Uncertain Correlated Parameters," *IEEE Transactions on Automatic Control*, to be submitted 1988.

Sinha, N. K., and B. Kuszta, *Modelling and Identification of Dynamic Systems* (Van Nostrand: New York), 1983.

Skogestad, S., and M. Morari, "Control of Ill-Conditioned Plants: High Purity Distillation," *AIChE Annual Meeting*, paper 74a, Miami, Florida, November 1986.

Skogestad, S., and M. Morari, "Implications of Large RGA-Elements on Control Performance," *AICHE Annual Meeting*, paper 6d, Miami Beach, Florida, November 1986.

Skogestad, S., and M. Morari, "Robust Performance of Decentralized Control Systems by Independent Designs," *Automatica*, submitted January, 1987.

Smith, O. J. M., "Closer Control of Loops with Dead Time," *Chemical Engineering Progress*, 53, 1957, pp. 217–219.

Smith, R. S., Personnal Communication, California Institute of Technology, June 19, 1987.

Smith, R. S., with J. C. Doyle, M. Morari, and A. Skjellum, "A Case Study Using μ: Laboratory Process Control Problem," *IFAC World Congress*, Munich, July 1987.

Statistical Abstract of the United States, U. S. Department of Commerce, 107th ed., 1987, pp. 660–661.

Statistical Yearbook 1983/1984, Department of International Economics and Social Affairs (United Nations: New York), 34th ed., pp. 686–687.

Tong, R. M., "Automatic Control of Grammage Profile on a Paper Machine," *Proceedings of the 3rd IFAC PRP Conference*, Brussels, Belgium, 1976, pp. 289–298.

Velguth, J., Personnal Communication, Voith Inc., Appleton, WI, November 2, 1987.

Wallace, B. W., "Economic Benefits Offered by Computerized Profile Control of Weight, Moisture, and Caliper," *Tappi*, 64, 1981, pp. 79-83.

White, F. M., *Fluid Mechanics* (McGraw-Hill, Inc.: New York), 1979, pp. 597–601.

Wilhelm, R. G. Jr., and M. Fjeld, "Control Algorithms for Cross Directional Control: the State of the Art," *Preprints of the 5th IFAC PRP Conference*, Antwerp, Belgium, October 11-13, 1983, pp. 139–150.

Wilkinson, A. J., and A. Hering, "A New Control Technique for Cross Machine Control of Basis Weight," *Preprints of the 5th IFAC PRP Conference*, Antwerp, Belgium, October 11-13, 1983, pp. 151–155.

Witham, G. S., *Modern Pulp and Paper Making: A Practical Treatise* (Reinhold Publishing Co.: New York), 2nd Ed., 1942.

Wrist, P. E., "Dynamics of Sheet Formation on the Fourdrinier Machine," *Oxford Symposium on Formation and Structure*, 1961, pp. 839–899.

Youla, D. C., with H. A. Jabr, and J. J. Bongiorno, Jr., "Modern Wiener-Hopf Design of Optimal Controllers: Part II," *IEEE Transactions on Automatic Control*, AC-21, 1976, pp. 319–338.

Ziegler, J. G., and N. B. Nichols, "Process Lags in Automatic-Control Units," *Transactions of the A.S.M.E.*, 65, July 1943, pp. 433–444.